PROBING QUARK GLUON PLASMA THROUGH PHOTON, DILEPTON AND STRANGENESS PRODUCTIONS IN RELATIVISTIC NUCLEAR COLLISIONS

By

JAJATI KESARI NAYAK
(PHYS04200704008)

VARIABLE ENERGY CYCLOTRON CENTRE
KOLKATA-700064, INDIA.

A thesis submitted to the
Board of Studies in Physical Sciences
In partial fulfillment of the requirements
For the degree of

Doctor of Philosophy

of

HOMI BHABHA NATIONAL INSTITUTE

November, 2012

STATEMENT BY AUTHOR

This dissertation has been submitted in partial fulfillment of requirements for an advanced degree at Homi Bhabha National Institute (HBNI) and is deposited in the Library to be made available to borrowers under rules of the HBNI.

Brief quotation from this dissertation are allowable without special permission, provided that accurate acknowledgement of source is made. Requests for permission for extended quotation from or reproduction of this manuscript in whole or in part may be granted by the Competent Authority of HBNI when in his or her judgement the proposed use of the material is in the interests of scholarship. In all other instances, however, permission must be obtained from the author.

Jajati Kesari Nayak

DECLARATION

I, hereby declare that the investigation presented in the thesis has been carried out by me. The work is original and has not been submitted earlier as a whole or in part for a degree/diploma at this or any other Institution/University.

Jajati Kesari Nayak

Dedicated to my parents
&
to my school teachers

Education enlightens
Education enriches
Education expands the horizon of knowledge
The education, hence should be free for all as the air.

Acknowledgement

First and foremost, I owe my deepest gratitude to my supervisor, Prof. Jan-e Alam, whose encouragement, guidance and support from the beginning enabled me to develop an understanding of the subject. This thesis would not have been in such a shape without his patience and guidance. I am grateful to Prof. Bikash Sinha, Homi Bhabha Professor & Ex-Director and Prof. Dinesh Srivastava, Director, VECC, who suggested me to work in the exciting field of ultra-relativistic heavy ion collisions. I felicitate my hearty thanks to the Doctoral committee members, Prof. Santanu Pal, Prof. Subhasish Chattopadhyay and Prof. Debadesh Bandopadhyay, who guided continuously when needed with their valuable suggestions. I am quite impressed with the behaviour and honesty of Prof. Pal especially for his encouraging words which boosts the morale of a young scientific mind. I also thank Prof. P. Barat, our ex-Dean, HBNI, VECC for his support to carry out Ph.D.

I would like to express my deepest gratitude to another dedicated researcher Prof. Asish Dhara who is like a wikipedia for me and played a crucial role for the development of my basic understandings. I express my sincere thanks to Dr. Bedangadas Mohanty and Dr. Sourav Sarkar for providing valuable inputs to some of the important topics of this thesis. If I bestow my thanks again and again still it would be less for Mrs. Payal Mohanty, who has been helping me constantly till the date of my submission. I also thank to Prof. Tapan Nayak and Dr. Premomay Ghosh, Prof. Ashis Chaudhuri the well wishers, some of whom went through my thesis and provided many useful suggestions. It is my pleasure to be a member of the Physics Group and to work in such a vibrant academic atmosphere. Continuous help from the group members like Partha, Jhilam, Prithiwish, Swagata, Sanjib and Gargidi increased the enthusiasm for my scientific research and development. The fruitful discussions with the year-long physics companion Partha helped me a lot to give the thesis a final shape. I thank Sarmisthadi, one of my inspiring collaborators who helped me in various ways. Thanks to all the staffs of my physics group where I received the strong foundation necessary for any academic endeavor. My fellow graduate classmates Samir, Supriya, Pratap, Tapan, Kaushik, Ratnesh, Dipu, Surajitda and Gopalda have also been a constant driving force in my studies. I am thankful to the timely suggestions and numerous help of Samir, Supriya and Pratap which enabled me to submit the thesis. Surajitda is the solution book to all the technical problems like latex, Ubuntu, net connection, program compilation, etc. I enjoyed the company of Hemendra Pandey('pandeyji'), Shashi, Pratap (RIB) and Himansu bhai. Also many thanks to Pandeyji's family for the good meals they have provided at some of my late office hours. Shashi's useful suggestions played an intricate role in my development as a researcher. I would not miss this oppertunity to thank Dr. V. S. Pandit for his interesting discussions on general physics in many occasions. Dr. Anand Dubey is another name not to be forgotten, especially for the exciting discussion of physics or discussions deviating physics, leaning towards literatures or bending towards politics at the odd hours of the day. I also thank Sabya, Hari, Santosh, Victor, Jamil, Rupa, Nihar, Sudipan, Abhisek, Trambak, Surashree, Nasim, Subhash, Somnath and Younus for the encouragement provided during thesis period. I am very much thankful to Dr. Atanu Talapatra, a friend in need, who has been encouraging continuously since the start of the thesis work. I would like to thank Prof. Pradip Roy and A. K Dutt-Mazumder of SINP for various help during my thesis period.

The company of Mr. Prafulla Behera since 2003 and the association of other friends like Pradip, Ankur, Jay, Subash and Mahant later on facilitated my work in several ways. I am indebted to Chinuapa and Bibhansubhai who are the other key ingredients of the smoothness of my academic endevour. The continuous encouragement and support from Gourahari, Biswa, Jaga and Rajib kept up my enthusiasm during the whole period. My apologies for those who helped me but I miss to acknowledge here.

Finally, I am forever indebted to my parents, members of my (joint) family, inlaws and relatives for the kind of support they have provided during my academic journey. Special thanks to my niece Saina, whose half-spell words took me away from the day-long work's tiredness. I am really indebted to my wife Deepti for her patience and tenderness without which it would have been difficult to complete.

Synopsis

Lattice quantum chromo dynamics (lQCD) based calculations predict that at very high temperature, and densities the hadronic matter undergoes a phase transition to a new state of matter called quark gluon plasma (QGP) due to asymptotic freedom and Debye screening of color charges. QGP is a thermodynamic state of matter where the properties of the system is governed by quarks and gluons. It is expected that the magnitude of temperature and/or density required for QGP-hadron transition can be achieved by colliding heavy nuclei at relativistic energies (such as at SPS, RHIC and LHC energies). Because of the transient nature of the matter produced at relativistic nuclear collisions it is very difficult to confirm the formation of QGP. Electromagnetic (EM) probes, such as photon and dilepton spectra, have been proposed as one of the most promising tools to characterize the initial state of the collisions. Because of the very nature of their interactions, photons and dileptons suffer minimum rescattering but produced at every space time points, therefore, can be used as an efficient tool to extract the initial temperature of the system. By comparing the initial temperature and the transition temperature estimated from lattice QCD, one can infer whether QGP is formed or not. In the present work we study the EM probes emanating from the system formed in nuclear collisions at SPS, RHIC and LHC energies. The spectra of photons and dileptons have been studied considering an extensive set of partonic and hadronic interactions within the framework of thermal field theory. The space time evolution of the matter is studied using boost invariant relativistic hydrodynamic model. The theroetical results on the photon and dilepton spectra have been compared with experimental data obtained by PHENIX and NA60 collaboration (respectively for RHIC

and SPS energies). The transverse momentum (p_T) spectra of photons, dileptons and their ratios for various lepton pair mass bins have been evaluated and shown that a less model dependent information of the initial temperature of the system can be extracted from the ratio. We study the evolution of radial flow v_r using both photon and dilepton spectra and argue that v_r can be quantified from the simultaneous measurements of photons and lepton pairs with a judiciuos choice of kinematic variables.

Production of strangeness in heavy ion collisions has also been studied to detect the QGP expected to be formed in nuclear collisions. For the production of strange mesons and baryons a microscopic calculation has been employed using momentum integrated Boltzmann transport equation. The results have been compared with the experimental data for K/π ratio obtained by CERES, NA49, STAR, PHENIX collaborations at AGS, SPS and RHIC energies. The 'horn' like structure observed in the measurement of K^+/π^+ ratio with different center of mass energies ($\sqrt{s_{NN}}$) has been explained with the assumption of an initial partonic phase beyond a threshhold in center of mass energy. However an initial hadronic scenario fails to explain the data at higher center mass energies. K^-/π^- data also have been explained within the same formalism.

Contents

Notation and Conventions

In the thesis, the natural units have been used, $\hbar = c = k_B = 1$. The matric tensor used is $g^{\mu\nu} = diag(1, -1, -1, -1)$. Variables in bold face denote 3-vectors. Most of the notation is introduced during the discussion and the frequently used notations are enlisted below:

$N - N$	Nucleon-Nucleon
$p - p$	proton-proton
$p - A$	proton-Nucleus with mass number A
$A - A$	Nucleus-Nucleus with mass number A
$s,\ t,\ u$	Madelstam Variables, where $s = (p_1 + p_2)^2,\ t = (p_1 - p_3)^2,\ u = (p_1 - p_4)^2$
$\mu_B = \mu$	Baryonic chemical potential
τ	Proper time ($= \sqrt{t^2 - z^2}$)
y	Particle rapidity ($= \frac{1}{2} \ln \left[\frac{E+p_z}{E-p_z}\right]$)
η	Space-time rapidity ($= \tanh^{-1}(t/z)$), thus $t = \tau \cosh \eta$ and $z = \tau \sinh \eta$
M	Invariant mass of lepton pairs
p_T	transverse momentum
m_T	transverse mass of lepton pair ($m_T^2 = M^2 + p_T^2$)
ϵ	Energy density
P	Thermodynamic pressure
s	Entropy density
V	Vector mesons
τ_i	Thermalization time
T_i	Thermalization temperature
T_c	Transition temperature
T_{ch}	Chemical freeze-out temperature
T_f	Thermal freeze-out temperature
d^4x	four-volume
K	average pair momentum ($= (p_1 + p_2)/2$), off-shell
q	relative pair momentum ($= p_1 - p_2$), off-shell

List Of Publications

The thesis is primarily based on the work published in the following peer reviewed journals and unreviewed conference proceedings.

Referred Journals:

1. **Kaon production in Heavy Ion Collisions,**
   Jajati K. Nayak, J. Alam, P. Roy, A. K. Dutt-Mazumder, B. Mohanty,
   Acta. Phys. Slova. 56, 27 (2006).
   Preprint : Nucl-th/0511023.

2. **Thermal radiation from Au+Au collisions at $\sqrt{s}$=200 GeV/A,**
   J. Alam, Jajati K. Nayak, P. Roy, A. K. Dutt-Mazumder and B. Sinha,
   J. Phys. G, 34, 871 (2007),
   Preprint : Nucl-th/0508043.

3. **Thermal photon to dilepton ratio in high energy nuclear collisions,**
   Jajati K. Nayak, J. Alam, S. Sarkar and B. Sinha,
   Phys. Rev. C, 78, 034903 (2008),
   Preprint : Nucl-th/0705.1591.

4. **Measuring initial temperature through photon to dilepton ratio in heavy ion collision,**
   Jajati K. Nayak, J. Alam, S. Sarkar and B. Sinha,

J. Phys. G, 35, 104161 (2008),

Preprint : Nucl-th/0806.0447.

5. **Measuring radial flow of partonic and hadronic phases in relativistic heavy ion collision,**

   Jajati K. Nayak, J. Alam,

   Phys. Rev. C, bf 80, 064906 (2009),

   Preprint : Nucl-th/0907.3036.

6. ***Radial Flow from Electromagnetic Probes and Signal of Quark Gluon Plasma.**

   Payal Mohanty, Jajati K Nayak, Jan-e Alam, Satosh K Das.

   Phys. Rev. C, 82, 034901 (2010).

   Preprint : Nucl-th/0910.4856

7. **The horn in the kaon to pion ratio,**

   Jajati K. Nayak, S. Banik and J. Alam,

   Phys. Rev. C, 82, 024914 (2010),

   Preprint : Nucl-th/1006.2972.

8. **Kaon and Lambda productions in relativistic heavy ion collisions,**

   Jajati K. Nayak, S. Banik and J. Alam,

   Nucl. Phys. A, 862-863, 286 (2011),

   Preprint : Nucl-th/1101.3187.

9. **Muon pairs from In+In collision at energies available at the CERN Super Proton Synchrotron,**

Jajati K. Nayak, J. Alam, T. Hirano, S. Sarkar and B. Sinha,

Phys. Rev. C. 85, 064906 (2012).

Preprint : Nucl-th/0902.0446.

Review Article/Book:

1. ***Two introductory lectures on high energy QCD and heavy ion collisions**

   Debasish Benarjee, Jajati K. Nayak and Raju Venugopalan,

   Lectures Given at QGP Winter School, Jaipur, India, 1-3 Feb, 2008,

   Article in the book **"Physics of Quark Gluon Plasma"**,

   published by **Springer Berlin/Heidelbarg** in **Lect. Notes Phys. 785:105-137, (2010)**.

   Preprint : arxiv:0810.3553.

Axiv Submission:

1. *** Phi productions at RHIC: characterisation of co-existence phase,**

   Jajati K. Nayak, J. Alam, B. Mohanty, P. Roy, A. K. Dutt-Mazumder,

   Preprint : Nucl-th/0509061.

Conference Proceedings:

1. **Invariant mass spectra of dimuons from In+In collisions at $\sqrt{s_{NN}}$ =17.3 GeV,**

   Jajati K. Nayak, J. Alam, S. Sarkar,

   DAE-BRNS Symposium on Nuclear Physics, Vol. 56(2011).

2. **Strangeness to equilibrium entropy: a signal of phase transition,**

   Jajati K. Nayak, Sarmistha Banik and Jan-e Alam,

   DAE-BRNS Symposium on Nuclear Physics, Vol. 55(2010).

3. **Kaon and Lambda productions in heavy ion collisions,**

   Jajati K. Nayak, Sarmistha Banik and Jan-e Alam,

   Proceedings of ICPAQGP-2010 .

4. **Probing quark gluon plasma through the radial flow of the thermal electromagnetic radiations,**

   Jajati K. Nayak, Payal Mohanty, Jan-e Alam & Santosh Das,

   Proceedings of ICPAQGP-2010 .

5. **Radial flow from photon to dilepton ratio,**

   Jajati K. Nayak, Jan-e Alam, Sourav Sarkar and Bikash Sinha,

   DAE-BRNS Symposium on Nuclear Physics, Vol. 53(2008) 553.

6. **Measuring initial temperature through photon to dilepton ratio in heavy ion collision,**

Jajati K. Nayak, Jan-e Alam, Sourav Sarkar and Bikash Sinha,

Proceedings of Quark Matter-2008.

7. ***Thermalisation in Ultra-Relativistic Heavy Ion collision,** Santosh K Das, Payal Mohanty, Jajati K. Nayak and Jan-e Alam.

   Proceedings of Quark Matter-2008.

8. **Thermal photons to dileptons ratio in the Relativistic Heavy-Ion collision,**

   Jajati K Nayak, Jan-e Alam, Sourav Sarkar and Bikash Sinha,

   DAE-BRNS Symposium on Nuclear Physics, Vol. 52(2007) 553.

9. ***Freeze out time in Ultra-Relativistic Heavy Ion Collisions,**

   Santosh K Das, Payal Mohanty, Jajati K Nayak and Jan-e Alam,

   DAE-BRNS Symposium on Nuclear Physics, Vol .52(2007) 521.

10. **Thermal photons to dilepton ratio at LHC,**

    Jajati K. Nayak, Jan-e Alam, Sourav Sarkar and Bikash Sinha,

    Presented at workshop on Heavy Ion Collisions at LHC: Last call for predictions, CERN, Geneva, Switzerland,

    Edited by N. Armesto and published in J.Phys.G**35**:054001(153-156), 2008.

11. *** Phi production at RHIC,**

    Jajati K Nayak, Jan-e Alam, Bedangadas Mohanty, Pradip Roy and Abhee K Dutt-Mazumder,

    Pramana J. Phys., Vol. 67, (2006) No. 5, 973.

12. **Thermal radiation from Au+Au collisions at roots =200 GeV/A,**

    Jajati K. Nayak, Jan-e Alam, Pradip Roy, Abhee K Dutt-Mazumder, Bikash Sinha

    DAE-BRNS Symposium on Nuclear Physics, Vol.50(2005)407.

13. **Kaons from Heavy Ion Collisions,**

    Jajati K. Nayak, Abhee K Dutt-Mazumder, Pradip Roy, Jan-e Alam, Bikash Sinha,

    DAE-BRNS Symposium on Nuclear Physics, Vol. 47(2004)400.

The works in the star(*) marked papers although have been published in reviewed journal or presented in any symposia/conferences during the Ph.D. period but not included in this thesis.

List of Figures

List of Tables

Chapter 1

Introduction

"What are we made up of or made from" led the mankind to think and search for the fundamental entities or building blocks of matter. Since the dawn of the civilization, this question puzzled the human minds. Few thousand years ago Indian [1, 2] as well as Greek philosophers proposed five basic elements of nature namely; earth (kshiti), water (aap), fire (tejas), air(marut), Aether(vyom). The Greek philosopher Democritus, asked more specific question: what would happen if we take a lump of some material, and keep dividing it into smaller ones? He concluded that the continuation of this division would lead to a stage where one can't divide the material any more. He referred it as the smallest unit of matter or 'atom'. The 'atom' is a Greek word which means 'uncuttable' or 'indivisible'. Different kinds of atoms were postulated then with different specific properties. In modern times, people started the journey from the

[1] Many also believe that Indian philosopher, Kanad originated the idea of smallest unit of indivisible matter known as 'anu' [1], similar to the atom. He also told that anu's of similar types combine to form 'dvyanuka' and 'tryanuka' as atoms form diatomic and triatomic molecules.

macroscopic world to the microscopic world to know the structure of matter *i.e.,* from the visible matter to the molecules, atoms, nuclei, nucleons, and finally reached up to the quarks. With the advent of modern accelerators, the journey of exploration of the microscopic world has taken a new dimension. It has become the saga of the discoveries of fundamental particles. The kinetic energy from the remarkably high-speed collisions in particle accelerators produce matter of new particles consistent with energy-mass equivalence and the conservation principles of energy as well as momentum. Here we discuss various fundamental particles those act as the building blocks of the matter.

1.1 Basic building blocks of matter and the fundamental interactions

During the last century, our understanding of the fundamental building blocks of the universe has changed dramatically because of the construction of more powerful and energetic particle accelerators. Along with the development of accelerator technology, the formulation of new theoretical frame work, 'the standard model' has also accelerated the journey with the successful predictions of new particles; including the recently discovered new meson of mass 125 GeV (might be Higgs boson). The scattering experiments have been proved to be key to reveal the structure of the matter. The matter that we see in the naked eye are made up of molecules which contains atoms. Atoms already unimaginably small, are built of even more minute particles-electrons, neutrons and protons. Neutrons and protons are comprised of quarks which are bound by the gluons. The quarks, like electrons, appear to be indivisible. Indeed all present day experiments

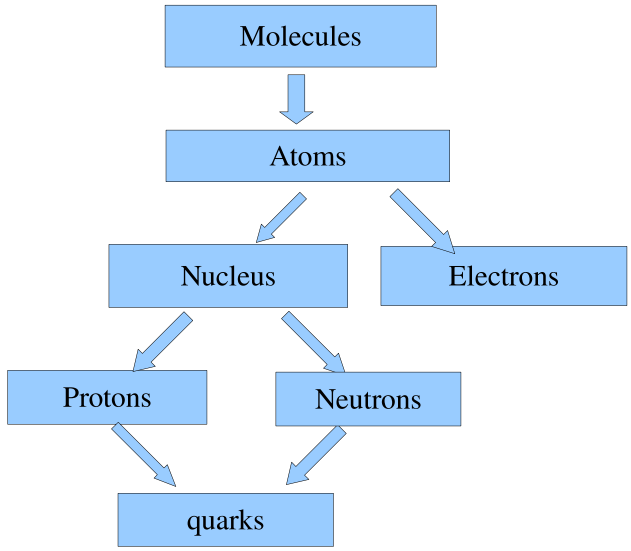

Figure 1.1: Hierarchal structure of visible matter

have failed to display any substructure of the quarks. The hierarchical structure of visible matter can be shown as in Fig. 1.1. Although this figure Fig. 1.1 tells about the constituents of matter but it is not sufficient to know the properties of matter, only from the constituents. It is necessary to understand how they interact among themselves. The interaction can tell us how the constituents are bound together inside a molecule, atom, proton, or neutron. Also the interaction can answer the question like what happens when two constituents (like molecules, atoms, nucleons or quarks) come close to each other. The answers to these questions are relevant for understanding various reactions, such as chemical reactions, nuclear reactions and reactions involving quarks. This issue has been addressed with four kind of fundamental interactions that nature exhibits- **Gravitational, Electromagnetic, Weak and Strong** interactions. In every day life the effect of two interactions are experienced by us namely gravitational interaction acting between any two particle having mass and the electromagnetic

Table 1.1: Elementary particles as in Standard model

Particle types	particles
Quarks	u_1, u_2, u_3 d_1, d_2, d_3 c_1, c_2, c_3 s_1, s_2, s_3 t_1, t_2, t_3 b_1, b_2, b_3
Leptons	(e, ν_e) (μ, ν_μ) (τ, ν_τ)
Gauge bosons	gluons $(g_1, ..., g_8)$ photon (γ) W^+, W^-, Z Higgs ϕ

interaction acting between two charged particles. The other two interactions which we do not observe in our day to day life are the weak interaction, responsible for radioactive β decay and the strong interaction that binds the quarks inside a neutron or proton. Strong interaction is also responsible for the binding of protons and neutrons inside the nucleus. Apart from the gravitational interaction all other three interactions are well described by the mathematically consistent theory, the 'Standard Model'. This theory has been successful in explaining most of the experimental results involving elementary particles. The elementary particles predicted by standard model are tabulated in the table 1.1 The anti particles of these particles are also considered for the sake of completeness. For example- a quark and an anti quark form a meson and three quarks form a baryon. Standard model predicts both stable and unstable mesons and baryons that are formed from the interaction of quarks and anti quarks. Some unstable mesons and baryons are only observed in the particle accelerators. The particle zoo owing to the

Table 1.2: Types of microscopic particles excluding gauge bosons

Particle family	what does the word means	Particles	What are the particles made of ?
Leptons	Light	Electron, muon and tau lepton, neutrinos	fundamental (till now)
Mesons	Medium	pion, kaon, J/ψ, upsilon, *etc.*	quark + anti quarks
Baryons	Heavy	proton, neutron, sigma, cascade, delta *etc.*	three quarks
Quarks		up, down, top, bottom, charm and strange	fundamental (till now)

elementary particles and their interactions as predicted by standard model is shown in Fig. 1.2. All these particles in the zoo have the intrinsic properties called spin. These particles can be categorized as fermions (half integer spin) and bosons (integer spin) according to their spin. It turns out that **the fermions like leptons and quarks are the fundamental building blocks of matter while the gauge bosons are the force carriers**.

1.2 The theory of strong interaction and quark gluon plasma (QGP)

The strong interaction which is the interaction between color charged particles, quarks and gluons, is described by quantum chromo dynamics (QCD). As a part of the Yang-Mills theory [3] QCD describes the fundamental forces between colored fermions, the quarks mediated by the gauge bosons, the gluons. QCD is very similar to *Quantum*

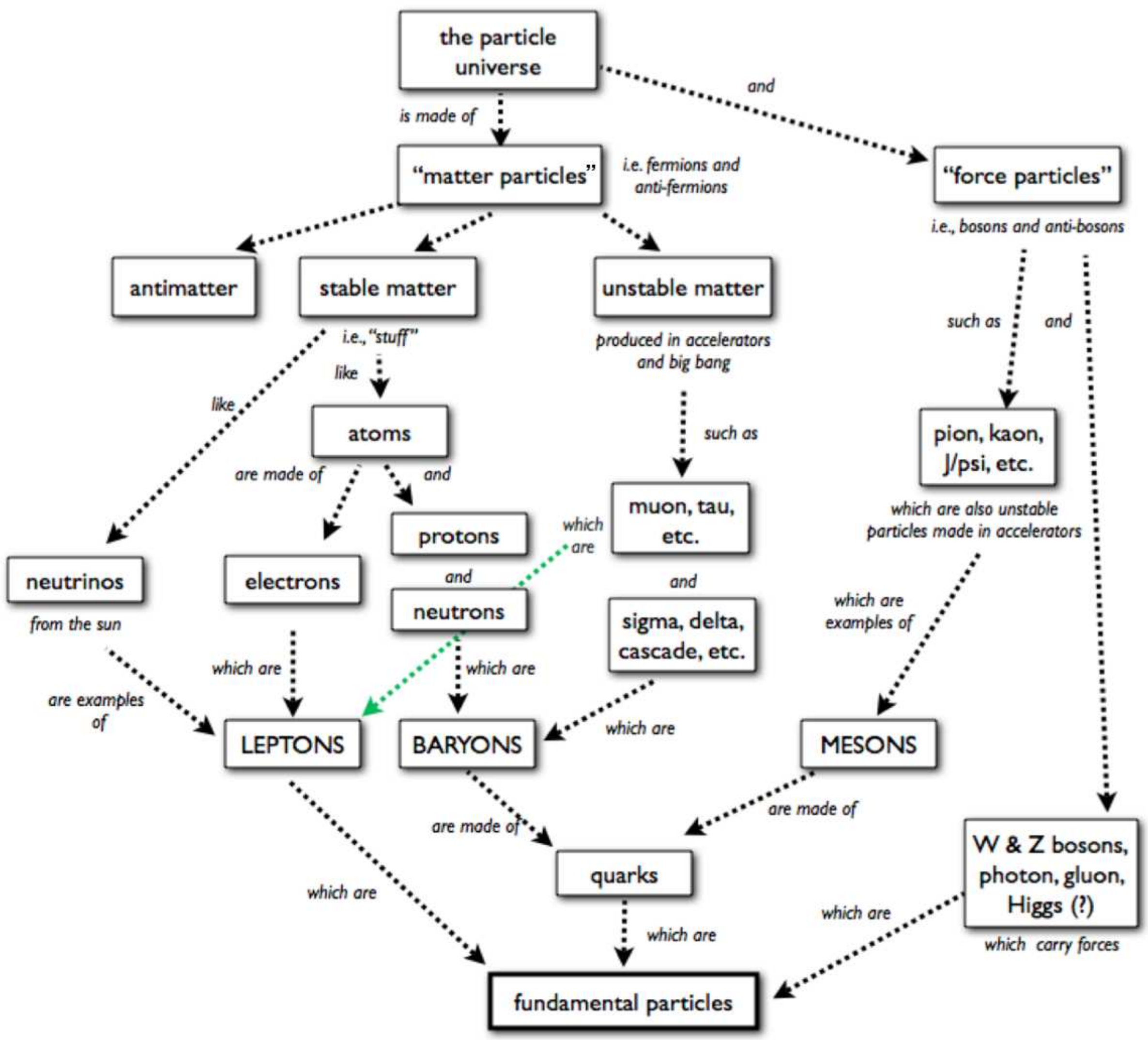

Figure 1.2: Particle Zoo : This called particle zoo as the wide varieties of particles can be understood by what they are made of (e.g., their fundamental constituents) or what they make (e.g., stable matter, unstable matter, or forces). Courtesy: Facilitator's Guide High Resolution Graphics

Electrodynamics (QED), the gauge theory corresponding to commuting symmetry group $U(1)$ with massless photons as gauge bosons. In contrast to QED, it is a non abelian gauge theory of color fields corresponding to non-commuting local symmetry group SU(3). The color charged gluons, unlike the photons (in QED) have self-interactions. This makes QCD non abelian and more complex compared to the abelian QED.

The QCD, Lagrangian density which describes the interactions of quarks and gluons is expressed as follows; [4, 5, 6],

$$\mathcal{L}_{QCD} = \mathcal{L}_{inv} + \mathcal{L}_{gauge} + \mathcal{L}_{ghost} \tag{1.1}$$

$\mathcal{L}_{inv}$ is the classical Lagrangian density, invariant under local SU(N_c) gauge transformation, with $N_c = 3$ for QCD. This can be expressed in the following way [3];

$$\begin{aligned}
\mathcal{L}_{inv} \quad &= \sum_f \bar{\psi}_f (i\not{D} - m_f)\psi_f - \frac{1}{4}F^2 \\
&= \sum_{f=1}^{N_f} \sum_{\alpha,\beta=1}^{4} \sum_{i,j=1}^{N_c} \bar{\psi_{f,\beta,j}} \left[i\gamma^{\mu}_{\beta\alpha} D_{\mu,ji} - m_f \delta_{\beta\alpha}\delta_{ji} \right] \psi_{f.\alpha,i} \\
&-\frac{1}{4} \sum_{\mu,\nu=0}^{3} \sum_{a=1}^{N_c^2-1} F_{\mu\nu,a} F^{\mu\nu}_a
\end{aligned} \tag{1.2}$$

where $\mathcal{L}_{inv}$ is a function of quark and gluon fields, represented by ($\psi_{f,\alpha,i}$) and ($A_{\mu,a}$) respectively with Dirac indices α, β (μ, ν) for quark fields (gluon fields). The color indices for quark (gluon) fields are denoted by $i, j(a)$. m_f, is the mass of quark. There are N_f independent quark fields. $'f'$ stands for quark flavors (See Fig. 1.3 for the properties of different flavors of quarks).

$D_{\mu,ij}$ - is the co-variant derivative in N_c-dimensional representation of $SU(N_c)$, which

Quarks	Charge	Mass	Baryon Number	Isospin
u up	+ 2/3	~ 4 MeV	1/3	+1/2
d down	-1/3	~ 7 MeV	1/3	-1/2
c charm	+2/3	~ 1.5 GeV	1/3	0
s strange	-1/3	~ 135 MeV	1/3	0
t top	+2/3	~ 175 GeV	1/3	0
b bottom	-1/3	~ 5 GeV	1/3	0

Figure 1.3: Properties of six flavors of quark according to the Standard Model [7].

acts on the spinor quark field in Eq. 1.1, with color indices i=1, ..., N_c. The covariant derivative $D_{\mu,ij}$ and the non-abelian field tensor $F_{\mu\nu,a}$ are defined as,

$$D_{\mu,ij} = \partial_\mu \delta_{ij} + igA_{\mu a}(T_a^{(F)})_{ij}. \tag{1.3}$$

$$F_{\mu\nu,a} = \partial_\mu A_{\nu,a} - \partial_\nu A_{\mu,a} - gC_{abc}A_{\mu b}A_{\nu c} \tag{1.4}$$

. $F_{\mu\nu,a}$ is defined in terms of the gluon vector field A_a^μ, with $N_c^2 - 1$ group components a; N_c being the "number of color". "g" is the QCD ("strong") coupling and C_{abc} is known as the structure constants of $SU(N_c)$, a,b,c=1,...,$N_c^2 - 1$ are real numbers, defining its Lie Algebra. The Lie Algebra is defined by commutator relation of the $N_c^2 - 1$; $N_c \times N_c$ matrices $(T_a^{(F)})_{ij}$ that appear in the definition of $D_{\mu,ij}$ (E. (1.3)),

$$\left[T_a^{(F)}, T_b^{(F)}\right] = iC_{abc}T_c^{(F)} \tag{1.5}$$

These commutation relations define the algebra. Here $T_a^{(F)}$ are known as the Gell-Mann matrices.

Under local gauge transformation, quark fields transform as;

$$\psi'_{f,\alpha,j}(x) = U_{ij}(x)\psi_{f,\alpha,i}(x) \tag{1.6}$$

where

$$U_{ij}(x) = \left[\exp \left\{ i \sum_{a=1}^{N_c^2-1} \beta_a(x) T_a^{(F)} \right\} \right]_{ij} \tag{1.7}$$

with $\beta_a(x)$ real. $U_{ij}(x)$ for each x is an element of the group SU(N_c), which acts on the local invariance that has been built into the theory. The gluon field can be expressed in terms of an $N_c \times N_c$ matrix, $A_\mu(x)$

$$[A_\mu(x)]_{ij} = \sum_{a=1}^{N_c^2-1} A_{\mu a}(x)(T_a^{(F)})_{ij}, \tag{1.8}$$

The gluonic field transforms as,

$$A'_\mu(x) = U(x)A_\mu(x)U^{-1}(x) + \frac{i}{g}[\partial_\mu U(x)]U^{-1}(x) \tag{1.9}$$

The $\mathcal{L}_{inv}$, following the above transformation rules, remain invariant under local gauge transformation. But the gauge invariance of $\mathcal{L}_{inv}$ actually makes it difficult to quantize. This problem is solved by adding to $\mathcal{L}_{inv}$ a gauge fixing ($\mathcal{L}_{gauge}$) term and ghost densities ($\mathcal{L}_{ghost}$).

$$\mathcal{L}_{gauge} = \begin{cases} -\frac{\lambda}{2}\sum_{a=1}^{N_c^2-1}\left(\partial_\mu A_a^\mu\right)^2 \, , \; ; \quad 1 < \lambda < \infty \\ \\ -\frac{\lambda}{2}\sum_{a=1}^{N_c^2-1}\left(n.A_a\right)^2 , \; \lambda \rightarrow \infty \end{cases} \tag{1.10}$$

where n^μ is a fixed vector. The first defines the set of "covariant" gauges, the most familiar having $\lambda = 1$, the *Feynman gauge*. The second defines the "axial" or "physical" gauge, since taking λ to infinity eliminates the need for ghost field. Here, picking n^μ to be light-like, $n^2 = 0$, defines the *light-cone gauge*. For $\lambda \rightarrow \infty$, a non zero value of $n.A$ leads to infinite action and for this reason the physical gauges are often called "$n.A = 0$" gauges. Finally, in covariant gauges we must add a ghost Lagrangian [8, 9],

$$\mathcal{L}_{ghost} = (\partial_\mu \bar{c_a})(\partial^\mu \delta_{ab} - gC_{abd}A_b^\mu)c_d, \tag{1.11}$$

where $c_a(x)$ and $\bar{c_a}(x)$ are scalar ghost and antighost fields respectively. In the quantization procedure, ghost fields anti-commute, despite the fact that they are scalars. In SU(N_c) theory, the ghost field ensures that the gauge fixing does not spoil the unitarity of "physical" S matrix that governs the scattering of quarks and gluons in perturbation theory.

Feynman rules for QCD

While calculating the scattering cross section in perturbation theory, the interaction between particles (which is stated by their interacting Lagrangian) can be described by starting from free fields which describe the incoming and outgoing particles. The amplitude for scattering is the sum of each possible interaction history over all possible intermediate particle states. Feynman gave a prescription for calculating the amplitude for any given diagram from a field theory Lagrangian, known as Feynman rules. Here we summarize the Feynman rules for calculating different interactions following QCD in Fig 1.4.

1.2.1 Properties of QCD

Quantum Chromo Dynamics shows the properties of 'Confinement' and 'Asymptotic Freedom'. When two quarks are separated then the force between them does not decrease rather increases and an infinite amount of energy is required to separate them.

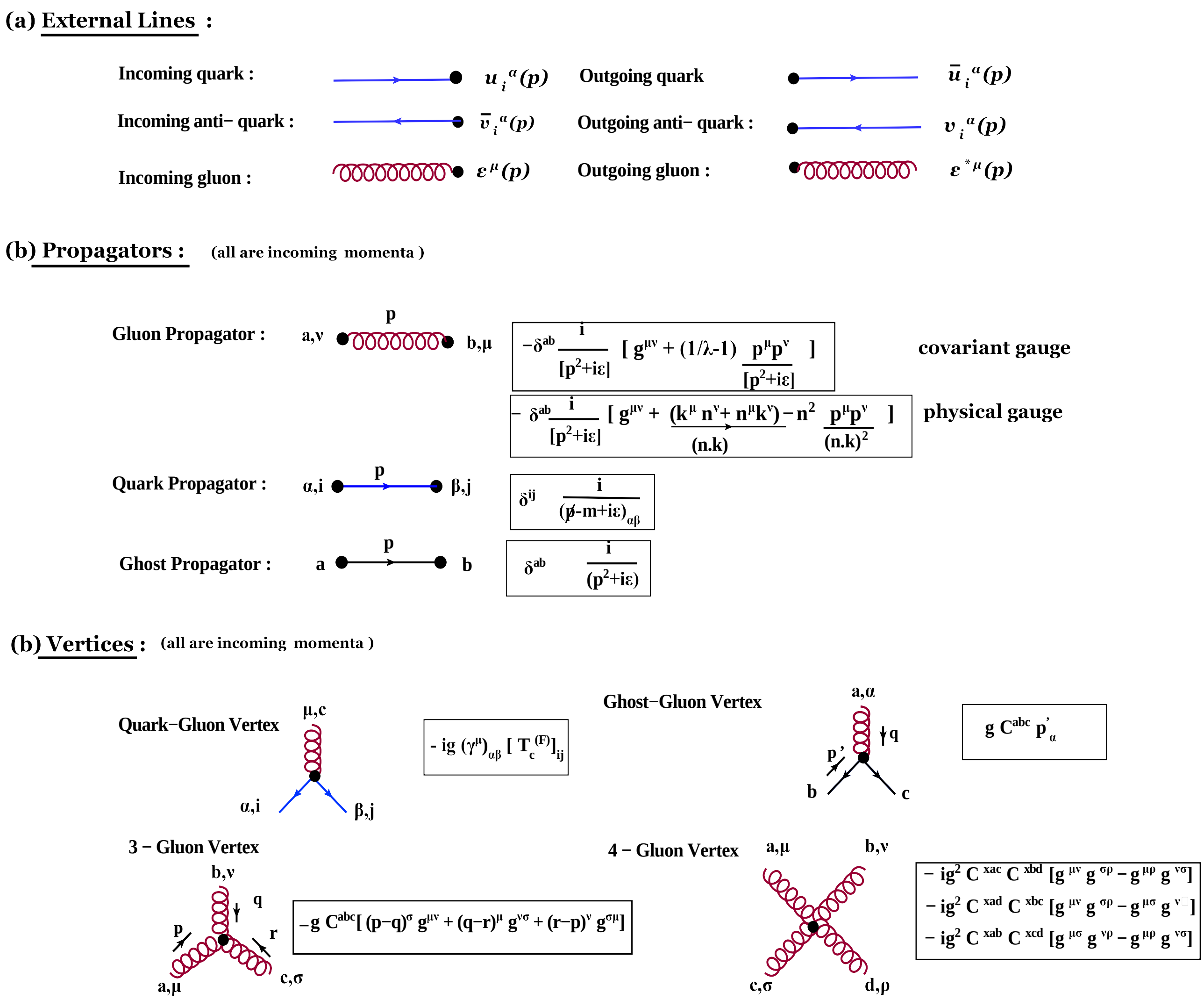

Figure 1.4: Feynman Rules for QCD in covariant gauge for gluons (red curly line), quarks (blue line) and ghost field (black line).

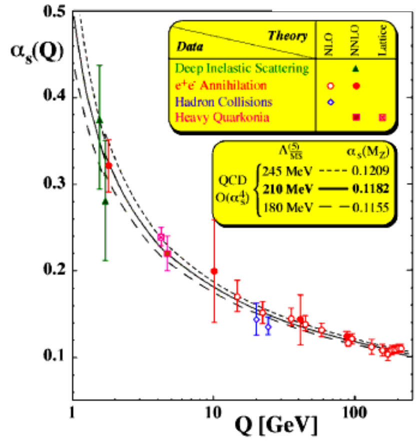

FIG. 1: QCD running coupling constant

Figure 1.5: Running coupling constant α_s established by various types of measurements at different scales, compared to the QCD prediction for $\alpha_s(M_z)$=0.118 $\pm$ 0.003. The open circles are results based on global event shape variables [10]. Q is the momentum transfer

.

That's why they are permanently bound to hadrons like baryons and mesons. This is the 'Confinement' property of QCD. On the other hand, at very high energy reactions when two quarks are close to each other, then they interact very weakly as if they are free. This is called 'Asymptotic Freedom' , first discovered by David Politzer, Frank Wilzek and David Gross [8, 11]. At low energy there is confinement [12] in QCD and at high energy there is asymptotic freedom. These two remarkable features of QCD can be explained from the coupling parameter α_s.

The effective strong coupling constant α_s depends on momentum transfer between the interacting hadrons. The QCD running coupling constant, α_s $(= g^2/4\pi)$ can be written in perturbative QCD (pQCD) as [5]:

$$\alpha_s(Q^2) = \frac{12\pi}{(33 - 2n_f)\ln(Q^2/\Lambda^2)} \tag{1.12}$$

The number of participating quark flavor(n_f) is determined by the available energy characterized by Q^2. The parameter Λ has to be determined by comparing QCD predictions to experimental results and is commonly given as $\Lambda \sim 250$ MeV. The Q dependence of $\alpha_s(Q^2)$ (shown in Fig 1.5) reproduces the phenomenologically determined behavior of quarks:

- For small values of Q, the interaction strength between quarks is strong (as the α_s is large) and hence they remain confined within the hadrons and not seen isolated in nature. This is known as **confinement**.
- On the other hand, for large Q which corresponds to small distance, the α_s vanishes asymptotically. Due to the weak coupling the quarks behave like free particles. This feature is known as **asymptotic freedom**.

1.2.2 Deconfinement: QCD at extreme temperature and/or density

Collins and Perry [13] showed that at extreme conditions of density, hadronic matter goes to a deconfined phase where it exhibits asymptotic freedom. In low coupling regime, the asymptotically vanishing nature of α_s does not allow the quarks to remain intact inside the hadronic matter; rather they move freely due to anti-screening of color charges forming a new deconfined state of quarks and gluons. The deconfined phase of QCD where the bulk properties of matter are governed by fundamental degrees of freedom -quarks and gluons, in a finite volume is known as quark gluon plasma (QGP). Quantum Chromo Dynamics, the theory of strong interactions predicts the formation of QGP phase at a temperature 170 MeV [14] (170×10^{10} oK) for zero baryonic chemical potential based on the lattice gauge theory calculations. Heavy ion collisions at

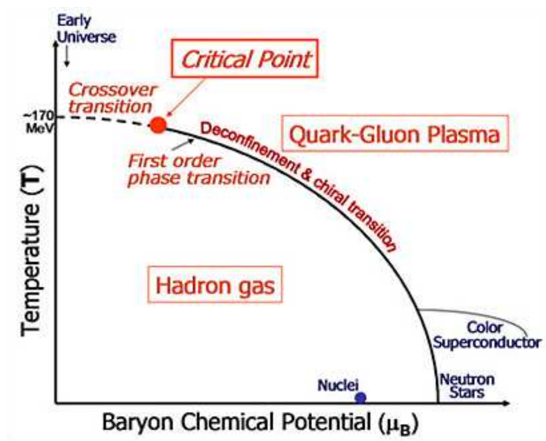

Figure 1.6: Phase diagram of Temperature (T) vs baryonic chemical potential (μ_B) showing the transition from hadronic phase to a deconfined QGP phase.

ultra-relativistic energies have been targeted to create a hot and dense thermally equilibrated system of partons or quarks & gluons, called Quark Gluon Plasma (QGP) in the laboratory and to observe the properties of this system under extreme conditions of temperature and/or pressure. Efforts have been made experimentally to produce such a state of matter at extreme temperature at the above mentioned facilities. Careful theoretical investigations have also been carried out to explain the experimental observables and to understand the properties of matter formed in these heavy ion collisions. Before going to quark gluon plasma, let's discuss the history of the term 'plasma', as a special form of matter and its relevance to the quark gluon plasma.

1.3 Cell Plasma, electromagnetic plasma and quark gluon plasma

When various corpuscles are removed from blood, there remains a transparent fluid, which the Czech medical scientist Johannes Purkinje (1787-1869) called as "plasma". This is termed after the Greek word "$\pi\lambda\alpha\sigma\mu\alpha$" which means moldable substance or jelly [15]. In 1927, American Chemist Irving Langmuir was reminded of the blood plasma which carries white and red corpuscles and resembles the ionized gas as electrical fluid which carries electrons and ions and used this term to describe ionized gas. This is the electromagnetic plasma discovered by Langmuir. Similarly the term quark gluon plasma is coined by Russian-American physicist E. V. Shuryak for the assemblage of quarks and gluons in 1980 [16]. But its physics was already discussed much before in 1975 by Collins and Perry [13]. They predicted that at extreme conditions of temperature and pressure the hadrons lead to a de-confined state of color charged particles (quarks and gluons). This is nothing but quark gluon plasma. This phenomenon is explained by the property of gauge theory called Asymptotic Freedom [11]. Big Bang theory suggests the existence of such a state of thermalised partons, Quark Gluon Plasma at the very early time, after few microseconds of the creation of the Universe. Also the core of the neutron star is expected to be in quark gluon plasma phase.

When a structured system is formed then its binding energy is larger than the ambient thermal energy. If the ambient thermal energy is more then the system will be unbound and decompose to its constituent particles. Hence, at extreme conditions of temperature and pressure, the structured system decomposes e.g., the crystal melts, molecule dissociates into atoms, atom ionizes to electrons and nuclei, nucleus breaks giving nucleons, nucleon produces quarks.

If we consider a system which contains a particular type of atoms and is placed in an extreme conditions of temperature such that the ambient thermal energy is near or exceeding the atomic ionization energies. The atoms decompose into negatively charged electrons and positively charged ions. The charged particles are by no means free rather they are strongly affected by each other's electromagnetic fields. Again the charges are no longer bound; their assemblage becomes capable of exhibiting collective motions. Such an assembly is basically the electromagnetic plasma. Multiple collisions inside the system lead towards an equilibrium state. This assembly does not exclude some fraction of neutral atoms since all atoms may not be ionized in a particular time scale. Hence one can say it is a collection of charged and neutral particles showing the property of collective behavior and quasi-neutrality. The quasi-neutrality refers to an approximately equal value of number density of both positive and negative charged particles on a macroscopic length scale (i.e. $n_+ = n_-$). Quasi-neutrality is not the necessary criteria for a system to be called as plasma. There are non-neutral plasmas containing one type of charged particles which are created in the laboratory. More specifically an ionized gas can be called as plasma if it satisfies the following criteria [17, 18];

(i) $\lambda_D << L$

(ii) $\omega_p \tau_c \sim 1$

(iii) $N_D >> 1$

where λ_D, ω_p, τ_c are respectively the Debye screening length, plasma frequency and mean collision time. Debye screening length is the length scale within which the potential of a test particle put inside the plasma is screened to 1/e of its value. L is the dimension of plasma. N_D is the number of the particles within the Debye sphere. N_D is defined for each type of particle separately. The plasma is predominantly characterized by the excitation of various collective dynamic modes. Few examples of such electromagnetic plasma are; plasma inside the core of the sun, flame of a gas stove, tube light, ionosphere of earth etc. These above plasmas are basically weakly coupled plasma (gas like behavior). There are also examples of strongly coupled electromagnetic plasma such as dusty plasma.

Now let's come to a hadronic (particularly nucleonic) system where the constituent particles are hadrons. We know that quarks, anti-quarks and gluons are confined or bound within the hadrons due to strong interactions. Now if this system is subjected to an extreme conditions of temperature and pressure such that ambient thermal energy is near exceeding than their binding energies then the nucleonic system or hadronic system deconfines to its constituent color charged particles-quarks and gluons. The system is fully color neutral. Here the colored particles are affected by short range strong interactions unlike the long range coulomb interactions in case of electromagnetic plasma. This collection of color charged particles (quarks, anti-quarks and gluons) where the system properties are manifested by color degrees of freedom, is called as quark gluon plasma. As discussed already such a situation is created by colliding heavy nuclei at relativistic energy using accelerator facility. Several experimental facilities have been developed to collide heavy ion like Au+Au, Pb+Pb and to create QGP in the laboratory. Different experiments are carried out by different large collaborations under the relativistic heavy ion collision program. A history of the QGP search has been summarized in the next section.

1.4 History of the search for the QGP

The advent of the QCD and its application to the thermodynamics of strong interactions urged us to create hot and dense nuclear matter in the laboratory. As the ideas about the QGP formation in relativistic nuclear collisions matured [19] around eighties, challenges were how to create the QGP and to distinguish it from the gas of hadrons. Heavy ion collisions at ultra relativistic energies were first studied at Bevelac ($E_{lab} \sim 1$ GeV) at Lawrence Berkeley Laboratory, USA and at JINR (Joint Institute for Nuclear research, Dubna) Russia. Next level of experiments were done at the Alternating Gradient Synchrotron (Brook Haven National Laboratory, USA) during nineteen-eighties. The first round of experiments were done with Silicon(Si) beam (with Au, Cu and Al) at beam energy 14.6 A.GeV. With further developed technologies, the experiments were carried out at Super Proton Synchrotron, CERN, Geneva with oxygen(O) and sulphur (S) beam with energies 60-200 AGeV during 1986-1990 [20]. In the period 1990-1993 experiments were done with 14.6 A.GeV Gold (Au) beams at AGS and 200 A.GeV sulphur beams at the SPS. Also asymmetric collision between S+Au at 200 A.GeV were performed at SPS followed by lead+lead (Pb+Pb) collisions at 158 A.GeV. Then the Relativistic Heavy Ion Collider (RHIC, BNL) came up around 2000. Here also several heavy ion collision experiments were done for different centre of mass energies. The experimental data were taken by PHENIX, STAR, BRAHMS and PHOBOS collaborations. In the mean time collaborations like NA49 used the SPS facility to collide Pb+Pb (E_{lab}=40, 80 and 158 A GeV) and NA60 to collide In+In (E_{lab}=158 A GeV or centre of mass energy, $\sqrt{s_{NN}}$= 17.3 GeV). Presently at 2012, the Large Hadron Collider(LHC) at CERN and the upcoming Facility for Anti-Proton and Ion Research (FAIR, GSI, Germany) are the major focii to create and study the hot dense matter. Different collaborations like ALICE, ATLAS and CMS are involved in the measurement of experimental data. At LHC, we reached up to the $\sqrt{s_{NN}} \sim 2.76$ TeV. Simultaneously the low energy RHIC scan program is complementing the observations for the search of QGP. It is very important to know whether the matter which is produced in the collisions is QGP or not. The theoretical efforts are simultaneously complementing the experimental data to infer about the production of QGP in these collisions. Several signals have been proposed to detect the QGP. The observations at higher SPS energy and RHIC indicates the formation of a state of dense matter with observed collective partonic properties [21, 22]. This might be the QGP.

1.5 Ultra-relativistic heavy-ion collisions and QGP

Heavy Ions like Oxygen (O), Sulphur (S), Silicon (Si), Gold (Au), lead (Pb) were accelerated up to relativistic energies and collided at different facilities like AGS (BNL), SPS(CERN), RHIC (BNL) and LHC (CERN) with an energy range from 2 A.GeV to few TeV per nucleon. The matter density produced there is few times the normal

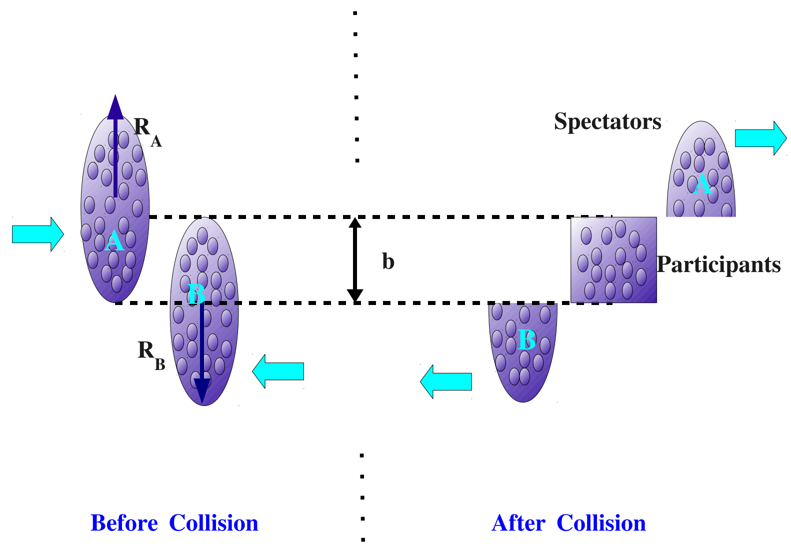

Figure 1.7: Rapidity distribution of heavy ion collision in different scenarios

nuclear matter density. In the fixed target experiment a heavy ion or nucleus collides with the other nucleus within a thin layer, (for example, 0.1 mm Au (projectile) on 1 mm of S (target) material [20]) unlike the collider experiments where both (target and projectile) nuclei are accelerated to collide. The amount of energy density created at the point of collision depends on the amount of nuclear stopping. The amount of nuclear stopping is defined as the percentage of kinetic energy loss of the projectile nucleons in the nucleus-nucleus collisions. The schematic diagram of the heavy ion collision is in figure 1.7.

Those nucleons from both the target and projectile nuclei which take part in primary collisions are called 'participants' and the non-interacting nucleons are called 'spectators'. Since the nuclei move with relativistic energies they are represented with Lorentz

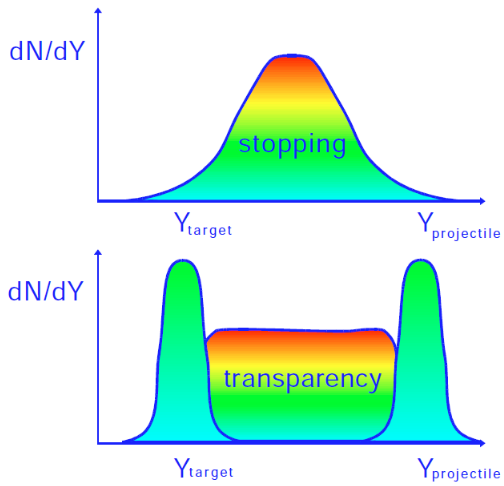

Figure 1.8: A schematic diagram of heavy ion collision

contracted shapes along the direction of motion.

The stopping of the participant nucleons during the collision is generally explained in two different models *i.e.,* Fermi-Landau Model and Bjorken- Mclerran model. New particles are produced because of the energy deposited at the point of collision, thus, it leads to the formation of a hot-dense matter which expands dynamically and cools gradually. The view of stopping are expressed in relativistic hydro dynamical model where energy, momentum, entropy, and baryon numbers are conserved. The interacting nucleons are treated as fluid of nuclear matter which are extremely compressed via propagation of shock waves.

The particles, produced at the collision zone might be quarks(anti-quarks), gluons or hadrons. The particles re-scatter among themselves and leads towards a equilibrium. Then the equilibrated system which is at very high temperature, let's say, at T_i, expands with time and cools subsequently. The expansion can be simulated by a relativistic hy-

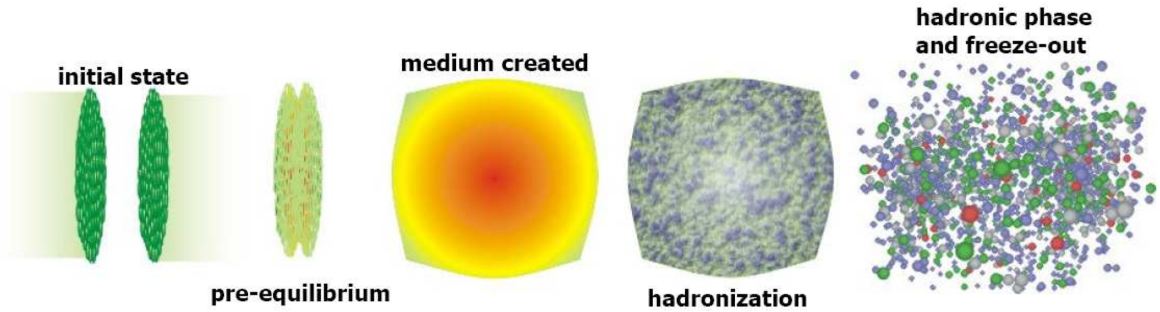

Figure 1.9: Schematic representation of the evolution of the matter produced in relativistic nuclear collisions. Picture:Courtesy to prof. Steffan Bass

drodynamic model (if mean free path is less than the system dimension). The expansion is likely to be adiabatic , which means no dissipation will occur during the expansion. Therefore is-entropic expansion is presumed. This is explained using relativistic hydrodynamics in the later chapter. Before applying hydrodynamics to heavy ion collision one has to be cautious about the thermal equilibrium of the produced system since the transverse momentum distributions of the particles produced in p+p collision show the Boltzman like behavior($e^{-\frac{m_T}{T}}$) where $m_T = \sqrt{p_T^2 + m^2}$. This observations restrict the straight forward interpretation of an exponential transverse momentum spectrum in heavy ion collisions as the evidence of thermalization [23].

1.6 Formation and evolution of QGP in relativistic nuclear collisions

Depending upon the energy density created due to the deposition of energy by the colliding nuclei into the collision zone, the initial state of the heavy ion collision after undergoing sufficient re-scatterings may go to a QGP phase or a hadronic phase. The re-scatterings among the initial hadrons or partons owing to the initial energy density leads towards a local thermal equilibrium state. The equilibrium is achieved shortly. Now this is like an hot-fire ball system with large pressure which expands dynamically. Because of the expansion, the system cools down gradually. The evolution of the equilibrated hot-fire ball may follow the following scenarios;

1. (a) QGP $\rightarrow$ Mixed Phase $\rightarrow$ Hadron Phase $\rightarrow$ Freeze out (1st order transition)

   (b) QGP $\rightarrow$ Hadron Phase $\rightarrow$ Freeze out (Continuous or cross over transition)

2. Hadron Phase $\rightarrow$ Freeze out

The scenario 1 describes the formation of a QGP with high energy density (ϵ_i) and pressure. If it is a weakly coupled QGP that is the interactions among the quarks and gluons are small then the energy density and pressure can be calculated using thermal perturbation theory. But if a strongly coupled QGP is formed then the calculation of energy density and pressure is very difficult. And mostly in the recent experiments there are evidences of the formation of strongly coupled QGP. The QGP expands and the energy density or temperature decreases due to the expansion. The temperature falls gradually and when it reaches to a certain value, T_c such that the quarks and gluons no more become free, then the quarks combine to form hadrons; and the QGP phase goes to a hadronic phase. This phase transition may be a 1st order transition with an intermediate mixed phase where the latent heat liberated because of the hadronisation keeps the temperature of the system constant for certain time till all the quarks get hadronised to hadrons. In case of the 1st order QGP-hadron phase transition there is a jump or discontinuity in the entropy density like other 1st order transition(e.g., liquid-gas). It may also happen that the QGP phase can directly go to the hadronic phase continuously without any abrupt change in entropy density. This is 2nd order or continuous phase transition. The other possibility that the QGP system may encounter a crossover without any discontinuity at all, which the quantum chromo dynamics based on lattice calculation predicts at zero baryon chemical potential [14]. Actually, by definition, the crossover can't distinguish two phases. In a naive sense, in case of crossover one phase is above and the other phase is below the pseudo-transition temperature. When an ionised (electrically charged ions) gas converts to plasma such type of crossover scenario is also observed.

The temperature, due to continuous expansion, again decreases to a value T_{ch} leading to chemical freeze-out, where the ratios of the particle (hadron) numbers get fixed. On further decrease to a temperature T_f, the system leads to kinetic freeze-out following the free-stream of the particles towards the detector. The scenario (2) explains the formation of initial hadronic mater which expands and cools from T_i to T_f following the freeze out scenarios as described above.

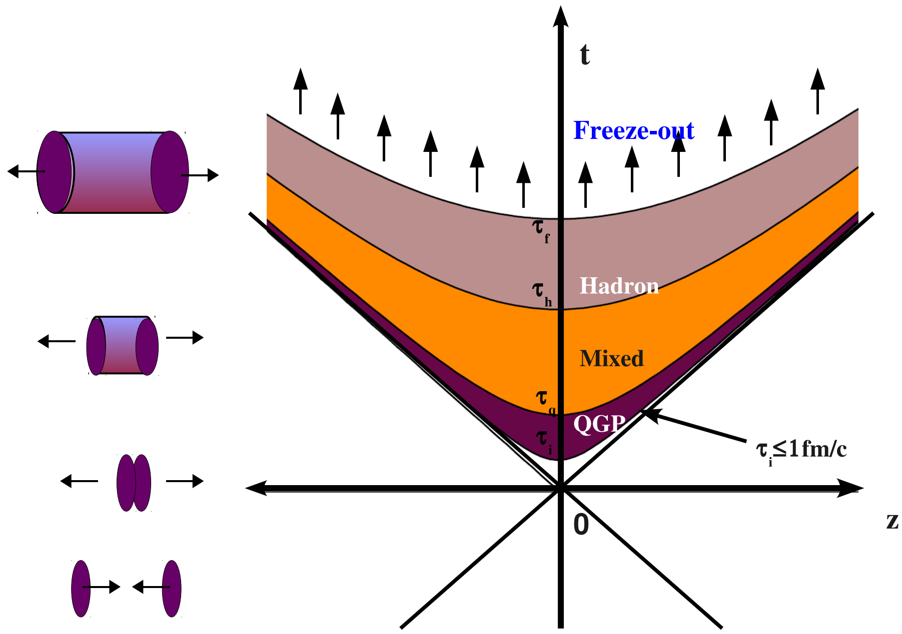

Figure 1.10: Space time evolution for a first order phase transition in the light cone picture. If there is a crossover or 2nd order phase transition then there would be no mixed phase in the light cone diagram.

1.7 Signals of QGP

Several signals have been proposed to detect the hot and dense matter produced in the heavy ion collisions. The life span and size of the formed system is very small. Hence to get the information of the system by inserting a direct probe into it looks impossible with the present day technology. Hence the radiations emanated from the system during its evolution are considered as efficient signals. Some of the important signals are (i) electromagnetic radiations-spectra of photons and lepton pairs, (ii) strange hadrons-strangeness enhancement, (iii) Charmonium or quarkonium productions- J/ψ, Υ (Upsilon) production and suppression, (iv) Jet quenching *etc.*.

1.7.1 Electromagnetic radiations: Photons and dileptons

Probing the QGP formation in the relativistic heavy ion collision experiments using the electromagnetic radiations such as photons and lepton pairs ($e^+e^-, \mu^+\mu^- \& \tau^+\tau^-$) has a special importance because of their nature of interactions with the medium in which they are produced. The leptons respond to either weak or electromagnetic interactions. Photons respond to electromagnetic interactions. When two heavy nuclei are collided with relativistic energies then it is expected that either an initial quark-gluon matter or a hadronic matter is formed depending upon the energy density created at the point of collision. Whatever may be the produced initial system(quark-gluon matter or hadronic matter), the properties of the state are governed by strong interactions although there may be electromagnetic interactions. The produced system evolves in space & time and eventually the particles decouple from each other and get detected in the detector. During this whole evolution process, the entire system remains dominated by the strong interactions (here coupling is stronger compared to electromagnetic interactions). The photons and lepton pairs are emanated from each stages of the evolution. Since these particles interact via electromagnetic interactions, their cross-section in such medium is less or in other words the mean free path is more. That is why they come out of the system after their productions without interacting with other particles of the system and keeps the information of the system as such. A simple estimation says that the mean free path ($\lambda \equiv c\tau_{relax}$) of photons in QGP with energies 0.5, 1, 2 and 3 GeV at 200 MeV are 270, 356, 505 and 639 fm respectively [24]. The mean free path in hadronic gas is of the same order. Since the production of these particles depend on the intensive thermodynamic parameters like temperature, the study of their spectra has been proposed to be a promising probe for the extraction of the information of temperature of the system. The initial temperature of the system extracted from the spectra of electromagnetic particles gives an indirect signal for the QGP formation. Like photons the study of the lepton pairs is equally important with similar reasons and also sometimes more advantageous because of the extra kinetic variable (invariant mass) involved in the calculation. The importance of the electromagnetic probes was first proposed by Feinberg in 1976 [25]. The details of this signal have been discussed in the later chapters 2 and 4.

1.7.2 Strangeness enhancement

The abundance of strange flavored hadrons *i.e.,* strange mesons and baryons in the relativistic nuclear collisions provide an opportunity to detect the quark gluon plasma and study its properties. This has been proposed as a signal [26] in the following way in 1980 [27]. Assuming equilibrium in the quark gluon matter, the density of strange quarks (two spins and three colors) at any temperature T is given by,

$$\frac{N_s}{V} = \frac{\bar{N}_s}{V} = 6\int \frac{d^3p}{(2\pi)^3} e^{-\sqrt{p^2+m_s^2}/T} = 3\frac{Tm_s^2}{\pi^2} K_2(m_s/T) \tag{1.13}$$

(Neglecting the perturbative corrections and weak decays). Here $N_s(\bar{N}_s)$, V are the number of strange quarks (anti quarks) and volume of the produced system respectively. m_s is the mass of the s-quark in the perturbative vacuum. Boltzmann distribution is used as density of strangeness is relatively low. The light flavor quarks or anti quarks (u and d) density is given as;

$$\frac{N_q}{V} = \frac{\bar{N}_q}{V} = 6\int \frac{d^3p}{(2\pi)^3} e^{-|p|/T-\mu_q/T} = e^{-\mu_q/T} T^3 \frac{6}{\pi^2}, \tag{1.14}$$

Table 1.3: Different experimental collaborations taken data for strangeness studies

Experiments	Collaborations	Colliding Nuclei	Colliding Energy
AGS	E802	Si+Au, Si+Cu, Si+Al	E_{lab}=14.6 A GeV
AGS	E866/E917	Au+Au	E_{lab}=11.6 A GeV
SPS	NA44	Pb+Pb	E_{lab}=158 A GeV (E_{cm}=17.3 GeV)
SPS	NA49	Pb+Pb	E_{lab}=40, 80 and 158 A GeV (E_{cm}=9, 12 and 17.3 GeV)
RHIC	BRAHMS	Au+Au	E_{cm}=200 and 130 GeV
RHIC	STAR	Au+Au	E_{cm}=9.2 GeV

where the quark chemical potential μ_q=$\mu_B/3$, μ_B being baryonic chemical potential. From both the equations it is clear that there are more $\bar{s}$ quarks compared to $\bar{u}$ and $\bar{d}$ in the high energy nuclear collisions at finite μ_B. The ratio of $\bar{s}$ to $\bar{q}$ (q is the light flavor) is

$$\frac{N_{\bar{s}}}{N_{\bar{q}}} = \frac{1}{2}\frac{m_s}{T}^2 K_2(m_s/T)e^{\mu_B/(3T)} = \frac{T}{2}x^2 K_2(x)e^{\mu_B/(3T)} \tag{1.15}$$

The function $x^2K_2(x)$ varies between 1.3 to 1.0 for x lying between 1.5 to 2.0. We therefore always have more $\bar{s}$ quarks compared to $\bar{q}$. At $\mu_B \rightarrow 0$ we have almost same number of $\bar{s}$, $\bar{u}$ and $\bar{d}$ quarks. When hadronisation occurs, the quarks form mesons and baryons. The $s, \bar{s}$ forms strange mesons and baryons like K mesons ($K^+= u\bar{s}$, $K^- = \bar{u}s$, $K^0 = d\bar{s}$, $\bar{K^0} = \bar{d}s$), $\phi = s\bar{s}$, baryons (Λ=uds), $\bar{\Lambda}$, Σ; $\Sigma^+ = uus$, $\Sigma^0 = uds$, $\Sigma^- = dds$, $\Omega(sss)$ *etc.*). The light flavors q and $\bar{q}$ dominantly produce pions along with other mesons and baryons.

Strange quarks s and $\bar{s}$ are produced in equal abundance. Due to the initial conditions in the heavy ion collisions, non strange quarks (light flavors u, d) will be more abundantly available than non-strange anti quarks ($\bar{u}, \bar{d}$) since colliding nuclei carry finite μ_B or μ_q. For $\bar{s}$ quarks this opens the possibility to form mesons K^+, K^0, ϕ while for s quarks it is easy to form Λ (uds) compared to $K^-, \bar{K^0}$ as availability of $\bar{u}$ and $\bar{d}$ is less (μ_B=450 MeV in case of normal nuclear matter). The available phase space for Λ production is less compared to $K^-, \bar{K^0}$, K^+ and K^0. Because of the phase space the total Λ production is also less compared to K^+, K^0. But the production is more compared to $K^-, \bar{K^0}$ as there is a probability of absorption of $K^-, \bar{K^0}$ in a nucleonic medium. Thus an enhancement of K^+, K^0 and Λ is expected compare to $K^-, \bar{K^0}$ and $\bar{\Lambda}$. The ratio of K^+/K^- yield should be larger than 1. This was observed in several experiments [28, 29, 30]. But the things are not that straight forward as the K^+ may also come from associated production channels which are absent in K^-. Hence a detail microscopic calculation is required where the production mechanisms are taken into account. In the chapter 8 of this thesis we discuss the production rates of strange quarks(hadrons) in detail.

The strangeness production will be more if a QGP phase is produced at heavy ion collision since the strange degrees of freedom in QGP is more compared to hadronic medium. It is also expected that the $p+p$ collision, where the probability of formation of a medium is less compared to heavy ion collision, will have less strange particles produced. Several theoretical arguments have been proposed for the strangeness enhancement in the heavy ion collisions. Statistical model with canonical phase space suppression is one of them. This tells about the canonical suppression of strangeness in small systems as a source of strangeness enhancement in high energy heavy ion collisions. The strangeness conservation laws require the production of an $\bar{s}$ quark for each s quark in the strong interaction. The main argument in such model is that the energy and space-time extensions in smaller systems may not be sufficiently large. This leads to the suppression of strange hadron production in small collision system [31, 32, 33]. But the enhancement for the strange meson ϕ lies between strange hadrons having net strangeness=1 ($K^-$and$\bar{\Lambda}$) and net strangeness=2 (cascade hyperon). The enhancement for ϕ mesons is to be higher at $\sqrt{s_{NN}}$=200 GeV compared to 62.4 GeV. These observations for the produced $\phi(s\bar{s})$mesons clearly suggest that, at these collision energies, the source of enhancement of strange hadrons is related to the formation of a dense partonic medium in high energy nucleus-nucleus collisions and can not be alone due to the canonical suppression of their production in smaller system [34]. Then Gadzicki proposed the ratio of K^+ to π^+ as a signature of quark gluon plasma [35]. When the ratio of the measured multiplicities of K^+ to π^+ is plotted with centre of mass energies of the colliding nuclei a 'horn' like structure appears. There are different models to explain the horn structure which tells the formation of QGP beyond the threshold in energy (at which the horn appears) [35, 36, 37, 38]. Also some other hadronic models (without assuming QGP) also tried to explain the horn [32, 39, 40, 41] but these models do not talk about the dynamics of the productions. We evaluate microscopically the kaon and lambda productions in heavy ion collision using transport equations and compared with the experimental data with different initial conditions which is described in chapter 8. A strong rapidity dependence (as the energy density is maximum at mid rapidity) of the ratio K^+/π^+, K^+/K^- and K^+/K^- reveals the thermal origin of strange quarks. The strangeness production in detail will be presented in Chapter 8.

1.7.3 Quarkonia productions & suppression

Quarkonia ($Q\bar{Q}$) are the bound states of a heavy quark and anti-quark pair, and those are stable under the strong decay. The concept of quarkonium suppression as a 'smoking gun' was first put forward by Matsui and Satz [42] and considered as a good probe for the thermal properties of hot and dense matter created in heavy ion collision. Being highly massive, $Q\bar{Q}$ pairs are formed at very early stages of the collisions and their properties can be studied using non-relativistic (potential theory) quantum mechanics. Hence, the quarkonium spectrum can be calculated using Schroedinger equation.

$$\left\{2m_Q + \frac{1}{m_Q}\nabla^2 + V(r)\right\}\psi_{n,l} = M_{n,l}\psi_{n,l} \tag{1.16}$$

where the Cornell potential $V(r) = \sigma.r - \frac{\alpha_s}{r}$, contains the confining long-distance part $\sigma.r$ and a Coulomb like short distance part $\frac{\alpha_s}{r}$. Here σ and r are the string tension and the distance of separation between static quark and anti-quark. α_s is the coupling constant. For different values of principal (n) and orbital (l) quantum number, the masses $M_{n,l}$ and the wave functions $\psi_{n,l}(r)$ of different quarkonium states J/ψ, χ, ψ', Υ *etc.* in vacuum are obtained in terms of the constants m_Q, σ and α_s. Inside medium the potential gets screened as follows;

$$V(r, r_D) = \sigma.r(\frac{1 - e^{-r/r_D}}{r/r_D}) - \frac{\alpha_s.e^{-r/r_D}}{r} \tag{1.17}$$

The screening is a global feature of the medium, shortening the range of the binding potential. Once r_D becomes sufficiently small, the bound states begin to disappear. The following table 1.4 taken from [43] gives an overview of the spectrum of quarkonia.

In a deconfined (partonic) medium the heavy quark potential gets screened and at a sufficiently high temperature, the screening radius would be smaller than the typical size of the quarkonium state. As a result the screened potential no longer can support the formation of the bound states. The screening of the potential strongly depends on the number density of color charges. This is similar to the QED plasma, where the screening radius, r_D depends the number density n through $r_D = 1/(g\sqrt{n/T})$. The rapid rise of parton density with temperature results the rapid decrease of screening radius and decides the fate of the quarkonium bound states. This qualitative argument suggests the quarkonium suppression to consider as a probe for the formation of partonic phase.

However the difficulty in using the concept of suppression is because of the following reasons. Although the long distance (infrared) properties of QCD prohibits the formation of heavy quark bound state at high temperature, but the effective smaller size of the bound state (on the typical scale of QCD, $1/\Lambda_{QCD} \sim 1$ fm) urges the screening to be strong enough to modify the short distance part of the QCD potential. Hence different length scales play crucial role and needs to be understood in detail before establishing the quarkonia suppression as unique signature.

The other point to the concept of suppression considered in [42] is that creation of a $Q\bar{Q}$ pair in heavy ion collision is a rare event; it is assumed that $Q\bar{Q}$ pair created in dense medium would separate there after and both Q and $\bar{Q}$ would no more find another heavy quark partners to form the bound state again during the hadronisation. This might be a good approximation at SPS energy but the scenario would be different for RHIC and LHC energies. Then the process of recombination during the cooling of

Table 1.4: Quarkonia spectroscopy

State:	J/ψ	χ_c	ψ'	Υ	χ_b	Υ'	$\chi_b{}'$	Υ''
M (GeV)	3.10	3.53	3.68	9.46	9.99	10.02	10.26	10.36
Δ E (GeV)	0.64	0.20	0.05	1.10	0.67	0.54	0.31	0.20
Δ M (GeV)	0.02	-0.03	0.03	0.06	-0.06	-0.06	-0.08	-0.07
r (fm)	0.25	0.36	0.45	0.14	0.22	0.28	0.34	0.39

(m_c=1.25 GeV, m_b=4.65 GeV, $\sqrt{\sigma}$=0.445 GeV, α=$\pi/12$)

hot plasma [44, 45] and subsequent pairing of heavy quarks originating initially from different creation processes (statistical hadronisation) [46, 47] are considered. Hence the suppression scenario might be changed.

1.7.4 Jet quenching

Jet quenching is considered as a very efficient signal of QGP. The high energy partons of the colliding nucleons may produce energetic partons which fragments in to a set of hadrons (pions, kaons *etc.*), called **Jets**. A Jet is basically a collimated set of hadronic decay products of a parent parton. In general we can say that the collision of high energy particles can produce jets of elementary particles that emerge from the collisions. In case of high energy p+p collisions, the partons inside the protons collide and produce jets, which has been observed since from 1980's [48]. These Jets are produced at the early stage of the collisions. Then the Jets will propagate in the produced medium. If there is a medium then the Jets loose their energy during the propagation. If we compare the p+p and A+A collisions then the probability of formation of a medium and a large volume is more in case of A+A collision. Hence the energy loss of Jets in A+A collision is more. According to QCD, high momentum partons produced in the

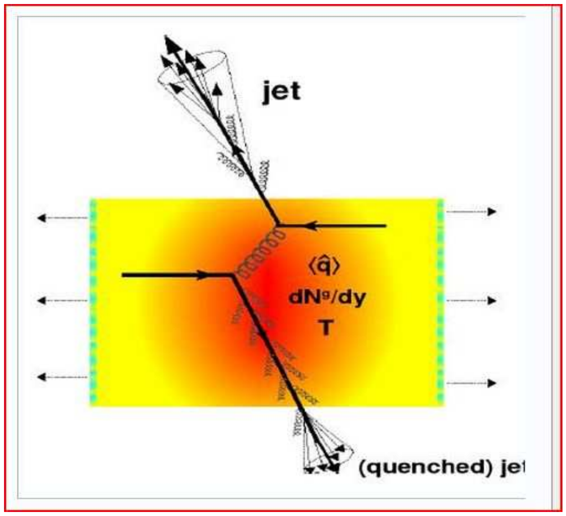

Figure 1.11: Schematic diagram of back to back Jet Productions.

initial stage of the nucleus-nucleus collision will undergo multiple interactions inside the collision region prior to hadronization. In these interactions the partons loose energy through collisional energy loss and medium induced gluon radiation. The later one is a dominant mechanism in case of QGP. If there is QGP phase then the energy loss of energetic partons or Jets will be more which happens more likely in A+A collisions. The magnitude of the energy dissipation depends on the density and temperature of the produced medium. The energy loss is quantified in terms of nuclear suppression factor, R_{AA}. The $R_{AA} = \frac{(\mathrm{Y}ield)_{AA}}{N_{coll}\times(\mathrm{Y}ield)_{pp}}$ is used to study the properties of QGP. The energy loss of high energy partons leading to suppression in yields of high p_T particles is called is called **Jet Quenching** [49, 50]. The variation R_{AA} with A is used to know the transport properties of the medium.

1.8 Motivation and organisation of the thesis

Search for the novel phase of primordial matter, quark gluon plasma, is quite exciting and challenging in the field of high energy nuclear physics. Creating QGP in the laboratory is not only challenging experimentally, its detection through theoretical analysis is also equally interesting and motivating.

We have discussed several signals for probing the nuclear collision and studying the properties of produced matter. Among them we have already discussed the importance of the electromagnetic radiations; real and virtual photons which are more effective in providing the information about the produced matter because of their nature of interaction with the medium they are produced. In this thesis we present the phenomenological study of two important signals; electromagnetic probes and strange probes - *i.e.,* the study of photon productions, lepton pair productions and strangeness productions to diagonise the QGP in the relativistic nuclear collisions. It is already mentioned that the photons and lepton pairs have large mean free path compared to the size of the system, once produced they are emanated out of the system with unscathed thermodynamic information of the medium. The thesis is organized as follows. In chapter 2, we have discussed the emission rate of thermal photons and dileptons from quark gluon plasma and hadronic matter.

Photons are emitted from different stages of the space time evolution. We consider them from different sources according to their emission era as follows;

1. *Prompt photons :* The photons produced from the hard scatterings of the partons of the colliding nuclei are known as prompt photons. The spectra of these photons are evaluated using perturbative quantum chromo dynamics(pQCD).

2. *Thermal photons:* Photons originating from the thermalized phases of the systems; i.e QGP phase or hadronic phase are called thermal photons. Here p_T spectra are calculated by folding the rate of production with space time evolution. The thermal spectra provides the temperature information of the system and gives the indirect evidence whether QGP is formed in heavy ion collision or not.

3. *Photons from hadronic decays:* Photons arising from the decay of hadrons and their resonances after the system freezes out or the hadrons decouple from each other, fall in to this category.These are the background photons and are important for the separation of thermal photons from the total measured photons.

Similar to photons, the dileptons are also emitted from different stages and categorized as follows;

1. *Drell-Yan :* The lepton pairs originating from the hard scatterings of the partons of the colliding nuclei falls to this category. The dilepton spectra from the Drell-Yan processes are evaluated using pQCD.

2. *Thermal :* The lepton pairs coming from the thermalised phase (QGP or Hadronic phase) from the decay of vector mesons like ρ, ω, ϕ *etc.*

3. *Dalitz decays :* The lepton pairs or dileptons emitted from the decay of hadrons like π^0, η *etc.* in the post freeze out era come under this category.

The relativistic ideal hydrodynamics(boost invariant with cylindrical symmetry) has been discussed in chapter 3 to explain the space time evolution of the thermalised system.

The photon productions at SPS, RHIC and LHC energies are discussed in chapter 4. The invariant yield in terms of transverse momentum (p_T) spectra (dN/d^2p_Tdy) are valuated. The p_T spectra of photons for Pb+Pb collision at SPS energy $\sqrt{s_{NN}}$=17.3 GeV [51], Au+Au collision at RHIC energy, $\sqrt{s_{NN}}$=200 GeV [52, 53] are evaluated and compared with the data taken by WA98 and PHENIX collaborations. There is also prediction for LHC energy [54, 53].

The chapter 5 discusses, the virtual photon or lepton pair productions at SPS energy. Those are equally important as real photons for extracting the thermodynamic information. Here instead of p_T spectra we calculate $m_T = \sqrt{{p_T}^2 + M^2}$ spectra *i.e.,* $\frac{\mathrm{d}N}{\mathrm{m}_T dm_T}$, since the lepton pair has extra kinematic variable invariant mass (M) unlike the zero mass of photons. Like photons they are also emitted from different stages of the evolution and categorized in a similar way. The thermal lepton pair spectra provides the temperature information of the system and indicates the possibility of QGP formation in the heavy ion collision. The m_T spectra for In+In collision at $\sqrt{s_{NN}}$=17.3 GeV has been evaluated and compared with the data measured by NA60 Collaboration [55].

Because of the extra kinematic variable, M, associated with lepton pair, the invariant mass spectra (dN/dM) are also calculated which tells about the medium properties of hadrons (ρ, ϕ, ω etc). The invariant mass spectra for In+In collision at $\sqrt{s_{NN}}$ for $\sqrt{s_{NN}}$=17.3 have been evaluated and compared with the data taken by NA60 collaboration [55].

While calculating the individual spectra of photons or dileptons, certain uncertainties enters in to the calculation through hydrodynamic input parameters. To get rid of the uncertainties associated with the input parameters we evaluate the ratio (R_{em}) of spectra and extract the temperature information of the system [53]. This is discussed in chapter 6. The collectivity of the system developed gradually during expansion is studied using the photon and lepton pair momentum spectra. Here the collectivity in terms of radial flow v_r is discussed in chapter 7 and an attempt has been made to extract v_r using both photon and lepton pair($\mu^+\mu^-$). We argue that the simultaneous measurements of photons and dileptons will enable us to estimate the value of radial flow $v_{\rm r}$ for various invariant mass windows of the lepton pairs [56, 51] and the variation of $v_{\rm r}$ with invariant mass M gives the information of QGP formation.

In chapter 8 the strangeness productions; s and $\bar{s}$ quarks in QGP phase and K^+, K^-, $K^0, \bar{K^0}$ mesons, Λ baryons in hadronic phase have been studied. The evolution of strangeness with time has been studied using momentum integrated Boltzmann equations [57]. Finally we evaluate $K^+/\pi^+, K^-/\pi^-$ and Λ/π^+ ratio for different centre of mass energies using different initial conditions and compare with the experimental data available from E802, E866, E917, NA44, NA49, BRAHMS, STAR collaborations at AGS, SPS and RHIC energies [58, 59, 60, 61, 28, 29, 30, 34]. The observed horn, a non-monotonic variation in the K^+/π^+ ratio with colliding energies is reproduced. The non-monotonic behavior has been explained by assuming an initial partonic phase beyond threshold energy $\sqrt{s_{NN}} \geq 7.6$ GeV [38, 62]. Finally, in the last chapter we summarize our work.

Chapter 2

Thermal emission rates of real and virtual photons from quark gluon plasma and hadronic matter

Photons and dileptons(virtual photons) are important signals to probe the formation of quark gluon plasma in relativistic nuclear collisions. Here the rate of photon and dilepton productions in a thermal medium like quark-gluon plasma or hadronic matter is discussed within the frame-work of thermal field theory.

2.1 Introduction

Just after the collision of two heavy nuclei at relativistic energies, the produced system expands in time and may achieve thermal equilibrium after a certain time called thermalisation time. We can categorize the state of evolving system as pre-equilibrium, thermal equilibrium(local) and freeze out state. Freeze out state is the post thermal equilibrium state *i.e.,* where the interactions among the particles cease to exist - consequently they free stream towards the detector. The importance of electromagnetic radiations, photons and lepton pairs (l^+l^-), in probing the matter produced in heavy ion collisions have been discussed in chapter 1. Photons and lepton pairs are produced from every space time point of the evolving matter and they escape out of the system as their mean free path is larger than the size of the system produced in heavy ion collisions. Hence they keep the footprints of every stages of evolution. Since their production depends on temperature, the thermodynamic informations of the system can be obtained from the study of their invariant mass and p_T spectra. These photons and dileptons can be categorized according to the evolution of the system. The photons which are emanated before the system attains equilibrium, are categorized as pre-equilibrium and prompt photons. Similarly, the dileptons produced at very early stage (before equilibrium) generally come from Drell-Yan sources. The photons (dileptons) which come from the thermal equilibrium state follow a thermal distribution and are called as thermal photons (dileptons). In the post equilibrium era, photons are emitted from the decays of hadrons. The dileptons are also produced from the Dalitz decays after the thermal freeze out. The photons excluding those coming from decay of hadrons and their resonances are called as direct photons since they are produced from the direct interactions of partons or hadrons. In this chapter we will discuss the thermal emission rates of both photons and dileptons. In fact it is important to realize that thermal emission rates of dileptons and photons are intimately connected, both being based on the e.m. current-current correlator, albeit evaluated in distinct kinematic domains, *i.e,* time-like ($M^2 = q_0^2 - q^2 > 0$) vs. light-like ($M^2 = 0$), respectively.

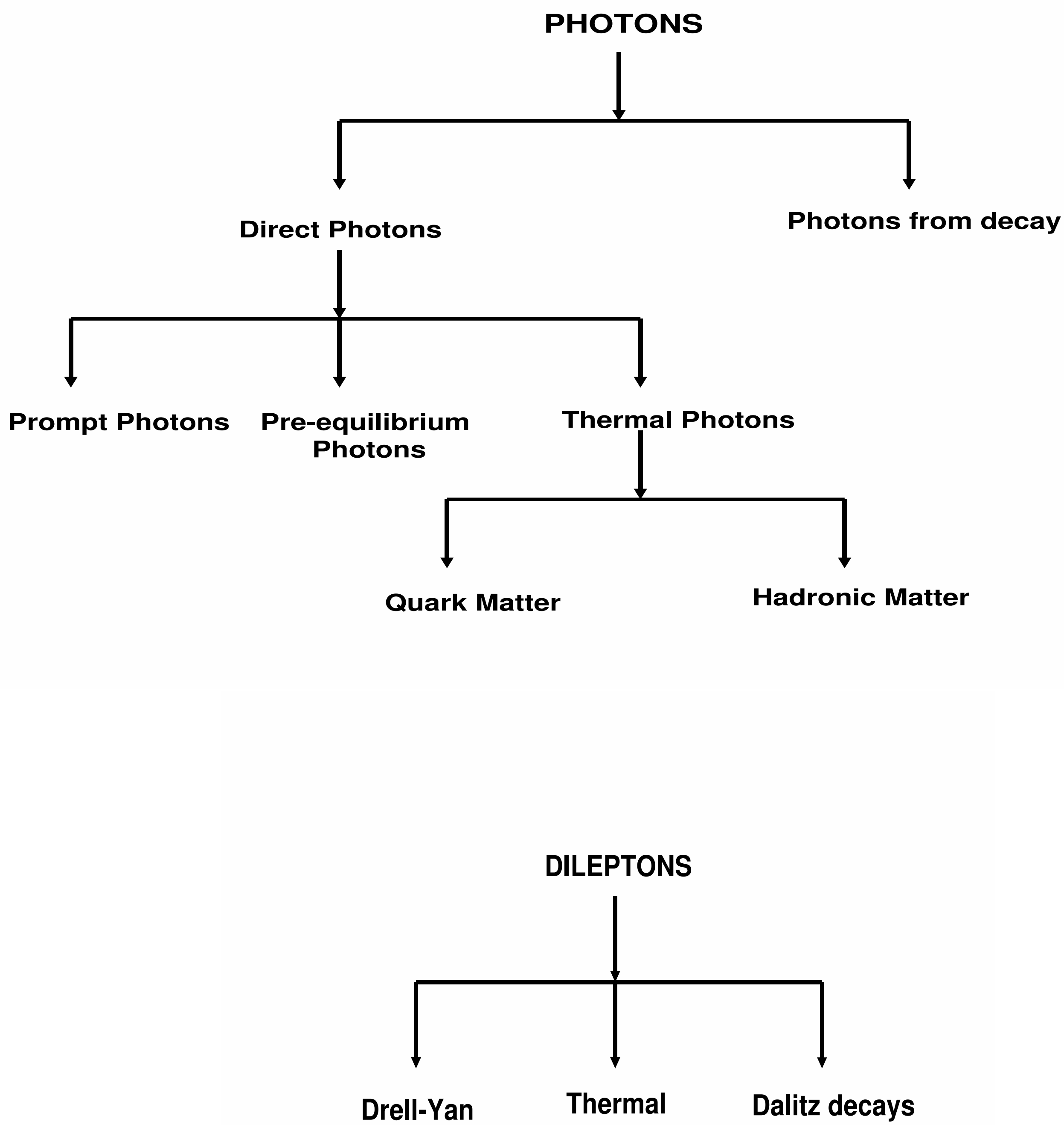

Figure 2.1: Categorization of photons and dileptons.

The sources of photons can be categorized and summarized as in 2.1; In this thesis we are mainly concentrating on thermal productions or thermal spectra.

2.2 Emission rates of photons and dileptons from a thermal medium

2.2.1 Dilepton emission rate from a thermal medium

(A) Spectral function approach:

Let's discuss the inclusive virtual photon(γ^*) or dilepton emission rate from a thermal system produced in heavy ion collisions. Before the collision, the heavy nuclei are in an asymptotic initial state $|I>$. The interaction of heavy nuclei producing lepton pairs l^+l^- can be represented as $|I>\rightarrow |F;l^+l^->$, where F is for the others particles produced along with the lepton pairs. We closely follow the Weldon's work [63]. The inclusive differential probability for emission of leptons into dimensionless cells $Vd^3p/(2\pi)^3$ of phase space is given by,

$$\sum_F |<F;l^+l^-|S|I>|^2 \frac{Vd^3p_1}{(2\pi)^3}\frac{Vd^3p_2}{(2\pi)^3} \tag{2.1}$$

where p_1, p_2 are the momenta of l^- and l^+. Sum over F represents the sum over final states. S is the scattering matrix for the transition, $|I>\rightarrow |F;l^+l^->$. The free lepton states are assumed to be normalized in a box of volume V. The inclusive probabilities are not normalized to unity. Elementary counting results shows that integrating over two particle inclusive probability yields the two particle multiplicity [64]. The multi-

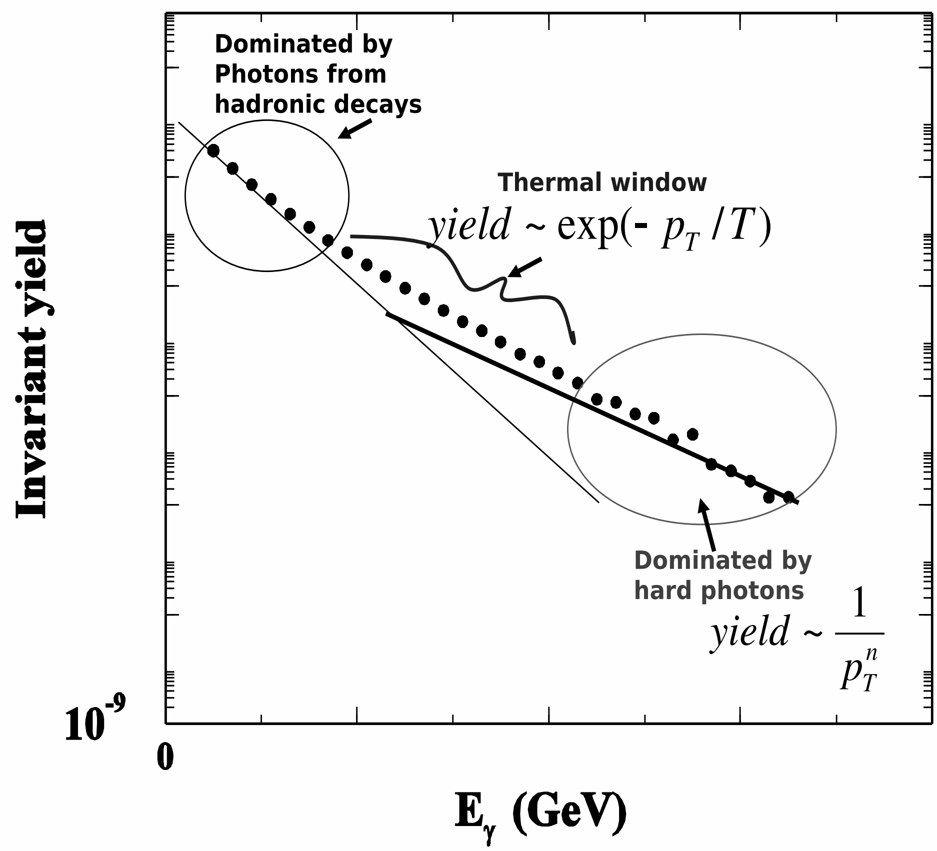

Figure 2.2: Schematic representation:- Dominance of different category of photons in the invariant spectra .

plicity obtained from 2.1 depends on the specific initial state $|I>$. The thermalisation deletes all information about a specific initial state $|I>$. Hence the informations can be replaced by an ensemble average over all initial states $|I>$ each weighted by a Boltzmann factor. Integration of inclusive probabilities over all initial states then leads to multiplicity, hence the thermally averaged lepton pair multiplicity is

$$\begin{aligned} N &= \sum_I \sum_F |<F; l^+l^-|S|I>|^2 \frac{Vd^3p_1}{(2\pi)^3} \frac{Vd^3p_2}{(2\pi)^3} \frac{e^{-\beta E_I}}{Z_c} \\ &= \sum_I \sum_F |S_{FI}|^2 \frac{Vd^3p_1}{(2\pi)^3} \frac{Vd^3p_2}{(2\pi)^3} \frac{e^{-\beta E_I}}{Z_c} \end{aligned} \tag{2.2}$$

where $Z_c = Tr[exp(-\beta H)]$ is the canonical partition function with $\beta = 1/T$, T is the temperature and H is the Hamiltonian. E_I is the energy of the initial state. $|S_{FI}|^2$ is the probability amplitude for the the initial state $|I>$ going to final state$|F; l^+l^->$. The above expression 2.2 describes the multiplicity in local rest frame of the produced system. If the thermal system is expanding then the 4-velocity of the fluid element $u^\mu(=(\gamma, \gamma\vec{v}))$ defined in the rest frame of the fluid then the energy E_I which is appearing in the Boltzmann factor is replaced by $u^\mu p_\mu$. Where the four momentum is $p^\mu = (E, \vec{p})$. The partition function also becomes $Z_c = Tr[exp(-\beta u^\mu p_\mu)]$. Feinberg [25] in 1976 showed that the emission rates in a thermalized system can be related quantum mechanically to the electromagnetic current -current correlation function in a non-perturbative manner. The production of a particle which interact weakly with the background thermal medium can be expressed in terms of the discontinuities or imaginary parts of the self energies of that particle. It is important to note that the produced particle may interact strongly with same species of particles [65, 66]. In Heisenberg picture let's define A^μ as the exact Heisenberg field which is the source of leptonic current ${J^l}_\mu$. Considering to a lowest order of electromagnetic coupling one can

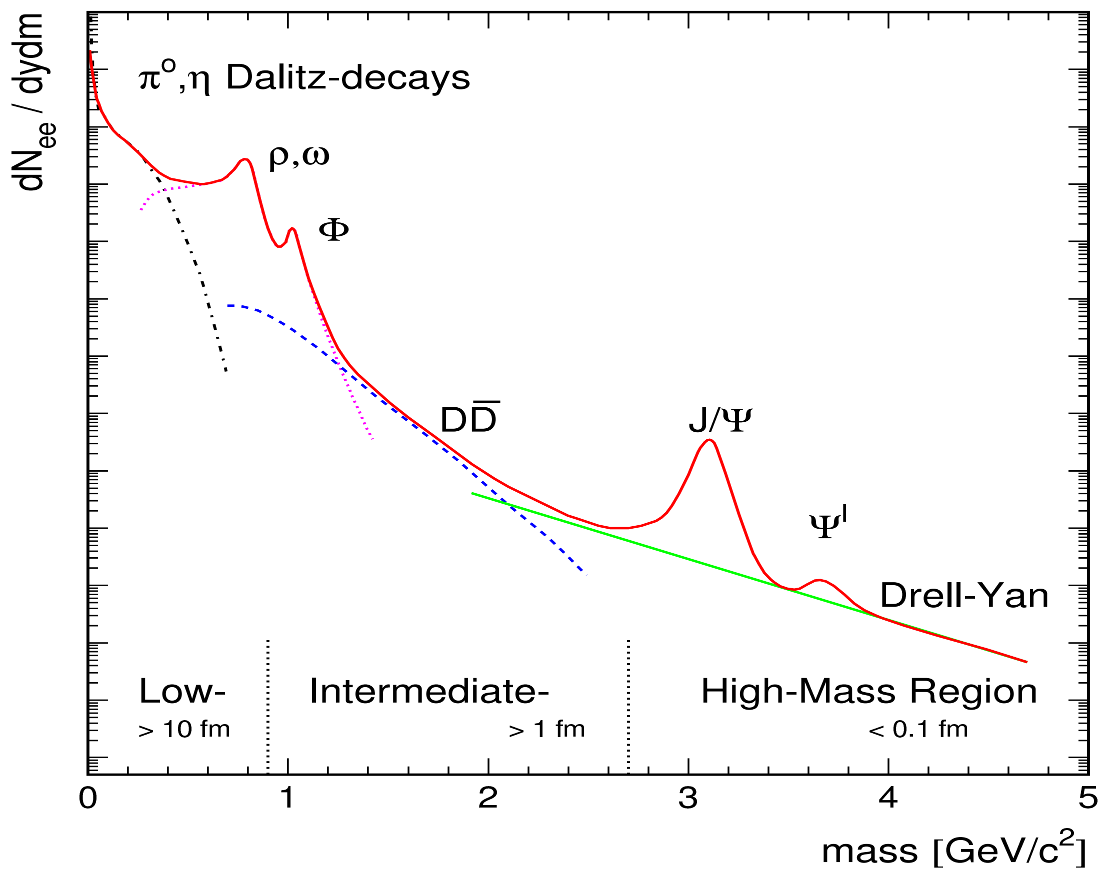

Figure 2.3: Schematic representation:- Dominance of known sources of dileptons in different mass windows of the invariant mass spectra . Courtesy-Prof. Ralf Rapp.

define the scattering matrix element, S_{FI}(amplitude),

$$\begin{aligned} S_{FI} =< F; l^+l^-|S|I > &= < F; l^+l^-|e^{i\int \alpha_I d^4x}|I > \\ &\equiv i < F; l^+l^-|\int \alpha_I d^4x|I > \\ &= ie_0 \int < F; l^+l^-|{J^l}_\mu(x^\mu)A^\mu(x^\mu)|I > d^4x \end{aligned} \quad (2.3)$$

Here the parameter 'e_0' is the un-renormalized charge and α_I is the interacting part of the Lagrangian density=$e_0 j^\mu A_\mu$. The produced lepton pairs are assumed not to interact with the medium. Hence one can write

$$< F; l^+l^-|{j^l}_\mu(x^\mu)A^\mu(x^\mu)|I >=< F|A^\mu(x^\mu)|I >< l^+l^-|{J^l}_\mu(x^\mu)|0 > \quad (2.4)$$

$|0>$ is the vacuum state. For high energy lepton pairs produced by a single virtual photon γ^*, let's call the four momentum of the lepton pair(γ^*) as $q^\mu = (q_0, \vec{q})$ with energy $q_0 = E_1 + E_2$ and momentum $\vec{q} = \vec{p}_1 + \vec{p}_2$. Then the leptonic current can be written as ${J^l}_\mu(x) = e_0\bar{\psi}(x)\gamma^\mu\psi(x) = \frac{e_0}{V}\sqrt{\frac{{m_l}^2}{E_1E_2}}e^{-i(p_1+p_2).x}[\bar{u}(p_1, s_1)\gamma_\mu v(p_2, s_2)]$, where m_l is the mass of the single lepton, $\bar{u}(p_1, s_1)$ and $v(p_2, s_2)$ are the Dirac spinors for l^- and l^+. E_1, E_2, p_1, p_2 and s_1, s_2 are their respective energies, momenta and spins. γ_μ are the Dirac matrices. e_0 is the unnormalized charge. The four vector q^μ is represented as q and x^μ as x. Putting the value of ${J^l}_\mu(x)$ we get

$$\begin{aligned} S_{FI} &= e_0\frac{\bar{u}(p_1, s_1)\gamma_\mu v(p_2, s_2)}{V\sqrt{2E_1 2E_2}}\int d^4x e^{i(p_1+p_2)x} < F|A^\mu(x)|I > \\ &= e_0\frac{\bar{u}(p_1, s_1)\gamma_\mu v(p_2, s_2)}{V\sqrt{2E_1 2E_2}}\int d^4x e^{iqx} < F|A^\mu(x)|I > \end{aligned} \quad (2.5)$$

Squaring the scattering amplitude we get

$$|S_{FI}|^2 = e_0\frac{\bar{u}(p_1, s_1)\gamma_\mu v(p_2, s_2)}{V\sqrt{2E_1 2E_2}}\int d^4x e^{iqx} < F|A^\mu(x)|I > \times$$

$$
\begin{aligned}
& \left[e_0 \frac{\bar{u}(p_1, s_1)\gamma_\nu v(p_2, s_2)}{V\sqrt{2E_1 2E_2}} \int d^4 y e^{iqy} < F|A^\mu(y)|I > \right]^* \\
= & \frac{e_0^2}{V^2} \bar{u}(p_1)\gamma_\mu v(p_2)\bar{v}(p_2)\gamma_\nu u(p_1) \frac{1}{2E_1 E_2} \times \\
& \int d^4 x d^4 y e^{iq(x-y)} < F|A^\mu(x)|I >< I|A^\nu(y)|F > \qquad (2.6)
\end{aligned}
$$

Then the dilepton multiplicity N can be written as

$$
\begin{aligned}
N = & \sum_I \sum_F \frac{e_0^2}{V^2} \bar{u}(p_1)\gamma_\mu v(p_2)\bar{v}(p_2)\gamma_\nu u(p_1) \frac{1}{2E_1 E_2} \times \\
& \int d^4 x d^4 y e^{iq(x-y)} < F|A^\mu(x)|I >< I|A^\nu(y)|F > \frac{V d^3 p_1}{(2\pi)^3} \frac{V d^3 p_2}{(2\pi)^3} \frac{e^{-\beta E_I}}{Z_c} \qquad (2.7)
\end{aligned}
$$

Normalizing the lepton spinors $\bar{u}u = 2m$ and $\bar{v}v = -2m$ we can write the above eq. 2.7 as

$$
N = e_0^2 L_{\mu\nu} M^{\mu\nu} \frac{d^3 p_1}{(2\pi)^3 E_1} \frac{d^3 p_2}{(2\pi)^3 E_2} \qquad (2.8)
$$

where lepton tensor $L_{\mu\nu}$ and photon tensor $M^{\mu\nu}$ are;

$$
\begin{aligned}
L_{\mu\nu} &= \frac{1}{4} \sum_{spins} \bar{u_1}\gamma_\mu v_2 \bar{v_2}\gamma_\nu u_1 \\
&= p_{1\mu} p_{2\nu} + p_{2\mu} p_{1\nu} - (p_1.p_2 + m^2) g_{\mu\nu} \qquad (2.9)
\end{aligned}
$$

and

$$
M^{\mu\nu} = \sum_F \sum_I \int d^4 x d^4 y e^{iq(x-y)} < F|A^\mu(x)|I >< I|A^\nu(y)|F > \frac{e^{-\beta E_I}}{Z_c} \qquad (2.10)
$$

We can write the energy of initial states, $E_I = E_F + q_0$, where $q_0 = E_1 + E_2$ and simplify the photon tensor $M^{\mu\nu}$. Because of the translational invariance, the matrix element depend only on the difference $(x - y = x')$. The four dimensional integration over $x' + y$ gives total space time volume Ω. Hence the photon tensor can be written as,

$$
M^{\mu\nu} = \Omega e^{-\beta q_0} 2\pi \rho^{\mu\nu}(q) \qquad (2.11)
$$

$$\rho^{\mu\nu}(q) \equiv \int \frac{d^4y}{2\pi} e^{iq.y} \sum_F < F|A^\mu(y)A^\nu(0)|F > \frac{e^{-\beta E_F}}{z_c} \tag{2.12}$$

Changing the dummy index y to x we can write,

$$\rho^{\mu\nu}(q) \equiv \int \frac{d^4x}{2\pi} e^{iq.x} \sum_F < F|A^\mu(x)A^\nu(0)|F > \frac{e^{-\beta E_F}}{z_c} \tag{2.13}$$

$\rho^{\mu\nu}$ is a symmetric tensor ($e^{-\beta q_0}\rho^{\mu\nu}(q_0, \vec{q}) = \rho^{\nu\mu}(-q_0, -\vec{q})$) called the photon spectral function at finite temperature. At $T = 0$ it reduces to the usual spectral function because the only state $|F>$ that survives $\beta \to \infty$ is the vacuum. Now we can write the multiplicity N in eq. 2.8 as

$$N = 2\pi e_0^2 \Omega L_{\mu\nu}\rho^{\mu\nu}(q)e^{-\beta q_0} \frac{d^3p_1}{(2\pi)^3 E_1} \frac{d^3p_2}{(2\pi)^3 E_2} \tag{2.14}$$

Since N is the total multiplicity in the entire four volume Ω, we can write $\frac{N}{\Omega} = \frac{dN}{d^4x}$ and the above equation can be written as

$$\frac{dN}{d^4x} = 2\pi e_0^2 L_{\mu\nu}\rho^{\mu\nu}(q)e^{-\beta q_0} \frac{d^3p_1}{(2\pi)^3 E_1} \frac{d^3p_2}{(2\pi)^3 E_2} \tag{2.15}$$

The above equation gives the multiplicity of dileptons at finite temperature in terms of the spectral function $\rho^{\mu\nu}(q)$. The same result can be expressed in terms of matrix elements of current as given by Mclerran and Toimela [67]. Using Maxwell's equation for A^μ and A^ν, let's define the tensor

$$W^{\mu\nu}(q) = \int \frac{d^4x}{2\pi} e^{-iq.x} \sum_F < F|J^\mu(x)J^\nu(0)|F > \frac{e^{-\beta E_F}}{z_c} \tag{2.16}$$

This is related to $\rho^{\mu\nu}(-q)$ by Maxwell's equation. Then above eq. 2.15 can be written in terms of $W^{\mu\nu}$ as

$$\frac{dN}{d^4x} = e_0^4 L_{\mu\nu} \frac{W^{\mu\nu}(q)}{q^4} \frac{d^3p_1}{(2\pi)^3 E_1} \frac{d^3p_2}{(2\pi)^3 E_2} \tag{2.17}$$

This is the result described by Mclerran and Toimela. The calculation of spectral function $\rho^{\mu\nu}$ or correlation function $W^{\mu\nu}$ plays the central role for the evaluation of the multiplicity.

Spectral function

It is useful to express the dilepton production rate in terms of photon spectral function since the spectral function can be related directly to the photon proper self energy(one-photon-irreducible self energy). The spectral function is related to imaginary part of the thermal propagator as follows,

$$\rho^{\mu\nu}(q_0,\vec{q}) = -\frac{1}{\pi}\frac{e^{\beta q_0}}{e^{\beta q_0}-1} ImD_F^{\mu\nu}(q_0,\vec{q}) \tag{2.18}$$

where $ImD^{\mu\nu}(q) = (1+\frac{2}{exp(q_0/T)-1})D_F^{\mu\nu}(q)$. The thermal propagator $D^{\mu\nu}$ as a function of q is calculated from the Fourier transform of the propagator represented in coordinate space. If we express the real time thermal propagator in coordinate space,

$$D^{\mu\nu}(x) = -2\pi i\theta(t)\rho^{\mu\nu}(x) - 2\pi i\theta(-t)\rho^{\mu\nu}(-x) \tag{2.19}$$

Taking the Fourier transform (over t and $\vec{x}$) and looking to the imaginary part we get,

$$ImD^{\mu\nu}(q_0,\vec{q}) = -\pi(1+e^{-\beta q_0})\rho^{\mu\nu}(q_0,\vec{q}) \tag{2.20}$$

The propagator $D_F^{\mu\nu}$ can be related to proper self energy $\Pi^{\mu\nu}$ through Schwinger-Dyson equation

$$(q^2 g_\lambda^{\mu\nu} - \Pi_\lambda^\mu){D_F}^{\lambda\nu} = -g^{\mu\nu} + \frac{\alpha q^\mu q^\nu}{q^2} \tag{2.21}$$

where α is a gauge parameter. From the current conservation we can have $q_\mu \Pi^{\mu\nu} = 0$. At $T = 0$ self energy is finite and the $T \geq 0$ contributions do not change this. Thus

$$\Pi^{\mu\nu}(q) = (1-\frac{1}{Z_3})(q^2 g^{\mu\nu} - q^\mu q^\nu) + \frac{1}{Z_3}\Pi_f^{\mu\nu} \tag{2.22}$$

Where Z_3 is the $T = 0$ wave function renormalization constant and $\Pi_f^{\mu\nu}$ is a finite function of q^μ, T and the renormalized charge e. Current conservation requires that it to be linear combination of two conserved tensors [68, 69].

$$\Pi_f{}^{\mu\nu} = \Pi_T P_T{}^{\mu\nu} + \Pi_L P_L{}^{\mu\nu} \tag{2.23}$$

In the rest frame of the fluid the tensors are $P_T^{00} = 0$, $P_T^{rs} = -\delta^{rs} + \frac{q^r q^s}{|q|^2}$, $P_L^{00} = -\frac{|q|^2}{q^2}$, $P_L^{0s} = -\frac{q^0 q^s}{q^2}$, $P_L^{rs} = -\frac{q^r q^s}{q^2}\left[\frac{q^0}{|q|}\right]^2$. These tensors $P_T^{\mu\nu}$ and $P_L^{\mu\nu}$ are transverse and longitudinal projection tensors. They are orthogonal to q_μ. The 3-tensors P_T^{rs} and P_L^{rs} are transverse and longitudinal to the three vector q^s. These tensors are idempotent ($P_T P_T = P_T, P_L P_L = P_L$) and orthogonal ($P_T P_L = P_L P_T$=0); also they sum up to $g^{\mu\nu} - \frac{q^\mu q^\nu}{q^2}$. The solution of Eq. 2.21 gives

$$D_F^{\mu\nu}(q) = -\frac{Z_3 P_T^{\mu\nu}}{q^2 - \Pi_T} - \frac{Z_3 P_L^{\mu\nu}}{q^2 - \Pi_L} + q^\mu q^\nu \tag{2.24}$$

With the substitution of the $D_F^{\mu\nu}$ eq. 2.18, we get the spectral function becomes

$$\rho^{\mu\nu}(q) = -\frac{Z_3}{\pi}\frac{e^{\beta q_0}}{e^{\beta q_0} - 1}(\rho_T P_T^{\mu\nu} + \rho_L P_L^{\mu\nu}) + q^\mu q^\nu. \tag{2.25}$$

Here

$$\rho_j = \frac{Im\Pi_j}{(q^2 - Re\Pi_j)^2 + (Im\Pi_j)^2} \tag{2.26}$$

j is for T or L. Substituting the spectral function into the expression of multiplicity 2.15 and renormalizing the bare charge e_0 with the factor Z_3 *i.e.,* $Z_3 e_0^2 = e^2$ we have the simplified expression

$$\frac{dN}{d^4x} = 2e^2 L_{\mu\nu}(P_T^{\mu\nu}\rho_T + p_L^{\mu\nu}\rho_L)\frac{d^3p_1}{(2\pi)^3 E_1}\frac{d^3p_2}{(2\pi)^3 E_2}\frac{1}{(e^{\beta q_0} - 1)} \tag{2.27}$$

The contribution from the last term vanishes. This above expression depends on the direction of momenta $\vec{p_1}, \vec{p_2}$. If the data are binned only by the total q^μ, then the integration gives,

$$\int \frac{d^3p_1}{E_1}\int \frac{d^3p_2}{E_2}\delta^4(p_1 + p_2 - q)L_{\mu\nu}(p_1, p_2) = \frac{2\pi}{3}\left[1 + \frac{2m^2}{q^2}\right]\left[1 - \frac{4m^2}{q^2}\right]^{1/2}(q_\mu q_\nu - q^2 g_{\mu\nu}) \tag{2.28}$$

m is the mass of the lepton. Contracting this equation with $P_T^{\mu\nu}$ and $P_L^{\mu\nu}$ we get the differential multiplicity as follows;

$$\frac{dN}{d^4xd^4q} = -\frac{\alpha}{12\pi^4}q^2L(m^2)(2\rho_{\mathcal{T}} + \rho_{\mathcal{L}})\frac{1}{(e^{\beta q_0} - 1)}$$
$$\frac{dR}{d^4q} = -\frac{\alpha}{12\pi^4}L(m^2)q^2(2\rho_{\mathcal{T}} + \rho_{\mathcal{L}})\frac{1}{(e^{\beta q_0} - 1)}. \tag{2.29}$$

The term $L(m^2) = \left[1 + \frac{2m^2}{q^2}\right]\left[1 - \frac{4m^2}{q^2}\right]^{1/2}$ arises from the Dirac spinor. α is the fine structure constant. This is the exact expression for the dilepton emission rate from a thermal medium of interacting particles. $Im\Pi_j$ is negative for $q_0 \geq 0$ [70]. This expression are valid for a plasma at rest. But in our case the plasma expands in space and time. Hence the term q_0 appearing in the exponent in the Eq. 2.29 should be replaced by $q^\mu u_\mu = q.u$, where u_μ is the fluid four velocity. The above expression is the production rate of dilepton $(e^+e^-, \mu^+\mu^-)$ at a finite temperature. The validity of the above equation 2.29 is for small wave length compared to system size *i.e.,* the mean free path of the photons must be larger compared to the system size. The imaginary and real parts of Π are proportional to electromagnetic coupling α hence they are very small for large q^2. So for large q^2 we get

$$\rho_j = \frac{Im\Pi_j}{(q^2 - Re\Pi_j)^2 + (Im\Pi_j)^2} = \frac{Im\Pi_j}{q^4} \tag{2.30}$$

Then the dilepton rate becomes,

$$\frac{dR}{d^4q} = -\frac{\alpha}{12\pi^4}L(m^2)\frac{2Im\Pi_T + Im\Pi_L}{q^2}\frac{1}{(e^{\beta q_0} - 1)} \tag{2.31}$$

This is the expression for dilepton production. We can also express this equation in terms of retarded photon self energy or retarded propagator.

In most of the cases the dilepton production rate from a thermal system is calculated with the approximation $\Pi_T = \Pi_L = \Pi$, then the expression for dilepton production rate becomes,

$$\frac{dR}{d^4q} = -\frac{\alpha}{12\pi^4 q^2} L(m^2) Im\Pi^\mu_\mu \frac{1}{(e^{\beta q_0} - 1)} \tag{2.32}$$

This is the most widely used and known result for dilepton production rate [66]. Here the self energy Π is calculated from the retarded thermal propagator $D_R^{\mu\nu}$ [1] using Schwinger-Dyson equation as the retarded thermal propagator is analytic. Here multiple re-scatterings or interactions virtual photons and multiple emission in the thermal bath are neglected hence the result is valid up to order $O(e^2)$. But the expression is true for all orders of strong interaction. Changing the notation from Π to Π^R (R for retarded) we write the equation as

$$\frac{dR}{d^4q} = -\frac{\alpha}{12\pi^4 q^2} L(M^2) Im\Pi^{R\mu}_\mu f_{BE}(q_0) \tag{2.33}$$

where $f_{BE}(q_0) = \frac{1}{(e^{\beta q_0} - 1)}$.

(B) Emission rate from current-current correlation function:

The dilepton emission rate can also be calculated from electromagnetic current-current correlation function [67]. We denote the hadronic part of the current operator by J^h_ν and the leptonic part of the current operator J^l_μ. The free propagator which is the photon propagator is denoted by $\bar{D_0^{\mu\nu}}$. The scattering matrix element for this transition can then be written as

$$\begin{aligned} S_{FI} = < F; l^+l^-|S|I > &= < F; l^+l^-|e^{i\int \alpha_I d^4x}|I > \\ &= i < F; l^+l^-| \int \alpha_I d^4x|I > \end{aligned}$$

[1] $D_R^{\mu\nu}(q_0, \vec{q}) = \int d^4x e^{iqx}\theta(t) \sum_F < F| [A^\mu(x)A^\nu(0)] |F > e^{-\beta E_F}$
$\rho^{\mu\nu} = -\frac{1}{\pi} Im D_R^{\mu\nu}$

$$\begin{aligned} &= i < F; l^+l^- | \int J^l{}_\mu(x) A^\mu(x) d^4x | I > \\ &= ie_0 \int < F; l^+l^- | J^l{}_\mu(x) D_O^{\bar{\mu\nu}}(x-y) J_h^\nu(y) | I > d^4x d^4y \end{aligned} \tag{2.34}$$

where $A^\mu(x)$ the photon current obtained from the hadron current as

$$A^\mu(x) = \int D_O^{\bar{\mu\nu}}(x-y) J_h^\nu(y) d^4y \tag{2.35}$$

Using the Fourier transform of photon propagator and squaring the matrix element we can get the dilepton production rate in terms of retarded current-current correlator, given by ,

$$W_R{}^{\mu\nu}(q) \equiv i \int d^4x e^{iq.x} \theta(t) \sum_F < F | \left[J_h{}^\mu(x) J_h{}^\nu(0) \right] | F > \frac{e^{-\beta E_F}}{z_c} \tag{2.36}$$

With further simplification one can end up the relation

$$\frac{dR}{d^4q} = -\frac{\alpha}{12\pi^4 q^2} L(m^2) Im P_\mu^{R\mu} f_{BE}(q_0) \tag{2.37}$$

where $P_\mu^{R\mu} = g^{\mu\nu} P^R{}_{\mu\nu} = 2P^R{}_T + P^R{}_L$ and $P_R{}^{\mu\nu}$, the improper self energy is defined in the coordinate space (we have to take the Fourier transform. $P_R{}^{\mu\nu} = -W_R{}^{\mu\nu}(q)$) as follows,

$$iP_R{}^{\mu\nu} \equiv \theta(t) \sum_F < F | \left[J_h{}^\mu(x) J_h{}^\nu(0) \right] | F > \frac{e^{-\beta E_F}}{Z_c} \tag{2.38}$$

This calculation is essentially non-perturbative till this point. Calculation to the order of α or $O(e^2)$ improper self energy P reduces to proper self energy $\Pi(=PD_0D^{-1})$ and equation 2.37 reduces to 2.33

$$\frac{dR}{d^4q} = -\frac{\alpha}{12\pi^4 q^2} L(m^2) Im \Pi_\mu^{R\mu} f_{BE}(q_0) \tag{2.39}$$

For the details of the current-current correlation formalism and the relation between current-current correlation function and spectral function see [71].

Dilepton emission rate from the resonance decay

When a thermal medium at temperature T $(= \beta^{-1})$ contains unstable particles like $\rho, \omega, \phi, J/\psi$ mesons, then the electromagnetic decay of these particles may provide crucial information of the system. An off-shell vector meson V with four momentum (q, where $q^2 = M^2$) may decay into a lepton pair e^+e^- or $\mu^+\mu^-$ and others depending upon the 4-momentum transfer. The emission rate of these lepton pairs or dileptons is given by [72],

$$\frac{dR}{d^4q} = \frac{2M}{(2\pi)^3} \rho^V{}_{\mu\nu} P^{\mu\nu} f_{BE}(q_0) \Gamma_{V \to l^+ l^-} \tag{2.40}$$

where $\rho^V{}_{\mu\nu}$ is the spectral function of the off-shell vector meson. This is similar to the previous description 2.13 where the photon field is replaced by the vector meson field. The spectral function $\rho^V_{\mu\nu}$ is given as is expressed in terms of retarded self energy $(\Pi^R_T = \Pi^R_L = \Pi^R)$ $\rho^V_{\mu\nu} = \frac{1}{\pi} \frac{Im\Pi^R}{(q^2 - m_V^2 + Re\Pi^R)^2 + (Im\Pi^R)^2} P_{\mu\nu}$ where $P_{\mu\nu} = \sum \epsilon_\mu \epsilon^*_\nu = -g_{\mu\nu} + \frac{q_\mu q_\nu}{q^2}$ is the projection operator for vector meson V with the property $P^{\mu\nu} P_{\mu\nu} = (2J + 1)$, J being the spin of vector meson. $\Gamma_V \to l^+ l^-$ is the partial decay width of the decay. The dilepton emission rate for the resonance decay is then given by

$$\frac{dR}{d^4q} = 2 \frac{(2J+1)}{(2\pi)^3} f_{BE} M \Gamma_{V \to l^+ l^-} \left[\frac{1}{\pi} \frac{Im\Pi^R}{(q^2 - m_V^2 + Re\Pi^R)^2 + (Im\Pi^R)^2} \right] \tag{2.41}$$

The retarded self energy is calculated using thermal field theory.

2.2.2 Photon emission rate from a thermal medium

The photon emission rate is calculated in the similar way to that of dilepton rate. The photon emission rate differs from the dilepton rate in the following way; the factor $e^2 L_{\mu\nu}/q^4$ appearing in the dilepton rate 2.32 which is nothing but the product of electromagnetic vertex $\gamma^* \to l^+ l^-$, the leptonic current involving Dirac spinors and the square of the photon propagator should be replaced by the factor $\sum \epsilon^\mu \epsilon^*_\nu (=-g_{\mu\nu})$. And the phase space factor $\frac{d^3p_1}{(2\pi)^3 E_1}\frac{d^3p_2}{(2\pi)^3 E_2}$ should be replaced by $\frac{d^3p}{(2\pi)^3 p_0}$. Then the photon emission rate becomes

$$\begin{aligned} p_0 \frac{dR}{d^3p} &= \frac{g^{\mu\nu}}{(2\pi)^3} Im\Pi_{\mu\nu} \frac{1}{e^{\beta p_0} - 1} \\ \frac{dR}{d^2p_T dy} &= \frac{g^{\mu\nu}}{(2\pi)^3} Im\Pi_{\mu\nu} \frac{1}{e^{\beta p_0} - 1} \end{aligned} \tag{2.42}$$

where p_T is the transverse momentum y is the rapidity ($y = \frac{1}{2} ln \frac{E+p}{E-p}$). The above emission rate is correct up to O(e^2) in electromagnetic interaction. But this is exact to all order of strong interactions. The imaginary part of the photon self energy can be calculated using thermal cutting rules [73, 74, 75]. The imaginary part of the n-loop amplitude can be expressed in terms of physical amplitude of lower order. If the photon self-energy is approximated by carrying out a loop expansion to some finite order, then the formulation of Eq. (2.42) is equivalent to relativistic kinetic theory, *i.e.,* when the imaginary part of the self energy is calculated up to L^{th} order loop where L satisfies $(x + y) < L + 1$, then one obtains the photon emission rate for the reaction
x particles $\to$ y particles + γ and the above formalism 2.42 becomes equivalent to the relativistic kinetic theory formalism [24].

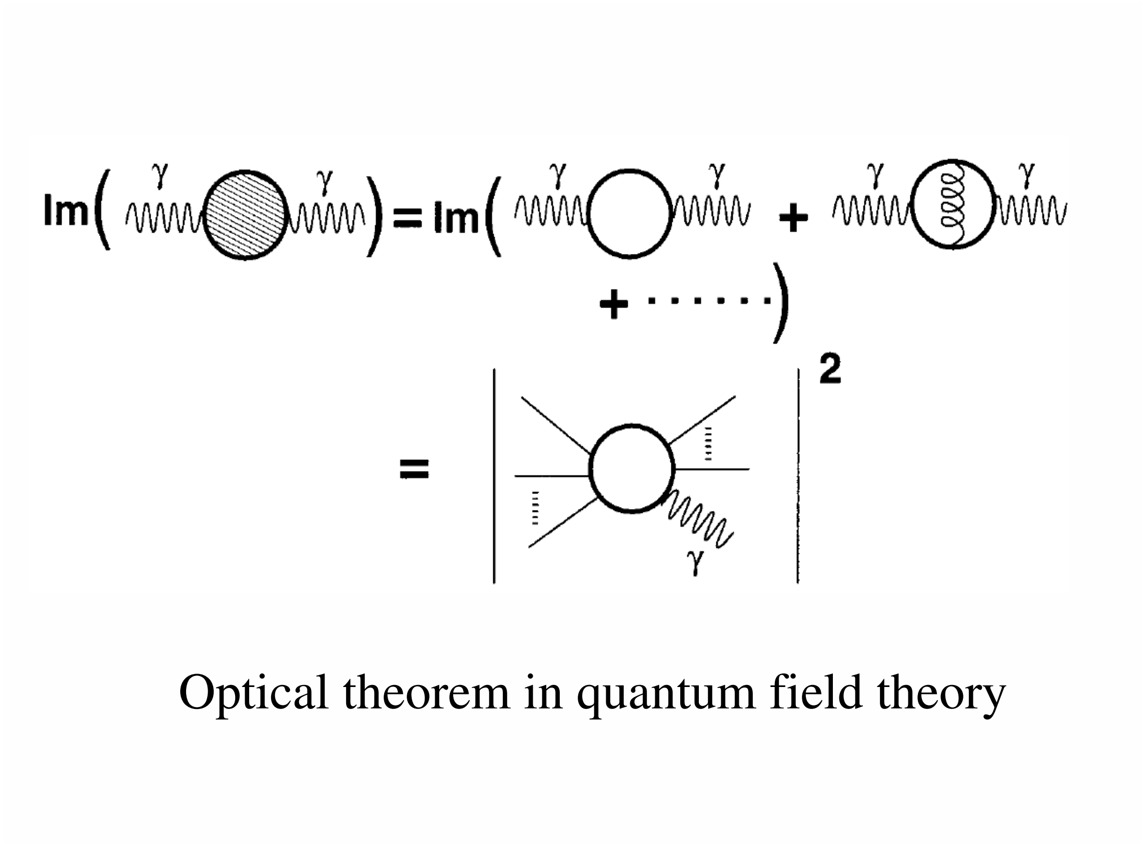

Figure 2.4: Cutkosky rules: Imaginary part of the n-loop amplitude is expressed in terms of physical amplitude of lower order.

1. **Photon emission from thermal medium using kinetic theory**

According to relativistic kinetic theory formulation, the production of i-type particles from the reaction of type $1(p_1)$+2 $(p_2) \rightarrow 3$ (p_3) + i(p_i) is given by [24, 76]:

$$\begin{aligned} \mathcal{R}_i &= \mathcal{N} \int \frac{d^3p_1}{2E_1(2\pi)^3} \frac{d^3p_2}{2E_2(2\pi)^3} f_1(E_1) f_2(E_2) (2\pi)^4 \delta({p_1}^\mu + {p_2}^\mu - {p_3}^\mu - p^\mu) \\ &\times |\mathcal{M}_i|^2 \frac{d^3p_3}{2E_3(2\pi)^3} \frac{d^3p}{2E(2\pi)^3} [1 \pm f_3(E_3)] \end{aligned} \tag{2.43}$$

where $\mathcal{N}$ is the over all degeneracy, $\mathcal{M}_i = \mathcal{M}_{1+2\rightarrow 3+1}$, is the matrix element which gives the amplitude ($\sim |M|^2$) of the process under consideration. f_j's are the (Fermi-Dirac or Bose-Einstein) thermal distribution functions of the incoming and outgoing particles. The term $[1 \pm f_3(E_3)]$ represents the Bose enhancement or Pauli suppression of the phase space of particle 3. p_1, p_2, E_1, E_2 carry their usual meanings. Here we are looking for the inclusive productions of photon (particle i). p is the Monet of produced photon. δ-function takes care of the energy-momentum conservation of the process. The matrix element is a function of Mandelstem variables $s = (p_1 + p_2)^2$, $t = (p_1 - p_3)^2$ and $u = (p_1 - p)^2$; $M_i = M_i(s, t, u)$. Using the Mandelstem variables we can write the differential photon production rate as:

$$\begin{aligned} E\frac{d\mathcal{R}_i}{d^3p} &= \frac{\mathcal{N}}{(2\pi)^7} \frac{1}{16E} \int dsdt\ |\mathcal{M}_i(s,t)|^2 \int dE_1 dE_2 f_1(E_1) f_2(E_2) \\ &\times [1 \pm f_3(E_1 + E_2 - E)] \theta(E_1 + E_2 - E)(a{E_1}^2 + bE_1 + c)^{-1/2} \end{aligned} \tag{2.44}$$

where,

$$\begin{aligned} a &= -(s+t)^2, \\ b &= 2(s+t)(Es - E_2 t), \\ c &= st(s+t) - (Es + E_2 t)^2. \end{aligned} \tag{2.45}$$

We denote $\mathcal{R}_i$ as $\mathcal{R}$ from now onwards. Further simplification of the above rate equation gives

$$
\begin{aligned}
E\frac{dR}{d^3p} &= \frac{\mathcal{N}}{16(2\pi)^7 E} \int_{(m_1+m_2)^2}^{\infty} ds \int_{t_{\min}}^{t_{\max}} dt\, |\mathcal{M}|^2 \int dE_1 \\
&\quad \times \int dE_2 \frac{f(E_1)\, f(E_2)\, [1+f(E_3)]}{\sqrt{a_1 E_2^2 + 2b_1 E_2 + c_1}},
\end{aligned} \tag{2.46}
$$

where

$$
\begin{aligned}
a_1 &= -(s+t-m_2^2-m_3^2)^2 \\
b_1 &= E_1(s+t-m_2^2-m_3^2)(m_2^2-t) + E[(s+t-m_2^2-m_3^2)(s-m_1^2-m_2^2) \\
&\quad -2m_1^2(m_2^2-t)] \\
c_1 &= -E_1^2(m_2^2-t)^2 - 2E_1E[2m_2^2(s+t-m_2^2-m_3^2) - (m_2^2-t)(s-m_1^2-m_2^2)] \\
&\quad -E^2[(s-m_1^2-m_2^2)^2 - 4m_1^2m_2^2] - (s+t-m_2^2-m_3^2)(m_2^2-t) \\
&\quad \times(s-m_1^2-m_2^2) + m_2^2(s+t-m_2^2-m_3^2)^2 + m_1^2(m_2^2-t)^2 \\
E_{1\min} &= \frac{(s+t-m_2^2-m_3^2)}{4E} + \frac{Em_1^2}{s+t-m_2^2-m_3^2} \\
E_{2\min} &= \frac{Em_2^2}{m_2^2-t} + \frac{m_2^2-t}{4E} \\
E_{2\max} &= -\frac{b_1}{a_1} + \frac{\sqrt{b_1^2-a_1c_1}}{a_1}.
\end{aligned}
$$

2. **Dilepton emission from thermal medium using kinetic theory** Similar to photon the dilepton production rate according to relativistic kinetic theory for the process $1(p_1)+2(p_2) \rightarrow l^+(p_l^+)l^-(p_l^-)$ can be written as,

$$
\begin{aligned}
R_i &= \int \frac{d^3p_1}{2E_1(2\pi)^3} f(p_1) \int \frac{d^3p_2}{2E_2(2\pi)^3} f(p_2) \int \frac{d^3p_{l^+}}{2E_{l^+}(2\pi)^3} \int \frac{d^3p_{l^-}}{2E_{l^-}(2\pi)^3} \\
&\quad | \mathcal{M} |^2_{1+2\rightarrow l^+l^-} \, (2\pi)^4 \delta^{(4)}(p_1+p_2-p_{l^+}-p_{l^-})
\end{aligned} \tag{2.47}
$$

where $f(p_j)$'s are the thermal distribution functions. The Pauli blocking of the lepton pair in the final state has been neglected.

2.3 Photon emission rate from quark gluon plasma and hadronic matter

2.3.1 Photon emission rate from quark gluon plasma

The photon productions from QGP phase has been evaluated using hard thermal loop (HTL) approximations. QGP at very high temperature ($T >> T_c$) can be studied using QCD perturbation theory since at very high temperature the coupling constant α_s is very small. But naive perturbation theory at high temperature has two difficulties-(i) the problem of infrared divergence and (ii) it has the problem of gauge dependence of the physical quantities *e.g.,* the gluon damping rate. The gauge dependence of the gluon damping rate was cured by Braaten and Pisaraski [77] using HTL frame work. In HTL frame work one has to basically expand the current-current correlation function in terms of effective vertices and propagators not with the bare propagator and vertices. Where effective quantities are the corresponding bare quantities plus the high temperature limit of one loop corrections. But the HTL formalism could not solve the infrared divergence problem. The quantities (in emission rate) which are quadratically divergent in naive perturbation theory becomes logarithmic divergent in effective theory and the quantities which have logarithmic divergence in naive perturbation theory becomes finite in effective theory due to the application of HTL re-summation method. The hard photon emission rate (photon with energy $E >> T$) falls to this category. The divergence was cured by isolating the region of divergence by putting infrared cut-off.

The Lagrangian density for different processes of photon productions in QGP phase is given by

$$\mathcal{L}_{QGP} = \mathcal{L}_{QCD} + \mathcal{L}_{\gamma q} \tag{2.48}$$

where,

$$\begin{aligned} \mathcal{L}_{QCD} &= -\frac{1}{4}\sum_{a=1}^{g} G^a_{\mu\nu}G^{a\mu\nu} + \sum_{f=1}^{N_f} \bar{\psi}_f(i\gamma^\mu\partial_\mu - g_s\gamma^\mu G^a_\mu \frac{\lambda^a}{2})\psi_f \\ \mathcal{L}_{\gamma q} &= -\frac{1}{4}F_{\mu\nu}F^{\mu\nu} - \sum_{f=1}^{N_f} e_f\bar{\psi}_f\gamma^\mu A_\mu\psi_f \end{aligned} \tag{2.49}$$

$G^a_{\mu\nu}$ is the non-abelian field tensor for the gluon field G^a_μ of color $a.$, ψ_f is the Dirac field, for the quark flavor f, g_s is the color charge, e_f is the effective (fractional) electric charge of quark flavor f, λ^a are the Gell-Mann matrices, $F_{\mu\nu}$ is the electromagnetic field tensor and A^μ is the photon field. The main processes for photon productions from QGP are the (i) annihilation of quark and anti quark- $q\bar{q} \rightarrow g\gamma$ and (ii) the Compton processes - $q(\bar{q})g \rightarrow q(\bar{q})\gamma$. The production rates from these processes have the difficulties of divergence due to the exchange of massless particles. This is a well known problem in thermal perturbative expansion of non-abelian gauge theory which suffers from infrared divergence. This can be demonstrated if we look at the production cross section of a particular process. The differential cross-section for mass less particles can be written in terms of the matrix element as,

$$\frac{d\sigma}{dt} = \frac{|\mathcal{M}|^2}{16\pi s^2} \tag{2.50}$$

The cross-sections for annihilation and Compton processes (with mass-less quarks) are:

$$\frac{d\sigma^{\text{annihilation}}}{dt} = \frac{8\pi\alpha\alpha_s}{9s^2}\frac{u^2+t^2}{ut} \tag{2.51}$$

and

$$\frac{d\sigma^{\text{Compton}}}{dt} = \frac{-\pi\alpha\alpha_s}{3s^2}\frac{u^2+s^2}{us} \tag{2.52}$$

The total cross-section can be obtained after integrating over t. Here the differential cross sections have singularities at t and/or $u = 0$. Now to get rid of these singularities one has to isolate the region of phase space causing the divergences [24] The integration is done by introducing a lower cut-off k_c to make the integrals finite.

$$-s + {k_c}^2 \leq t \leq -{k_c}^2, \;\; 2{k_c}^2 \leq s \leq \infty, \tag{2.53}$$

where $T^2 \gg {k_c}^2 > 0$ is an infrared cut-off.

Now the divergence is regulated treating u and t symmetrically and maintaining the identity for mass less particles $s + t + u = \sum_i m_i^2 = 0$.

In the limit that ${k_c}^2 \to 0$,

$$E\frac{d\mathcal{R}^{\text{Compton}}}{d^3p} = \frac{5}{9}\frac{\alpha\alpha_s}{6\pi^2}T^2 e^{-E/T}[\ln(4ET/{k_c}^2) + C_F] \tag{2.54}$$

$$E\frac{d\mathcal{R}^{\text{annihilation}}}{d^3p} = \frac{5}{9}\frac{\alpha\alpha_s}{3\pi^2}T^2 e^{-E/T}[\ln(4ET/{k_c}^2) + C_B] \tag{2.55}$$

where

$$C_F = \frac{1}{2} - C_{\text{Euler}} + \frac{12}{\pi^2}\sum_{n=2}^{\infty}\frac{(-1)^n}{n^2}\ln\; n = 0.0460.., \tag{2.56}$$

$$C_B = -1 - C_{\text{Euler}} - \frac{6}{\pi^2}\sum_{n=2}^{\infty}\frac{1}{n^2}\ln\ n = -2.1472... \tag{2.57}$$

These expressions have been obtained using the thermal distribution functions as Fermi-Dirac (FD) or Bose-Einstein (BE) functions in the final state. Using the Boltzmann distribution instead FD or BE functions in the final state we get [24]

$$E\frac{d\mathcal{R}^{\text{Compton}}}{d^3p} = \frac{5}{9}\frac{2\alpha\alpha_s}{\pi^4}T^2e^{-E/T}[\ln(4ET/{k_c}^2) + \frac{1}{2} - C_{Euler}] \tag{2.58}$$

$$E\frac{d\mathcal{R}^{\text{annihilation}}}{d^3p} = \frac{5}{9}\frac{2\alpha\alpha_s}{\pi^4}T^2e^{-E/T}[\ln(4ET/{k_c}^2) - 1 - C_{Euler}]. \tag{2.59}$$

The factor $5/9[=(2/3)^2+(1/3)^2]$ arises from the sum of the squares of the electric charges of the u and d quarks, the factor $\alpha\alpha_s$ comes from the topological structure of the diagrams, a factor T^2 comes from phase space which gives the overall dimension of the rate, and we have the Boltzmann factor $e^{-E/T}$ for photons of energy E. In this approach the many body effects shield the infrared divergence.

The photon rate using the soft part of the phase space is handled using HTL resummation technique. For hard photon in HTL calculation, one of the soft quark propagator should be replaced by effective quark propagators in the photon self energy diagram, which consists of the bare propagator and high temperature limit of one loop corrections (Fig. 2.5). When soft and hard contributions are added the emission rate becomes finite because of the Landau damping of the exchanged quark in thermal bath and the cut-off scale is canceled. The emission rate of hard photons then becomes

$$E\frac{dR_\gamma^{QGP}}{d^3q} = \frac{5}{9}\frac{\alpha\alpha_s}{2\pi^2}T^2\,e^{-E/T}\,\ln(2.912E/g_s^2T). \tag{2.60}$$

where α_s is the strong coupling constant. Apart from the annihilation and Compton processes, the bremsstrahlung contribution to photon emission rate has also been taken

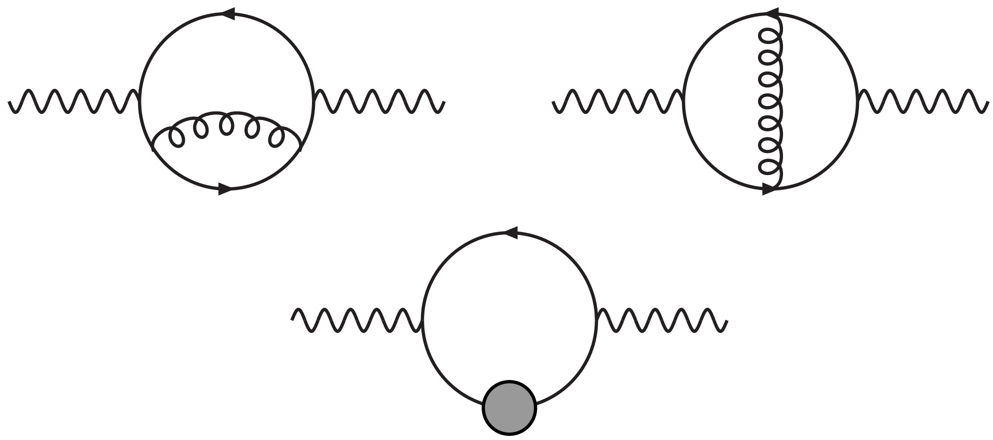

Figure 2.5: Two loop contribution to the photon self energy. A diagram interchanging the blob in the internal line of the third diagram should also be considered.

into account as computed in [78, 79, 80, 81] by evaluating the photon self energy in two loop HTL approximation. The physical processes arising from two loop contribution (Fig. (2.6)) are the bremsstrahlung of quarks, antiquarks and quark anti-quark annihilation with scattering in the thermal bath. The rate of photon production due to bremsstrahlung process for a two flavor thermal system with $E > T$ is given by [78]

$$E\frac{dR_{\gamma}^{QGP}}{d^3q} = \frac{40}{9\pi^5}\,\alpha\alpha_s T^2\, e^{-E/T}\,(J_T - J_L)\ln 2, \tag{2.61}$$

and the rate due to $q\bar{q}$ annihilation with scattering in the thermal bath is given by,

$$E\frac{dR_{\gamma}^{QGP}}{d^3q} = \frac{40}{27\pi^5}\,\alpha\alpha_s ET\, e^{-E/T}\,(J_T - J_L)\,, \tag{2.62}$$

where $J_T \approx 4.45$ and $J_L \approx -4.26$. The most important implication of this work is that the two loop contribution is of the same order of magnitude as those evaluated at one loop [24, 82] due to the larger size of the available phase space. Here in Fig.2.7 we show the Feynman diagrams for the processes considered for photon productions in QGP phase. The Photon rate from QGP to the order α_s has been considered with

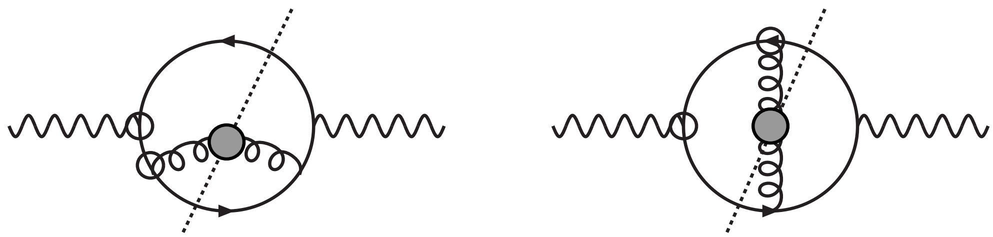

Figure 2.6: Two loop photon diagram relevant for bremsstrahlung processes. The blob on the gluon (spiral line) indicates effective gluon propagator. The circle on the vertices represent those required to evaluate the imaginary part of the photon self energy in the framework of thermal cutting rules

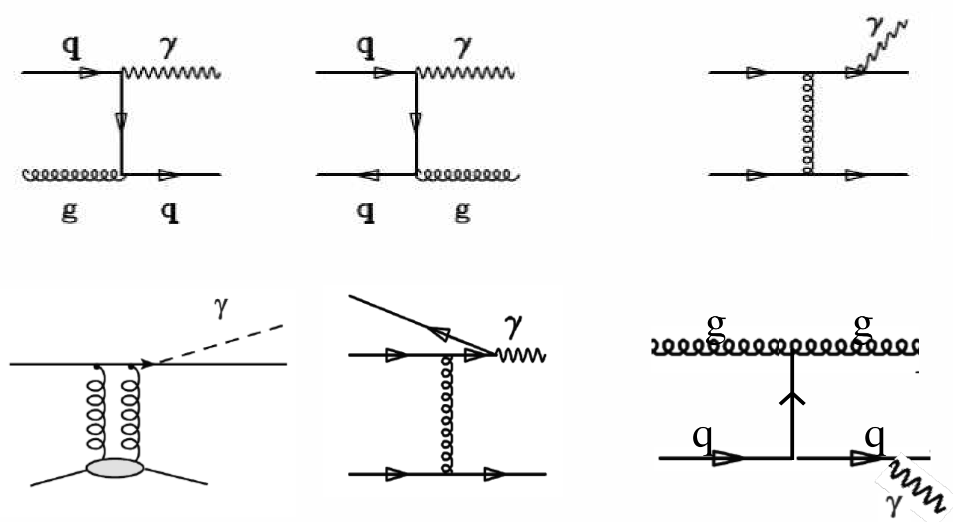

Figure 2.7: Compton, annihilation and bremsstrahlung processes considered for photon productions in QGP phase: $qg \to q\gamma$, $q\bar{q} \to g\gamma$, $q_1q_2 \to q_1q_2\gamma$, $qq\bar{q} \to q\gamma$, $gq \to gq\gamma$ etc.

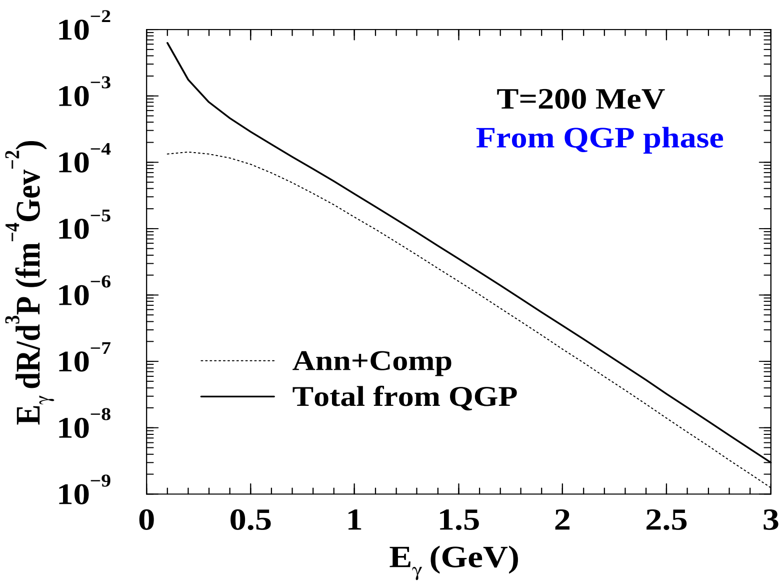

Figure 2.8: Photon production rates from Compton, annihilation processes and the total (including bremsstrahlung) are displayed

re-summed ladder diagrams in the effective theory as in [83, 84]. Here we have used the temperature dependence of strong coupling constant taken from [85]. The rates from different processes have been displayed in Fig. 2.8

Photons from passage of jets through QGP

The productions of jets in heavy ion collisions are already discussed in the introduction chapter and jet quenching is believed to be one of the important signals for probing quark gluon plasma. The produced jets or high energetic partons loose energy while traveling through a medium like QGP. They are produced at a time scale $\tau \sim 1/p_T$ (p_T is the transverse momentum of the energetic partons) before the medium is formed at τ_i. When they travel in the medium like QGP they interact with the thermal quarks, antiquarks or gluons via annihilation or Compton processes. These interaction lead to photon productions. The high energy photon productions due to jet-plasma interactions are called jet-photon conversion [86]. It may be noted that the photon productions due to jet-plasma interactions have not been considered in our evaluation of photon spectra at SPS, RHIC and LHC energies.

2.3.2 Photon emission rate from hadronic matter

The photon productions from hadrons have been evaluated using the above described thermal field theory frame work from a hot mesonic matter using massive Yang-Mills (MYM) approach, extended to the SU(3) (strangeness sector) as in [87]. Some more processes beyond MYM framework have also been considered. The photon production rate can be written as

$$p_0 \frac{dR_\gamma}{d^3p} = E_\gamma \frac{dR_\gamma}{d^3p} = -\frac{\alpha}{\pi^2}\, f^B(p_0;T)\ \mathrm{Im}\Pi^T_{\mathrm{em}}(p_0 = p;T)\ . \tag{2.63}$$

$f^B(p_0;T) = \frac{1}{\exp(p_0/T)-1}$ is the Bose-Einstein distribution function. Vector meson dominance model (VDM) relates the self energy Π_{em} to in-medium vector-meson spectral functions [88] thus making suitable for non-perturbative model calculations at low and moderate energies and momenta.

For the productions from the hadronic phase we consider the Lagrangian as in [89, 90] which describes the hadronic gas consisting of light pseudo-scalar, vector and axial vector mesons (π, K, ρ, K^*, a_1). The massive Yang-Mills (MYM) approach has been adopted to this Lagrangian which gives various hadronic phenomenology at tree level with a limited set of adjustable parameters. In an effective nonlinear σ-model Lagrangian vector and axial vector fields are considered as massive gauge fields of the chiral U(3)$_L\times$ U(3)$_R$ symmetry[89, 90]:

$$
\begin{aligned}
\mathcal{L} \;=\; & \tfrac{1}{8}F_\pi^2 \mathrm{Tr} D_\mu U D^\mu U^\dagger + \tfrac{1}{8}F_\pi^2 \mathrm{Tr} M(U + U^\dagger - 2) \\
& -\tfrac{1}{2}\mathrm{Tr}\left(F^L_{\mu\nu}F^{L\mu\nu} + F^R_{\mu\nu}F^{R\mu\nu}\right) + m_0^2 \mathrm{Tr}\left(A^L_\mu A^{L\mu\nu} + A^R_\mu A^{R\mu}\right) + \\
& \gamma \mathrm{Tr} F^L_{\mu\nu} U F^{R\mu\nu} U^\dagger \gamma \mathrm{Tr} F^L_{\mu\nu} U F^{R\mu\nu} U^\dagger \\
& -i\xi \mathrm{Tr}\left(D_\mu U D_\nu U^\dagger F^{L\mu\nu} + D_\mu U^\dagger D_\nu U F^{R\mu\nu}\right) \; .
\end{aligned} \tag{2.64}
$$

In the above,

$$
\begin{aligned}
U = \exp\left(\frac{2i}{F_\pi}\sum_i \frac{\phi_i \lambda_i}{\sqrt{2}}\right) &= \exp\left(\frac{2i}{F_\pi}\boldsymbol{\phi}\right) \; , \\
A^L_\mu &= \tfrac{1}{2}(V_\mu + A_\mu) \; , \\
A^R_\mu &= \tfrac{1}{2}(V_\mu - A_\mu) \; , \\
F^{L,R}_{\mu\nu} &= \partial_\mu A^{L,R}_\nu - \partial_\nu A^{L,R}_\mu - i g_0 \left[A^{L,R}_\mu, A^{L,R}_\nu\right] \; , \\
D_\mu U &= \partial_\mu U - i g_0 A^L_\mu U + i g_0 U A^R_\mu \; , \\
M &= \frac{2}{3}\left[m_K^2 + \frac{1}{2}m_\pi^2\right] - \frac{2}{\sqrt{3}}(m_K^2 - m_\pi^2)\lambda_8 \; .
\end{aligned} \tag{2.65}
$$

λ_i is a Gell-Mann matrix, $F_\pi = 135$ MeV. ϕ, V_μ and A_μ are matrices of the pseudo-scalar, vector and axial vector meson fields of the Lagrangian. The strange and non-strange fields are treated coherently. The reactions from the above Lagrangian Eq. (2.64) can be categorized as: $X + Y \to Z + \gamma$, $\rho \to Y + Z + \gamma$ and $K^* \to Y + Z + \gamma$. For X, Y, Z we have each combination of ρ, π, K^*, K mesons which respect to the conservation of charge, isospin, strangeness and G-parity defined for non-strange mesons. All possible s, t and u channels(Born graphs) are taken into account including all possible isospin combinations. The axial a_1 meson has been considered as exchange particle only (the

$a_1 \rightarrow \pi\gamma$ decay is automatically incorporated via s-channel $\pi\rho$ scattering). The Feynman diagrams for all possible isospins of particular process $\pi\rho \rightarrow \pi\gamma$ and $\rho \rightarrow \pi\pi\gamma$ have been displayed in Fig. 2.9. The production from the process $\rho \rightarrow \pi\pi\gamma$ is not considered from the above mentioned Lagrangian rather we consider

$$\mathcal{L} = \mid D_\mu\Phi \mid^2 - m_\pi^2 \mid \Phi \mid^2 - \frac{1}{4}\rho_{\mu\nu}\rho^{\mu\nu} + \frac{1}{2}m_\rho^2\rho_\mu\rho^\mu - \frac{1}{4}F_{\mu\nu}F^{\mu\nu} \tag{2.66}$$

where,

$$D_\mu = \partial_\mu - ieA_\mu - ig_\rho\rho_\mu,$$

Φ is the complex pion field(pseudo scalar field), $\rho_{\mu\nu}$ is the ρ field strength and $F_{\mu\nu}$ is the photon field tensor. The thermal photon production rates are obtained from the coherently summed matrix elements in each channel, and convenient parameterizations are used as in [87]. We assume a standard dipole form for each hadronic vertex appearing in the amplitudes to take care of the finite size effect,

$$F(t) = \left(\frac{2\Lambda^2}{2\Lambda^2 - t}\right)^2 . \tag{2.67}$$

Λ is taken as 1 GeV [91]. The four-momentum transfer is approximated in a given t-channel exchange of meson X by its average $\bar{t}$ according to

$$\left(\frac{1}{m_X^2 - \bar{t}}\right)^2 \left(\frac{2\Lambda^2}{2\Lambda^2 - \bar{t}}\right)^8 = \frac{1}{4E^2}\int_0^{4E^2} \frac{dt(2\Lambda^2)^8}{(m_X^2 + t)^2(2\Lambda^2 + t)^8} . \tag{2.68}$$

. Here the form factors are considered for t-channel only. Since for high energy photons, the t-channel diagram dominates over s-channel diagram because of the large $\frac{1}{t^2}$ enhancement when there is a direct exchange between the incoming particle 1 and emitted photon, and the small $\frac{1}{s^2}$ factor for the s-channel (phase space which favors larger s, for higher photon energy). As cross section is dominated by t-channel diagram the

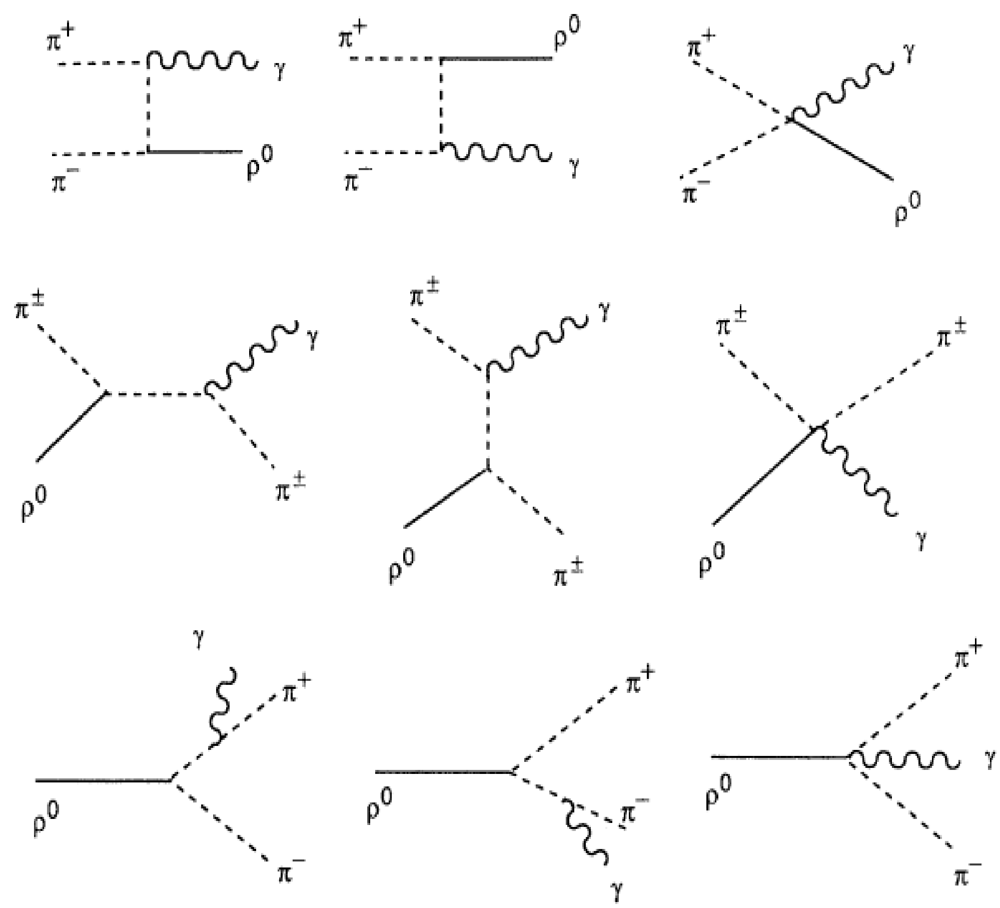

Figure 2.9: Feynman diagrams for all isospin combinations of reactions $\pi\rho \rightarrow \pi\gamma$ and $\rho \rightarrow \pi\pi\gamma$

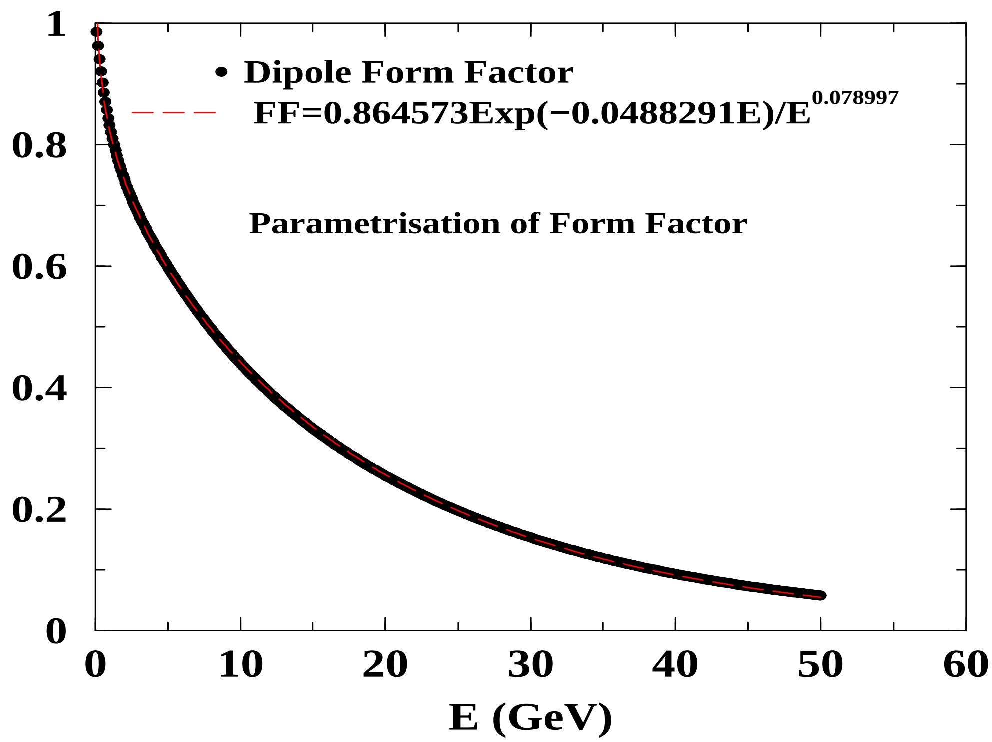

Figure 2.10: Parametrization of the form factor

form factor is evaluated assuming an exchange of particle X in a t-channel diagram. The form factor is parametrized as shown in Fig. 2.10.

The photon productions processes from non strange hadrons can be written as; $\pi\rho \to \pi\gamma$, $\pi\pi \to \rho\gamma$, $\pi\pi \to \eta\gamma$, $\pi\eta \to \pi\gamma$, $\rho \to \pi\pi\gamma$, $\omega \to \pi\gamma$. Similarly the reactions included in strange sector are: $\pi K^* \to K\gamma$, $\pi K \to K^*\gamma$, $K\rho \to K\gamma$, $KK \to \rho\gamma$, $KK^* \to \pi\gamma$, and $K^* \to \pi K\gamma$. All possible isospin combinations are accounted for in the rate calculations [87]. For a temperature of 200 MeV, the leading production channels are shown in Fig. 2.11, with the inclusion of form factor expressed in 2.68. The contribution from strange sector is displayed in Fig 2.12. The comparison from the

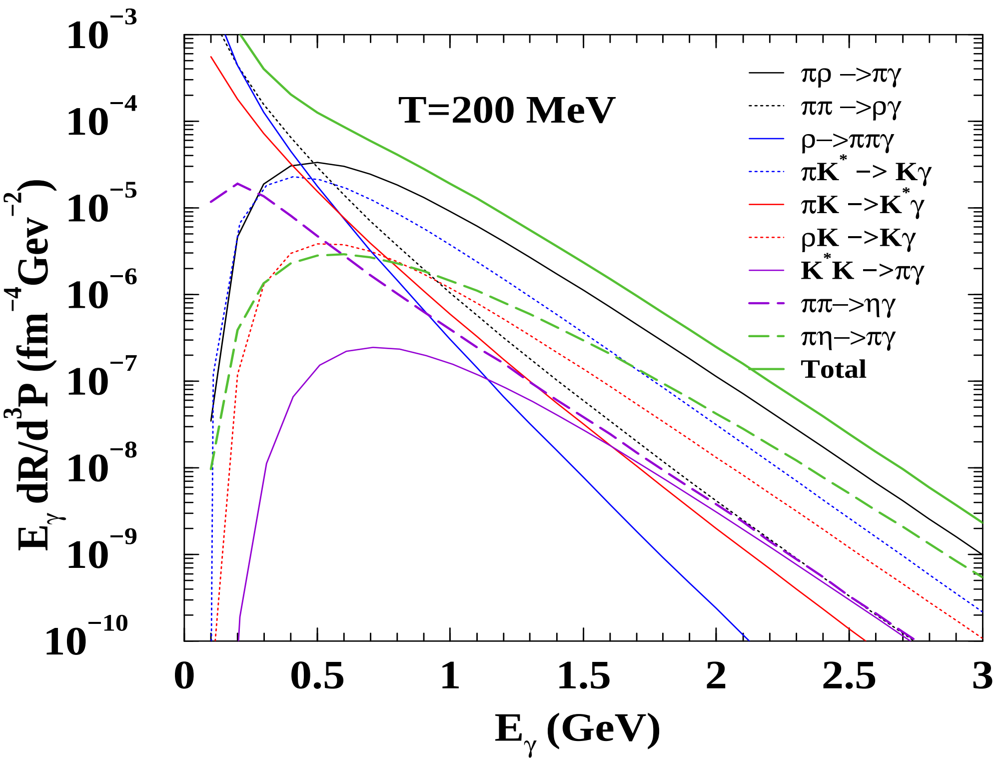

Figure 2.11: Photon rates from different processes

contributions from strange sector and non strange sectors are displayed in Fig. 2.13.

The contributions from $KK \to \rho\gamma$ and $K^* \to \pi K\gamma$ have negligible contributions. At all energies $E_\gamma \geq 0.5$ GeV [2], the $K^*\pi \to K\gamma$ reaction, shows to be the dominant source of photon emission source for strange sector and the $\pi\rho \to \pi\gamma$ reaction in the non-strange sector. Finally we show the comparison of photon production rate from hadronic matter and QGP matter at a temperature 200 MeV. Now it is clear from the Fig. 2.14 that the photon production rates at temperature $T \sim 200$ MeV from QGP and hadronic matter are similar at very low energy or p_T. But the QGP rate is higher compared to hadron rate by a factor of 1.5 for E= 1-3 GeV.

[2]photon energy $E_\gamma = q_0 = E$

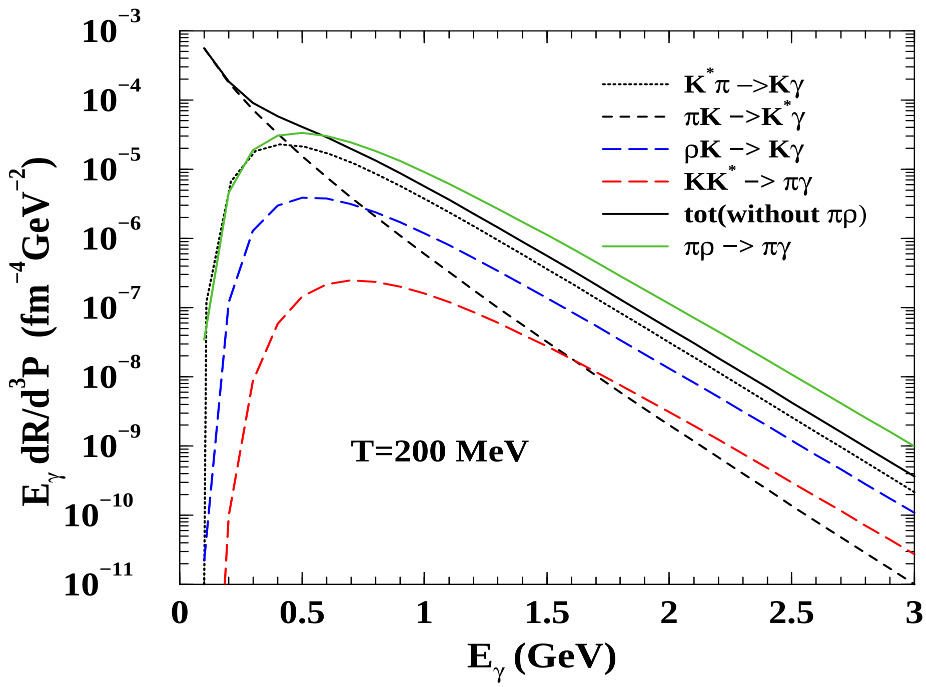

Figure 2.12: Photon rates from processes involving strange mesons

2.4 Dilepton emission rate from QGP and hadronic matter

Thermal dilepton production per unit space-time volume per unit four momentum is given by[67, 92, 69]

$$\frac{dR}{d^4q} = -\frac{\alpha^2}{6\pi^3 q^2} L(M^2) f_{\rm BE}(q_0) W^\mu_\mu(q_0, \vec{q}) \tag{2.69}$$

where α is the electromagnetic coupling, W^μ_μ is the correlator of electromagnetic currents and $f_{\rm BE}(q_0, T)$ is the thermal phase space factor for bosons. The factor

$$L(M^2) = \left(1 + 2\frac{m^2}{M^2}\right)\sqrt{1 - 4\frac{m^2}{M^2}} \tag{2.70}$$

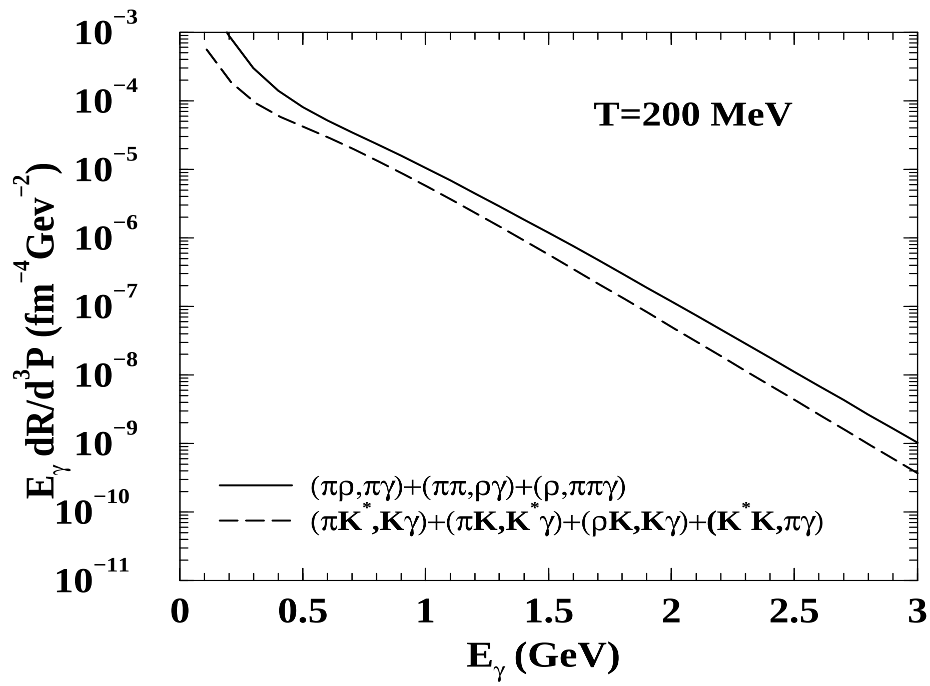

Figure 2.13: Photon rates from processes involving strange mesons

arises from the final state leptonic current involving Dirac spinors of mass m (in this case muon) and $q^2(=q_\mu q^\mu)=M^2$ is the invariant mass square of the lepton pair.

2.4.1 Dilepton emission rate from hadronic matter

In hadronic matter, this Eq. 2.69 can be simplified using vector meson dominance model to give (see [93] for details) [3],

$$\frac{dR}{dM^2 q_T dq_T dy} = \frac{\alpha^2}{\pi^2 M^2} L(M^2) f_{\rm BE}(q_0) \sum_{V=\rho,\omega,\phi} A_V(q_0,\vec{q}) \tag{2.71}$$

[3] $\frac{dR}{d^4q} = \frac{dR}{\pi dM^2 q_T dq_T dy}$

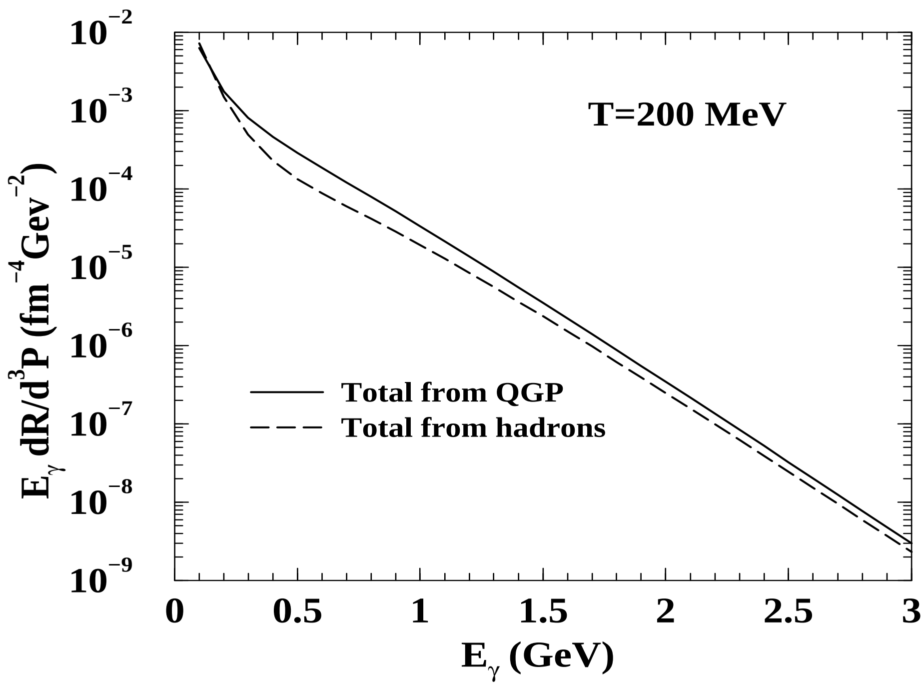

Figure 2.14: Photon rates from QGP and Hadron at T=200 MeV

where M is the invariant mass and q_T is the transverse momentum of the pair, y is the rapidity. Where the spectral function of the vector mesons consists of a pole and continuum,

$$A_V = A_V^{\text{pole}} + A_V^{\text{cont}} \tag{2.72}$$

For the ρ, the continuum part is parametrized as [71, 94]

$$A_\rho^{\text{cont}} = \frac{M^2}{8\pi}\left(1 + \frac{\alpha_s}{\pi}\right)\frac{1}{1 + \exp(\omega_0 - q_0)/\delta} \tag{2.73}$$

with $\omega_0 = 1.3$ GeV and $\delta = 0.2$ GeV and the pole part is given by [93]

$$\begin{aligned} A_\rho^{\text{pole}} \quad = \quad & -\frac{f_\rho^2 m_\rho^2}{3}\left[\frac{2\sum \text{Im}\Pi_t^R}{(q^2 - m_\rho^2 - \sum \text{Re}\Pi_t^R)^2 + (\sum \text{Im}\Pi_t^R)^2}\right. \\ & \left. + \frac{q^2 \sum \text{Im}\Pi_l^R}{(q^2 - m_\rho^2 - q^2 \sum \text{Re}\Pi_l^R)^2 + q^4(\sum \text{Im}\Pi_l^R)^2}\right] \end{aligned} \tag{2.74}$$

with $f_\rho = 0.130$ GeV. As we have included the continuum in the vector mesons spectral functions four pion annihilation process [95] is not considered here to avoid over counting. The self-energy Π contains contributions from mesons as well as baryons in the thermal medium so that

$$\Pi = \Pi_M + \Pi_B \tag{2.75}$$

The longitudinal and transverse components of the meson part Π_M have been evaluated in detail for one loop $\pi - h$ graphs with $h = \pi, \omega, h_1, a_1$ in the real time formulation of thermal field theory [93]. The baryonic contribution Π_B has been estimated in the approach of Eletsky et al [96] using resonance dominance in the low energy region and a Regge model at higher energies. Dilepton emission from the ω and the ϕ have also been included. The width of the ω in thermal bath is taken from the calculation of Ref [97]. For the ϕ only the vacuum width has been considered.

2.4.2 Dilepton emission rate from QGP

In the QGP phase the emission rate of non-thermalized dileptons or lepton pairs are calculated by factorizing the electromagnetic current and focusing on the emission rate of a time-like virtual photon with energy $p_0 = E$ and invariant mass M. In this approach the dilepton rate is of the form [67, 63]

$$\frac{dR}{d^4q} = \frac{dR}{\pi dM^2 q_T dq_T dy} = \frac{\alpha}{12\pi^4 M^2}\Gamma(q) \tag{2.76}$$

where $\Gamma(q)$ is the virtual photon emission rate from the quark gluon plasma (summed over all polarization). The lowest order comes from the quark anti-quark annihilation.

The rate from Born terms is

$$\Gamma^{(0)}(q) = N_c e_q^2 \int \frac{d^4p}{(2\pi)^4} Tr\gamma_\mu S^-(q-p)\gamma^\nu S^-(p) \tag{2.77}$$

where S^- are the cutting fermionic propagator and given as,

$$S^-(p) = 2(\theta(-p_0) - n_F(p))\pi\delta(p^2)\gamma^\mu p_\mu \tag{2.78}$$

n_F is the usual Fermi-Dirac weight. N_c is the number of colors. Further simplification with N_c=3 gives

$$\Gamma^{(0)}(q) = \frac{10\alpha}{3} M^2 e^{-E/T}(1 + O(T/E)) \tag{2.79}$$

Here only $u\bar{u}$ and $d\bar{d}$ annihilations are taken into account. This term is leading one when the energy and mass M is higher than temperature T. If the dilepton mass becomes small compared to the energy and temperature then the higher order terms contribute significantly. The annihilation of quark-antiquark pair is the major source of dilepton production ($q\bar{q} \rightarrow l^+l^-$) in the partonic phase. The rate of production from this processes at finite temperature and quark (1/3$\times$baryonic) chemical potential is taken from [98]. The next order contributions (first order QCD radiative corrections) come from the diagrams shown in Fig. 2.15. With first order correction, the rate of virtual photon production for processes like gluon emission (quark anti-quark annihilation, $q\bar{q} \rightarrow g\gamma^*$) and the Compton reaction ($q(\bar{q})g \rightarrow q(\bar{q})\gamma^*$) is given by

$$\Gamma^1(q) = \frac{20\alpha}{3} m_\beta^2 e^{-E/T} \left[ln\frac{2ET}{M^2} - 1 - \gamma + \frac{ln2}{3} + \frac{\xi'(2)}{\xi(2)} \right] \tag{2.80}$$

where $m_\beta^2 = 2\pi\alpha_s T^2/3$ and ξ is the Riemann zeta function. Other first order process like gluon absorption ($q\bar{q}g \rightarrow \gamma^*$) and virtual corrections also can contribute to the net rate. But these processes are kinetically suppressed because of phase space constraint [99].

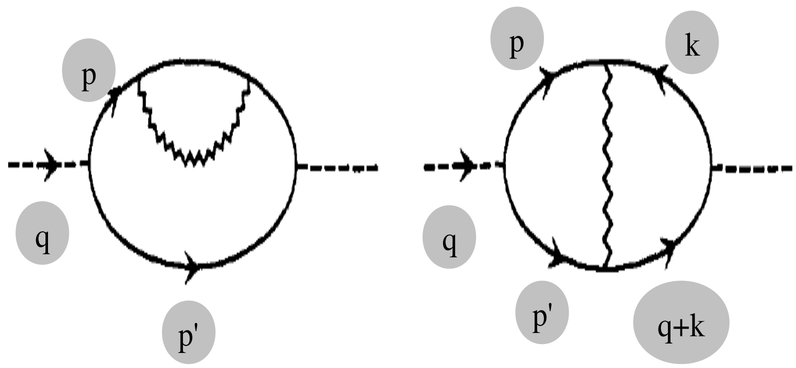

Figure 2.15: Diagrams for the 1st order QCD correction

Here we have considered the dilepton production (from the virtual photon productions) up to $\mathbf{O}(\alpha^2\alpha_s)$ corrections according to Ref. [99, 100]. However, we found that the effects of this corrections is about 8% for $M \sim 0.3$ GeV and it is negligible at higher M.

The Eqs. 2.71 and 2.76 have been integrated over q_T (for y=0) and the rates (of dimuon-$\mu^+\mu^-$) from QGP and hadronic matter have been displayed in Fig. 2.16.

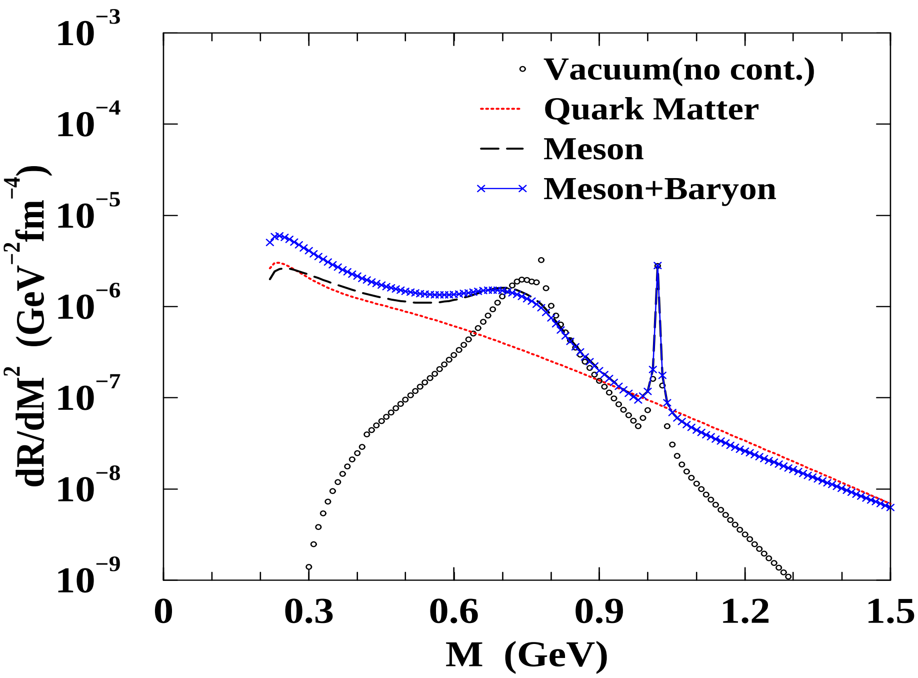

Figure 2.16: Rate of dilepton production from thermal medium. The curve with open circles is from the vacuum contribution (no continuum). The dotted curve represents the rate from quark matter only. The long-dashed curve represents the rate from hadronic medium where the self energy contains the contribution from mesons only. The solid (with star) curve represents the dilepton rate from hadronic matter where self energy contains the contributions from both mesons and baryons.

Chapter 3

Expansion scenario in the relativistic nuclear collisions

This chapter discusses the dynamics of the expansion of the system produced in heavy ion collision. Here we discuss the relativistic ideal hydrodynamics with boost invariance and cylindrical symmetry. We also outline the boundary conditions and different equation of states considered as the inputs to our calculation.

The hot and dense system formed in the relativistic nuclear collisions expands due to the high pressure gradient created at the collision zone. It is assumed that the system attains the local thermal equilibrium shortly due to the re-scattering among the particles. The expansion of the system can be treated by relativistic hydrodynamics. Hydrodynamics is the long wavelength and long-time effective theory of macroscopic systems [101, 102, 103]. The hydrodynamic equation (to be discussed later) along with the equation of state gives a complete description of the system evolving with space and time. The simplest version of the theory is ideal hydrodynamics that assumes the thermal (local for expanding system) equilibrium to be maintained through out the evolution of the system neglecting all the dissipative effects. If the scattering time of the constituents is much smaller than the expansion time and the mean free path of the system is smaller than the system size then it is safe to apply hydrodynamics. The relativistic hydrodynamics developed over the years [104, 105, 106, 107, 108], and now reformulated in the context of heavy ion collision [109, 110, 111, 112, 113, 114, 115, 116, 117, 118] is found to be successful in describing many of the observables like transverse momentum spectra of hadrons, photons, lepton pairs, invariant mass spectra of lepton pairs, flow, rapidity distribution of hadrons *etc* [51, 52, 55, 119, 120, 121]. Here in this chapter we discuss the basics of relativistic hydrodynamics [101, 122] related to our calculation.

3.1 Relativistic hydrodynamics of ideal fluid

As the system reaches thermodynamic equilibrium we treat the system to be an ideal fluid. Then from the basic conservation laws, we get,

$$\partial_\mu T^{\mu\nu} = 0 \qquad \text{Energy-momentum conservation} \tag{3.1}$$

$$\partial_\mu {j_B}^\mu = 0 \qquad \text{Baryon number conservation} \tag{3.2}$$

where $T_{\mu\nu}$ is the energy-momentum tensor and ${j_B}^\mu$ is the baryon-number-current with μ, ν=0,1,2 and 3. Here we assume fluid to be homogeneous and isotropic *i.e.,* the properties of the fluid element in the concerned frame of reference is isotropic. Also we assume the fluid to be composed of a single particle species. we need to construct the energy momentum tensor-$T_{\mu\nu}$ with the definition of velocity from a frame of reference.

3.1.1 Choice of frame

We consider the rest frame where the momentum of the fluid element is zero. The thermodynamic variables are to be defined in this rest frame. The thermodynamic variables of our interest are energy density ϵ, pressure P and number density n_B that are associated with the fluid element. The fluid-four velocity is defined as

$$u^\mu = (u^0, u^i) = \gamma(1, \vec{v}) = \gamma(1, v_x, v_y, v_z)$$
$$\text{and} \qquad u^\mu u_\mu = 1 \tag{3.3}$$

where the Lorentz factor $\gamma=\frac{1}{\sqrt{1-v^2}}$ and the metric tensor is $g^{\mu\nu}$=diag(1,-1,-1,-1). The derivative of γ is written as $d\gamma = \gamma^3 v^i dv^i$ and $vdv = \gamma^{-3}d\gamma$. where $v = \sqrt{v_x^2 + v_y^2 + v_z^2} = \sqrt{v_\perp^2 + v_z^2}$ and $v_\perp$ is the magnitude of transverse velocity. The total time derivative in the Cartesian co-ordinates reads as

$$\frac{d}{dt} = \frac{\partial}{\partial t} + v_x \frac{\partial}{\partial x} + v_y \frac{\partial}{\partial y} + v_z \frac{\partial}{\partial z} \tag{3.4}$$

In cylindrical coordinates it has the form,

$$\frac{d}{dt} = \frac{\partial}{\partial t} + v_\perp cos\alpha \frac{\partial}{\partial r} + \frac{v_\perp sin\alpha}{r} \frac{\partial}{\partial \phi} + v_z \frac{\partial}{\partial z} \tag{3.5}$$

α is the angle between the transverse velocity $v_\perp$ and radial velocity v_r i.e., v_r=$v_\perp cos\alpha$, $v_\phi = v_\perp sin\alpha$.

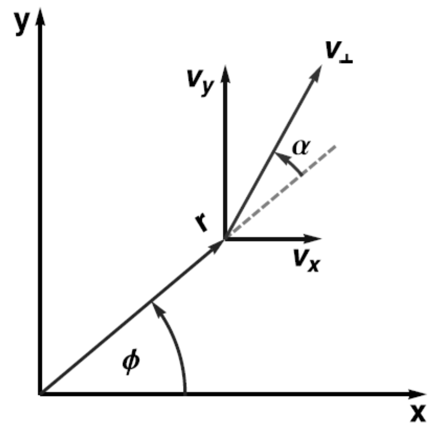

Figure 3.1: Velocity components

3.1.2 Construction of the energy-momentum tensor

The energy momentum tensor of the fluid element in the local rest frame is given by,

$$T_0^{\mu\nu} = diag[\epsilon, -P, -P, -P] \tag{3.6}$$

$$T_0^{\mu\nu} = \begin{pmatrix} \epsilon & 0 & 0 & 0 \\ 0 & -P & 0 & 0 \\ 0 & 0 & -P & 0 \\ 0 & 0 & 0 & -P \end{pmatrix} \tag{3.7}$$

Since these thermodynamic variables are isotropic in the rest frame of the fluid element, the other non-diagonal component of the energy momentum tensor *i.e.,* the energy flux T_{i0} and the momentum density T_{0j} would vanish in the rest frame of the fluid. *i.e,* $T_{ij} = P\delta_{ij}$. Now let's go to a frame which is moving with velocity $\vec{v}$. In this frame the $T^{\mu\nu}$ is given by,

$$T^{\mu\nu} = \Lambda_\alpha{}^\mu \Lambda_\beta{}^\nu T_0{}^{\alpha\beta} \tag{3.8}$$

where Λ, the Lorentz transformation matrix [101, 123] that contains the velocity components is given by;

$$\Lambda = \begin{pmatrix} 1 & v_x & v_y & v_z \\ v_x & 1 & 0 & 0 \\ v_y & 0 & 1 & 0 \\ v_z & 0 & 0 & 1 \end{pmatrix} \tag{3.9}$$

The 4 energy-momentum tensor for an arbitrary fluid velocity becomes,

$$T^{\mu\nu} = \begin{pmatrix} \epsilon & (\epsilon + P)v_x & (\epsilon + P)v_y & (\epsilon + P)v_z \\ (\epsilon + P)v_x & P & 0 & 0 \\ (\epsilon + P)v_y & 0 & P & 0 \\ (\epsilon + P)v_z & 0 & 0 & P \end{pmatrix} \tag{3.10}$$

which can be written in a compact form;

$$T^{\mu\nu} = (\epsilon + P)u^{\mu}u^{\nu} - Pg^{\mu\nu}. \tag{3.11}$$

This is the energy momentum-tensor for an ideal fluid.

3.1.3 Solution of the conservation Equations

The conservation of the energy momentum tensor of the perfect fluid in its most general form is

$$\partial_{\mu}[(\epsilon + P)u^{\mu}u^{\nu} - Pg^{\mu\nu}] = 0 \tag{3.12}$$

The first law of thermodynamics gives

$$
\begin{aligned}
d\epsilon &= Tds - pdV + \mu dn \\
dP &= sdT + nd\mu \qquad (3.13)
\end{aligned}
$$

where s is the entropy density, T is the temperature, $p = P/V$ and μ is the chemical potential (baryonic). The entropy density is given by the Durham-Gibbs relation

$$
\begin{aligned}
s &= \frac{\epsilon + P}{T} - \alpha n \\
Ts &= (\epsilon + P) - \mu n \qquad (3.14)
\end{aligned}
$$

where $\alpha = \frac{\mu}{T}$. For $\mu = 0$ we get $Ts = (\epsilon + P)$ and $dP = sdT$. With these substitution we have,

$$Tu^\nu \partial_\mu (su^\mu) + su^\mu \partial_\mu (Tu^\nu) = s\partial^\nu T. \qquad (3.15)$$

Multiplying both sides by u_ν and using the normalization condition for the 4-velocity, $u_\nu u^\nu = 1$ we arrive at

$$T\partial_\mu (su^\mu) + su^\mu T u_\nu \partial_\mu u^\nu + su^\mu \partial_\mu T = su_\nu \partial^\nu T. \qquad (3.16)$$

The term $u_\nu \partial_\mu u^\nu = 0$ because of the 4 velocity normalization condition. Thus above expression simplifies to

$$
\begin{aligned}
&T\partial_\mu (su^\mu) + su^\mu \partial_\mu T = su_\nu \partial^\nu T \\
&\text{which gives,} \qquad \partial_\mu (su^\mu) = 0. \qquad (3.17)
\end{aligned}
$$

This equation expresses the entropy conservation in the system - the hydrodynamic expansion is adiabatic. Putting Eq. 3.17 in to the Eq. 3.15, we get

$$u^\mu \partial_\mu (Tu^\nu) = \partial^\nu T \qquad (3.18)$$

The Eq. 3.18 is the acceleration equation which is nothing but the the relativistic generalization of the Euler equation for the classical fluid dynamics. The final form of the hydrodynamic equations in the co-variant form are

$$u^\mu \partial_\mu (T u^\nu) = \partial^\nu T$$
$$\partial_\mu (s u^\mu) = 0 \tag{3.19}$$

These equations do not form a closed system since they contain five independent variables T, s, v_x, v_y,and v_z. An additional equation, that is the equation of state (EoS) is required to close them. Since the equations are in T ans s we need the EoS in terms of T and s ($c_s^2 = \frac{\partial P}{\partial \epsilon} = \frac{s}{T}\frac{\partial T}{\partial s}$). Similarly here we can also construct the hydrodynamic equations in terms of energy density and pressure. We can write the equations of temperature and entropy in non-covariant way as follows;

$$\frac{\partial}{\partial t}(T\gamma v^i) + \nabla^i (T\gamma) = v^j \nabla^i (T\gamma v^i) - v^j \nabla^j (T\gamma v^i)$$
$$\frac{\partial}{\partial t}(s\gamma) + \nabla.(s\gamma v) = 0 \tag{3.20}$$

1. **Boost invariance (Cartesian coordinates):** The particle yields do not vary much with rapidity at mid-rapidity region. One can safely consider the number of particle per unity rapidity (dN/dy) is constant in the range of $|y| \leq 1$. Hence the mid rapidity zone can be assumed to be boost invariant and the symmetry demands that the longitudinal component of velocity has the form $v_z = z/t$ [124]. The thermodynamic scalar variables like temperature and entropy density are the functions of proper time $\tau = \sqrt{t^2 - z^2}$ and the transverse coordinates x and y. That is we can solve the hydrodynamic equation for $z = 0$ and by using Lorentz transformations we obtain the solution for $z \neq 0$.

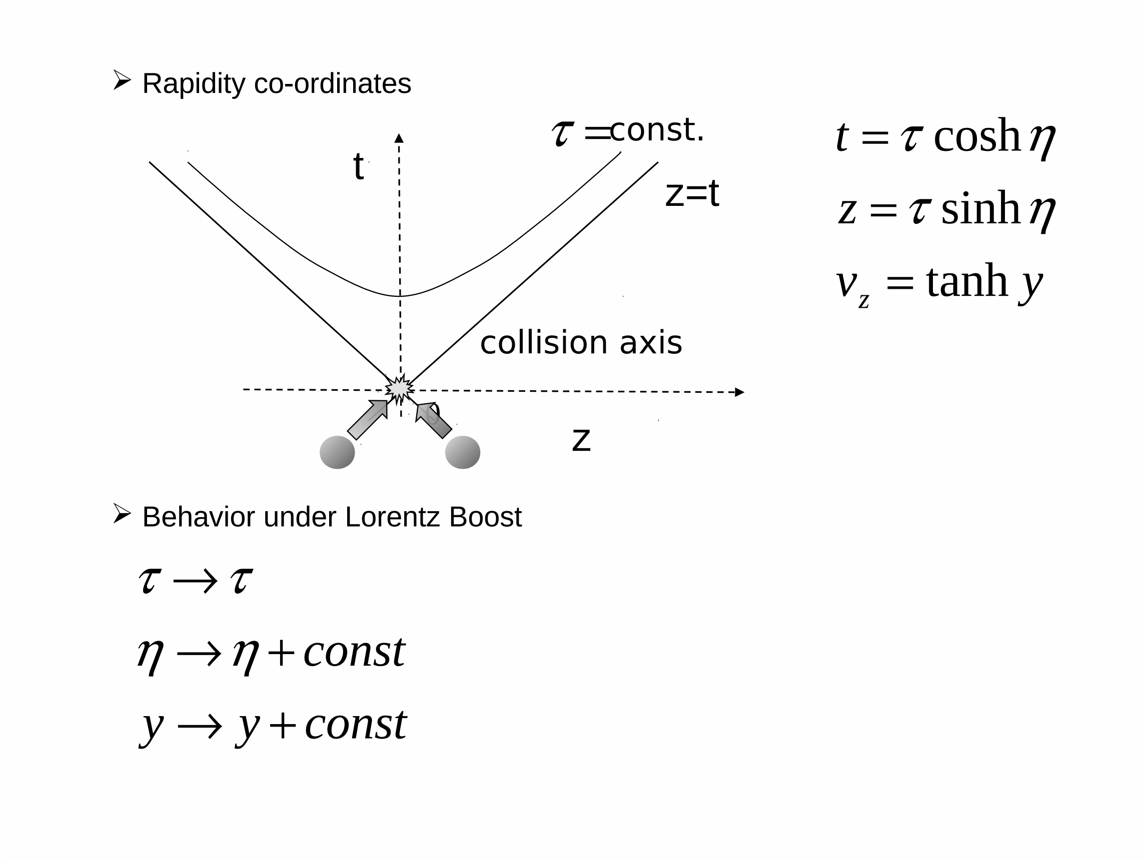

Figure 3.2: Boost invariance.

Azimuthal symmetry or cylindrical symmetry with boost invariance

If we assume azimuthal symmetry with the boost invariance along z-axis then the hydrodynamic equations will be simpler. In this case the temperature equations in Cartesian co-ordinates become,

$$(v^2-1)\frac{\partial lnT}{\partial t}+\frac{dlnT}{dt}+\frac{1}{1-v^2}v\frac{dv}{dt}=0. \tag{3.21}$$

$$(1-v^2)\frac{\partial lnT}{\partial z}+v_z\frac{dlnT}{dt}+\frac{dv_z}{dt}+\frac{v_z}{1-v^2}v\frac{dv}{dt}=0. \tag{3.22}$$

These equations have the same form in cylindrical coordinates. Combining both the boost invariance and cylindrical symmetry gives us only one independent equation

$$v_r\frac{\partial lnT}{\partial t}+\frac{\partial lnT}{\partial r}+\frac{1}{1-v_r^2}\frac{\partial v_r}{\partial t}+\frac{v_r}{1-v_r^2}\frac{dv}{dt}=0 \tag{3.23}$$

[*It may be noted that in the case of first order phase transition at zero baryon chemical potential, another equation is required to deal with the the fraction of hadron (or QGP) in the mixed phase.*] The entropy equation for cylindrical symmetry with boost invariance becomes

$$\frac{\partial lns}{\partial t}+v_r\frac{\partial lns}{\partial r}+\frac{v_r}{1-v_r^2}\frac{\partial v_r}{\partial t}+\frac{1}{1-v_r^2}\frac{\partial v_r}{\partial r}+\frac{v_r}{r}+\frac{1}{t}=0 \tag{3.24}$$

To make it simpler let's change the coordinates from $(t,\vec{r})=(t,x,y,z)=(t,r,\phi,z)$ to (τ,r,ϕ,η), where η can be expressed as;

$$\eta=\frac{1}{2}\ln\left[\frac{t+z}{t-z}\right]=\tanh^{-1}(z/t) \tag{3.25}$$

The fluid velocity is expressed as

$$u^\mu=\gamma_T(\tau,r)(t/\tau,v_r(\tau,r),z/\tau) \tag{3.26}$$

where

$$\gamma_T = 1/\sqrt{1 - v_r^2} \quad , \qquad v_r^2 = v_x^2 + v_y^2 = v_\perp^2 \tag{3.27}$$

where the radial velocity v_r and transverse velocity $v_\perp$ of the fluid element are same.$\tau = \sqrt{t^2 - z^2}$ is the proper time. The assumption of boost invariance and azimuthal asymmetry simplifies the hydrodynamic equations. Now let's describe the hydrodynamic equations in terms of energy density ϵ and pressure P with fluid velocities as a function of r and τ.

$$T^{00} = (\epsilon + P)u^0u^0 - P \tag{3.28}$$

and

$$T^{01} = (\epsilon + P)u^0u^1 \tag{3.29}$$

the hydrodynamic equations are [125]

$$\partial_r T^{00} + \frac{1}{r}\partial_r(rT^{01}) + \frac{1}{\tau}\partial_r(T^{00} + P) = 0 \tag{3.30}$$

and

$$\partial_r T^{01} + \frac{1}{r}\partial_r[r(T^0 + P)v_r^2] + \frac{1}{\tau}T^{01} + \partial_r P = 0 \tag{3.31}$$

These equations are solved numerically with the following boundary conditions (initial and final conditions).

3.2 Boundary Conditions and EoS

Hydrodynamic equations are boundary value problems which require initial and final conditions to describe the dynamics of a system at any intermediate stage. Here in case of ideal hydrodynamics for heavy ion collision we need the initial temperature (or energy density), velocity profile, initial time (here called as thermalisation time) and equation of state (EoS). We need a freeze out temperature (T_f) or energy density(ϵ_f) to stop the calculation.

1. Initial conditions

The matter formed after ultra-relativistic heavy ion collisions is assumed to undergo space-time evolution [125] with longitudinal boost invariance [124] and cylindrical symmetry. The initial conditions for the hydrodynamical evolution are not unambiguously known. Some parametrization based on Glauber approach or some other form of the initial stage may be considered so that the final multiplicity of the observed charge hadrons is reproduced. In case of Glauber approach a mixture of soft and hard collisions (90% soft, 10% hard for RHIC energies and it depends on the colliding energy) are accounted to reproduce the centrality dependence of charge hadron multiplicity spectra where a novel parametrization of longitudinal structure of initial fireball is assumed [126, 127]. One can also consider the initial conditions (like the space-time dependence of initial energy density) using Color Glass Condensate (CGC) model [128].

Here we consider a simple initial energy density $\epsilon(\tau_i, r)$ (with a central flat region) and radial velocity, $v_r(\tau_i, r)$ profiles as follows:

$$\epsilon(\tau_i, r) = \frac{\epsilon_0}{1 + e^{\frac{r-R_A}{\delta}}} \tag{3.32}$$

and

$$v_r(\tau_i, r) = v_0 \left(1 - \frac{1}{1 + e^{\frac{r-R_A}{\delta}}}\right), \tag{3.33}$$

which reproduce the charge hadron multiplicity with proper value of ϵ_0. where the surface thickness, $\delta = 0.5$ fm. An smooth energy density profile with a peak at the center may require higher ϵ_0 to explain the spectra (of photons and dileptons in our case) compared to the one we consider here. $\epsilon_0 = \epsilon_i$ is the initial central energy density which is calculated from the initial temperature constrained with initial thermalisation time τ_i from the experimentally measured multiplicity as follows [129];

$$T_i^3\tau_i \approx \frac{2\pi^4}{45\xi(3)}\frac{1}{4a_{eff}}\frac{1}{\pi R_A^2}\frac{dN}{dy}. \tag{3.34}$$

where, dN/dy= hadron multiplicity, R_A is the radius of the system, $\xi(3)$ is the Riemann zeta function and $a_{eff} = \pi^2 g_{eff}/90$, where g_{eff} is the effective degeneracy of the produced initial system. If it is QGP then the effective degeneracy $g_{eff} = 2 \times 8 + 7 \times 2 \times 2 \times 3 \times N_F/8$ assuming massless quarks and gluons. N_F=number of flavors. The above expression is valid for isentropic expansion (at mid-rapidity). Here it is important to mention that in this thesis we have assumed the initial states in the heavy ion collisions to be QGP or hadronic phase depending on the colliding energies of different nucleus-nucleus collisions.

2. Equation of state (EoS)

EoS is the thermodynamic relationship between two thermodynamic parameters. It is an important ingredient for hydrodynamic calculation. Here we express the pressure, P in terms of the energy density ϵ , *i.e.*, $P = f(\epsilon)$. The relevant equation of states for the high energy nuclear collisions are

(a) **MIT BAG Model equation of state:** The energy density and pressure of QGP according to this model is given by,

$$\begin{aligned}
\epsilon_{qgp} &= \frac{\pi^2}{30} g_{qgp} T^4 + B \\
P_{qgp} &= \frac{\pi^2}{90} g_{qgp} T^4 - B
\end{aligned} \tag{3.35}$$

where B is the Bag constant and from hadron spectroscopy the value is $\sim$ 200 MeV. g_{qgp} is the effective degeneracy of qgp (g_{eff}). The above equation gives $\epsilon - 3P = 4B$. This leads to

$$P_{qgp} = \frac{\epsilon_{qgp} - 4B}{3} \tag{3.36}$$

It gives,

$$\frac{\partial P_{qgp}}{\partial \epsilon_{qgp}} = \frac{1}{3} or \qquad c_s^2 = \frac{1}{3} \tag{3.37}$$

Where c_s is the velocity of sound. Similarly in the hadronic phase the parameters are

$$\begin{aligned}
\epsilon_{had} &= \frac{\pi^2}{30} g_{had} T^4 \\
P_{had} &= \frac{\pi^2}{90} g_{had} T^4
\end{aligned} \tag{3.38}$$

Here an first order phase transition is assumed occur from hadronic phase to QGP phase at a temperature T_c called transition temperature. From the above equations 3.38, the equation of state with velocity of sound is given by

$$\begin{aligned}
P_{had} &= \frac{\epsilon_{had}}{3} \\
\frac{\partial P_{had}}{\partial \epsilon_{had}} &= \frac{1}{3} \\
or \qquad {c_s}^2 &= \frac{1}{3}
\end{aligned} \tag{3.39}$$

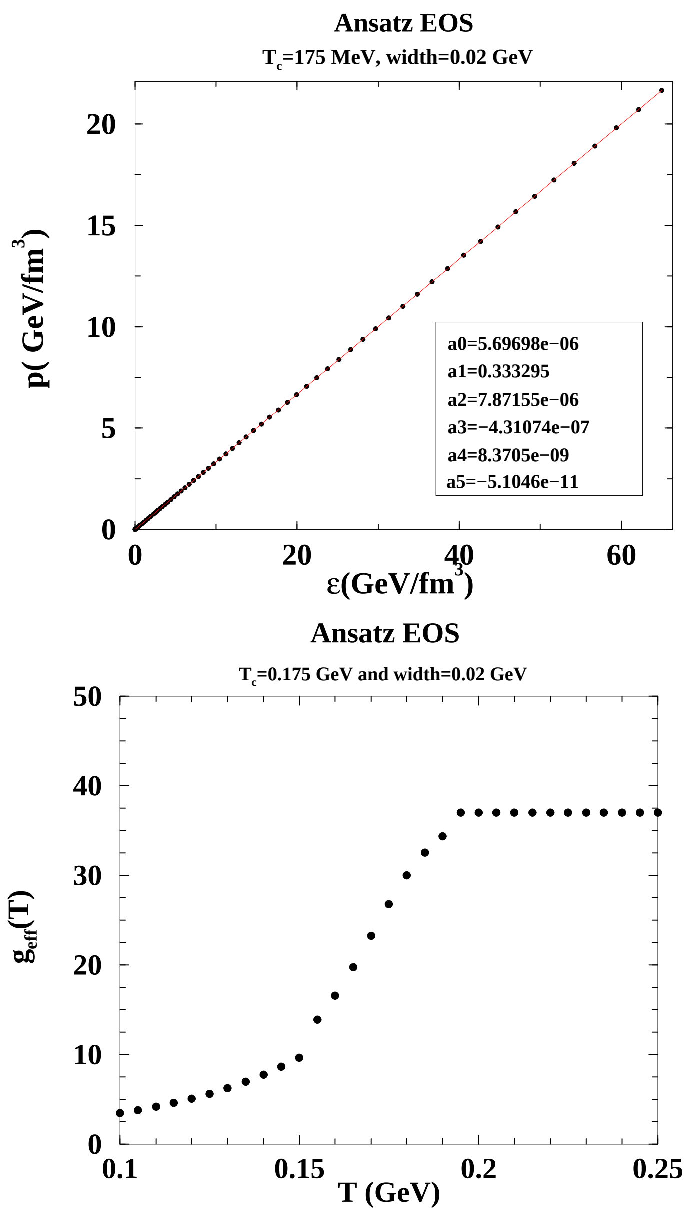

Figure 3.3: **(a)**Top panel: Pressure vs energy density is plotted for ansatz EoS with T_c=175 MeV and width Γ=20 MeV. Which is a weak first order transition. **(b)**Bottom panel: Effective degeneracy extracted from ansatz EoS is plotted with temperature$T$ for T_c=175 MeV and width Γ=20 MeV. Which is a weak first order transition

(b) **BAG-HRG equation of state:** In the BAG-HRG EoS, We use BAG model EoS for QGP phase and for the hadronic phase an EoS is constructed considering a non interacting gas of all the stable hadrons and their resonances up to mass $\leq$ 2.5 GeV. The later one for hadronic phase is called hadronic resonance gas (HRG) EoS. Here also a first order phase transition is assumed from hadronic to QGP phase. In case of first order transition we assume a fast hadronization due to lack of the concrete knowledge of the hadronization.

(c) **Ansatz equation of state:** The ansatz equation of state has been constructed from BAG EoS and HRG EoS. For $T \geq T_c$ the BAG EoS is used to describe the QGP matter and the HRG EoS is used to describe system below T_c. Here it is assumed that the transition does not happen suddenly but within a range Γ, called width of the transition. The transition region is parametrized smoothly using a tan-hyperbolic function. Basically the entropy density which is parametrized [130] as follows;

$$s = f(T)s_q + (1 - f(T))s_h \tag{3.40}$$

where s_q (s_h) is the entropy density of the QGP(hadron) phase at transition temperature T_c. The f is the fraction of QGP at any time during the transition and is given by

$$f(T) = \frac{1}{2}(1 + \tanh(\frac{T - T_c}{\Gamma})) \tag{3.41}$$

The Γ can be varied to make a strong or weak first order. Similarly also we construct the ansatz EoS by replacing BAG EoS with the Lattice EoS. Figure 3.3 shows the variation of P with ϵ for T_c=175 MeV and width Γ=20

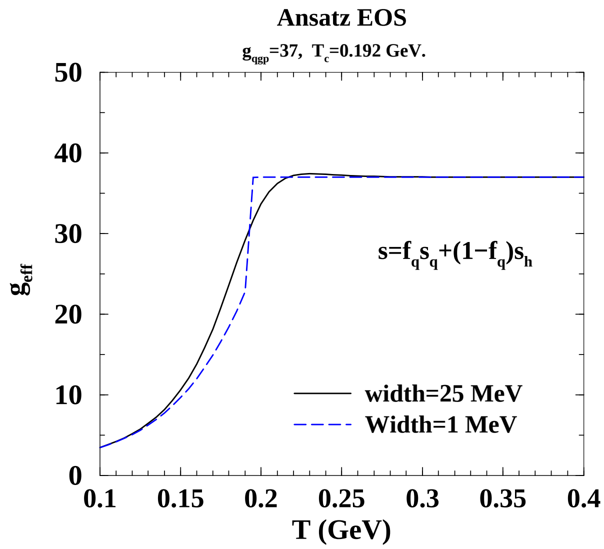

Figure 3.4: Effective degeneracy extracted from ansatz EoS for two different width plotted with temperature$T$ for T_c=192 MeV The difference between strong like first order and a weak first order transition

MeV. Which is like a weak first order transition. The effective degeneracy which shows a smooth continuous change from hadronic QGP phase around the temperature T_c=175 MeV.

(d) **Lattice equation of state** The EoS is constructed at finite temperature from QCD partition function by numerical computations. The QCD Lagrangian is given by,

$$\mathcal{L} = -\frac{1}{4}F^a_{\mu\nu}F^{\mu\nu}_a - \Sigma_f \bar{\psi}^f_\alpha (i\gamma^\mu\partial_\mu + m_f - g\gamma^\mu A_\mu)^{\alpha\beta}\psi^\alpha_\beta \qquad (3.42)$$

with

$$F^a_{\mu\nu} = \partial_\mu A^a_\nu - \partial_\nu A^a_\mu - g f^a_{bc} A^b_\mu A^c_\nu. \qquad (3.43)$$

where A^a_μ denotes the gluon field of color a(a=1,2,....8) and ψ^f_α the quark field of color α (α=1,2,3) and flavor f; the input bare quark masses are given by

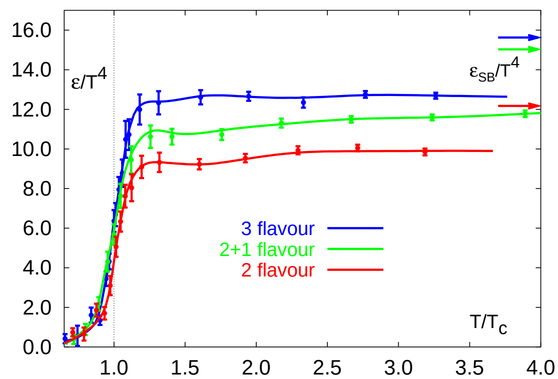

Figure 3.5: Energy density with temperature [131]

m_f. The thermodynamic quantities are obtained from the partition function,

$$Z(T,V) = \int dAd\psi d\bar{\psi} exp(-\int_V d^3x \int_0^{\frac{1}{T}} d\tau \mathcal{L}(A,\psi,\bar{\psi})) \tag{3.44}$$

which is expressed as a functional integral, that involves the Lagrangian density defining the theory. The spatial integration in the exponent of Eq.3.44 is performed over the entire spatial volume V of the system (in the thermodynamic limit it becomes infinite). The time component x_0 is "rotated" to make it purely imaginary, $\tau = ix_0$, thus turning the Minkowski manifold, on which the field A and ψ are originally defined into a Euclidean space. The integration over τ in Eq.3.44 runs over a finite slice whose thickness is determined by the temperature of the system. From the partition function the energy density and pressure are calculated as

$$\begin{aligned} \epsilon &= (T^2/V)(\frac{\partial lnZ}{\partial T})_V \\ P &= T(\frac{\partial lnZ}{\partial V})_T \end{aligned} \tag{3.45}$$

For the study of the critical behavior, long range correlations and multi particle interactions are of crucial importance; hence perturbation theory can not be used. The necessary non-perturbative regularization scheme is provided by the lattice formulation of QCD [12]; it leads to a form which can be evaluated numerically by computer simulation [132].

The energy-density and pressure calculated on the lattice are given as [133]

$$\begin{aligned} P &= cT^4[1 - a(\frac{m_{th}}{T})^2] = cT^4[1 - ag^2(T)] \\ \epsilon &= 3cT^4[1 - ag^2(T) - \frac{2am_{th}}{3}(\frac{dg}{dT})] \end{aligned} \quad (3.46)$$

where c and a are the color and flavor dependent positive constants. m_{th} is the thermal mass of quarks and gluons $m_{th} \equiv g(T)T$ [134, 135, 136]. In the Fig. 3.5 the energy-density calculated from lattice [131] is plotted with temperature.

3. **Freeze out conditions** The last stage of the evolution of a system in heavy ion collision is the freeze out. The two phenomena which keeps the particles in a local equilibrium are; the interactions within the system and the expansion of the system. The particles do interact strongly in heavy ion collision system and the system expands and the particles recede away from each other with the decrease of temperature. When the interactions are not sufficient enough compared to the expansion of the system then the particles start decoupling and lead towards freeze out. There are two freeze out scenarios, chemical and kinetic freeze out which occur sequentially. As temperature falls owing to expansion to a certain value T_{ch} then the inelastic scatterings stop inside the system, that is, the new particle productions are closed and the particle ratios remain fixed. This we call as the chemical freeze out. Still the interactions or scatterings with

momentum changes occur or elastic scatterings still dominate. However, further decrease in temperature to a lower value T_f, leads to the scenario where even the change of momenta between particles stop or the elastic scatterings stop. The particle interactions fails to compete with the expansion to keep it as a system. This is called kinetic freeze out. Then the spray of particles free stream towards the detector. Different species of particles have different freeze out temperatures. For the sake of simplicity we assume all the hadrons to have a single freeze out scenario. The freeze out temperature is obtained by constraining the p_T spectra of hadrons.

Chapter 4

Photon productions at SPS, RHIC and LHC energies

The rate of photon productions from QGP and hadron phase have been discussed in chapter 2. Here we discuss the photon productions at SPS ($\sqrt{s_{NN}}$=17.3 GeV or E_{lab} = 158 A GeV) & RHIC ($\sqrt{s_{NN}}$=200 GeV) energies considering the dynamical evolution of the system as discussed in chapter 3. The photon productions have been evaluated in terms of invariant momentum spectra $E\frac{dN}{d^3p}$ or $\frac{dN}{d^2p_T dy}$ and compared with the experimental observations made by WA98 and PHENIX collaborations for Pb+Pb and Au+Au collisions respectively. The experimental data are explained reasonably well with the assumption of an initial QGP phase with a temperature T larger than the transition temperature T_c, predicted by the lattice quantum chromodynamic calculation.

4.1 Introduction

Pb+Pb nuclei were collided at 158 A GeV energy (=E_{lab})in a fixed target experiment at CERN Super Proton Synchrotron aiming to create QGP in the laboratory. Out of several observables measured by different experimental collaborations, WA98 collaboration measured the direct photon invariant momentum spectra [137]. After a decade, the Au+Au collision were made at Relativistic Heavy Ion Collider, BNL at centre of mass energy 200 GeV to create and study the properties of QGP. At RHIC the photon spectra were measured by the PHENIX collaboration [138].

Hence, on the experimental side substantial progress has been made in measuring the transverse momentum spectra of photons to study the properties of the matter formed in the nuclear collisions at SPS and at RHIC. In contrast to the earlier approach [138] PHENIX collaboration has analyzed the data by using a novel technique and reported [139] excess direct photons over the next to leading order perturbative QCD (NLO pQCD) processes for $Au + Au$ collisions at $\sqrt{s_{NN}} = 200$ GeV. In this chapter, the photon spectra ($\frac{dN}{d^2p_Tdy}$) at SPS energy at $\sqrt{s_{NN}}$=17.3 GeV have been evaluated and compared with the data measured by the WA98 [137] collaboration. Also the transverse momentum (p_T) spectra for RHIC energy $\sqrt{s_{NN}}$=200 GeV have been evaluated and compared with the new experimental data [139]. The sensitivity of the results on various input parameters *e.g.* transition temperature(T_c), strong coupling constant (α_s), equation of states etc are presented for $\sqrt{s_{NN}}$=200 GeV.

The photon productions are given by

$$\left(\frac{dN}{d^2p_Tdy}\right)_{total} = \left(\frac{dN}{d^2p_Tdy}\right)_{prompt} + \left(\frac{dN}{d^2p_Tdy}\right)_{thermal} + \left(\frac{dN}{d^2p_Tdy}\right)_{decay} \tag{4.1}$$

The total photons as mentioned originate from three primary sources which are categorized according to the evolution of the system.

4.1.1 Prompt photons

The first term of the R.H.S of eq. 4.1, $(\frac{dN}{d^2p_T dy})_{prompt}$ represents the yield of photons emanating from the collisions of partons from the nucleus of the colliding nuclei. These prompt photons are the best understood part of the total photon productions as the perturbative QCD calculation works here. The prompt photon yield follow a power law kind of behavior and dominates at large p_T region of the spectra. Large momentum transfer results in small coupling constant which justifies the use of perturbative techniques. However, in experiments the collision of nuclei occurs which leads to the collision of partons.This nuclear collision comes under the domain of non-perturbative regime. There is a link required between the partonic interactions taken care by pQCD and hadronic interaction (interaction of nuclei in the experiment) which falls to non-perturbative regime. Hence the experimentally measured hadronic interaction cross-section is connected to theoretically calculated partonic interaction via *factorization method*. So *factorization method* is the technique to bridge the short-distance (perturbative) and the long-distance (non-perturbative) behavior. The factorization method can be written as follows [140]:

$$d\sigma = F(\mu, \Lambda_{QCD}) \otimes d\hat{\sigma}(Q, \mu) \tag{4.2}$$

where the $d\hat{\sigma}$ is the differential partonic cross-section which is calculated perturbatively. This is a function of α_s which takes care of the short distance effect. The other factor, $F(\mu, \Lambda_{QCD})$ which also depends on α_s contains all long distance effects. Although it depends on α_s but it becomes large enough which results non-perturbative situation and therefore, is obtained from data of various type of hard scattering processes. The factorization scale μ (an arbitrary parameter) is considered to be the scale which separates the long and short-distance physics. Hence when a parton emitted with small p_T *i.e.*, $p_T < \mu$, that is considered as a part of hadron structure and is absorbed into the parton distribution function. The processes which contribute to prompt photon

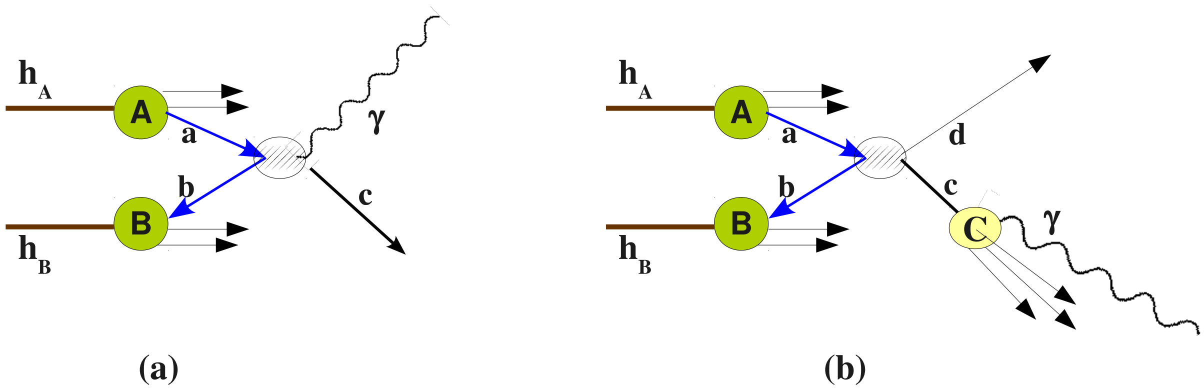

Figure 4.1: The inclusive photon production in collision of particles A and B in partonic level by the direct partonic subprocess and the fragmentation of partons is shown in (a) and (b) respectively.

productions are (i)Compton scattering ($qg \to g\gamma$), (ii)quark anti-quark annihilation process ($q\bar{q} \to g\gamma$) and quark fragmentation ($q \to q\gamma$) of the partons of the nucleons in colliding nuclei (shown in Fig. 4.1) and are well controlled by pQCD techniques [141]. The contribution from the annihilation process $q\bar{q} \to \gamma\gamma$ is negligible because both the vertices here are electromagnetic.

The invariant cross section of the reaction($A + B \to X + \gamma$) can be written in the factorized form as in [142]:

$$E_\gamma \frac{d\sigma}{d^3p_\gamma} = \sum_{a,b,c} \int [dx_a dx_b F_1^a(x_a, \mu) F_2^b(x_b, \mu) \times \{E_\gamma \frac{d\hat{\sigma}}{d^3p_\gamma}(a + b \to \gamma)$$
$$+ \int dz_c E_\gamma \frac{d\hat{\sigma}}{d^3p_\gamma}(a + b \to c) D_3^c(z_c, \mu)\}], \tag{4.3}$$

where a, b are the partons inside the hadrons A and B respectively. c is the produced partons from the interaction of a and b. $F_{1,2}(x,\mu)$ is the parton distribution functions and $D_3(z,\mu)$ is the fragmentation function. $\hat{\sigma}$ is the partonic cross section. In

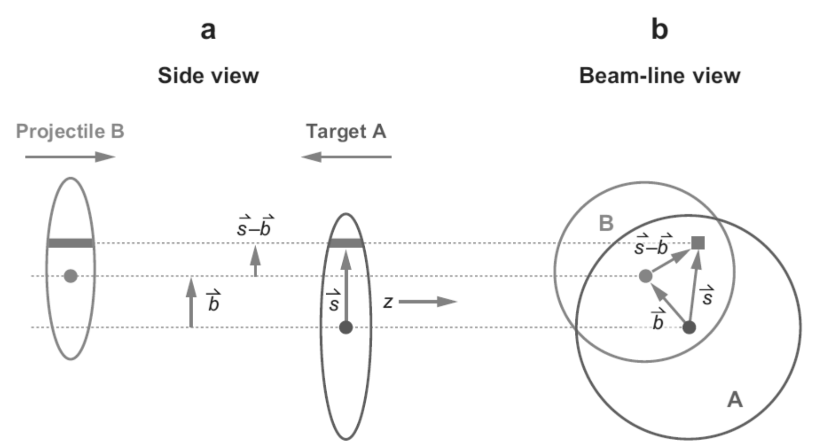

Figure 4.2: Schematic diagram for the nucleus nucleus collision in Glauber model in the optical limit approximation. Figure is taken from Miller *et al.* [143]

the Eq. 4.3, the partonic cross sections are leading order cross-sections and have been written in two different terms. The first term represents the direct partonic processes like -Compton scattering and annihilation processes (see Fig 4.1(a)), and the second term represents the quark fragmentation process (see Fig 4.1 (b)). The yield of prompt photons is given by,

$$\left(\frac{dN^{AB}}{d^2p_T dy}\right)_{prompt} = \frac{N_{coll}(b)}{\sigma_{in}^{pp}} \frac{d\sigma^{NN}}{d^2p_T dy} = T_{AB}(b) \frac{d\sigma^{NN}}{d^2p_T dy} \tag{4.4}$$

where, $T_{AB}(b)$ is the nuclear overlap function and given by $\hat{T_{AB}}(b) = \int \hat{T_A}(\mathbf{s})\hat{T_B}(\mathbf{s}-\mathbf{b})d^2\mathbf{s}$, where $\hat{T_A}(\mathbf{s})$ is the probability per unit transverse area of a given nucleon being located in the target flux tube (according to optical Glauber model figure 4.2). $\hat{T_A}$ is given by the equation $\hat{T_A}(\mathbf{s}) = \int \hat{\rho_A}(\mathbf{s}, z_A)dz_A$ with $\hat{\rho_A}(\mathbf{s}, z_A)$ is the probability per unit volume, normalized to unity for finding the nucleon at $(\mathbf{s}, z_A)$. Here the two flux tubes (target and projectile) are located at a displacement $\mathbf{s}$ from the centre of the target nucleus and $(\mathbf{s}-\mathbf{b})$ from the centre of the projectile nucleus. b is the impact parameter.

$N_{coll}(b)$ is the number of binary inelastic nucleon-nucleon collisions and σ_{in}^{NN} is the inelastic cross-section of nucleon-nucleon scattering. The $T_{AB}(b)$ and $N_{coll}(b)$ is calculated using Glauber model [144] and σ_{in}^{NN} is calculated by using pQCD.

4.1.2 Thermal photons

The second term of the R.H.S of the Eq. 4.1 represents the thermal contribution of the photon productions *i.e.,* and given by,

$$\left(\frac{dN}{d^2p_T dy}\right)_{thermal} = \sum_{i=phases} \int_i \frac{dR}{d^2p_T dy} d^4x \tag{4.5}$$

where i represents the different thermally equilibrated phases of the evolution of the system. $\frac{dR}{d^2p_T dy} = E\frac{dR}{d^3p}$ is the static rate of production. The static rate is convoluted with the expansion dynamics through the integration over d^4x. This is taken care of by the boost invariant relativistic hydrodynamics with cylindrical symmetry [125] as explained in chapter 3. The formalism for the calculation of the thermal rates are already discussed in chapter 2.

When an initial QGP phase with 1st order phase transition is assumed then the above Eq. 4.5 becomes

$$\left(\frac{dN}{d^2p_Tdy}\right)_{thermal} = \int_{QGP} \frac{dR}{d^2p_Tdy}d^4x + \int_{Mix} \frac{dR}{d^2p_Tdy}d^4x + \int_{Had} \frac{dR}{d^2p_Tdy}d^4x \qquad (4.6)$$

representing the contributions from QGP, mixed and hadronic phases. For a continuous transition only QGP and hadron phases are assumed to contribute. In case of crossover the QGP phase moves to hadronic phase smoothly without any discontinuity around the pseudo-transition temperature. Here also, the contributions from QGP (above pseudo-transition temperature) and hadrons (below pseudo-transition temperature) are assumed.

The last part of the R.H.S of the Eq. 4.1 $(\frac{dN}{d^2p_Tdy})_{decay}$ is for the contribution from decay of hadrons occurring after the thermal freeze-out of the system. The experimental data for SPS and RHIC energies are available after the subtraction of decay contribution. Hence in the present analysis the photons from post freeze out hadronic decays are ignored and we evaluate,

$$\left(\frac{dN}{d^2p_Tdy}\right)_{direct} = \left(\frac{dN}{d^2p_Tdy}\right)_{prompt} + \left(\frac{dN}{d^2p_Tdy}\right)_{thermal}. \qquad (4.7)$$

4.2 Photons from Au+Au collisions at $\sqrt{s_{NN}}$=200 GeV RHIC energy.

Theoretically the prompt photons and thermal photons have been evaluated at this energy and compared with the direct photon data taken by PHENIX collaboration [139].

4.2.1 Prompt photons at $\sqrt{s_{NN}}$=200 GeV

Let us identify the possible sources of "excess" photons above those coming from the decays of π^0, η mesons etc. as provided by the data. Photons from the decays of π^0, η etc.. are subtracted from the data and hence will not be discussed here. For the transverse momentum spectra of the photon, first we focus on the high p_T domain. These are populated by the prompt photons that originate from the hard collisions of initial state partons in the colliding nuclei. We use next -to- leading order (NLO) predictions by Gordon and Vogelsang [145] from pp collisions and scale it up by the number of binary collisions for $Au+Au$ interactions to obtain the prompt contributions. It should be noted here that NLO prediction does not require any intrinsic k_T smearing to explain the $p-p$ data [146]. This effect is ignored in the analysis of $Au+Au$ data in the present work. The fast quarks propagating through QGP lose energy due to gluon radiation and hence produce photons with reduced energy via fragmentation processes. This indicates that photon production by these processes will be suppressed. However, the induced emission of photons by the hard partons due to multiple scattering in the QGP will enhance the photon radiation. It is shown in Ref. [80] that the enhancement due to induced radiation compensates the suppression due to jet energy loss for the p_T domain considered here. Therefore, we ignore these mechanisms in the current analysis. Photon productions from the interaction of thermal gluons and non-thermal quarks were first considered in [147] within the framework of Fokker Planck equation. Contributions from the hard partons undergoing annihilation and Compton processes with the quarks and gluons in the thermal medium [86] have been evaluated and their importance has been highlighted recently in [148]. The duration of the pre-equilibrium stage will be small since the thermalization time taken here is small (~ 0.2 fm) and hence the contribution from this stage is assumed to be small. Photons from the pre-equilibrium stage and hard-thermal conversion are neglected here. The current experimental data are explained without these contributions.

4.2.2 Thermal photons at $\sqrt{s_{NN}}$=200 GeV

The estimation of the thermal contribution depends on the space-time evolution scenario that one considers. In case of a de-confinement phase transition, which seems to be plausible at RHIC energies, we assume that QGP is formed initially. The equilibrated plasma then expands in space and time, cools as temperature falls. Then at a point it reverts back to hadronic matter and finally freezes out at a temperature $\sim$ 120 MeV. Hence the thermal radiations are from the quark-gluon fireball and also from luminous hadronic fireball which has to be evaluated properly in order to have a reliable estimate of the initial temperature. The photon emission rate from QGP due to Compton ($q(\bar{q})g \rightarrow q(\bar{q})\gamma$) and annihilation ($q\bar{q} \rightarrow g\gamma$) processes was evaluated [24, 82] by using Hard Thermal Loop (HTL) approximation(described in chapter 2). Later it was shown [78] that photon production from the reactions, $gq \rightarrow gq\gamma$, $qq \rightarrow qq\gamma$, $qq\bar{q} \rightarrow q\gamma$ and $gq\bar{q} \rightarrow g\gamma$ contribute in the same order as annihilation and Compton processes. However, this calculation does not incorporate suppression due to multiple scattering during the emission process. This point was later clarified in Ref. [83]. The complete calculation of photon emission rate from QGP to order α_s has been completed by resuming ladder diagrams in the effective theory [84]. We use the results of Ref. [84] in the present work. The parameterizations of the emission rates for various processes are available in Ref. [149]. The temperature dependence of the strong coupling constant is taken from Ref. [85]. While evaluating the photons from hadronic phase we consider an exhaustive set of hadronic reactions and the radiative decay of higher resonance states [150, 151, 152, 153]. The relevant reactions and decays for photon productions are: (i) $\pi\,\pi \;\rightarrow\; \rho\,\gamma$, (ii) $\pi\,\rho \;\rightarrow\; \pi\gamma$ (with π, ρ, ω, ϕ and a_1 in the intermediate state [152]), (iii)$\pi\,\pi \;\rightarrow\; \eta\,\gamma$ and (iv) $\pi\,\eta \;\rightarrow\; \pi\,\gamma$, $\rho \;\rightarrow\; \pi\,\pi\,\gamma$ and $\omega \;\rightarrow\; \pi\,\gamma$. The corresponding vertices are obtained from various phenomenological Lagrangians described in detail in Ref. [150, 151, 152, 153]. Contributions from other decays, such as $K^*(892) \rightarrow K\,\gamma$, $\phi \rightarrow \eta\,\gamma$, $b_1(1235) \rightarrow \pi\,\gamma$, $a_2(1320) \rightarrow \pi\,\gamma$ and $K_1(1270) \rightarrow \pi\,\gamma$ have been found to be small [154] for $p_T > 1$ GeV. All the isospin combinations for the above reactions and decays have properly been taken into account.

Various experiments suggest that the spectral functions of hadrons are modified in a dense nuclear environment [155, 156, 157, 158, 159, 160, 161]. The enhancement of lepton pair yield in CERES data [162] below the ρ-mass can only be explained by assuming the in-medium modifications of the ρ meson [163, 164, 165, 166]. The photon spectra measured by WA98 collaboration at CERN-SPS energies have been reproduced by assuming the reduction of hadronic masses in the thermal bath [167, 168]. It was shown in Ref. [168] that the p_T distribution of photons changes significantly with a reduced mass scenario and is almost unaffected by the broadening [168] of the vector meson spectral function in the medium. On the other hand the invariant mass distribution of the lepton pairs is sensitive to both the reduction in vector meson masses [164, 165] as well as the enhanced width of the vector mesons [163, 166]. Thus, by looking only at the dilepton spectra, it is difficult to differentiate the above scenarios. We need to analyze both the photon and dilepton spectra simultaneously.

Although the NA60 data favors the broadening of the spectral function of low mass vector meson, the issue of the medium modification is yet to be understood. The shift in hadronic spectral function depends on the temperature and (baryonic) chemical potential of the thermal bath created after the collisions. The value of baryonic chemical potential for system produced after the collision at $\sqrt{s_{NN}} = 200$ GeV is much smaller [169] compared to the other lower energy collisions [170]. Therefore, the extrapolation of the nature of change observed in these low energy experiments to RHIC energy may suffer from various uncertainties, because for matter formed at RHIC collision the net baryon number is very small (baryon - anti-baryon ~ 0). Because of these reasons and the insensitivities of photon spectra on broadening we consider the reduction of hadronic masses to evaluate photon productions from hadronic matter to estimate T_i. The nature of changes in the hadronic spectral function at non-zero temperature and density is not known from first principle at present. Thus one has to rely on calculations based on various phenomenological models (see [71, 163, 171] for a review). In this particular work we use Brown-Rho (BR) scaling scenario [173] (see also [174]) for in-medium modifications of hadronic masses (except pseudo scalars). BR scaling has been used here to indicate how far the value of initial temperature is affected when the reduction of the hadronic mass is incorporated in evaluating the photon spectra. The BR scaling indicates stronger reduction of hadronic masses as compared to Quantum Hydrodynamics (QHD) [175]. As the abundances of hadrons increase with the reduction in their masses, photon yield is expected to increase from hadronic phase with BR

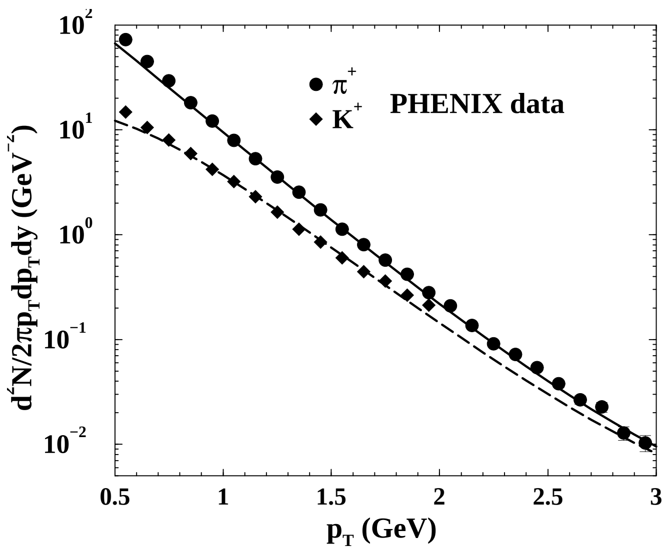

Figure 4.3: π^+ (filled circle) and K^+ (filled diamond) spectra at $\sqrt{s_{NN}} = 200$ GeV are measured by PHENIX Collaboration. Solid (dashed) line depicts the pion (kaon) spectra obtained in the hydro dynamical model. The data is taken from [172] for Au + Au collisions at $\sqrt{s_{NN}} = 200$ GeV for $(0-5)\%$ centrality. Type I EoS has been considered here with $T_i = 400$ MeV, $\tau_i = 0.2$ fm and $T_f = 120$ MeV.

scaling. Therefore, in this scenario a conservative estimate of the photons from QGP phase and hence a conservative value of the initial temperature is obtained.

Table 4.1: Different sources of photon productions.

Prompt		$qg \to q\gamma$, $q\bar{q} \to g\gamma$, NLO (Vogelssang) $q_1q_2 \to q_1q_2\gamma$	Included
Thermal	QGP	$qg \to q\gamma$ (Compton), $q\bar{q} \to g\gamma$ (Gluon emission), $q_1q_2 \to q_1q_2\gamma$, $qq\bar{q} \to q\gamma$, $gq \to gq\gamma$	Included
	Hadronic	$\pi\rho \to \pi\gamma$, $\pi\pi \to \rho\gamma$, $\pi\pi \to \eta\gamma$, $\pi\eta \to \pi\gamma$, $\rho \to \pi\pi\gamma$, $\omega \to \pi\gamma$, $\pi K^* \to K\gamma$, $\pi K \to K^*\gamma$, $K\rho \to K\gamma$, $KK \to \rho\gamma$, $KK^* \to \pi\gamma$, $K^* \to \pi K\gamma$.	
Decay		$\pi \to \gamma\gamma$, $\eta \to \gamma\gamma$	Not included

• **Space time evolution :**

The ideal relativistic hydrodynamics with longitudinal boost invariance [124] and cylindrical symmetry [125] has been used for the space time evolution. This is described in chapter 3.

• **Initial Condition :**

In case of isentropic expansion the experimentally measured hadron multiplicity can be related to the initial temperature and thermalization time by the following equation [129]:

$$T_i^3(b)\tau_i = \frac{2\pi^4}{45\zeta(3)\pi R_A^2 4a_k}\frac{dN}{dy}(b) \tag{4.8}$$

where $\frac{dN}{dy}(b)$ is the hadron (predominantly pions) multiplicity at a given impact parameter b, R_A is the radius of the system, τ_i is the initial thermalization time, $\zeta(3)$ is the Riemann zeta function and $a_k = (\pi^2/90)g_{eff}$ and g_{eff} is the effective statistical degeneracy of the system. The hadron multiplicity resulting from $Au + Au$ collisions is related to that from pp collision at a given impact parameter and collision energy by

$$\frac{dN}{dy}(b) = [(1-x)N_{part}(b)/2 + xN_{coll}(b)]\,\frac{dN_{pp}}{dy} \tag{4.9}$$

where x is the fraction of hard collisions. N_{part} is the number of participants and N_{coll} is the number of collisions evaluated by using Glauber model. $dN^{ch}_{pp}/dy = 2.5 - 0.25ln(s) + 0.023ln^2 s$, is the multiplicity of the produced hadrons in pp collisions at centre of mass energy, $\sqrt{s}$ [176]. We have assumed that 25% hard (i.e. $x = 0.25$)and 75% soft collisions are responsible for initial entropy production.

We further assume that the system is formed in a thermalized phase of quarks and gluons at the initial thermalization time $\tau_i = 0.2$ fm. Taking the number of flavors, $N_F = 2.5$, $dN/dy \sim 1100$ and solving Eq. 4.8 the value of the initial temperature (T_i) is obtained as $T_i = 400$ MeV. The initial energy density profiles is considered as:

$$\epsilon(\tau_i, r) = \frac{\epsilon_0}{1 + e^{(r-R_A)/\delta}} \tag{4.10}$$

where ϵ_0 is the central energy density calculated from the initial temperature T_i ($\frac{\pi^2}{30}g_{eff}T_i^4$), The value of the g_{eff} is obtained from the equation of state considered for that phase. Similarly the radial velocity profile is given by,

$$v(\tau_i, r) = v_0\left[1 - \frac{1}{1 + e^{(r-R_A)/\delta}}\right] \tag{4.11}$$

where v_0=0 and $\delta \sim 0.5$ fm.

4.2.3 Equation of state (EoS)

Two types of equation of state are used here to study the photon spectra to indicate the sensitivity of the results. (I)BAG-HRG EoS: Bag model type EoS has been used for QGP and for the hadronic matter the equation of state has been constructed considering all the resonances with mass < 2.5 GeV $/c^2$ (HRG EoS). The velocity of sound is taken as $c_s^2 = 1/3$ and $1/5$ [177] for QGP and hadronic phase respectively. The effect of baryonic chemical potential is neglected here.

(II) EoS from lattice QCD [178] has also been used here to show the sensitivity of our results on the equation of state and to find out the conservative value of T_i.

The transition temperature is taken as $T_c \sim 190$ MeV guided by the lattice QCD [179, 180]. However, the sensitivity of the results on T_c will also be demonstrated. The freeze-out temperature, T_f has been fixed by studying the transverse momentum distribution of hadrons.

4.2.4 Results for the p_T spectra at RHIC

First we use the type I EoS and initial conditions described above to solve the relativistic hydrodynamic equations for studying the p_T spectra of pions and kaons. To reproduce the transverse momentum distribution of pions and kaons (Fig. 4.3) measured experimentally by PHENIX collaboration [172], the required value of $T_f \sim 120$ MeV.

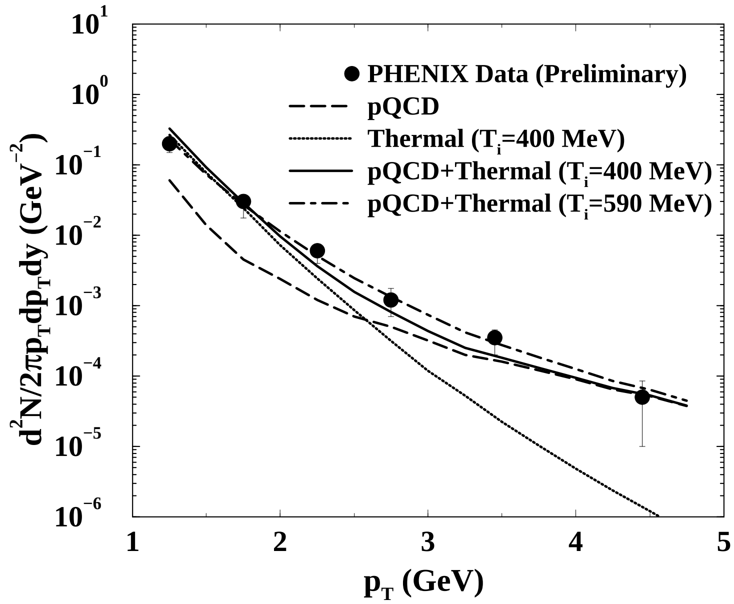

Figure 4.4: Direct photon spectra at RHIC energies measured by PHENIX Collaboration for $(0-20)\%$ centrality. Dashed line indicates hard photons from NLO pQCD calculations [145]. Solid (dot-dashed) line depicts the total photon yield obtained from QGP initial state with $T_i = 400$ MeV and $\tau_i = 0.2$ fm ($T_i = 590$ MeV $\tau_i = 0.15$ fm). Type I EoS has been used to obtain the thermal contributions shown in this figure. In medium effects on hadrons are included (ignored) in the results shown by solid (dot-dashed) line. Photon production rate from QGP is taken from [84].

In all the results shown below the value of the freeze-out temperature is fixed at 120 MeV. The dependence of the p_T distributions of hadrons on the initial temperature is rather weak for the p_T values under consideration. It is assumed here that the chemical equilibrium is maintained down to T_f. Now we evaluate the p_T spectra of photons and compare the resulting spectra with the recent PHENIX measurements of direct photons in Fig. 4.4. We observe that the data is reproduced with $T_i = 400$ MeV and $\tau_i = 0.2$ fm with in-medium modification of hadrons and type I EoS. It is found that the contributions from quark matter and hadronic matter to the photon production are similar in

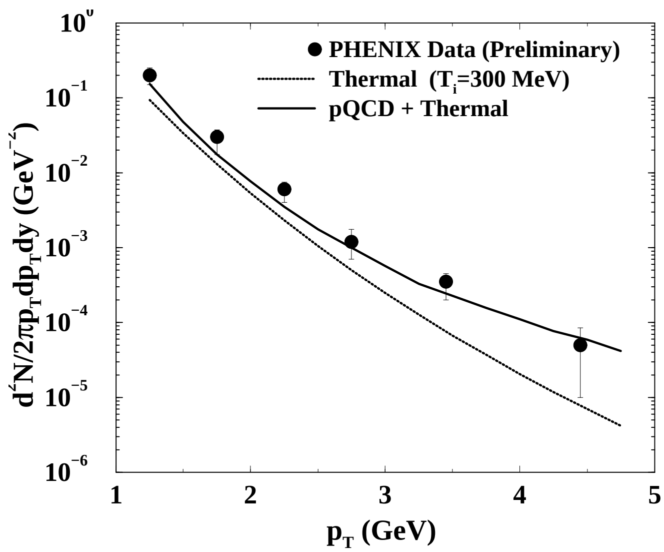

Figure 4.5: Same as Fig. 4.4 for type II EoS, with T_i = 300 MeV, τ_i = 0.5 fm and T_f = 120 MeV. Photon production rate from QGP is taken from [84].

the p_T interval, $1 \leq p_T$(GeV)≤ 3, the range where thermal contribution dominates. In Ref. [181] the initial temperature and thermalization time are taken as 590 MeV and 0.15 fm respectively to evaluate the photon spectra. They have used the hadronic photon production rates of Ref. [87]. We reproduce the photon spectra with this initial condition by using the hadronic emission rates of photons from [150, 151, 152, 153]. As in Ref. [181] the medium effects are neglected in this case. The resulting photon spectrum is also shown in Fig. 4.4 for comparison. If we fix $\tau_i = 0.15$ fm then the data can also be described reasonably well for $T_i = 440$ MeV (keeping $T_i^3\tau_i \propto dN/dy$ fixed) if the medium effects on hadrons are taken into account. It may be mentioned here that photons from strange hadrons [87] is down by a factor of 2 (at $p_T \sim 2$ GeV) compared to the production rates from non strange hadrons $(\pi, \rho, \omega, \eta)$. The contributions involving η mesons are neglected in Ref. [87]. As mentioned earlier the reduction of hadronic masses in a thermal bath increases their abundances and hence the rate of photon emission gets enhanced [71, 150, 151]. As a result a smaller initial temperature compared to the one obtained in Ref. [181], is seen to reproduce the data reasonably well. The variation of hadronic masses with temperature in QHD model [71, 175] is slower than the BR scaling. As a result the PHENIX photon data requires higher value of T_i in QHD than BR scaling scenario. Hence to pinpoint the actual initial temperature through photon spectra it is imperative to understand the properties of hadrons in hot and dense environment. However, it is clear that the initial temperature obtained in the present analysis is more than the value of T_c obtained from lattice QCD calculations. The initial temperature obtained from the analysis of the RHIC data is $\sim$ 400 MeV in the present work and $\sim$ 590 MeV in [181]. This may be compared with the value of the initial temperature obtained from the analysis of SPS data. The value of initial temperature obtained from the analysis of the single photon data from Pb + Pb collisions at SPS [137] is within the range $\sim 200 - 230$ MeV [167, 168, 182, 183, 184, 185]. A much higher value of $T_i \sim 335$ MeV is obtained in [186] by assuming a very small value of $\tau_i \sim 0.2$ fm for SPS energy.

To show the sensitivity of the results on the EoS we evaluate the photon spectra using type II EoS (lattice QCD) in hydro-dynamical evolution. It is seen (Fig. 4.5) that the data can be reproduced with lower initial temperature, $T_i \sim 300$ MeV (and hence larger thermalization time scale ~ 0.5 fm). This is so because in the case of type II EoS the space time evolution of the system for temperature below the transition temperature is slower than type I EoS. Hence the hadronic phase lives longer for type II EoS, radiating more photons from this phase. However, it should be mentioned here that the slope of the p_T spectra of hadrons can not be reproduced by type II EoS with the value of the initial temperature mentioned above.

It may be mentioned at this point that the photon emission rates obtained in [84] are valid in weak coupling limit, although the QGP formed after $Au + Au$ collisions at RHIC energy could be strongly coupled[187]. However, photon production from strongly coupled QGP is not available from thermal QCD. Therefore, results in strong coupling limit would be useful even if it comes from a theory which is not real QCD. Recently, results from $\mathcal{N} = 4$ Super-symmetric Yang Mills (SYM) theory have been made available [188, 189] in the strong coupling limit. The rate obtained in this case could be treated as an upper limit of photon production from QGP. The thermal photons obtained in this case are compared with that from thermal QCD in Fig. 4.6. Photons from SYM is enhanced by about 20% as compared to thermal QCD in the p_T region ~ 2 GeV. When the results obtained from SYM is added with thermal photons from hadronic phase and photons from pQCD it describes the data reasonably well (see Fig. 4.7). The initial temperature and time are taken as 300 MeV and 0.5 fm respectively. The type II EoS is used here. It should be mentioned here that for type I EoS and production rate from SYM, $T_i \sim 400$ MeV and $\tau_i \sim 0.2$ fm is required to reproduce the data. In Fig. 4.8 the dependence of photon spectra from QGP phase on strong coupling is demonstrated. The temperature dependence of α_s has been taken from [85]. The difference in photon spectra at $p_T \sim 3$ GeV for $\alpha_s = 0.3$ and temperature dependent α_s is about 13%. A 20% enhancement is obtained at $p_T \sim 2$ GeV in total thermal photon production if transition temperature is increased from 170 to 190 MeV (Fig. 4.9). Photons from hadronic phase populate mainly the low p_T region of the spectra. Larger value of transition temperature means that hadrons survive up to larger

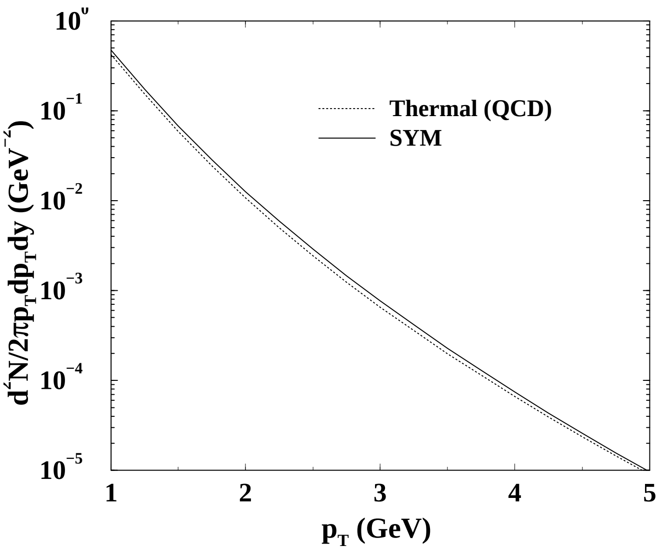

Figure 4.6: Solid (dotted) represents p_T spectra of thermal photons when photons from QGP is evaluated within the ambit of SYM theory (thermal QCD). The values of $T_i = 590$ MeV, $\tau_i = 0.15$ fm and $T_f = 120$ MeV. Type II EoS has been used here.

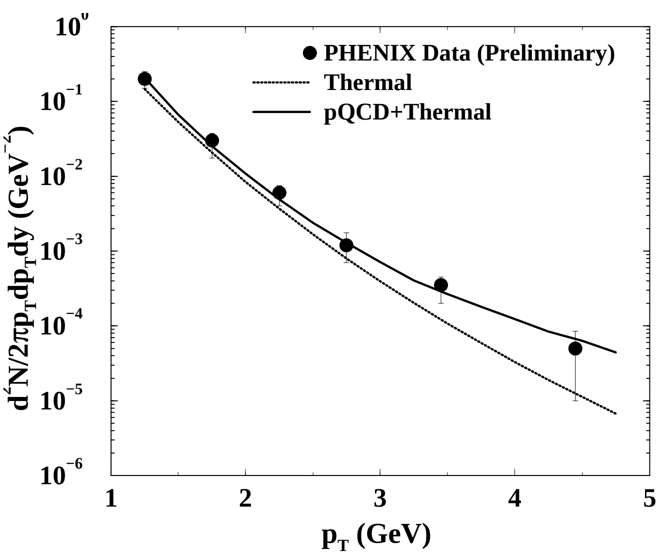

Figure 4.7: Direct photon spectra at RHIC energies measured by PHENIX Collaboration. Solid (dotted) line depicts the pQCD + thermal (thermal) photon yield. Thermal photons from QGP phase is obtained from SYM theory [84]. Here $T_i = 300$ MeV and $\tau_i = 0.5$ fm. Type II EoS is used to obtain the thermal contributions.

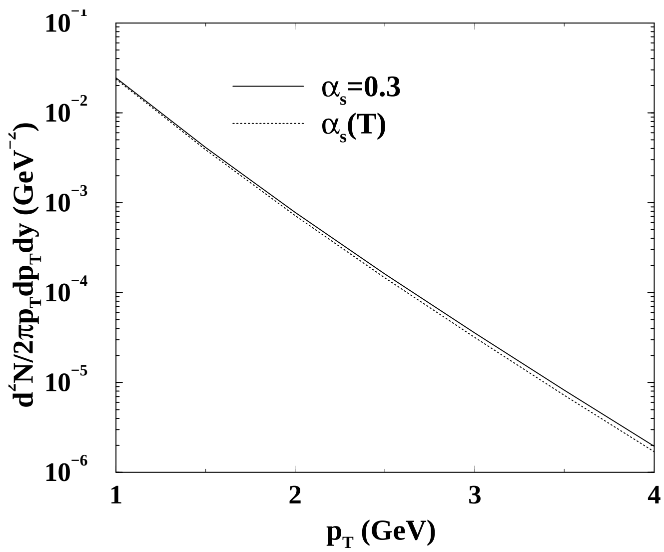

Figure 4.8: Photon emission from QGP phase for two values of strong coupling constant α_s. Solid (dotted) line indicates results for $\alpha_s = 0.3$ (temperature dependent coupling). Here $T_i = 400$ MeV, $\tau_i = 0.2$ fm and $T_f = 120$ MeV. Type I EoS has been used here.

temperature and emit more photons at low p_T region. All the results presented above are obtained with vanishing initial radial velocity *i.e.* for $v_0 = 0$ in Eq. 4.11. Finally, we demonstrate the sensitivity of results on the value and shape of the initial velocity profile. In Fig. 4.10 we show the results for $v_0 = 0$ (solid line) and $v_0 = 0.2$ (dashed line) in Eq. 4.11. The difference in results is rather small. However, for a different velocity profile, $v_r(\tau_i, r) = v_0^1\, r/R_A$ a substantial change in the spectra is observed for $v_0^1 = 0.2$, because this gives a stronger radial velocity distribution of the fluid compared to Eq. 4.11. It will be interesting to put constrains on the initial velocity profile from experimental data on the p_T distributions of various types of hadrons [55].

We have also evaluated the p_T spectra of direct photons for different centralities for Au+Au collisions at $\sqrt{s_{NN}}$=200 GeV. It is important to mention here that while

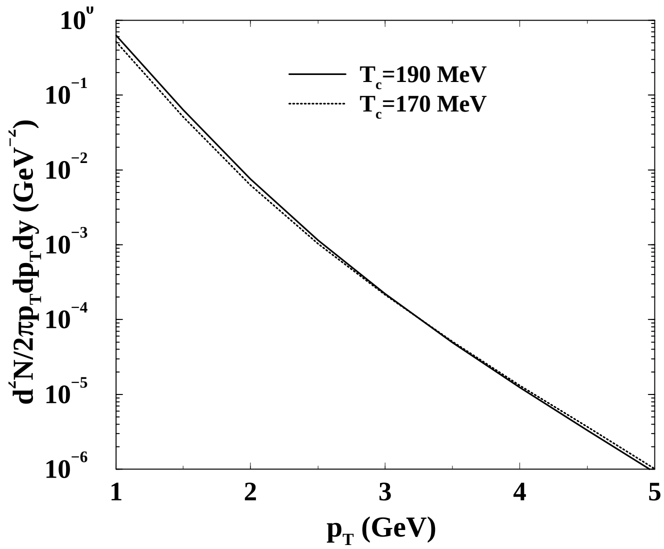

Figure 4.9: Photon emission from QGP phase for two values of transition temperature, T_c. Solid (dotted) line indicates results for $T_c = 190(170)$ MeV. Here $T_i = 400$ MeV, $\tau_i = 0.2$ fm and $T_f = 120$ MeV. Type I EoS has been used here.

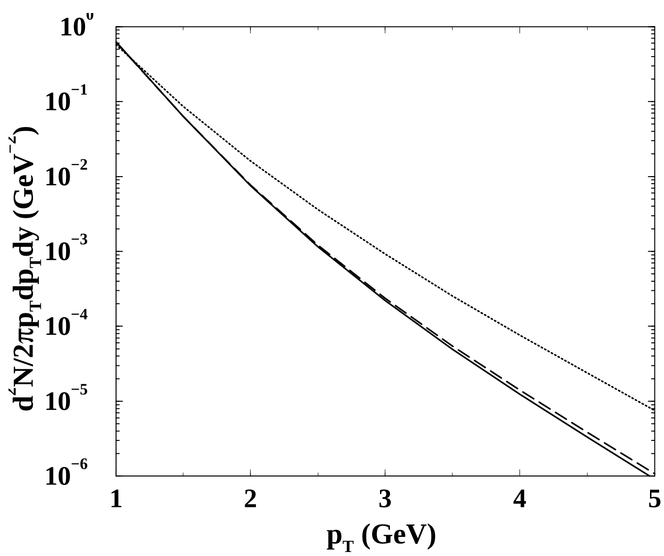

Figure 4.10: Thermal photon spectra with different initial velocity profile. Solid (dashed) line indicates results for v_0=0 (0.2) for the radial velocity profile given in expression 4.11. Result for different velocity profile $v_r(\tau_i, r) = v_0^1 r/A$ with v_0^1=0.2 is shown in dotted line. Here T_i=400 MeV, τ_i=0.2 fm, T_f=120 MeV and Type-I EoS.

evaluating the spectra for different centralities we have assumed the value of x (fraction of hard collision) to be 0.1 and calculate the initial entropy production in terms of hadronic multiplicities dN/dy using Glauber model. Also we have considered the thermal photon productions from hadronic phase by using the non-linear sigma model Lagrangian described in chapter 2. The results are compared with the experimental data [190] and shown in [51]. The initial conditions taken for different centralities are mentioned in table 4.2.

Table 4.2: The values of various parameters - thermalization time (τ_i), initial temperature (T_i) and hadronic multiplicity dN/dy - used for the calculations at SPS [137] and for RHIC [190]

$\sqrt{s_{NN}}$	centrality	$\frac{dN}{dy}$	$\tau_i(fm)$	T_i(MeV)
17.3 GeV	0-06%	700	1.0	200
200 GeV	0-20%	496	0.6	227
	20-40%	226	0.6	203
	min. bias	184	0.6	200

4.3 Photons from Pb+Pb collisions at $\sqrt{s_{NN}}$=17.3 GeV, SPS energy.

Similar to RHIC, the direct photons have been evaluated for $\sqrt{s_{NN}}$=17.3 GeV at SPS energy and compared with the available data for Pb+Pb collisions [51].

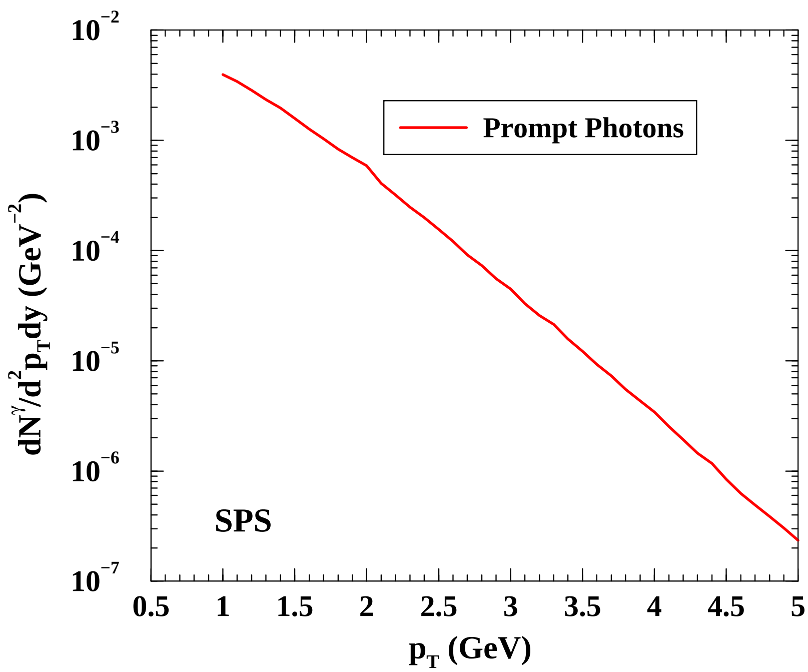

Figure 4.11: Transverse momentum spectra of prompt photons for Pb+Pb collision at $\sqrt{s_{NN}}$=17.3 GeV obtained by scaling the p+p collision at $\sqrt{s_{NN}}$=19.4 GeV

4.3.1 Prompt Photons at $\sqrt{s_{NN}}$=17.3 GeV

One can obtain the prompt photon contribution from A+A collision using the technique of pQCD as described 4.2. The prompt production from A+A collision can also be evaluated by scaling the photon productions from p+p collision [137] with number of binary collisions (in Au+Au). Here we have used the second way to evaluate the spectra at SPS energy, $\sqrt{s_{NN}}$=17.3 GeV. Since no data are available for p+p collision at this energy, we used the photon data for p+p collision at $\sqrt{s_{NN}}$=19.4 GeV and scale it for Pb+Pb collision at 17.3 GeV. Then we estimate the prompt photon production for Pb+Pb collision. The prompt photon spectra is displayed in Fig. 4.11.

4.3.2 Thermal photons at $\sqrt{s_{NN}}$=17.3 GeV

The formalism for the rate of thermal photon productions from the QGP phase is similar to RHIC and are already discussed in chapter 2. The emission from thermal hadrons have been considered from [87]. Here we discuss the initial conditions for the space time evolution and evaluate the spectra at $\sqrt{s}_{NN}$=17.3 GeV.

Initial Conditions for hydrodynamics:

We assume that the system reaches equilibration at a time τ_i after the collision. We take T_i=200 MeV, calculated from the relation 4.9 for the multiplicity dN/dy. The value of dN/dy for various beam energies and centralities are calculated from the above mentioned equation 4.9. and tabulated in table I. The number of collision, N_{coll} contribute to x fraction to the multiplicity dN_{pp}/dy measured in pp collision. The number of participants, N_{part} contributes to fraction $(1-x)$ of dN_{pp}/dy. The values of N_{part} and N_{coll} are estimated for this energy by using Glauber Model and the results are in agreement with [146]. We have used $dN_{pp}/dy = 2.43$ and $x = 0.1$ at $\sqrt{s_{NN}} = 200$ GeV. It should be mentioned here that the values of dN/dy (as depend on $N_{\rm part}$ and $N_{\rm coll}$) and T_i (through dN/dy in Eq. 6.2) depend on the centrality of the collisions. The values of R_A for different centralities have been evaluated by using the equation $R_A \sim 1.1 N_{\rm part}^{1/3}$. The initial energy density and radial velocity profiles are considered as taken for RHIC: with central energy density ϵ_i=$\frac{\pi^2}{30} g_{eff} T_i^4$. The values of T_i are tabulated above. The EoS obtained from the lattice QCD calculations by the MILC collaboration [191] has been used. All hadrons are assumed to freeze out thermally at the same time and the temperature is taken to be T_f=140 MeV. The chemical freeze out temperature where the hadrons decouple chemically are taken to be T_{ch} = 170

MeV obtained from the experimentally measured particle ratios [22, 192]. The system remains out of chemical equilibrium from $T_{\rm ch}$ to T_f. The deviation of the system from the chemical equilibrium is taken in to account by introducing chemical potential for each hadronic species. The chemical non-equilibration affects the yields through the phase space factors of the hadrons which in turn affects the productions of the EM probes. The value of the chemical potential has been taken in to account following Ref. [193]. It is expected that the chemical potentials do not change much for the inclusion of resonances above Δ. The p_T spectra of thermal photons at SPS energy $\sqrt{s_{NN}}$=17.3 GeV is displayed in Fig. 4.3.2. It is important to note that the different initial conditions with BAG-HRG equation of state or Ansatz equation of state as described in chapter 3 also explain the data. Although we discuss the effect of EoS on the photon spectra in chapter 5, still it is very much important to know the exact equation of state in case of A+A collisions.

4.3.3 Results at SPS

The thermal photons with initial temperature of 200 MeV along with the prompt contributions explain the WA98 data well [51] with the inclusion of non-zero chemical potentials for all hadronic species considered [193](see also [194]). In some of the previous works [167, 168, 186, 183, 195, 182, 196] the effect of chemical freeze-out is ignored. As a result either a higher value of T_i or a substantial reduction of hadronic masses in the medium was required [167, 168]. In the present work, the data has been reproduced without any such effects.

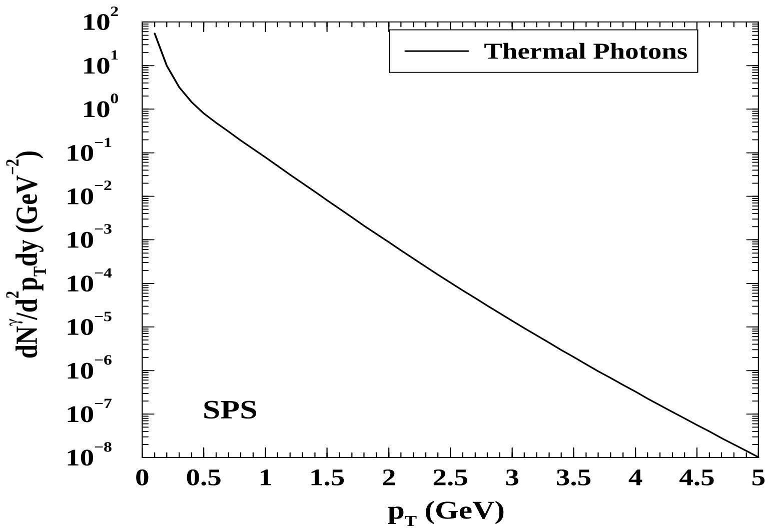

Figure 4.12: Transverse momentum spectra of photons at $\sqrt{s_{NN}}$=17.3 GeV SPS energy for Pb+Pb collision at mid-rapidity.

4.4 Photons at LHC energy

Using the same formalism for thermal photon productions discussed in the above section 4.3, the p_T spectra of (dN/d^2p_Tdy) thermal photons have been evaluated for LHC energy. The initial temperature T_i is considered to be 850 MeV and initial thermalisation time, τ_i, is taken as 0.08 fm.(for a hadron multiplicity 4000, see for details [54, 53]). Freeze out temperature is taken as 120 MeV. BAG-HRG EoS for a first order phase transition is assumed. The p_T spectrum is displayed in Fig. 4.13.

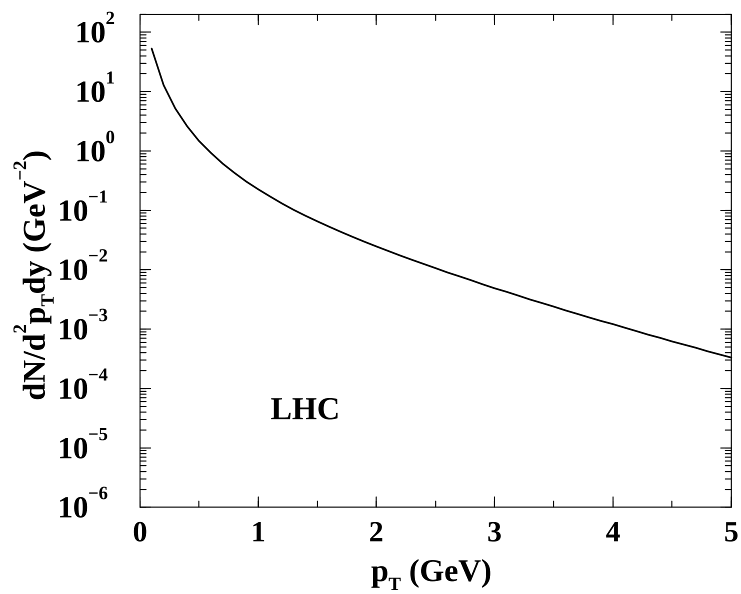

Figure 4.13: p_T spectra for LHC energy (assuming hadron multiplicity dN/dy=4000)

4.5 Summary & Conclusion

The transverse momentum spectra of direct photons at RHIC energy ($\sqrt{s}_{NN}$=200 GeV) for Au+Au collision and at SPS energy ($\sqrt{s}_{NN}$=17.3 GeV) for Pb+Pb collision have been studied using the formalism and expansion dynamics explained in chapter 2 and 3 respectively. For RHIC energy (mid rapidity) we take an initial temperature T_i=400 MeV and initial thermalisation time τ_i=0.2 fm being constrained together from that experimentally measured hadron multiplicity. The freeze out temperature T_f (assuming equal-time freeze out scenario) has been taken to be 120 MeV which is also constrained from the hadron (pion and kaon) p_T spectra. We observe that different boundary condition with different initial conditions can also explain the data well. All the cases we assume an initial QGP phase. If we assume an initial hadronic state for example in

Au+Au collision at RHIC energy then we can calculate the T_i for an effective hadronic degeneracy g_{eff}=10 (a large value) from the eq. 4.8 $T_i^3\tau_i = \frac{2\pi^4}{45\zeta(3)\pi R_A^2 4a_k}\frac{dN}{dy}$. This calculation is for mid-rapidity. Here $\zeta(3)$=1.2, $a_{eff} = \frac{\pi^2}{90}g_{eff}$=$\frac{\pi^2}{9}$, R_A=6 fm, $dN/dy = 1100$ for RHIC. Putting all these values we get $T_i^3\tau_i = 7.99 fm^-2$. If we take τ_i=10 fm which is a very unrealistic larger value then also we get T_i=185 MeV. With this value of T_i and g_{eff} the data for p_T spectra of photons is not reproduced for all p_T range. If we take a value of τ_i=1 fm then we get T_i=400 MeV. A lower value of g_{eff} leads to higher value of T_i and higher value of g_{eff} is not realistic for hadronic matter. This value of T_i is much larger than the value of the transition temperature T_c predicted by the lattice QCD at zero baryonic chemical potential. We can remind here that the baryonic chemical potential μ_B obtained from the particle ratios are of the order of 25 MeV for Au+Au collision at RHIC energy $\sqrt{s}_{NN}$=200 GeV. Which rules out the initial hadronic state at this energy again the theoretical evaluation of spectra with the assumption of an initial QGP phase explains the data nicely. The data for different centralities have also been explained with the same production and expansion mechanism. As we mentioned different EoS (Lattice EoS (MILC Collaboration) etc.) with different initial conditions also explain the data. Similarly photon spectra Pb+Pb collision at SPS energy ($\sqrt{s}_{NN}$=17.3 GeV or E_{lab}=158 A GeV) have been explained with initial temperature T_i=200 MeV and τ_i=1 fm with lattice EoS. From the initial temperature T_i inferred for spectra at both energies we conclude the data along with the theoretical evaluation supports the formation of an initial QGP phase at $\sqrt{s}_{NN}$=17.3 GeV, Pb+Pb collision and at $\sqrt{s_{NN}}$=200 GeV, Au+Au collision.

Chapter 5

Thermal dilepton productions from In+In collisions at SPS energy and the information of radial flow

---

The importance of the lepton pairs(μ^+ & μ^- pairs) for probing the state of the matter that is produced in the heavy ion collision has been discussed earlier. Here the production of lepton pairs in terms of invariant yield has been evaluated for In-In collision at $\sqrt{s_{NN}} = 17.3 GeV$ SPS energy. The theoretical estimations of invariant mass ($dN/dM_{\mu^+\mu^-}$) spectra and transverse mass spectra ($dN/m_T dm_T$) have been contrasted with the available experimental data measured by NA60 Collaboration. The assumption of an initial QGP state explains the data where the hadronic initial state fails to reproduce. While evaluating the invariant mass spectra we restrict our calculation up to M$\sim$1.5 GeV. The excess dimuon observed in the low mass region of the invariant mass spectra may be due to the melting of ρ meson due to the interactions with the thermal baryons and mesons. The non-monotonic behaviour of T_{eff} extracted from the transverse mass spectra indicates the presence of two different thermal sources (may be partonic or hadronic). The theoretical evaluation of the spectra after comparing with the experimental observations suggests the formation of QGP phase in relativistic In+In nuclear collisions.

5.1 Introduction

In this chapter, the thermal dimuon yields have been evaluated from a system formed in heavy ion collisions using thermal field theory and relativistic hydrodynamics as discussed in previous chapters 2 & 3. We compare our results [55] with the dimuon spectra ($m_T - M$ and M) measured by NA60 collaboration [197] from In+In collisions at beam energy 158A GeV (or center of mass energy, $\sqrt{_{NN}}$=17.3 GeV), SPS energy. The high quality data have been made available [197, 198, 199] for both the kinematic variables - the transverse momentum (p_T) and the invariant mass (M) of the muon pairs. The available data are excluded from the non-thermal sources like Drell-Yan and decay of vector mesons after the freeze out. Theoretically we evaluate invariant mass spectra $dN_{\mu^+\mu^-}/dM$ *i.e.,* the number of dimuons produced per unit invariant mass, $M = \sqrt{(E_1 + E_2)^2 - (P_1 + P_2)^2}$ of dimuons produced from In+In collision at SPS energy $\sqrt{s_{NN}}$=17.3 GeV. Here 1 &2 represents μ^+ and μ^- respectively. To compare with the experimental data we express the invariant mass spectra in terms of normalized spectra as $(dN/dMdy)/(dN_{ch}/dy)$ and plot with the invariant mass M. Here y is the rapidity and dN_{ch}/dy is the charge hadron multiplicity [55]. The evaluation is for different p_T windows. Also we evaluate the transverse mass spectra ($dN/m_T dm_T \equiv dN/p_T dp_T$) where $m_T = \sqrt{p_T^2 + M^2}$. p_T is the transverse momenta of the pair. The transverse mass spectra have been evaluated for different M widows and plotted against $m_T - M$ and finally compared with the data [55]. From the experimental observations an interesting result is obtained for the m_T spectra which gives an indication of the formation of QGP in In+In nuclear collision. A non-monotonic behavior of the inverse slope parameter, T_{eff} is observed when extracted from the transverse mass spectra of the thermal lepton pairs - as a function of invariant mass. This non-monotonic trend of $T_{\rm eff}$ may possibly indicate the origin of lepton pairs from a partonic phase formed initially in the collisions. T_{eff} has been extracted from the theoretical estimation of the m_T spectra of In+In collisions and compared with the data.

The probability that a muon pair of invariant mass, M with transverse momentum, p_T will be emitted from a thermal system at temperature T is determined by the Boltzmann factor $\sim e^{-\sqrt{M^2+p_T^2}/T}$. For a dynamically evolving system like the one produced after In-In nuclei collisions at ultra-relativistic energies - the temperature decreases with time because a part of the thermal energy is spent to develop the collective motion in the system. Consequently the Boltzmann factor is modified to $\sim e^{-\sqrt{M^2+p_T^2}/T_{\rm eff}}$, where $T_{\rm eff} \sim T_{\rm th} + Mv_r^2$ - here the first term represent thermal part and the second term stands for the flow part of the energy. It is expected that the large M thermal pairs are originated from early time when temperature is large and flow velocity is small and the small M pairs are originated from the late stage of the evolution when the temperature is low but flow velocity is large. Therefore, the variation of the $T_{\rm eff}$ with invariant mass, M may very naively be treated as a chronometer of the heavy ion collisions. A detail discussion on T_{eff} vs M would be given in the next chapter.

We assume the following two scenarios for the collisions: (i)In+In $\rightarrow$ quark gluon plasma (QGP) $\rightarrow$ mixed phase of quarks and hadrons $\rightarrow$ hadronic phase and (ii) In+In $\rightarrow$ hadronic phase and check by comparing with data which is the possible scenario realized in these collisions. Some earlier studies [194, 200, 201, 202] with the assumption for scenario-I are also available.

5.2 Dimuon productions at $\sqrt{s_{NN}}$=17.3 GeV fron In+In collision

Let's recall the rate of thermal dilepton production *i.e.,* the number of thermal pairs per unit space-time volume per unit four momentum volume (discussed in chapter 2), [63, 67, 92] as follows;

$$\frac{dR}{d^4p} = -\frac{\alpha^2}{6\pi^3 p^2} L(M^2) f_{\rm BE}(p_0) W^\mu_\mu(p_0, \vec{p}) \tag{5.1}$$

Recalling α as the electromagnetic coupling, W^μ_μ is the correlator of electromagnetic currents. $f_{\rm BE}(E,T)$ ($\vec{p}$, p_0 is nothing but the three momentum and energy, E of the pairs) is the thermal phase space factor for Bosons. For an expanding system the energy E appearing in the phase-space factor should be replaced by $u^\mu p_\mu$ having four velocity u^μ at each space-time point of the system. $p^2(=p_\mu p^\mu) = M^2$ is the invariant mass square of the lepton pair. The term $L(M^2) = \left(1 + 2\frac{m^2}{M^2}\right)\sqrt{1 - 4\frac{m^2}{M^2}}$ comes from the final state muonic current involving Dirac spinors, m is the muon mass.

When we consider the lepton pair production from quark gluon plasma phase then the major sources are the annihilation of quark anti-quark pairs($qq \rightarrow l\bar{l}$) [98]. In the present work the QCD corrections through the processes $q\bar{q} \rightarrow gl^+l^-$ $gq(\bar{q}) \rightarrow q(\bar{q})l^+l^-$ (see Ref. [99, 100]) have been taken into account. When we look into the lepton pair production from hadronic matter then we consider the decay of vector mesons to $\mu^+\mu^-$ and we use the vector meson dominance model. The the above equation 5.1 reduces to [93]

$$\frac{dR}{dM^2 p_T dp_T dy} = \frac{\alpha^2}{\pi^2 M^2} L(M^2) f_{\rm BE}(p_0) \sum_{V=\rho,\omega,\phi} A_V(p_0, \vec{p}) \tag{5.2}$$

where the spectral function of the vector meson A_V contains a pole part and continuum part. *i.e.,*

$$A_V = A_V^{\rm pole} + A_V^{\rm cont}. \tag{5.3}$$

Here we consider the vector mesons ρ(I=1, J=1, P=-1), ω(I=0, J=1, P=-1) and ϕ(I=0, J=1, P=-1) for the production of lepton pairs. Since our study of the invariant mass spectra is limited up to mass =1.5 GeV, the low mass region(LMR), we have not added the contribution from other thermal sources like J/ψ , $D\bar{D}$, Υ. These sources contribute substantially to the intermediate mass range (IMR: 1.5 < M(GeV) < 4.5 GeV). As mentioned before in the chapter-2 there are other non-thermal sources of productions. These non-thermal dimuons consists of Drell-Yan contributions resulting from hard interactions of partons of the colliding nuclei and from the decay of various mesons $(\pi, \eta, \omega, \eta', \rho, \phi$ etc.) after the freeze out of thermal system. The non-thermal contributions (apart from the decay of ρ meson) are subtracted from the data under consideration [197, 198, 199]. The contributions from the decay of ρ mesons after the freeze-out have been estimated as these have not been subtracted from the data. Cooper-Frye formula is used to evaluate the m_T distributions of dileptons originating from the decay of ρ mesons in the post freeze-out [203] period.

$$\begin{aligned}
\frac{dN_{\gamma^*}}{m_T dm_T} &= 2\pi \int dr \int d\eta \int d\phi \, r\tau \\
&\times \left(m_T \cosh(y-\eta) - \frac{\partial \tau}{\partial r} p_T \cos\phi \right) \\
&\times \rho(M) \Gamma_{V\to\mu^+\mu^-} / \Gamma_V^{\rm tot} f_{\rm unstable} \\
&dM^2 dy
\end{aligned} \tag{5.4}$$

Here r is the radial cordinate, τ is the proper time and ϕ is the azimuthal angle(from 0 to 2π), η is the space time rapidity and ρ(M) is the spectral function of the unstable vector meson ρ and f_{unstable} is the thermal phase space factor of the unstable vector meson. For a stable particle the spectral function is replaced by Dirac-delta function and consequently the usual thermal phase space factor is recovered. Γ_V^{tot} is the total decay width of the ρ vector meson. The f_{unstable} is given by

$$f_{\text{unstable}} = \frac{g}{(2\pi)^3} \frac{1}{\exp(\mathrm{p_0})/\mathrm{T} - 1} \rho(M) \tag{5.5}$$

where $p_0 = \sqrt{p^2 + M^2}$, g is the statistical degeneracy. As we have included the continuum in the vector mesons spectral functions four pion annihilation process [95] is not considered here to avoid over counting.

To evaluate the thermal dilepton spectra the static rate of emission $dR/d^2m_T dM^2 dy$ has to be integrated over the space time dynamics , governed by relativistic hydrodynamics as

$$\begin{aligned} \frac{dN}{m_T dm_T} &= 2\pi \sum_{phases} \int \left(\frac{dR}{d^2 m_T dy dM^2} \right)_{phase} \\ &\times dM^2 dy d^4x \end{aligned} \tag{5.6}$$

where d^4x is the 4 dimensional volume element, m_T is the transverse mass defined as $m_T = \sqrt{M^2 + p_T^2}$ and y is the particle rapidity ; p_z is the longitudinal momentum of the virtual photon(lepton pair). The limits for the integration over invariant mass M is fixed according to the experimental measurements for any desired mass windows ($M_{\min} \leq M \leq M_{\max}$). Similarly, the invariant mass spectra is obtained by integrating above Eq. 5.6 over the appropriate p_T windows. The space time evolution of the system (the integration over d^4x) has been studied using ideal relativistic hydrodynamics with longitudinal boost invariance [124] and cylindrical geometry [125] as already described in chapter 3. The system when produced after collision undergoes rapid thermalization process and reaches a thermalised state at a temperature T_i and time (τ_i). The initial temperature T_i and time τ_i are unknown quantities and constrained by the Eq. 3.34 for the hadron multiplicity, dN/dy= $\frac{3}{2}dN_{ch}/dy$, dN_{ch}/dy=110 for In+In collision. The effective radius R_A radius of the system is taken as 4 fm for impact parametre b=5.34 fm. The g_{eff} = 32 in the QGP phase is considered from the lattice QCD results for a 2 flavor QGP. The initial radial velocity, $v_r(\tau_i, r)$ and energy density, $\epsilon(\tau_i, r)$ profiles are taken similar to that photon productions (mentioned in the previous chapter) as follows:

$$v_r(\tau_i, r) = 0, \quad \epsilon(\tau_i, r) = \epsilon_0/(e^{\frac{r-R_A}{\delta}} + 1) \tag{5.7}$$

where surface thickness $\delta = 0.5$ fm. Initial energy density ϵ_0=4.5 GeV $/fm^3$.

The system thermalised at temperature T_i cools down to the freeze out temperature T_f, where the particles decouple and free stream towards the detector. It is already mentioned that we have assumed two kind of scenarios for the system produced in In-In collision; one with initial QGP phase that goes to hadron phase via first order phase transition and the other scenario with pure hadronic phase through out the evolution. When an initial QGP phase is assumed the temperature evolves as $T_i \longrightarrow T_c \longrightarrow T_f$ and in case of an initial hadronic phase it goes as $T_i \longrightarrow T_f$. The transition temperature T_c is taken to be 175 MeV [180, 204, 205]. Freeze out temperature is taken to be T_f=130 MeV which can reproduce the slope of ϕ spectra measured by NA60 collaboration for In-In collision [206]. We use Ansatz EoS: the bag model of equation of state for QGP phase and HRG EoS for the hadronic phase where all the resonances with mass $\leq$ 2.5

GeV have been considered [177]. The transition region has been parameterized as follows [130] :

$$s = f(T)s_q + (1 - f(T))s_h \tag{5.8}$$

where s_q (s_h) is the entropy density of the quark (hadronic) phase at T_c and

$$f(T) = \frac{1}{2}\left[1 + \tanh(\frac{T - T_c}{\Gamma})\right] \tag{5.9}$$

the value of the parameter Γ can be varied to make the transition strong first order or continuous. Γ=20 MeV. The ratios of various hadrons measured experimentally at different $\sqrt{s_{\rm NN}}$ indicate that the system formed in heavy ion collisions chemically decouple at a temperature ($T_{\rm ch}$) which is higher than the temperature for kinetic freeze-out (T_f)determined by the transverse spectra of hadrons [207]. T_{ch} is taken to be 170 MeV. Therefore, the system remains out of chemical equilibrium from $T_{\rm ch}$ to T_f. The chemical non-equilibration affects the dilepton yields at two levels: (a) the emission rate through the phase space factor and (b) the space-time evolution of the matter through the equation state. The value of the chemical potential and the its inclusion in the EoS has been taken in to account [193].

5.3 Results

The invariant mass spectra and transverse mass spectra using the above mentioned values of $T_i, \tau_i, T_c, T_{ch}, T_f$, EoS *etc* as inputs to hydrodynamics. First we discuss the results for scenario(I)-here it is assumed that a thermalised state of quarks and gluons

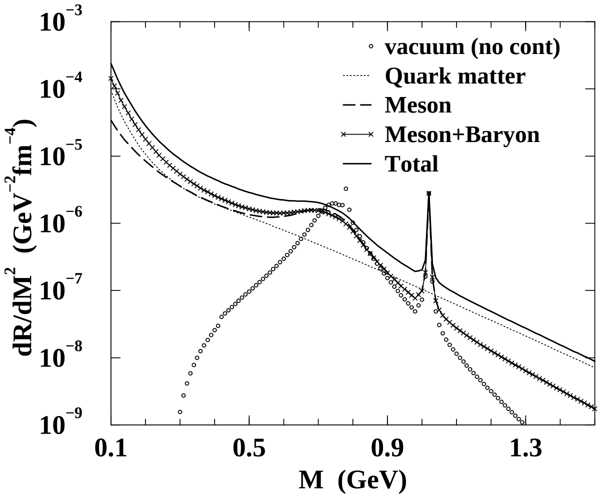

Figure 5.1: In variant mass spectra(acceptance corrected inclusive mass spectrum $p_T > 0$) of dimuon from quark gluon plasma and hadronic phase at T=0.175 GeV and μ_B=0.250 GeV.

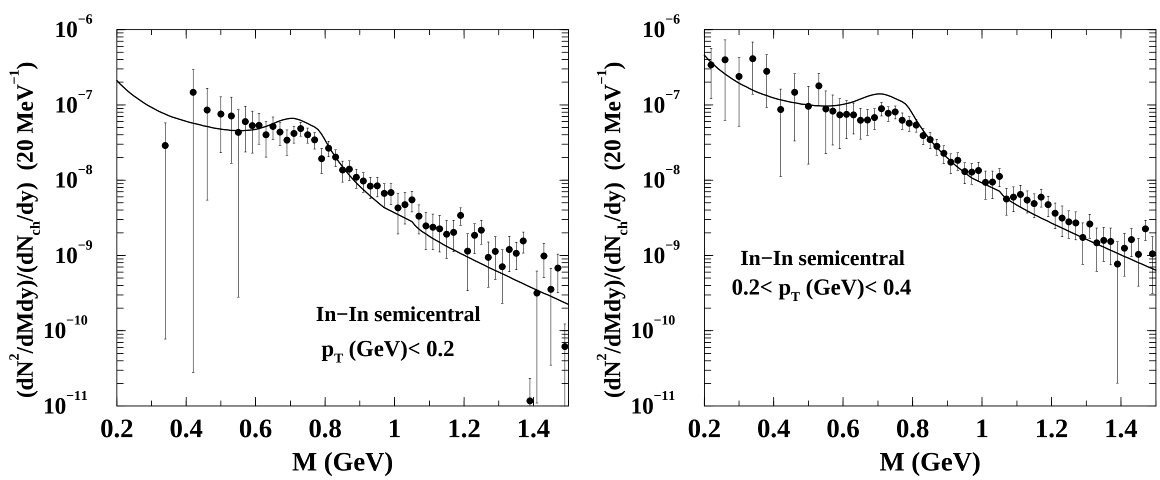

Figure 5.2: In variant mass spectra(acceptance corrected inclusive mass spectrum) for different p_T window (p_T <0.2 GeV and 0.2 < p_T (GeV)<0.4) of the dimuon measured by NA60 collaboration for semi central In-In collision ($\sqrt{s_{NN}}$=17.3 GeV). The solid line is the theoretical result for scenario-I.

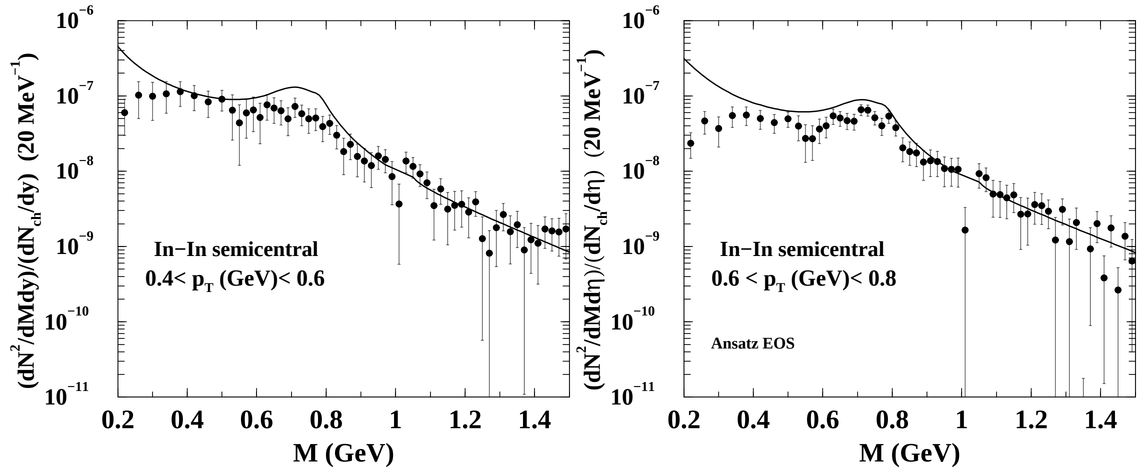

Figure 5.3: In variant mass spectra(acceptance corrected inclusive mass spectrum) for different p_T window (0.4<p_T(GeV) <0.6 GeV and 0.6 < p_T (GeV)<0.8) of the dimuon measured by NA60 collaboration for semi central In-In collision ($\sqrt{s_{NN}}$=17.3 GeV). The solid line is the theoretical result for scenario-I.

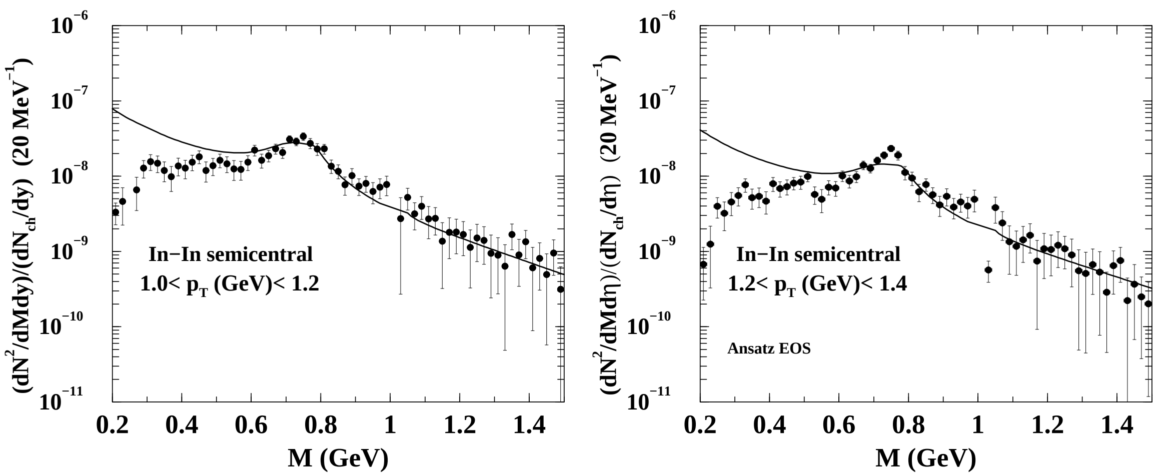

Figure 5.4: In variant mass spectra(acceptance corrected inclusive mass spectrum) for different p_T window (1.0<p_T(GeV) <1.2 GeV and 1.2 < p_T (GeV)<1.4) of the dimuon measured by NA60 collaboration for semi central In-In collision ($\sqrt{s_{NN}}$=17.3 GeV). The solid line is the theoretical result for scenario-I.

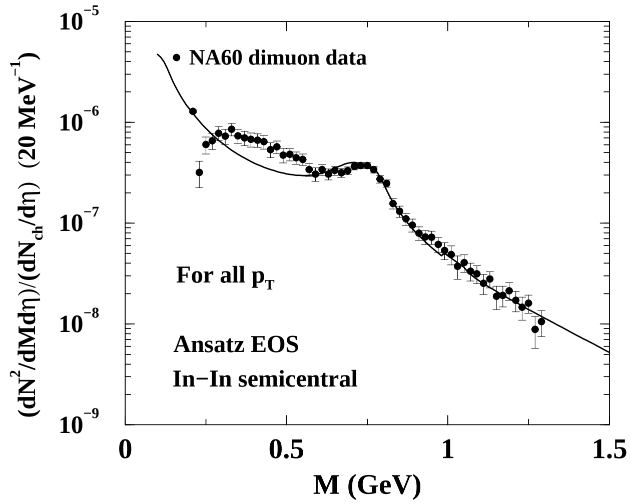

Figure 5.5: In variant mass spectra(acceptance corrected inclusive mass spectrum) for all p_T (p_T(GeV) <2.4 GeV) of the dimuon measured by NA60 collaboration for semi central In-In collision ($\sqrt{s_{NN}}$=17.3 GeV). The solid line is the theoretical result for scenario-I.

is formed after the collisions which reverts to hadronic phase through a weak first order phase transition. In Fig. 5.1 the static invariant mass spectrum (dR/dM^2 vs M) is plotted up to M=1.5 GeV. Vacuum (without continuum) contribution, the quark matter and hadronic matter (meson+baryon) contribution to the dimuon production rate is displayed in this Fig. 5.1. The curve with open circle shows the contribution from vacuum ρ in a hadronic matter. The long dashed curve shows the contribution when medium effects are considered with only meson loop and the solid line with star symbol represents the contribution when both meson and baryon loops are considered. It clearly says that the inclusion of baryon loops along with meson loops enhances the spectra substantially in the low mass region. The dotted curve is from quark matter. In the mass region $M < 0.5$ GeV and $M > 1.02$ GeV ($\sim m_\phi$) dilepton from the quark matter populate notably to the spectra.

In Figs. 5.2, 5.3 and 5.4 the invariant mass spectra are plotted for different p_T windows. Theoretical evaluation for low p_T window of the M spectra matches reasonably well with the measured data. But in the high p_T window $1.0 < p_T(GeV) < 1.2$, $1.2 < p_T(GeV) < 1.4$ theory over predicts the data in the low M region. In Fig. 5.5 the invariant mass spectra for all p_T ($0 < p_T(GeV) < 2.4$) is displayed and the theoretical evaluation matches quite well with the data except a slight disagreement in the very low mass region.

Before discussing the m_T spectra it is important to mention here that initially there is no transverse collective flow ($v(\tau_i, r) = 0$), the entire energy of the system is thermal at mid-rapidity. With the progress of time some part of the thermal energy gets converted to the collective (flow) energy for a system undergoing hydrodynamic expansion. The measured m_T spectra of muon pairs therefore, contains contributions from both thermal as well as collective degrees of freedom *i.e.* the inverse slope parameter, $T_{\rm eff}$ can be written as $T_{\rm eff} = T_{\rm th} + Mv_r^2$ as mentioned earlier. Therefore, it is important to know the domains of M where the thermal contributions from early (quark matter) and late (hadronic) phases dominate corresponding to small and large radial flow respectively.

We observe significant enhancement in the dilepton yield in the mass region below the ρ pole compared to vacuum, nevertheless the total dilepton yield in this region of M contains notable the contribution from the partonic phase. However, the thermal pairs for M beyond m_ϕ-peak is dominated by QGP phase. Therefore, it is expected that the slope parameters extracted from the transverse mass distribution of lepton pairs for mass region above the ϕ-peaks should reflect the properties of quark matter

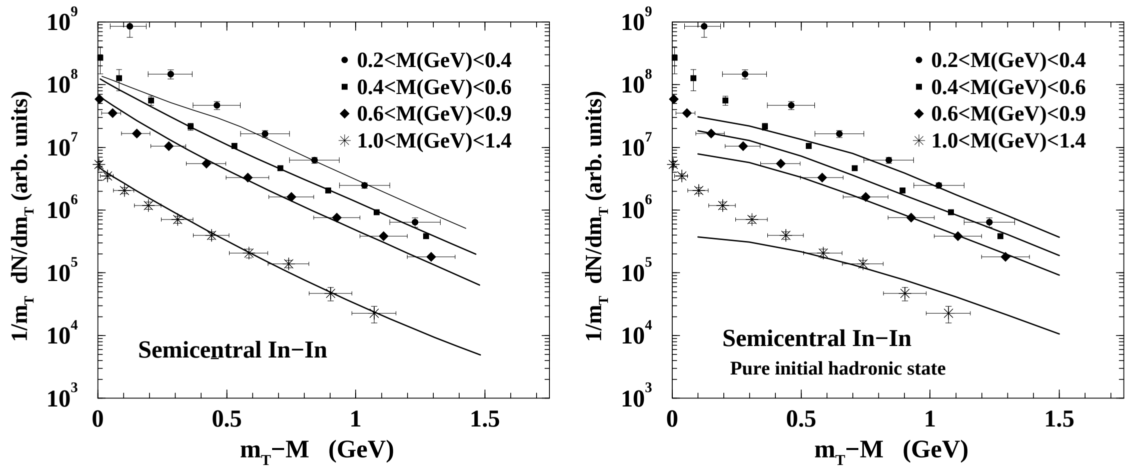

Figure 5.6: $m_T - M$ spectra of muon pair for different invariant mass ranges for semi central In+In collision at $\sqrt{s_{NN}}$=17.3 GeV. The solid line is the theoretical result for- *Left panel*: scenario-I (initial QGP phase) *Right panel*: scenario-II (initial hadronic state).

phase. Therefore, slopes at these M region will correspond to the early time when the radial follow is small. On the other hand the contributions in the region of ρ mass are overwhelmingly from the hadronic phase and hence the slope at this region correspond to the late time containing larger radial flow. For $M < m_\rho$ the situation is complex as it contains significant contributions from both the hadronic as well as the partonic phase. In Fig. 5.6 we plot the transverse mass spectra for various M windows. The resulting $m_T - M$ spectra of $\mu^+\mu^-$ are compared with the data for different mass window. The left panel of the Fig. 5.6 shows the calculation for scenario-I, where the initial QGP phase was assumed. For scenario (ii) with initial hadronic phase we keep dN/dy fixed and evaluate the initial temperature corresponding to a hadronic degrees of freedom g_{eff}. The right panel shows the calculation for an initial hadronic state (secnario-II). The data is very poorly explained with this scenario. In the scenario-II the p_T spectra

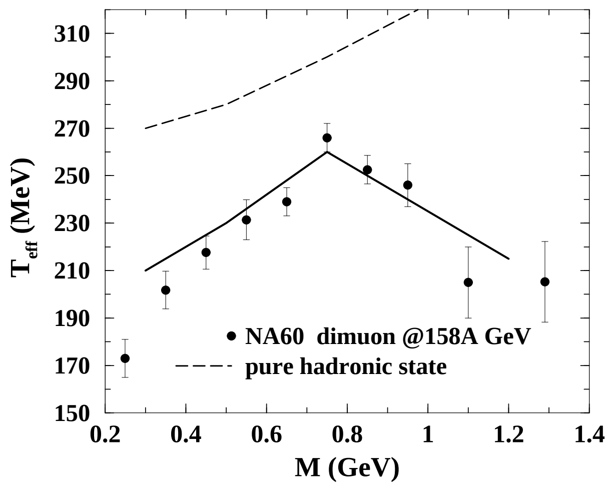

Figure 5.7: Inverse slope parametre obtained from the $m_T - M$ spectra of different mass ranges of muon pair for scenario-I and scenario-II. The long-dashed curve is for hadronic initial state.

have higher slopes i.e, because the system here has a long life time and development of flow velocity is more. The scenario-I calculation agrees well with the data for all the mass ranges shown.

Finally in Fig 5.7 the effective temperature obtained from the inverse slope of these spectra have been plotted and compared with the data. The slopes have been estimated from theoretical results (scenario-I by solid lines and scenario-II by long dashed lines) by parameterizing to an exponential function within the $(m_T - M)$ range $0.3 \leq m_T - M$(GeV)$\leq$ 1.0. It is clear from the results that the slope is reproduced well if the source is predominantly partonic. A similar non-monotonic behavior is observed in the variation of the elliptic flow (v_2) of photons as a of transverse momentum [208, 209].

The modification of hadronic spectral functions in a thermal bath and its effects on electromagnetic radiation is a field of great interest. The invariant mass distribution of lepton pairs are sensitive to both the pole shift and broadening [96, 163, 164, 165, 166, 168, 173, 210, 211, 212]. But the p_T spectra of the EM radiation is insensitive to the broadening of the spectral function provided the integration over the M is performed over the entire region. This is because broadening does not change the density of vector mesons significantly ([168]). However, the number density of vector mesons depends on the nature (shape) of the spectral function within the integration limit. Therefore, the p_T spectra may change due to broadening when the integration over M is done in a limited M domain.

5.4 Summary

Similar to photon productions the dimuon productions have been evaluated. Here the productions have been estimated considering two scenarios of the expanding system : (I) with the assumption of an initial QGP phase which goes to hadronic phase via a 1st order phase transition and (II) with the assumption of an initial hadronic state. For the productions from QGP we consider the lepton pair productions from the major sources like the annihilation of quark anti-quark pairs($qq \rightarrow l\bar{l}$). The QCD corrections through the processes $q\bar{q} \rightarrow gl^+l^-$ $gq(\bar{q}) \rightarrow q(\bar{q})l^+l^-$ have been taken into account. The lepton pair productions from hadronic matter have been considered from the decay of vector mesons (ρ, ω, ϕ) to $\mu^+\mu^-$ using the vector meson dominance model. Real time formalism is considered for the production from hadronic matter. Since our study of the invariant mass spectra is limited up to mass =1.5 GeV, the low mass region(LMR), we have not added the contribution from other thermal sources like J/ψ , $D\bar{D}$, Υ. These sources contribute substantially to the intermediate mass range (IMR: 1.5 < M(GeV) < 4.5 GeV). As mentioned before in the chapter-2 there are other non-thermal sources . These non-thermal dimuons are originated from Drell-Yan processes involving hard interactions of partons of the colliding nuclei and from the decay of various mesons $(\pi, \eta, \omega, \eta', \rho, \phi$ etc.) after the freeze out of thermal system. Since the non-thermal contributions apart from the decay of ρ meson are subtracted from the data under consideration. But the contributions from the decay of ρ mesons after the freeze-out are considered using Cooper-Frye formula as these have not been subtracted from the data. We do not consider four pion annihilation process (as some author considers) as we include the continuum in the vector mesons spectral functions to avoid over counting. The invariant mass spectra normalized with the charge hadron multiplicity, $(dN/dMdy)/(dN_{ch}/dy)$ have been evaluated as a function of invariant mass M for different p_T windows for scenario(I). Also we evaluate the transverse mass spectra $(dN/m_T dm_T \equiv dN/p_T dp_T)$ for different M widows as a function of $m_T - M$ for both scenarios (I) and (II) and finally compared with the data [55]. It has been observed that the scenario(I) with the initial QGP phase explains the data well. Our study restricts up to low mass region (LMR: $M < 1.5$ GeV). It is clear from the study that the excess dimuons in the very low mass region $(M < M_\rho)$ of the invariant mass spectra are due to the broadening of ρ spectral function due to the interaction with the thermal mesons and baryons. From the experimental observations an interesting result is obtained for the m_T spectra which gives an indication of the formation of QGP in In+In nuclear collision. A non-monotonic behavior of the inverse slope parameter, $T_{\rm eff}$ is observed when extracted from the transverse mass spectra of the thermal lepton pairs - as a function of invariant mass. This non-monotonic trend of T_{eff} may possibly indicate the origin of lepton pairs from a partonic phase formed initially in the collisions. The scenario-I reproduces the data when scenario-II fails to explain. The thermal dimuon pairs for M beyond m_ϕ-peak (M_ϕ=1.02 GeV) is dominated by QGP phase. Therefore, it is expected that the slope parameters extracted from the transverse mass distribution of lepton pairs for mass region above the ϕ-peaks should reflect the properties of quark matter phase. Therefore, slopes at these M region will correspond to the early time when the radial flow is small (T_{eff} is small). On the other hand the contributions in the region of ρ mass (0.77 GeV) are overwhelmingly from the hadronic phase where the radial flow is more (there by T_{eff} is more) and hence the slope at this region correspond to the late time containing larger radial flow. The theoretical analysis of both M-spectra and $m_T - M$ spectra supports the formation of QGP in In+In nuclear collision at $\sqrt{s_{NN}}$=17.3 GeV SPS energy.

Chapter 6

Ratio of the electromagnetic spectra and the initial temperature of the system formed in heavy ion collision

---

The ratios of the spectra of thermal photons to thermal dileptons have been evaluated at SPS, RHIC and LHC eneries. The ratio, $R_{em} = (dN_\gamma/d^2p_Tdy)_{y=0}/(dN_{\gamma^*}/d^2p_Tdy)_{y=0}$ *has been evaluated for different invariant mass windows of dileptons. Since the individual thermal spectra of photons and dileptons suffer from uncertainties present in the input parametres like* T_i*,* τ_i*, EoS,* T_c*,* v_r *etc., we evaluate the ratio to get rid of some of these uncertainties involved in the model while extracting the thermodynamic information of the system created in the heavy ion collision. It has been studied that while considering the ratio of the two spectra at various* p_T*, the ratio reaches a plateu beyond certain value of* p_T *and some of the uncertainties get cancelled away. The ratio is found to be least sensitive to* T_c*, EoS and* v_r *for the invariant mass window* $1.2 < M(GeV) < 1.3$ *of dileptons. But it is highly sensitive to* T_i*. Hence it is argued that the simultaneous measurements of photons, dileptons by choosing the mass window judiciously and thus evaluating ratio would help in extracting the temperature information of the initial stage of the system produced in heavy ion collision.*

6.1 Introduction

In the previous chapters we have discussed the importance of the study of photons and dileptons in heavy ion collision. The thermal photon productions and thermal dilepton/dimuon productions at SPS, RHIC and LHC energies have also been discussed in the last two chapters. As discussed, the thermodynamic information of the system can be obtained from the thermal spectra of photons and dileptons. However, this is a difficult task, because on the one hand the thermal radiation from QGP has to be disentangled from those produced in initial hard collisions and from the decays of hadrons and on the other hand the evaluation of thermal photon and dilepton spectra need various inputs *such as* initial temperature (T_i), thermalization time (τ_i), equation of state (EoS), transition temperature (T_c), freeze-out temperature (T_f) etc, which are not known unambiguously. The sensitivity of the photon spectra on these inputs are demonstrated in [52, 213]. Therefore, the theoretical results on the transverse momentum (p_T) spectra of photons and dileptons always suffer from these uncertainties. Of course, certain constraints can be imposed on these inputs from experimental results - *e.g.* transverse mass spectra of hadrons and hadronic multiplicities are useful quantities for constraining freeze-out conditions and initial entropy production. Here the aim is to get rid of these model dependence of the input parameters and to extract the thermodynamic information of the system. Therefore, in the present work we evaluate the ratio of the transverse momentum spectra of thermal photons and lepton pairs [53, 54]: in which most of the uncertainties mentioned above are expected to get canceled so that it provides accurate information [214, 215] about the state of the matter formed initially. We calculate the ratio, R_{em} for SPS, RHIC and LHC energies.

6.2 Ratio of electromagnetic probes

The ratio, $R_{\rm em}$ of the p_T spectra of thermal photons to dileptons can be written as follows [53]:

$$R_{em} = \frac{(\frac{d^2N_\gamma}{d^2p_Tdy})_{y=0}}{(\frac{d^2N_\gamma^\star}{d^2p_Tdy})_{y=0}} = \frac{\sum_i \int_i \left(\frac{d^2R_\gamma}{d^2p_Tdy}\right)_i d^4x}{\sum_i \int_i \left(\frac{d^2R_{\gamma^*}}{d^2p_Tdy dM^2}\right)_i dM^2 d^4x.} \tag{6.1}$$

The numerator (denominator) is the invariant momentum distribution of the thermal photons (lepton pairs). In Eq. 6.1 p_T, y and M denote the transverse momentum, rapidity and the invariant mass of the lepton pair. The summation in Eq. 6.1 runs over all phases through which the system passes during the expansion. $(d^2R/d^2p_Tdy)_i$ and $(d^2R/d^2p_TdydM^2)_i$ are the static rates of photon and dilepton productions from the phase i, which is convoluted over the expansion dynamics through the space-time integration over d^4x. The integration over M is done by selecting invariant mass windows - $M_{\rm min} \leq M \leq M_{\rm max}$ appropriately and we define $< M >= (M_{\rm min} + M_{\rm max})/2$.

6.3 Thermal photons and lepton pairs(e^+e^-)

The formalism for the thermal photon productions from QGP and hadronic phases considered here is same as described in sec. 4.3.2 of chapter 4. The mechanism of thermal dilepton productions from QGP phase are also discussed earlier in chapter 5. For the dilepton production from hadronic phase we use a parametrization to evaluate the decay of vector mesons. For a case study of how effectively the radial flow of the system can be extracted by using ratio,R_{em}, as a tool we consider the following parametrization [94, 210] to evaluate the dilepton emission rates from light vector mesons (ρ, ω and ϕ):

$$\begin{aligned} \frac{d^2R_{\gamma^*}}{dM^2d^2p_Tdy} &= \frac{\alpha^2}{2\pi^3}f_{\rm BE}[\frac{{f_V}^2M\Gamma_V}{(M^2-{m_V}^2)^2+(M\Gamma_V)^2} \\ &+\frac{1}{8\pi}\frac{1}{1+exp((w_0-M)/\delta)} \\ &\times(1+\frac{\alpha_s}{\pi})]. \end{aligned} \tag{6.2}$$

These parameterizations are consistent with the experimental data from $e^+e^- \rightarrow V(\rho,\omega$ or $\phi)$ processes [94, 163, 210]. Here, $f_{\rm BE}$, is the Bose-Einstein distribution. f_V is the coupling between the EM current and vector meson fields, m_V and Γ_V are the masses and widths of the vector mesons and ω_0 is the continuum threshold above which the asymptotic freedom is restored. We have taken $\alpha_s = 0.3$ (already we have shown in chapter 4 that the temperature dependent $\alpha_s(T)$ and the constant α_s with value 0.3 do not differentiate the p_T spectra substantially (see Fig. 4.8) , $\delta = 0.2GeV$, $\omega_0 = 1.3$ GeV for ρ and ω. For ϕ we have taken $\omega_0 = 1.5$ GeV and $\delta = 1.5$ GeV. The EM current in terms of ρ, ω and ϕ field can be expressed as $J_\mu = J_\mu^\rho + J_\mu^\omega/3 - J_\mu^\phi/3$. Therefore, the contributions from ω and ϕ will be down by a factor of 9 [53].

6.4 Initial conditions

For the space time evolution, the relativistic hydrodynamic equations are solved with the following initial conditions as described earlier in 5.7. The initial energy density,radial velocity are given as:

$$\epsilon(\tau_i, r) = \frac{\epsilon_0}{1+e^{\frac{r-R_A}{\delta}}} \tag{6.3}$$

and

$$v_r(\tau_i, r) = v_0 \left(1 - \frac{1}{1 + e^{\frac{r-R_A}{\delta}}}\right), \tag{6.4}$$

where the surface thickness, $\delta = 0.5$ fm. We have taken $v_0 = 0$. The energy density ϵ_0 is calculated from the T_i obtained from Eq. 3.34 constraining the hadron multiplicity dN/dy. The values of initial temperatures and thermalization times for various beam energies are shown in Table-6.1. In the present work we assume $T_c = 192$ MeV [180] and 175 MeV for comparison. In a first order phase transition scenario - we use the bag model EoS for the QGP phase and for the hadronic phase all the resonances with mass ≤ 2.5 GeV have been considered [177]. The effect of the chemical freeze out of the system before kinetic freeze out is included in the present study through non-zero chemical potential discussed before.

One point may be added here for other initial conditions. One can consider Glauber or CGC initial conditions. For example if the energy density profile $\epsilon_0(\tau_i, r)$ is smooth with a peak at the center unlike the simple one we consider here, then the required ϵ_0 or T_i would be larger. But it would have less effect as far as ratio of the spectra (photon to dilepton) are considered.

To show the sensitivity of the results on the EoS we also use the lattice QCD EoS for $T \geq T_c$ [191]. For the hadronic matter (below T_c) all the resonances with mass ≤ 2.5 GeV have been considered [177]. The transition region is obtained from the parametrization [130] of entropy as $s = f(T)s_q + (1 - f(T))s_h$. where s_q (s_h) is the entropy density of the quark (hadronic) phase at T_c and $f(T) = \frac{1}{2}(1 + \tanh(\frac{T-T_c}{\Gamma}))$. The value of the parameter Γ can be varied to make the transition strong or weak first

Table 6.1: The values of various parameters - thermalization time (τ_i), initial temperature (T_i), freeze-out temperature (T_f) and hadronic multiplicity dN/dy - used in the present calculations. dn/dy for LHC is taken from [216]

Accelerator	$\frac{dN}{dy}$	$\tau_i(fm)$	T_i(GeV)	T_f (MeV)
SPS	700	1	0.2	120
RHIC	1100	0.2	0.4	120
LHC	2100	0.08	0.7	120

order[1]. Results for various values of Γ are given below.

6.5 Results

The values of the initial and freeze-out parameters shown in table 6.1 along with the EoS mentioned above have been used as inputs to hydrodynamic calculations. The experimental data from SPS on p_T spectra of hadrons [217], photons [137] and m_T & M distribution of dileptons [162] have been reproduced in [218], [167, 168] and [164] respectively by using different input parameters mentioned in the table. The values of the initial parameters for SPS agree with the results obtained from the analysis of photon spectra in Refs. [182, 183, 184, 185]. Recently the data from PHENIX collaboration at RHIC [219, 220] has also been explained in [52] (see also [181]) with the parameters mentioned in table 6.1.

The emission rate of lepton pairs from hadronic and quark matter at a temperature of 200 MeV has been displayed in Fig. 6.1. The contribution from QGP dominates over its hadronic counterpart (without any medium effects) for $M < 600$ MeV and

[1]Although it is discussed earlier, here it is mentioned again for the ready reference

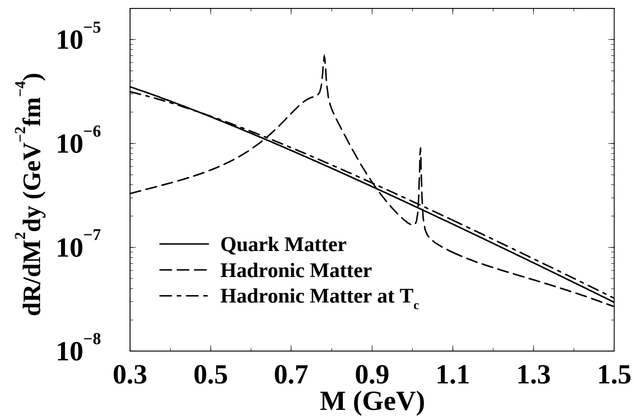

Figure 6.1: The invariant mass distributions of thermal dileptons from QGP and hadronic matter at $T = 200$ MeV. Solid (dashed) line indicates the emission rates from QGP (hadronic matter). The dot-dashed line stands for emission rate from hadronic matter at the transition temperature (see text).

$M > 1.1$ GeV, therefore, these windows are better suited for the detection of QGP. However, it should be mentioned here that the modification of the spectral functions of vector mesons (especially ρ and ω) - pole shift [173] or broadening [163] may give rise to dileptons at the lower M region making it difficult to detect contributions from QGP below ρ-peak. The change in the hadronic spectral function will enhance the dileptons from the hadronic contribution in the lower mass ($M < 600 MeV$) window, however the overall structure in the ratio, R_{em} will not change appreciably. At the transition temperature (~ 200 MeV) if one assumes the vector mesons masses go zero *a la* Brown-Rho scaling [173] then all the peaks in the dilepton spectra disappeared and the rates obtained from EM current-current correlator (dot-dashed line) are close to the rate from QGP, indicating that the $q\bar{q}$ interaction in the vector channel has become very weak, signaling the onset of deconfinement. This also indicates the quark-hadron duality [221, 222] near the transition point.

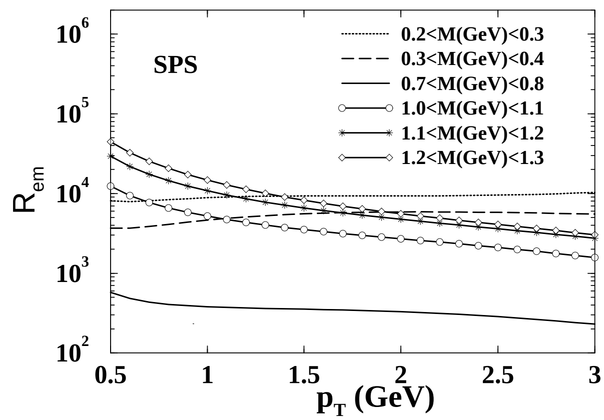

Figure 6.2: The thermal photon to dilepton ratio, R_{em} as a function of transverse momentum, p_T for various invariant mass window.

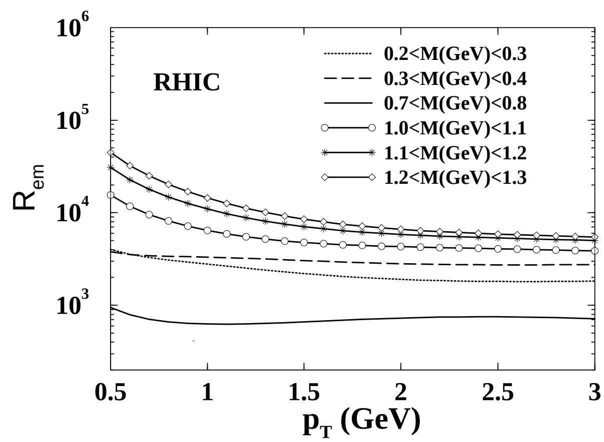

Figure 6.3: Same as Fig. 6.1 for RHIC energy

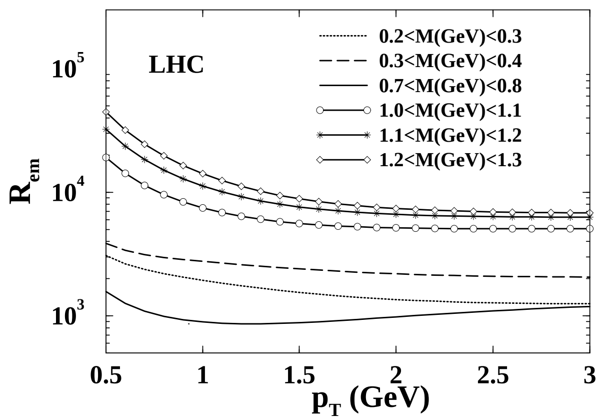

Figure 6.4: Same as Fig. 6.1 for LHC energy

The p_T dependence of the ratio, R_{em} for SPS, RHIC and LHC energies are shown in Figs. 6.2, 6.3 and 6.4 respectively. It is observed that at a given p_T, the ratio decreases with M, reaches a minimum around ρ-peak and increases beyond the ρ-peak. This trend is valid for all the cases, *i.e.* SPS, RHIC and LHC as expected because at a given p_T the R_{em} is actually the inverse of the invariant mass distribution of lepton pairs (the denominator *i.e.* the photon spectra is same for all the mass windows). It is observed from Figs. 6.2,6.3 and 6.4 that the ratio, R_{em} decreases with T_i for given p_T for M below the ρ-peak and the opposite behavior is observed above the ρ-peak. The slope of the ratio at low p_T also indicates substantial change with increasing M, the slope is minimum at the ρ-peak. Therefore, the minimum of the slope may be used to locate the effective mass of the vector meson in medium.

It is clear from the results displayed in Figs. 6.2 6.3 and 6.4 that the quantity, R_{em}, reaches a plateau beyond $p_T = 1.5$ GeV for all the three cases *i.e.* for SPS, RHIC and LHC. It may be noted here that the degree of flatness increases from SPS to RHIC and LHC. As mentioned before for all the three cases, except T_i all other quantities *e.g.* T_c, v_0 and EoS are same, so the difference in the value of R_{em} in the plateau region originates due to different values of initial temperature, indicating this can be a measure of T_i.

The following analysis will be useful to understand the origin of the plateau at high p_T region. The strong three momentum dependence in the dilepton and photon emission rates (Eqs. 2.69 and 2.42 respectively) originates from the thermal factor, $f_{\rm BE}(E,T)$. For a static system the energy, E can be written as $E = M_T \cosh y$, where $M_T = \sqrt{p_T^2 + M^2}$ $y = \tanh^{-1} p_z/E$. At high $p_T(>> M)$, $M_T \approx p_T$, the exponential momentum dependence become same for real photon ($M^2 = 0$) and dilepton ($M^2 \neq 0$) spectra and hence plateau is expected in the static ratio for large p_T for all the M values.

We recall that for an expanding system out of the two kinematic variables describing the dilepton spectra, p_T is affected by expansion but M remains unchanged. The range of M under present study is $0.3 < M(\text{GeV}) < 1.3$. The energy, E appearing in both the photon and dilepton emission rates should be replaced by $u^\mu p_\mu$ for a system expanding with space-time dependent four velocity u^μ. Under the assumption of cylindrical symmetry and longitudinal boost invariance u^μ can be written as

$$u^\mu = \gamma_r(t/\tau, v_r\cos\phi, v_r\sin\phi, z/\tau) \tag{6.5}$$

where $\tau = \sqrt{t^2 - z^2}$ $t = \tau\cosh\eta$, $z = \tau\sinh\eta$, $v_r(\tau, r)$ is the radial velocity, $\gamma_r(\tau, r) = (1 - v_r(\tau, r))^{-1/2}$. The four momentum, $p^\mu = (M_T\cosh y, p_T, 0, M_T\sinh y)$ where $p_L =$

$m_T\sinh y$. Therefore, for dilepton

$$u^\mu p_\mu = \gamma_r(M_T\cosh(y-\eta) - v_r p_T\cos\phi) \tag{6.6}$$

for photon the factor $u^\mu p_\mu$ can be obtained by replacing M_T in Eq. 6.6 by p_T. The p_T dependence of the photon and dilepton spectra originating from an expanding system is predominantly determined by the thermal factor $f_{\rm BE}$. Therefore, we discuss following three scenarios. (i)At high $p_T(>> M)$, $M_T \approx p_T$, the exponential momentum dependence become same for real photon and dilepton spectra, hence for large p_T a plateau is obtained in the ratio, R_{em} (Figs 6.2-6.4). In other words, the effect of radial flow on the photon and dilepton is similar at high p_T region. (ii)If the large M pairs originate from early time (when the flow is small) the ratio, R_{em} which includes space-time dynamics will be close to the static case and hence will show plateau. (iii) However, at late time when the radial flow is large and M is comparable to or larger than p_T the effect of flow on dilepton will be larger (receives larger radial kick due to non-zero M) than the photon and hence the plateau may disappear. Therefore, the disappearance of plateau structure in R_{em} in moderate or high M region will indicate the presence large radial flow. This can be understood from the results shown in Figs 6.5 and 6.6.

In Fig. 6.5 the ratio has been displayed only for quark matter. Here the flow is expected to be small within the present framework. A plateau is observed for all the M windows. It is observed that for high M ($\sim$ 1.2 GeV) and low M ($\sim$ 0.3 GeV) the ratio for QM is close to the total for LHC energy (not shown separately).

In Fig.6.6 the ratios has been displayed for hadronic matter only. Here the flow is expected to be very large. Within the ambit of the present modeling the contribution

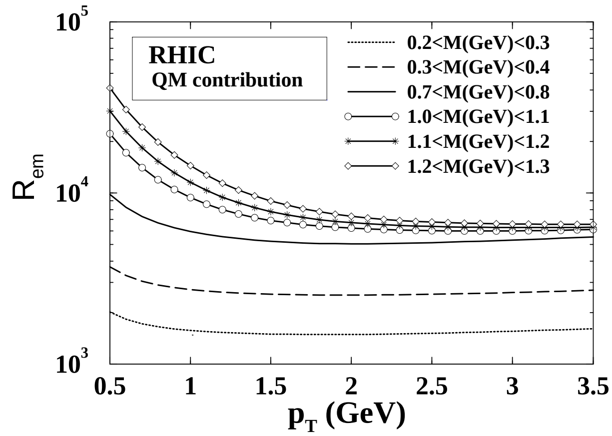

Figure 6.5: Same as Fig. 6.2 for quark matter phase only.

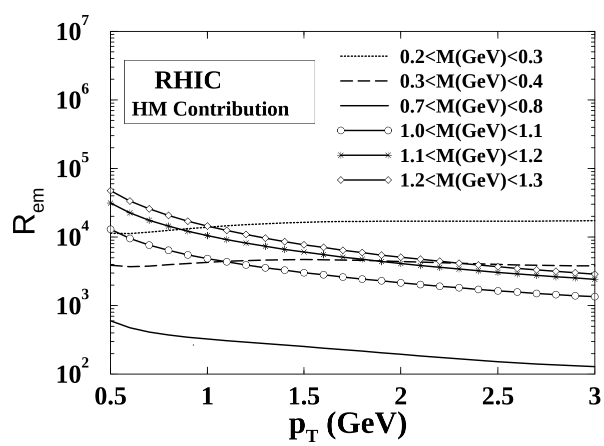

Figure 6.6: Same as Fig. 6.2 for hadronic phase only.

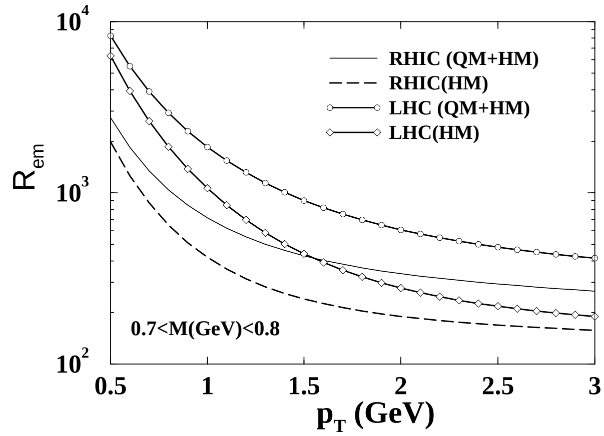

Figure 6.7: The variation R_{em} with p_T for invariant mass window, $M = 0.7 - 0.8$ GeV. An unrealistically large value to radial flow has been given initially to demonstrate that large flow can destroy the plateau structure of R_{em}. Other inputs are similar to those of Figs.6.3 and 6.4.

from the hadronic matter is overwhelmingly large in the M region, $0.7 < M < 0.8$ GeV. Therefore, this region will have large effects from the radial flow and hence it may destroy the plateau. This is clearly seen in Fig. 6.6 for the curve corresponding to $0.7 < M < 0.8$ GeV.

To demonstrate the effect of flow on the plateau we use an initial velocity profile (which gives rise to stronger radial flow than Eq. 6.4) of the form $v_r(\tau_i, r) = v_0' \frac{r}{R_A}$ with an unrealistically large value of $v_0' \sim 0.5$ (just to demonstrate the point). These inputs are used only for results shown in Fig.6.7, which clearly indicates the disappearance of plateau. Variation of R_{em} with p_T corresponding to hadronic phase is steeper than the total because of larger radial flow in the late stage of the evolution.

Now we demonstrate the effect of other parameters on R_{em}. We show the sensitivity of the results to T_c in Fig. 6.8 for two invariant mass windows. The results show that R_{em} is not very sensitive to T_c.

The EoS has a large effect on the individual spectra. At p_T=1 GeV if we observe the value in the p_T spectra of photons and dileptons for BAG-HRG and Lattice EoS (as here described) then photon spectra differ by 81 % and dilepton spectra by 96% within the ambit of the present calculation. But the R_{em} changes by 16 % only. The effect of the EoS on R_{em} is demonstrated in Fig. 6.9, by varying width parameter Γ. It is observed that the effect of EoS on R_{em} for both the mass windows are small. Again the effect of EoS on R_{em} differs for different mass windows. Similar to the effect of T_c, here also the larger mass window ($1.2 \leq M(\text{GeV}) < 1.3$) is less affected by the change in EoS. This is because the effect radial flow (and other hydrodynamic effects) are less at early times from where higher mass lepton pairs originate. Replacement of lattice QCD EoS for QGP phase by bag model shows negligible effects on R_{em}.

In Fig. 6.10 the dependence of $R_{em}(p_T = 2.5\text{GeV})$ is depicted as a function of T_i for $1.2 \leq M(\text{GeV}) < 1.3$. This mass window is selected because the contributions from the hot quark matter phase dominates this region and the effects of T_c, EoS etc are least here. $p_T = 2.5$ GeV is taken because R_{em} achieved a complete plateau at this value of transverse momentum. The change in R_{em} from SPS to RHIC is about 40% and from RHIC to LHC this is about 20%. A simultaneous measurements of photons and dileptons with required accuracy, will be useful to disentangle the effects of flow and true average temperature in a space-time evolving system formed in heavy ion collisions at ultra-relativistic energies.

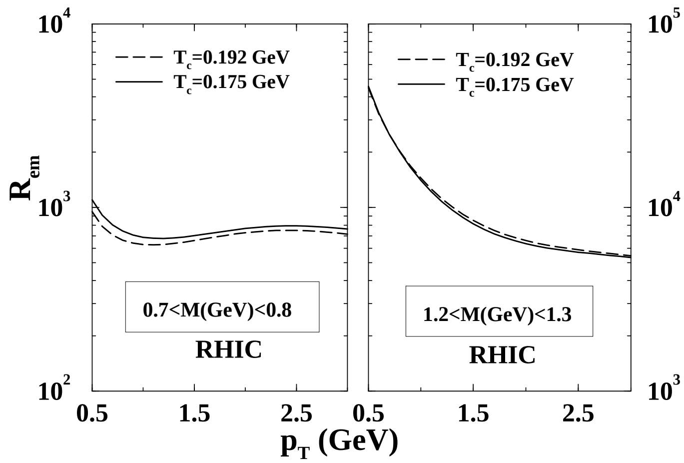

Figure 6.8: R_{em} as a function of p_T for different values of T_c for invariant mass windows, $M = 0.7 - 0.8$ GeV and $M = 1.2 - 1.3$ GeV.

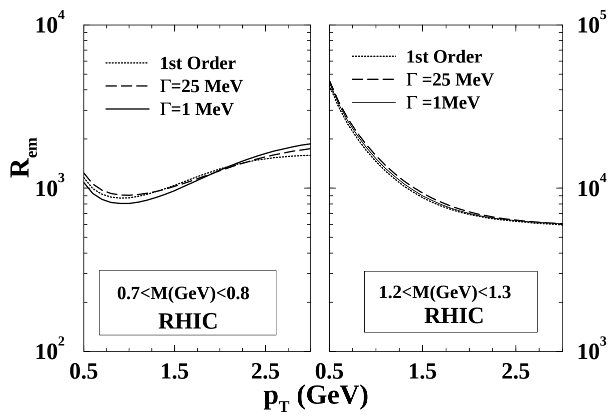

Figure 6.9: R_{em} as a function of p_T for different EoS for invariant mass windows, $M = 0.7 - 0.8$ GeV and $M = 1.2 - 1.3$ GeV.

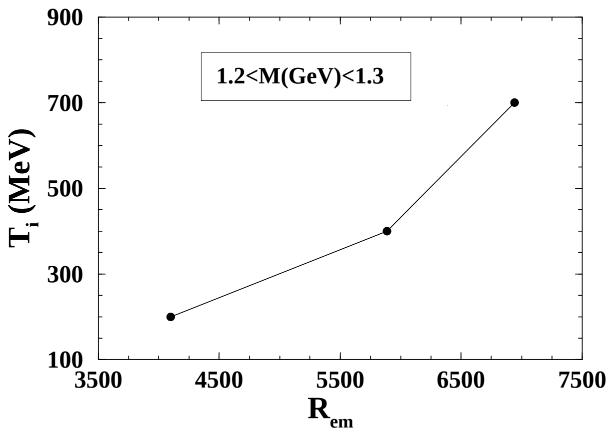

Figure 6.10: Initial temperature is plotted as function $R_{em}(p_T = 2.5\text{GeV})$ for the M window 1.2-1.3 GeV.

We have evaluated R_{em}^{pQCD}, the ratio $(d^2N_\gamma/d^2p_Tdy)_{y=0}/(d^2N_{\gamma^*}/d^2p_Tdy)_{y=0}$ for hard processes using pQCD (Fig. 6.11). The hard photon contributions has been constrained to reproduce the PHENIX data [223] for pp collisions at $\sqrt{s_{NN}} = 200$ GeV. We consider $q\bar{q} \to \gamma^* \to l^+l^-$, $q\bar{q}\to g\gamma^*$ and $qg(\bar{q})\to q\bar{q}\gamma^*$ for the lepton pair production. The M integration of lepton pair spectra is done over the range $0.2 \le M(\text{GeV}) \le 0.3$. We observe that R_{em}^{pQCD} increases for p_T up to ~ 3 GeV, above which it reaches a plateau. Therefore, for $p_T \sim 1-3$ GeV, R_{em} for the thermal and pQCD processes show different kind of behavior. The plateau arises from the fact that at large p_T both photon and dilepton show power law behavior [140, 142]. In the low p_T domain lepton pairs (photon) from pQCD processes indicate a Gaussian type [140] (power law) variation resulting in the increase of R_{em} with p_T.

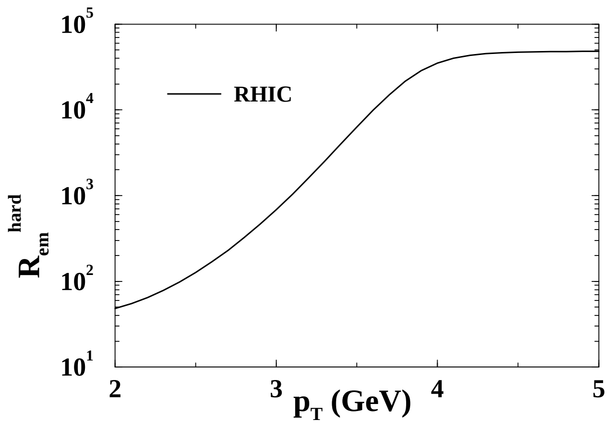

Figure 6.11: The variation R_{em} for hard photons to dileptons ratio as a function of p_T for $\sqrt{s_{NN}} = 200$ GeV and invariant mass window, $M = 0.2 - 0.3$ GeV.

6.6 Summary and Conclusions

We have studied the variation of R_{em}, the ratio of the transverse momentum spectra of photons and dileptons and argued that measurement of this quantity will be very useful to determine the value of the initial temperature of the system formed after heavy ion collisions. We have observed that R_{em} reaches a plateau beyond $p_T = 1.5$ GeV. The value of R_{em} in the plateau region depends on T_i. However, the effects of flow, the dependence on the values of T_c and v_0 get canceled away in the ratio, R_{em}. The effect of EoS on R_{em} is less in the mass window $1.2 < M(GeV) < 1.3$. For M above and below the ρ peak and $p_T \geq 2$ GeV the contributions from quark matter dominates, therefore these regions ($p_T \geq 2$ GeV and $1.2 < M(GeV) < 1.3$) could be chosen to estimate the initial temperature of the system formed after the collisions [53].

It is well known that T_{eff}, the inverse slope (see *e.g.* [197]) extracted from the p_T

spectra of EM radiation contains the effect of temperature as well as flow. We have seen that when the flow is less (in the initial stage of the evolution) the ratio, R_{em} shows a plateau for large $p_T(>> M)$, the height of the plateau in this region will give a good measure of the average temperature. However, a large flow can destroy the plateau and hence the deviation from the flatness of the R_{em} versus p_T curve may be used as a measure of flow. So a careful selection of M and p_T regions will be very helpful to disentangle the effect of average temperature and the flow (see also [224]).

We have included the effects of chemical off-equilibrium of mesons on the photon and dilepton production rates. This is implemented by appropriately introducing non-zero pionic chemical potential, μ_π ($\mu_\rho = 2\mu_\pi, \mu_\omega = 3\mu_\pi$) in the thermal factors [225] appearing both in photon and dilepton emission rates. We observed that the plateau structures in R_{em} do not change for RHIC and LHC, but for SPS it has little effect.

The change in hadronic spectral function at non-zero temperature and density is a field of high contemporary research interest as this is connected with the restoration of chiral symmetry in QCD. From the QGP diagnostics point of view the background contributions (photons and dileptons from thermalized hadrons) are affected due to medium effects on hadrons. Therefore, some comments on this issue are in order here.

We have checked that the p_T spectra of both photons and dileptons are sensitive to the pole shift of hadronic spectral function, as the reduction of hadronic masses [173] in a thermal bath increases their abundances and hence the rate of emission gets enhanced [150, 151, 167, 168, 210]. The invariant mass distribution of lepton pairs are sensitive to both the pole shift and broadening [55, 163, 164, 165, 166, 168]. But the p_T spectra of the EM radiation is insensitive to the broadening of the spectral function provided the integration over the M is performed over the entire region. This is because broadening does not change the density of vector mesons significantly (see also [168]). However, the number density of vector mesons depends on the nature (shape) of the spectral function within the integration limit. Therefore, the p_T spectra may change due to broadening when the integration over M is done in a limited M domain. We have checked that doubling the ρ width ($\sim 2 \times 150$ MeV) changes R_{em} by 10%. It is important to note that the change in mass and widths can not be arbitrary it should obey certain constraints as discussed in [226]. Therefore, simultaneous measurements of p_T spectra and invariant mass distribution of real and virtual photons could be very useful to understand the nature of medium effects on hadrons [168].

Chapter 7

Ratio of the spectra and radial flow of partonic & hadronic phases

---

In the previous chapters we discussed the production of photons and dileptons at different center of mass energies ($\sqrt{s_{NN}}$) measured by different experiments from different heavy ion collisions. Also we discussed the importance of the evaluation of ratio of the p_T spectra in extracting the thermodynamic (Temperature) information of the system in a less model dependent way. Here we study the collectivity in terms of radial flow, v_r developed in the system. The v_r has been extracted simultaneously using the p_T spectra of photons and dileptons at various invariant mass windows. The variation of v_r has been studied with the average temperature T_{av} and invariant mass M. The variation of v_r with M shows a non-monotonic behaviour for an initial QGP phase. v_r has been evaluated for RHIC and LHC energies for different invariant mass windows. Also an attempt has been made to extract v_r using the experimental data at SPS.

7.1 Introduction

The hot and dense matter formed in the partonic phase after ultra-relativistic heavy ion collisions expands in space and time due to high internal pressure. Consequently the system cools and goes to hadronic matter from the partonic phase. Initially (when the thermal system is just born) the entire energy of the system is thermal in nature and with progress of time some part of the thermal energy gets converted to the collective (flow) energy. In other words during the expansion stage the total energy of the system is shared by the thermal as well as collective degrees of freedom. The evolution of the collectivity within the system is sensitive to the EoS. Therefore, the study of the collectivity in the system formed after nuclear collisions will be useful to shed light on the EoS [193, 227, 228] of the strongly interacting system at high temperatures and densities. In this chapter we try to discuss the study of collectivity in terms of radial flow, v_r, developed in the system produced in the heavy ion collisions.

It is well known that the average magnitude of radial flow can be extracted from the transverse momentum (p_T) spectra of the hadrons. However, hadrons being strongly interacting objects can bring the information of the state of the system when it is too dilute to support collectivity. On the other hand electromagnetic (EM) probes *i.e.* photons and dileptons are produced and emitted from each space time points. Therefore, estimating radial flow from the EM probes is more advantageous and it sheds light on the time evolution of the collectivity in the system. The collectivity in terms of T_{eff} is demonstrated by NA60 collaboration [197, 229] through dilepton measurements in In+In collisions at SPS energy. The slope of the transverse mass spectrum of lepton pairs, T_{eff} of invariant mass M can be related to the space-timed averaged quantities like radial flow velocity $v_{\rm r}$ and the average temperature T_{av} as $T_{\rm eff} \sim T_{\rm av} + Mv_{\rm r}^2$. T_{eff} is estimated from dilepton spectra [197] shows a different kind of behavior [55, 194, 200, 201, 202, 225] as compared to that from hadronic spectra. T_{eff} when extracted from the spectra of hadrons it shows a monotonic increase with mass (mass ordering). But the effective temperature extracted from transverse mass spectra of dileptons increases linearly with invariant mass M up to ρ-mass and then falls. This is observed by NA60 Collaboration [197]. But the PHENIX data does not show this trend [230]. Here we show that although the above trend is maintained for RHIC energy but T_{eff} increases continuously with mass M for LHC energy without any decrease beyond ρ peak. In this work we also argue that $T_{\rm eff}$ may not be a direct answer to the radial flow since it depends on both average temperature of the system and flow velocity. We use both photon and dilepton transverse momentum spectra simultaneously to extract the radial flow for different invariant mass. In the previous chapter we have shown that the ratio ($R_{\rm em}$) of the p_T spectra of photons to lepton pairs has an advantage over the individual spectra because some of the uncertainties or model dependence pertaining to the individual spectra gets canceled in the ratio. Hence the ratio can be used as an efficient tool to understand the state of an expanding system. In the present work we focus on the extraction of the radial flow from ratio, R_{em} as in 6.1. We also argue that the simultaneous measurements of photons and dileptons will enable us to estimate the value of $v_{\rm r}$ for various invariant mass windows of the lepton pairs. The $v_{\rm r}$ obtained from the analysis of both the spectra vary with M non-monotonically. Such a behavior may be interpreted as due to the presence of two different kinds of thermal sources of lepton pairs of the expanding system.

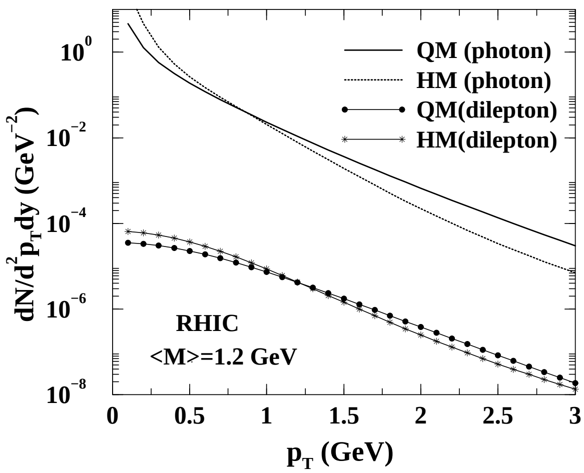

Figure 7.1: The p_T spectra of photons and dileptons from hadronic and quark matter at RHIC energy. The dilepton spectra is obtained by doing M integration from M =1.0 GeV to 1.4 GeV

.

While evaluating ratio, here, we have assumed T_c= 192 MeV as obtained in lattice QCD calculations [180]. The initial conditions are same as in the last chapter see 6.1.

7.2 Results and Discussion

In Fig. 7.1 the photon and dilepton spectra have been displayed for RHIC conditions. Results indicate that the photon spectra from QGP dominates over its hadronic counterpart for $p_T > 1.5$ GeV. The dilepton from QGP and hadrons are comparable in magnitude for entire range of p_T for $M \sim 1.2$ GeV (this is because of the inclusion of the continuum of the vector meson spectral functions [71, 94] without the continuum the quark matter part dominates). However, for $M \sim 0.75$ GeV the dileptons from the hadronic matter are overwhelmingly large compared to quark matter contributions (not shown in the figure). Therefore, an appropriate selection of p_T and M will be very useful to characterize a particular phase of the system.

Now we consider the variation of the ratio, R_{em} as a function of p_T for different invariant mass windows. The results are shown in the Fig. 7.2 and Fig. 7.3 below. The variation of R_{em} with respect to p_T can be parametrized as follows:

$$R_{em} \equiv A_3[\frac{m_T}{p_T}]^{B_3} exp[C_3(m_T - p_T)] \tag{7.1}$$

where A_3, B_3 and C_3 are constants and M_T, the transverse mass of the lepton pair is defined as, $M_T = \sqrt{p_T^2 + < M >^2}$. It is observed that the ratio decreases sharply and reaches a plateau beyond $p_T > 1.5$ GeV. This behavior of R_{em} as a function of p_T can be understood as follows: (i) for $p_T >> M$, $M_T \sim p_T$ and consequently $R_{em} \sim A_3$ giving rise to a plateau at large p_T. The height of the plateau is sensitive to the initial temperature of the system [53]. (ii) For $p_T < M$ $R_{em} \sim exp(-p_T/T_{eff})/p_T^{B_3}$ indicating a decrease of the ratio with p_T (at low p_T) as observed in the Fig. 7.2 and Fig. 7.3.

To indicate the effect of the radial flow velocity, v_r we have evaluated the R_{em} with and without radial flow (see Fig. 7.2 and Fig. 7.3). In case of vanishing radial flow the ratio can be parametrized as follows:

$$R^1{}_{em} \equiv A_1[\frac{m_T}{p_T}]^{B_1} exp[C_1(m_T - p_T)] \tag{7.2}$$

Here C_1 contains the information of the average temperature, T_{av} of the system ($C_1 \sim 1/T_{av}$).

In case of vanishing radial flow velocity the inverse slope of the photon and dilepton spectra represent the average temperature, $T_{\rm av}$ of the system. However, in case of non-zero radial flow the inverse slope contains the effect of average temperature as well as that of $v_{\rm r}$. Therefore, the difference in the slopes of the two cases will enable us to estimate the amount of collectivity in the system. As mentioned before for large initial temperature transverse momentum distribution of photons from QGP dominates over its hadronic counterpart for $p_T \geq 1.5$ GeV. However, in case of dileptons one has to select both the M and the p_T windows to observe QGP. For example the thermal dileptons from hadrons dominate over those from QGP for $M \sim 0.75$ GeV. Therefore, for estimating the radial velocity in the hadronic phase we chose $p_T \sim 0.5$ GeV and $M \sim 0.75$ GeV for demonstrative purpose. Similarly a p_T and M windows may be selected where contributions from QGP dominates.

The exponential slope of the ratio (C_3) can be related to the individual slopes of photons ($T_{{\rm e}ff1}^{-1}$) and dileptons ($T_{{\rm e}ff2}^{-1}$) as follows:

$$C_3 \times (m_T - p_T) = \frac{m_T}{T_{eff2}} - \frac{p_T}{T_{eff1}} \tag{7.3}$$

writing the effective (blue shifted) temperatures of the photon spectra and dilepton spectra as

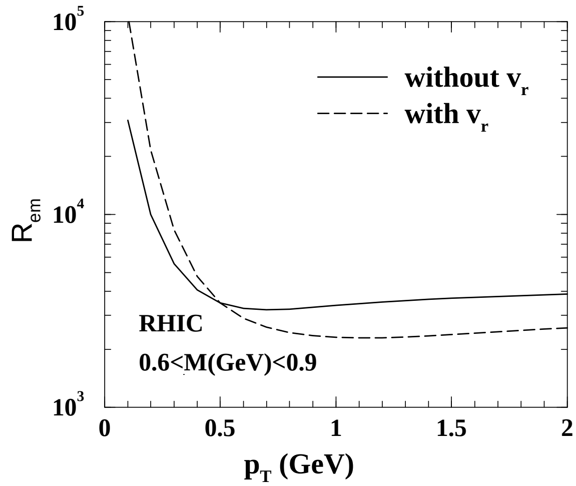

Figure 7.2: R_{em} as a function of p_T with and without radial flow for invariant mass $0.6 < M(GeV) < 0.9$. The spectra with radial flow is normalized to the one without radial flow at $p_T = 0.5$ GeV

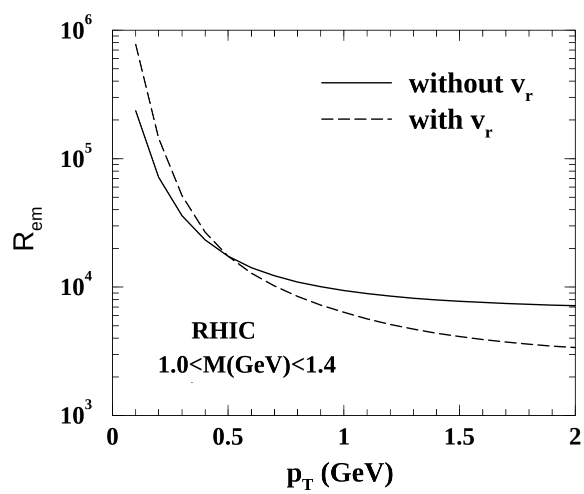

Figure 7.3: R_{em} as a function of p_T as in the above figure for invariant mass $1.0 < M(GeV) < 1.4$.

$$T_{eff1} = T_{av}\sqrt{\frac{(1+v_r)}{(1-v_r)}}, \tag{7.4}$$

$$T_{eff2} = T_{av} + M{v_r}^2 \tag{7.5}$$

we obtain,

$$C_3 \times (m_T - p_T) = \frac{m_T}{T_{av} + M{v_r}^2} - \frac{p_T}{T_{av}\sqrt{(1+v_r)/(1-v_r)}} \tag{7.6}$$

Further simplification leads to

$$aT_{av}^2 + bT_{av} + c = 0 \tag{7.7}$$

where a, b and c are functions of v_{r}. Solving Eq. 7.7 for a given C_3, M and p_T we obtain v_{r} as a function of the average temperature. The results are displayed in Figs. 7.4 and 7.5 for initial conditions of RHIC and LHC energies for invariant mass and p_T windows indicated. The contributions in the M and p_T windows shown in Fig. 7.4 are dominated by the hadronic phase *i.e.* from temperature range $T_c \sim 192$ MeV to $T_F \sim 120$ MeV. The radial velocity increases sharply with decrease in T_{av} in the hadronic phase.

We have estimated v_{r} with the EoS described earlier with two values of width parameter, Γ= 20 MeV and 1 MeV. A small value of $\Gamma \to 0$ mimick the first order transition. In Fig. 7.4, the v_{r} is plotted with T_{av} for two values of Γ. Indicating that the presence of the mixed phase (of hadrons and QGP) characterized by zero sound velocity slowed down the expansion of the system, resulting in a lower radial flow. Therefore, extraction of v_{r} from experimental data will be useful to understand the nature of the transition.

In Fig. 7.5 the radial velocity is displayed for (average) temperature range which is dominated by QGP phase. The results indicate a moderate v_r for RHIC but a large v_r

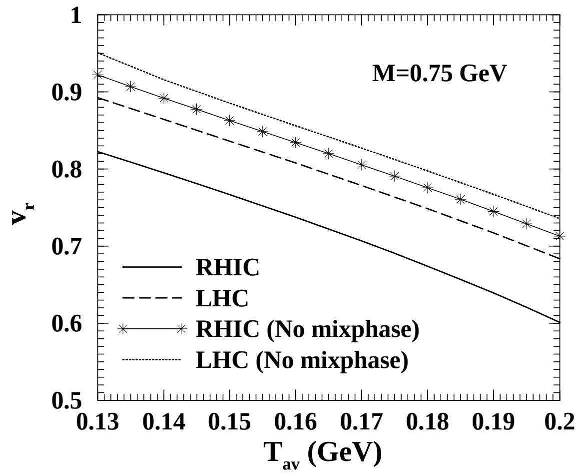

Figure 7.4: Variation of $v_{\rm r}$ with $T_{\rm av}$ for $M = 0.75$ GeV and $p_T = 0.5$ GeV. The solid (dashed) line indicate the results for RHIC (LHC) for EoS with first order phase transition. The line with asterisk (dotted line) stands for RHIC (LHC)for an EoS which excludes the mixed phase.

is achieved even in the QGP phase for LHC energies. The $v_{\rm r}$ for LHC is much larger than RHIC because of the longer life time and larger internal pressure of the partonic phase in LHC than RHIC.

In a first order phase transition scenario the QGP formed (at T_i) in heavy ion collisions returns to hadronic phase with a sharp change in entropy at T_c. We estimate the average values of the radial velocity ($v_{\rm i}soth$) on the constant temperature surfaces determined by the conditions: $T(r,\tau) = T_S$, for various values T_S. The variation of ($v_{\rm i}soth$) with T_S is depicted in Fig. 7.6 both for RHIC and LHC energies. $v_{\rm i}soth$ for LHC is larger than RHIC because of higher initial temperature and hence internal pressure. In contrast to the results shown in Figs. 7.4 and 7.5, the variation of $v_{\rm i}soth$ with T_S is not measurable as it does not depend on the kinematic variables, p_T and M. The

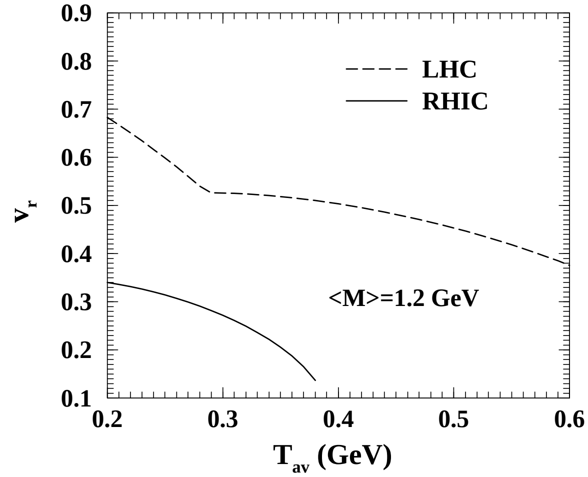

Figure 7.5: Variation of $v_{\rm r}$ with $T_{\rm av}$ for $M = 1.2$ GeV and $p_T = 0.5$ GeV at RHIC and LHC energies for EoS with a first order phase transition.

expansion is slower in the hadronic phase because of the softer EoS as compared to the QGP phase. For given T_c and T_F the life time of the hadronic phase is larger for softer EoS - allowing the system to develop large radial flow as evident from the results depicted in Fig. 7.6 for the low temperature part. The effective temperature extracted from the ratio is displayed in Fig. 7.7 as a function of M for RHIC energy. $T_{\rm eff}$ increases with M up to the ρ-peak and then decreases beyond ρ mass. The reduction of $T_{\rm eff}$ beyond ρ is indicating the dominance of the radiation from the high temperature phase in the high M region. For LHC, however, no clear reduction of $T_{\rm eff}$ beyond ρ - peak is observed (Fig. 7.8). At LHC the average temperature and the flow velocity in the early phase (from where large M pairs originate) are large (see Fig. 7.4). Hence the combination of both large v_r and large T_{av} does not allow $T_{\rm eff}$ to fall above the ρ-peak. The dependence of individual spectra on T_F is quite strong, however, we have observed that the slope of the ratio is insensitive to T_F and also to T_c. The slope of the ratio does

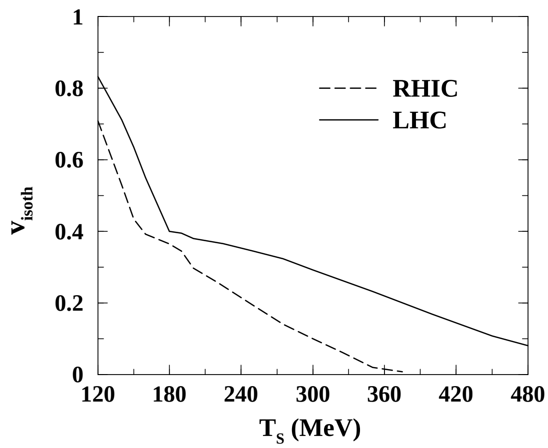

Figure 7.6: Variation of average radial velocity of the fluid on the constant temperature surface.

not change when the parameters like T_F changes from 0.120 GeV to 0.150 GeV and T_c from 0.192 GeV to 0.175 GeV. Eliminating $T_{\rm av}$ from Eq. 7.5 and taking the values of $T_{\rm eff1}$ and $T_{\rm eff2}$ from photon and dilepton spectra one can obtain the variation of v_r as a function of M. The results are shown in Fig. 7.9 for RHIC and LHC energies. A non-monotonic behavior of v_r with M is observed. Comparison of dilepton production from QGP and hadronic sources [53] indicate that in the low $M(< m_\rho)$ and high $M(> m_\phi)$ region the emission rate from QGP dominates over its hadronic counter part if the medium effects on the vector meson spectral functions are neglected. In other words, for a dynamically evolving system the low and high M pairs are emitted from early QGP phase, whereas lepton pairs with M around ρ - mass are emitted from the late hadronic phase. Therefore, low and high M domains represent early time where $v_{\rm r}$ is low and the $M \sim m_\rho$ domain represent late time - where $v_{\rm r}$ is large - giving rise to the observed variation in Fig. 7.9- indicative of a two different kinds of source in early and late times of the evolving system. For $< M >\sim 1.2$ GeV the flow velocity is not

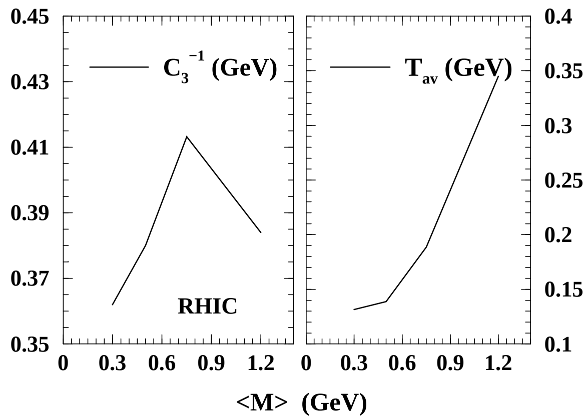

Figure 7.7: Left panel: The variation of the slope, C_3 with invariant mass obtained from the p_T spectra of ratio for RHIC energy is displayed in the left panel of the curve. Right panel: the variation of average temperature of the system. The left (right) vertical label is for left (right) panel of the curve

very small since this window is populated by both hadronic and partonic contributions almost equally. Again at LHC energy the partonic phase life time is more which favors the development of larger flow compared to RHIC energy. It is important to note at this point that for LHC, although the slope C_3 does not show a clear non-monotonic behavior with M, v_r does so. Because as described, before the slope C_3 depends not only on v_r but also on T_{av} and both are large in the partonic phase at LHC.

The two time scales - the life time of the partonic phase ($\tau_{\rm QGP}$) and the time an inward moving rarefaction wave takes to hit the center of the cylindrical geometry decide whether radial flow play any important role in the partonic phase or not. The later time scale is defined as $\tau_{\rm rw} \sim R/c_s$ where R is the transverse size of the system and c_s is the velocity of sound. If $\tau_{\rm Q}{}_{GP} \sim \tau_{\rm rw}$ then $v_{\rm r}$ will be large in the partonic phase. Therefore, an increase in τ_i ($\tau_{\rm Q}{}_{GP} \propto \tau_i$) will increase the radial flow in the partonic

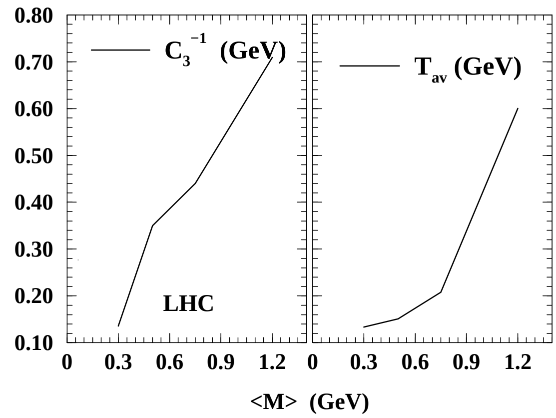

Figure 7.8: The variation of the slope, C_3 with invariant mass obtained from the p_T spectra of ratio for LHC. Please note that the scales in the left and the right panels are same.

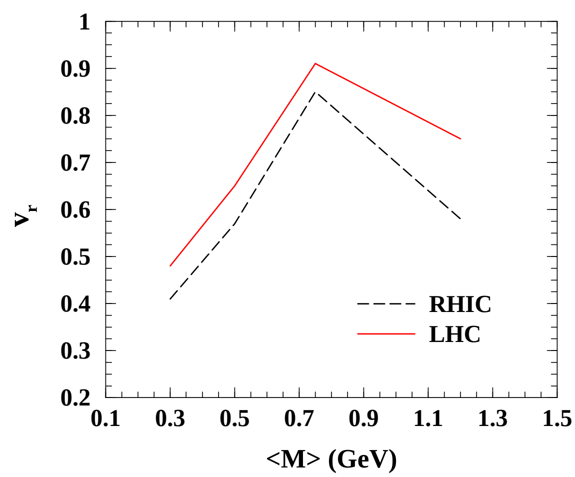

Figure 7.9: Radial velocity as a function of M for RHIC and LHC energies.

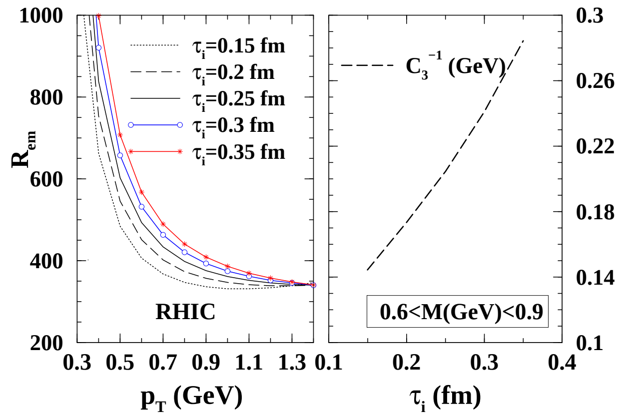

Figure 7.10: Left panel: Ratio of the p_T spectra for different initial thermalization time τ_i with all other parameters kept same. Right panel: variation of the effective slope C_3 as a function of initial thermalization time, τ_i. The left (right) vertical label is for left (right) panel of the curve

phase if the initial and the critical temperatures are kept fixed. However, an increase in τ_i from τ_1 to τ_2 produces same flow if the T_i decreases by a factor $(\tau_2/\tau_1)^{1/3}$. For a fixed T_i an increase in τ_i will increase the effective slope as evident from the right panel of Fig. 7.10. Therefore, the slope of the ratio may be used effectively to estimate the value of initial thermalization time.

At SPS energy, the p_T spectra of photons from Pb+Pb collision at $\sqrt{s_{NN}}$=19.4 GeV and the dimuon (m_T and M) spectra from In+In collision at $\sqrt{s_{NN}}$=17.3 GeV have been explained using the formalism described in chapter 4 and 5 [51]. The ratio has been evaluated for $\sqrt{s_{NN}}$=17.3 GeV and the v_r has been extracted. The non-monotonic variation of v_r with M is shown in [51].

7.3 Summary and Discussions

It has been shown that the p_T distribution of thermal photons and lepton pair spectra may be used simultaneously to estimate the magnitude of the radial velocity of different phases of the matter formed in nuclear collisions at ultra-relativistic energies. Judicious choices of the kinematic variables *e.g.* the invariant mass and the transverse momentum windows may be selected to estimate the flow velocity in the partonic and hadronic phases of the evolving matter. It has been observed that for RHIC and LHC energies the flow velocity increases with invariant mass up to the ρ peak beyond which it decreases. The T_{eff} may not decrease with mass beyond ρ peak if the average temperature and the flow velocity are large in the partonic phase as in case of LHC energy. By doing a simple analysis of photon and dilepton spectra we have extracted the radial flow velocity for various invariant mass windows. $v_{\rm r}$ varies with M non-monotonically. We argue that such a variation indicates the presence of two different types of thermal sources of lepton pairs.

Chapter 8

Strangeness production in heavy ion collision: kaon to pion and lambda to pion ratio

We study the strangeness productions in relativistic nuclear collisions at various centre of mass energies. A microscopic approach has been employed to study the kaon and Λ productions in heavy ion collisions. The momentum integrated Boltzmann equation has been used to study the evolution of strangeness in the system formed in heavy ion collision at relativistic energies. The kaon and Λ productions have been calculated for different centre of mass energies ($\sqrt{s_{\rm NN}}$) ranging from AGS to RHIC. The results for kaon productions have been compared with the available experimental data. We obtain a non-monotonic horn like structure for K^+/π^+ and Λ/π^+ when plotted with $\sqrt{s_{\rm NN}}$ with the assumption of an initial partonic phase beyond a certain threshold in $\sqrt{s_{NN}}$. However, a monotonic rise of K^+/π^+ is observed when a hadronic initial state is assumed for all $\sqrt{s_{\rm NN}}$. Experimental values of K^-/π^- are also reproduced within the ambit of the same formalism. Results from scenarios where the strange quarks and hadrons are formed in equilibrium and evolves with and without secondary productions have also been discussed.

8.1 Introduction

In the collision of two heavy nuclei at relativistic energies, some strange mesons and baryons are also detected along with other hadrons. Both strange particles and anti particles are produced keeping the net strangeness zero. Strangeness enhancement [37] has been proposed as a good signal for the production of QGP. Here the relative abundance of kaons (strange meson) to pions has been studied to analyze the QGP formation in the heavy ion collisions. For a simple understanding of the strangeness enhancement let us consider the baryon free system of non-interacting particles. While considering a hadronic system at thermodynamic equilibrium temperature , we can assume that the strangeness is contained in strange mesons and baryons, like K^- ($\bar{u}$ s), $\bar{K^0}$ ($\bar{d}$ s) and Λ (uds), Σ(uus, uds, dds) *etc.*; also in their corresponding antiparticles like K^+, $\bar{K^0}$ $\bar{\Lambda}$. The relative abundance of Λ, Σ is less compared to $K^-, \bar{K^0}$ since they have small phase space density because of higher masses. So in a hadronic system (at relatively small temperature compared to mass of Λ, Σ) the strangeness density is effectively decided by the kaon degrees of freedom (2 degrees of freedom-$K^-, \bar{K^0}$). Same argument is valid for K^+ and K^0 if antistrange particles are considered. In a quark gluon plasma phase the strangeness is carried by the s-quark ($\bar{s}$ quark if antistrange particles are considered). The strangeness density in QGP phase is more compared to a hadronic phase at the same temperature since the degrees of freedom of s-quark is more (6: 2 for spin and 3 for color) compared to kaons ($K^-, \bar{K^0}$) and the phase space is also more as mass of s-quark (current mass $\sim$ 150 MeV) is smaller than that of kaon ($\sim$ 490 MeV). Hence a partonic system formed at a temperature T will show more strangeness compared to a hadronic system at the same temperature. But if the system has some net baryons initially then strangeness density will change depending on the baryonic chemical potential (μ_B). The study of strangeness to entropy ratio is a subject of high interest and the ratios, $R^+ \equiv K^+/\pi^+$ and $R^\Lambda \equiv \Lambda/\pi^+$ are currently debated issues. R^+ is measured experimentally [231, 232, 233, 234] as a function of centre of mass energy ($\sqrt{s_{NN}}$). It is observed that the R^+ increases with $\sqrt{s_{NN}}$ and then decreases beyond a certain value of $\sqrt{s_{NN}}$ giving rise to a horn like structure, whereas the ratio, $R^- \equiv K^-/\pi^-$ increases faster at lower $\sqrt{s_{NN}}$ and tend to saturate at higher $\sqrt{s_{NN}}$.

Explanation of this structure has ignited intense theoretical activities [192, 235, 236, 237, 238, 239, 240, 241, 242]. Several authors have attempted to reproduce the experimental data of K^+/π^+ ratio using different approaches. While the authors in [236] use a hadronic kinetic model, in Ref. [237] high mass unknown hadronic resonances have been introduced through Hagedorn formula to describe the data. In Ref. [238] a transition from a baryon dominated system at low energy to a meson dominated system at higher energy has been assumed to reproduce the ratio K^+/π^+. The release of color degrees of freedom is assumed in [235] beyond a threshold in $\sqrt{s_{\rm NN}}$ (resulting in large pion productions) or the production of larger number of pions than kaons from higher mass resonance decays has also been employed [192] to explain the data. In the present work we employ a microscopic model for the productions and evolution of strange quarks and hadrons depending on the collision energy. Here we examine whether the K^+/π^+ experimental data can differentiate between the following two initial conditions or two scenarios - after the collisions the system is formed in: (I) the hadronic phase for all $\sqrt{s_{\rm NN}}$ or (II) the partonic phase beyond a certain threshold in $\sqrt{s_{\rm NN}}$. Other possibilities like formation of strangeness in complete thermal equilibrium and evolution in space time (III) without and (IV) with secondary productions of quarks and hadrons have been considered. (V) Results for an ideal case of zero strangeness in the initial state has also been presented. The ratio R^{Λ} has been evaluated for scenario (II).

In this work, we assume an initial state where non-strange sectors are in equilibrium but the strange degrees of freedom are out of equilibrium (having density below their equilibrium values). The strangeness production in a deconfined (partonic) phase is enhanced compared to the their production in the confined (hadronic) phase because of the higher mass and less degrees of freedom of the strange hadrons, K, Λ, ω *etc.* than the strange quarks. Therefore, the strangeness production during the space time evolution of the system for partonic initial state will be enhanced compared to the hadronic initial state, hence the enhanced production of strangeness could be an efficient signal for deconfinement [243, 244, 245]. In contrast to these studies Gazdzicki and Gorenstein [235, 246, 247] within the ambit of statistical model considered the strangeness production where both the strange and non-strange degrees of freedom are in thermal equilibrium and the production of strangeness during the expansion stage is ignored. In the present work we would like to compare the results on kaon to pion ratio from these two contrasting scenarios.

When the non-strange quarks and hadrons are in complete thermal (both kinetic and chemical) equilibrium and the strange quarks and strange hadrons are away from chemical equilibrium, the evolution of the strange sector of the system is governed by the interactions between the equilibrium and non-equilibrium degrees of freedom. The momentum integrated Boltzmann equation provides a possible framework to study the temporal evolution of strangeness in such scenarios. Similar approach has been used to study the sequential freeze-out of elementary particles in the early universe [248].

For the strangeness productions in the partonic phase we consider the processes of gluon fusion and light quarks annihilation. For the production of K^+ and K^- an exhaustive set of reactions involving thermal baryons and mesons have been considered. The time evolution of the densities are governed by the Boltzmann equation.

8.2 Strangeness productions

The productions of s and $\bar{s}$ in the QGP and the K^+ and K^- and Λ in the hadronic system are discussed below.

8.2.1 Strange quark productions in the QGP

The two main processes for the strange quark productions are gluon fusion ($gg \rightarrow s\bar{s}$) and quark(q)-antiquark ($\bar{q}$) annihilations ($q\bar{q} \rightarrow s\bar{s}$). The cross sections in the lowest order QCD is given by [243]:

$$\sigma_{q\bar{q}\rightarrow s\bar{s}} = \frac{8\pi\alpha_s^2}{27s}(1+\frac{2m^2}{s})w(s) \tag{8.1}$$

and

$$\sigma_{gg\rightarrow s\bar{s}} = \frac{2\pi\alpha_s^2}{3s}[G(s)\mathrm{t}anh^{-1}w(s) - \frac{7}{8} + \frac{31m^2}{8s}w(s)] \tag{8.2}$$

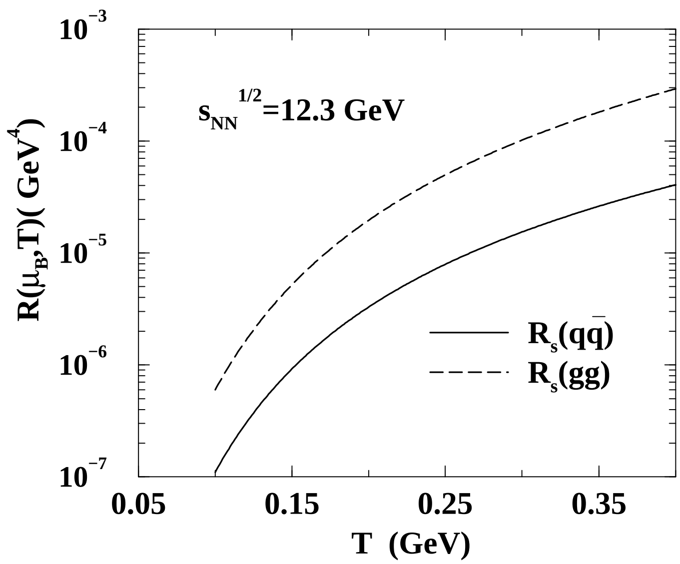

Figure 8.1: Rate of production of $\bar{s}$ quark from $gg \to s\bar{s}$ and $q\bar{q} \to s\bar{s}$ with temperature.

where m is the mass of strange quark, $s = (p_1 + p_2)^2$, is the square of the centre of mass energy of the colliding particles, p_i are the four momenta of incoming particles, $G = 1 + 4m^2/s + m^4/s^2$, $w(s)$=$(1 - 4m^2/s)$ and α_s is the strong coupling constant that depends on temperature [85].

8.2.2 Strange hadron(K^+ and K^- Λ) productions in the hadronic phase

The rate of $K^+(u\bar{s})$ and $K^-(\bar{u}s)$ and Λ productions in the hadronic phase can be categorized as due to (a) meson-meson (MM), (b) meson-baryon (MB) and (c) baryon-baryon (BB) interactions. Here we quote the main results [249] for kaon productions in the hadronic matter.

(a) For the first category $MM \rightarrow K\bar{K}$, we considered the following channels: $\pi\pi \rightarrow K\bar{K}$, $\rho\rho \rightarrow K\bar{K}$, $\pi\rho \rightarrow K\bar{K}^*$ and $\pi\rho \rightarrow K^*\bar{K}$. The invariant amplitude for these processes have been calculated from the following Lagrangians [249]. For the $K^*K\pi$ vertex the interaction is given by,

$$\mathcal{L}_{K^*K\pi} = g_{K^*K\pi} K^{*\mu} \tau [K(\partial_\mu \pi) - (\partial_\mu K)\pi] \tag{8.3}$$

Similarly for the ρKK vertex the interaction is,

$$\mathcal{L}_{\rho KK} = g_{\rho KK} [K\tau(\partial_\mu K) - (\partial^\mu K)\tau K]\rho^\mu \tag{8.4}$$

The isospin averaged cross section ($\bar{\sigma}$) for $MM \rightarrow K\bar{K}$ (i.e., $\pi\pi \rightarrow K\bar{K}$, $\rho\rho \rightarrow K\bar{K}$ and $\pi\rho \rightarrow K\bar{K}^*$, $\pi\rho \rightarrow K^*\bar{K}$) is evaluated by using,

$$\bar{\sigma} = \frac{1}{32\pi} \frac{P'}{sP} \int_{-1}^{1} dx M(s,x) \tag{8.5}$$

where P and P' are the three-momenta of the meson and kaons in the centre-of-mass frame, x is the cosine of the angle between P and P'. $M(s,x)$ is the iso-spin averaged squared invariant amplitude.

(b) For meson baryon interactions the dominant channels are ($MB \rightarrow YK$ (Y-hyperon)); $\pi\, N \rightarrow \Lambda\, K$, $\rho\, N \rightarrow \Lambda\, K$, $\pi\, N \rightarrow N\, K\, \bar{K}$ and $\pi\, N \rightarrow N\, \pi\, K\, \bar{K}$. The isospin averaged cross section is given by [250]:

$$\bar{\sigma}_{MB\rightarrow YK} = \sum_i \frac{(2J_i+1)}{(2S_1+1)(2S_2+1)} \frac{4\pi}{k_i^2} \frac{\frac{\Gamma_i^2}{4}}{(s^{\frac{1}{2}} - m_i)^2 + \Gamma_i^2/4} B_i^{in} B_i^{out} \tag{8.6}$$

J_i, Γ_i and m_i are the spin, width and mass of the resonances, $(2S+1)$ is the polarization states of the incident particles, k is the centre of mass momentum of the initial state.

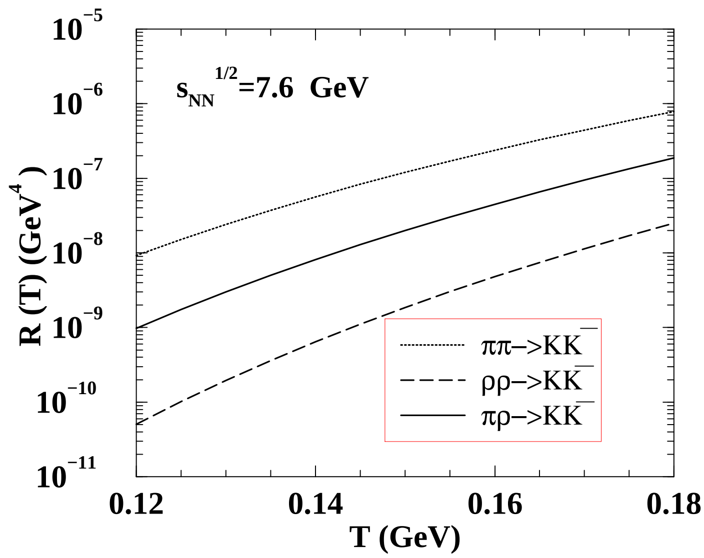

Figure 8.2: The rate of kaon production from dominant meson-meson interactions with temperature.

B^{in} and B^{out} are the branching ratios of initial and final state channels respectively. The index i runs over all the resonance states. For interactions $\pi N \to \Lambda K$, $\rho N \to \Lambda K$ we have considered $N_1^*(1650), N_2^*(1710)$ and $N_3^*(1720)$ as the intermediate states. Values of various hadronic masses and decay widths are taken from particle data book [250]. (c) For the last category of reactions *i.e.* for baryon baryon interactions ($BB \to BYK$) [251, 252, 253] the dominant processes are: $N\,N \to N\,\Lambda\,K$, $N\,\Delta \to N\,\Lambda\,K$, $\Delta\,\Delta \to N\,\Lambda\,K$, $N\,N \to N\,N\,K\,\bar{K}$, $N\,N \to N\,N\,\pi\,\pi\,K\,\bar{K}$ and $N\,N \to N\,N\,\pi\,K\,\bar{K}$.

The isospin averaged cross section of kaon production from the process like $N_1N_2 \to N_3\Lambda K$ is given by [251, 252, 254]

$$\bar{\sigma}_{NN\to N\Lambda K} = \frac{3m_N^2}{2\pi^2 p^2 s}\int_{W_{min}}^{W_{max}} dW W^2 k \times$$

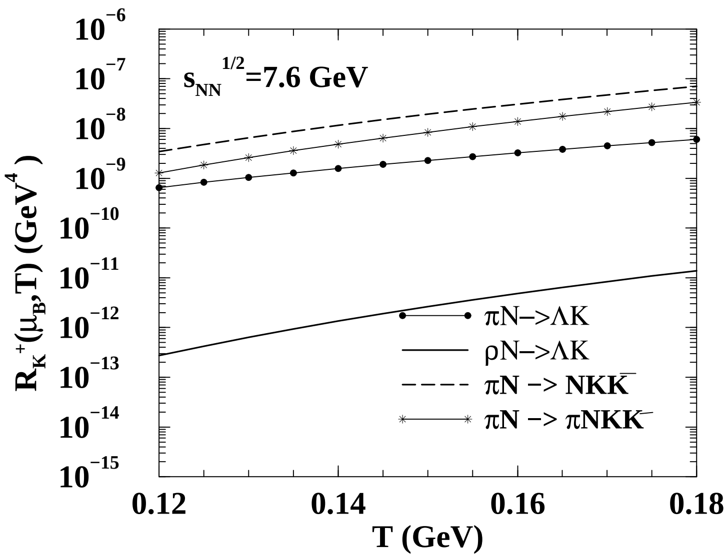

Figure 8.3: Rate of kaon productions from the meson-baryon interactions with temperature.

$$\int_{q_-^2}^{q_+^2} dq^2 \frac{f_{\pi NN}^2}{m_\pi^2} F^2(q^2) \frac{q^2}{(q^2 - m_\pi^2)^2} \bar{\sigma}_0(W; q^2). \tag{8.7}$$

Pion is the intermediate particle for the above interaction, m_N is the mass of N, W is the total energy in the centre of mass system of pion and N_2, $W_{min} = m_K + m_\Lambda$, $W_{max} = s^{1/2} - m_N$. Momentum of the pion, $k = \frac{1}{2W}\left[W^4 - 2W^2(M_\pi^2 + M_\Lambda^2) + (M_\pi^2 - M_\Lambda^2)^2\right]^{1/2}$. $q_\pm^2 = 2m_N^2 - 2EE' \pm 2pp'$ where p, p' are the momenta and E, E' are the energies of N_1 and N_3 respectively. We take $f_{\pi NN}$ =1 and to constrain the finite size of the interaction vertices we use the form factor $F = (\Lambda^2 - m_\pi^2)/(\Lambda^2 - q^2)$. $\bar{\sigma_0}$ is the isospin averaged cross section of $\pi N_2 \to \Lambda K$. Cross sections for the processes: $N\Delta \to N\Lambda K$ and $\Delta\Delta \to N\Lambda K$ have been taken from [252]. The cross section of other reactions *e.g.* $N\,N \to N\,N\,K\,\bar{K}$, $N\,N \to N\,N\,\pi\,\pi\,K\,\bar{K}$ and $N\,N \to N\,N\,\pi\,K\,\bar{K}$ have been taken from [253]. In a baryon rich medium, K^- gets absorbed due to its interaction with the baryons. The reactions $K^-p \to \Lambda\pi^0$, $K^-p \to \sigma\pi^0$, $K^-n \to \sigma p$, $K^-p \to \bar{K}^0 n$,

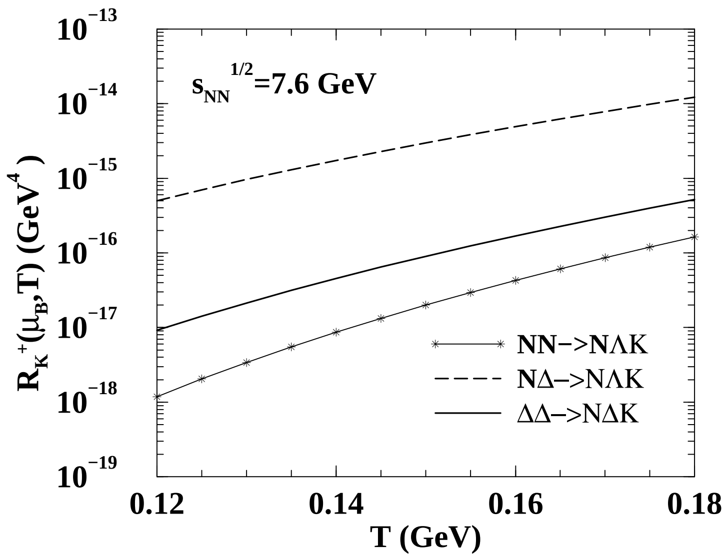

Figure 8.4: Rate of kaon productions from baryon-baryon interactions with temperature.

$K^- n \to K^- n$ have been considered for K^- absorption [253] in the nuclear matter.

8.2.3 Rate of strangeness productions

The number of s quarks produced per unit time per unit volume at temperature T and baryonic chemical potential μ_B is given by

$$R = \frac{dN}{d^4x} = \frac{dN}{d^4x} = \int \frac{d^3p_1}{(2\pi)^3} f(p_1) \int \frac{d^3p_2}{(2\pi)^3} f(p_2) v_{rel}\sigma \tag{8.8}$$

where p_i's are the momenta of the incoming particles and $f(p_i)$'s are the respective phase space distribution functions (through which the dependence on T and μ_B are introduced), $v_{\rm rel} = |v_1 - v_2|$ is the relative velocity of the incoming particles and σ is the production cross sections for the reactions. The same equation can be used for kaon production by appropriate replacements of phase space factor and cross sections.

8.3 Evolution of strangeness using Boltzmann transport equation

The possibility of formation of a fully equilibrated system in high energy nuclear collisions is still a fiercely debated issue because of the finite size and life time of system. In the present work we assume that the strange quarks or the strange hadrons (depending on the value of $\sqrt{s_{\rm NN}}$) produced as a result of the collisions are not in chemical equilibrium. The time evolution of the strangeness in either QGP or in hadronic phase is governed by the momentum integrated Boltzmann equation. We have assumed that the initial density of strange quarks or kaons (depending on the initial conditions (I) or (II)) is 20% away from the corresponding equilibrium density. We will comment on the amount of deviations from chemical equilibrium later.

8.3.1 Evolution in QGP and hadronic phases

The momentum integrated Boltzmann equations describing the evolution of i (particle) and j (anti particle) with proper time τ is given by:

$$\begin{aligned}
\frac{dn_i}{d\tau} &= R_i(\mu_B, T)[1 - \frac{n_i n_j}{n_i^{eq} n_j^{eq}}] - \frac{n_i}{\tau} \\
\frac{dn_j}{d\tau} &= R_j(\mu_B, T)[1 - \frac{n_j n_i}{n_j^{eq} n_i^{eq}}] - \frac{n_j}{\tau}.
\end{aligned} \tag{8.9}$$

where, n_i (n_j) and $n_i{}^{eq}$ ($n_j{}^{eq}$) are the non-equilibrium and equilibrium densities of i (j) type of particles respectively. R_i [1] is the rate of production of particle i at temperature T and chemical potential μ_B, τ is the proper time. First term on the right hand side of Eq. 8.9 is the production term and the second term represents the dilution of the system due to expansion. The time variation of temperature and the baryonic chemical potential of the thermal bath is governed by the hydrodynamic equations (next section). The indices i and j in Eq.8.9 are replaced by $s, \bar{s}$ quark in the QGP phase and by K^+, K^- in the hadron phase respectively.

8.3.2 Evolution in the mixed phase

For higher colliding energies i.e., $\sqrt{s} \geq 8.76$ GeV an initial partonic phase is assumed. The hadrons are formed at a transition temperature, $T_c = 190$ MeV through a first order phase transition from QGP to hadrons. The fraction of the QGP phase in the mixed phase at a proper time τ is given by [255, 256]:

$$f_Q(\tau) = \frac{1}{r-1}(r\frac{\tau_H}{\tau} - 1) \tag{8.10}$$

where τ_Q (τ_H) is the time at which the QGP (mixed) phase ends, r is the ratio of statistical degeneracy in QGP to hadronic phase. The evolution of the kaons are governed by [255]:

$$\begin{aligned} \frac{dn_{K^+}}{d\tau} &= R_{K^+}(\mu_B, T_c)[1 - \frac{n_{K^+}n_{K^-}}{n^{eq}_{K^+}n^{eq}_{K^-}}] - \frac{n_{K^+}}{\tau} + \\ & \frac{1}{f_H}\frac{df_H}{d\tau}(\delta n_{\bar{s}} - n_{K^+}) \end{aligned}$$

[1] It is noted that $R_{i/j}$ is the rate of production, reader should not be confused with the ratio

$$\frac{dn_{K^-}}{d\tau} = R_{K^-}(\mu_B, T_c)[1 - \frac{n_{K^+}n_{K^-}}{n^{eq}_{K^+}n^{eq}_{K^-}}] - \frac{n_{K^-}}{\tau} + \frac{1}{f_H}\frac{df_H}{d\tau}(\delta n_s - n_{K^-}) \tag{8.11}$$

Similar equation exist for the evolution of s and $\bar{s}$ quarks in the mixed phase (see [255] for details). In the above equations $f_H(\tau) = 1 - f_Q(\tau)$ represents the fraction of hadrons in the mixed phase at time τ. The last term stands for the hadronization of $\bar{s}(s)$ quarks to $K^+(K^-)$ [255, 257]. Here δ is a parameter which indicates the fraction of $\bar{s}(s)$ quarks hadronizing to $K^+(K^-)$. $\delta = 0.5$ indicates the formation of K^+ and K^0 in the mixed phase because half of the $\bar{s}$ form K^+ and the rest hadronize to K^0.

8.3.3 Space time evolution

The partonic/hadronic system produced in nuclear collisions evolves in space-time. The space-time evolution of the bulk matter is governed by the relativistic hydrodynamic equation:

$$\partial_\mu T^{\mu\nu} = 0 \tag{8.12}$$

with boost invariance along the longitudinal direction [258]. In the above equation $T^{\mu\nu} = (\epsilon + P)u^\mu u^\nu - g^{\mu\nu}P$, is the energy momentum tensor for ideal fluid, ϵ is the energy density, P is the pressure and u^μ is the hydrodynamic four velocity. The net baryon number conservation in the system is governed by:

$$\partial_\mu(n_B u^\mu) = 0 \tag{8.13}$$

where n_B is the net baryon density. Eqs. 8.12 and 8.13 have been solved (see [259, 260] for details) to obtain the variation of temperature and baryon density with proper time.

The initial temperatures corresponding to different $\sqrt{s_{\rm NN}}$ are taken from Table 8.2. The baryonic chemical potential at freeze-out are taken from the parametrization of μ_B with $\sqrt{s_{\rm NN}}$ [261](see also [192]) and the baryonic chemical potential at the initial state is obtained from the net baryon number conservation equation. The initial state might be a QGP or a hadronic that depends on the colliding energies. The baryonic chemical potential for both QGP and hadronic phase is obtained as follows.

For a QGP phase we treat the light flavors to be massless compared to the temperature of the system. The net baryon number is then given by

$$\begin{aligned} n_q^B = n_q - n_{\bar{q}} &= \frac{g_q}{2\pi^2}T^3[\exp\{\mu(T)/T\} - \exp\{-\mu(T)/T\}], \\ = \frac{g_q}{\pi^2}T^3\sinh(\frac{\mu}{T}). \end{aligned} \tag{8.14}$$

Assuming boost invariance and neglecting the transverse expansion, the baryon number conservation $\partial_\mu n_q^{B\mu} = 0$ leads to

$$\begin{aligned} n_q^B\tau &= const. \\ \frac{g_q}{2\pi^2}T^3\sinh(\frac{\mu}{T})\tau &= const. \end{aligned} \tag{8.15}$$

we get, Since, $T^3\tau = \text{const.}$, from Eq. 8.14 we get,

$$\frac{\mu}{T} = const. \tag{8.16}$$

where, $n_q^{B\mu}$ is the net baryon number density at temperature T and chemical potential μ_q. $\mu = \mu_q(= \mu_B/3)$ is the quark(baryonic) chemical potential. Eq.8.16 represents the temperature evolution of chemical potential in quark matter medium. Similarly, in hadronic medium, the net baryon density is given by

$$n_p^B = n_p - n_{\bar{p}}$$

$$= \frac{g_p}{\pi^2} m_p^2 T K_2(\frac{m_p}{T}) \sinh(\frac{\mu_B}{T}), \tag{8.17}$$

where $n_p, n_{\bar{p}}$ are the proton and anti proton densities in the hadronic system. Here K_2 is the modified bessel function of second kind of order two. Again, using baryon number conservation formula, we get

$$\frac{1}{T^2} K_2(\frac{m_p}{T}) \sinh(\frac{\mu_B}{T}) = const. \tag{8.18}$$

$$\frac{1}{T^2} K_2(\frac{m_p}{T}) \sinh(\frac{\mu}{T}) = \frac{1}{T_{ch}^2} K_2(\frac{m_p}{T_{ch}}) \sinh(\frac{\mu_{ch}}{T_{ch}}). \tag{8.19}$$

The chemical potential μ_{ch} at a temperature T_{ch} for different centre of mass energies ($\sqrt{s_{NN}}$) are given in the Table 8.2. The variation of temperature (see [38]) and net baryon density has been obtained from the solution of boost invariant relativistic hydrodynamics [124]. Then to start the equation we need the initial temperature (T_I) or energy density (ϵ_i). The initial temperatures of the systems formed after nuclear collisions have been evaluated from the measured hadronic multiplicity, dN/dy by using the relation 3.34: Initial temperatures for different $\sqrt{s_{NN}}$ are tabulated in Table 8.1

8.4 Results and discussions

The variation of the number of strange anti-quarks produced per unit volume per unit time with temperature has been displayed in Fig. 8.1 for a baryonic chemical potential $\mu_q = 107$ MeV. It is observed that the process of gluon fusion dominates over the $q\bar{q}$ annihilation for the entire temperature range under consideration, primarily because at high $\mu_B (= 3\mu_q)$ the number of anti-quarks is suppressed. In Fig. 8.2, the production rate of K^+ from the $MM \rightarrow K\bar{K}$ type of reactions has been depicted for $\sqrt{s_{\mathrm{NN}}} = 7.6$

Table 8.1: Initial conditions for the transport calculation. Colliding energies are in centre of mass frame

$\sqrt{s_{\rm NN}}$ (GeV)	T_i (GeV)	T_c (GeV)
3.32	0.115	-
3.83	0.128	-
4.8	0.150	-
6.27	0.160	-
7.6	0.187	-
8.76	0.210	0.190
12.3	0.225	0.190
17.3	0.25	0.190
62.4	0.3	0.190
130	0.35	0.190
200	0.40	0.190

GeV. The production rate from pion annihilation dominates over the reactions that involves ρ mesons, because the thermal phase space factor of ρ is small due its larger mass compared to pions and smaller production cross section. Results for interactions involving mesons and baryons are displayed in Fig. 8.3. It is observed that the interactions involving pions and nucleons in the initial channels dominate over that which has a ρ meson in the incident channel. In fact, contributions from the reactions $\rho\, N \rightarrow \Lambda\, K$ has negligible effect on the total productions from the meson baryon interactions. The kaon production from baryon-baryon interaction is displayed in Fig. 8.4. The contributions from $N\,\Delta \rightarrow N\,\Lambda\,K$ dominates over the contributions from $N\,N \rightarrow N\,\Lambda\,K$ and $\Delta\,\Delta \rightarrow N\,\Delta\,K$ for the temperature range $T = 120$ to 180 MeV. It has been investigated earlier in [252, 262] that $BB \rightarrow BYK$ has a dominant contribution to the rate at BEVELAC energies but here at these energies (from AGS to RHIC) the contribution from $BB \rightarrow BYK$ is not dominant but considered for the sake of completeness. In

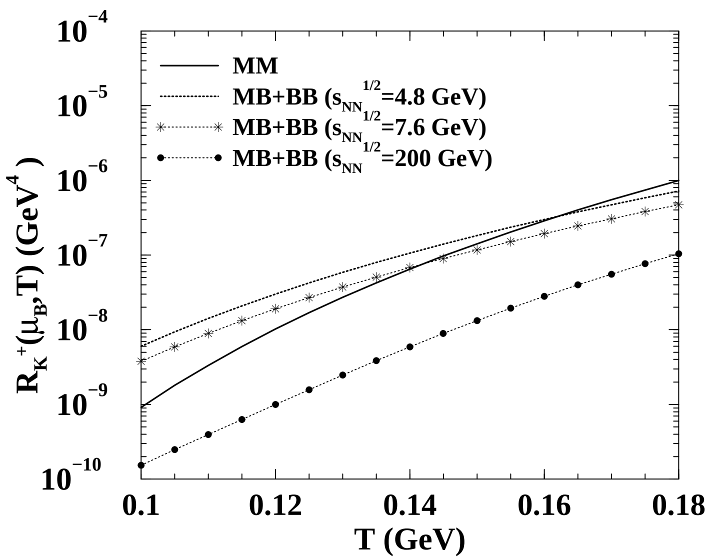

Figure 8.5: Rate of Kaon productions from meson-meson(MM) interactions, meson-baryon(MB) and baryon-baryon(BB) interactions at different center of mass energies

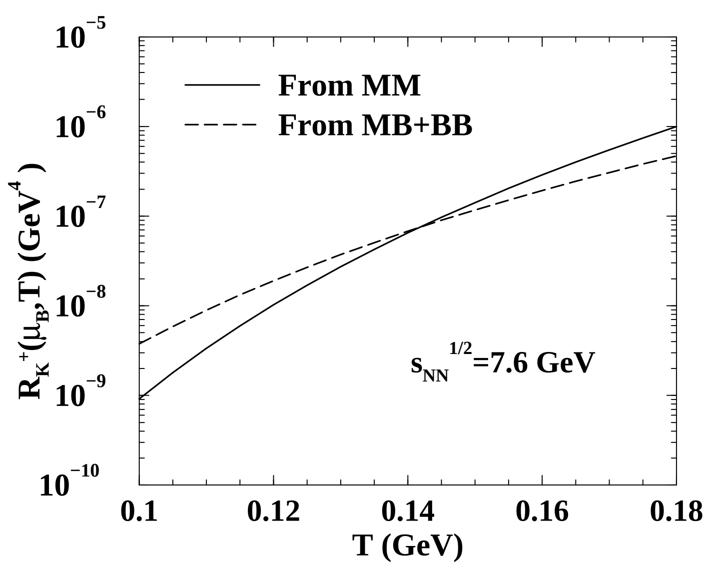

Figure 8.6: Comparison between rates of kaon productions from MM and MM + MB interactions with temperature.

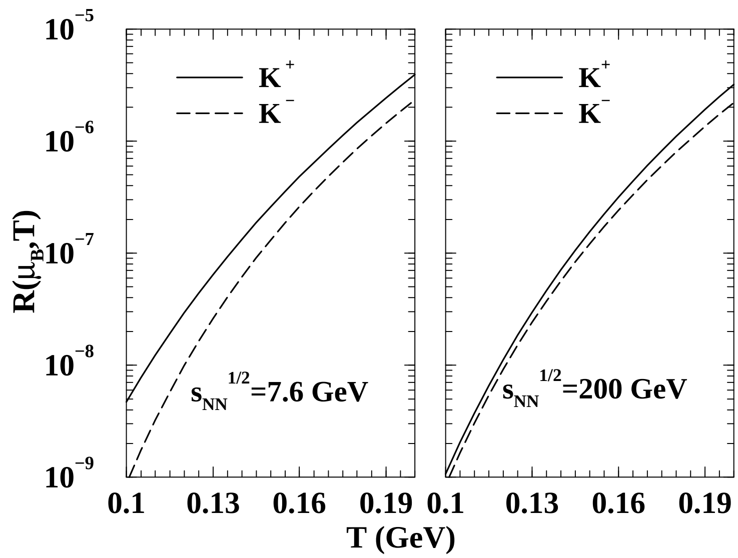

Figure 8.7: Total K^+ and K^- production rates with temperature at center of mass energy=7.6 GeV and 200 GeV.

Fig.8.5 the rates of K^+ productions from meson-meson interactions has been compared with those involving baryons *i.e.* with meson-baryon and baryon-baryon interactions for different $\sqrt{s_{\rm NN}}$ (different μ_B). The results clearly indicate the dominant role of baryons at lower collision energies which diminishes with increasing $\sqrt{s_{\rm NN}}$. At low temperature the baryonic contribution is more than the mesonic one for lower beam energy. Rate of productions (from MB+BB interactions) at $\sqrt{s_{\rm NN}}$=4.8 GeV is more compared to the rates at $\sqrt{s_{\rm NN}}$=7.6 and 200 GeV, since μ_B at $\sqrt{s_{\rm NN}}$=4.8 GeV is more (see Table 8.1). Production rate from pure mesonic interactions does not depend on μ_B hence same for all. It is quite clear from the results displayed in Fig.8.5 that more the baryonic chemical potential (lower the centre of mass energy), more is the rate from BB and MB interactions compared to MM interactions. For a system having lower chemical potential (higher centre of mass energy) the rate of production from mesonic interactions is dominant. A comparison is made between rates of kaon productions from meson meson

Table 8.2: Chemical potential for different centre of mass energies

Center of mass energy($\sqrt{s}_{NN}$) (in A GeV)	Chem. potential (μ_B) (MeV)
3.32	595
3.83	568
4.8	542
6.27	478
7.6	432
8.76	398
12.3	321
17.3	253
62.4	86
130	43
200	28

interactions (MM) and meson-baryon (MB) plus baryon-baryon (BB) interactions for $\sqrt{s_{\rm NN}} = 7.6$ GeV. At this energy baryons and mesons are equally important as shown in Fig. 8.6.

In Fig. 8.7 the net rates of productions for K^+ and K^- have been depicted for $\sqrt{s_{\rm NN}} = 7.6$ GeV (left panel) and 200 GeV (right panel). At $\sqrt{s_{\rm NN}} = 7.6$ GeV the production of K^+ dominates over K^- for the entire temperature range. However, for large $\sqrt{s_{\rm NN}}$ (low μ_B) the productions of K^+ and K^- are similar. The strong absorption of the K^- by nucleons in a baryon rich medium resulting in lower production yield of K^- compared to K^+. This may be contrasted with the experimental findings of BRAHMS experiment [233] where it is observed that at mid-rapidity (small μ_B due to nuclear transparency at RHIC energy) the K^+ and K^- yields are similar but at large

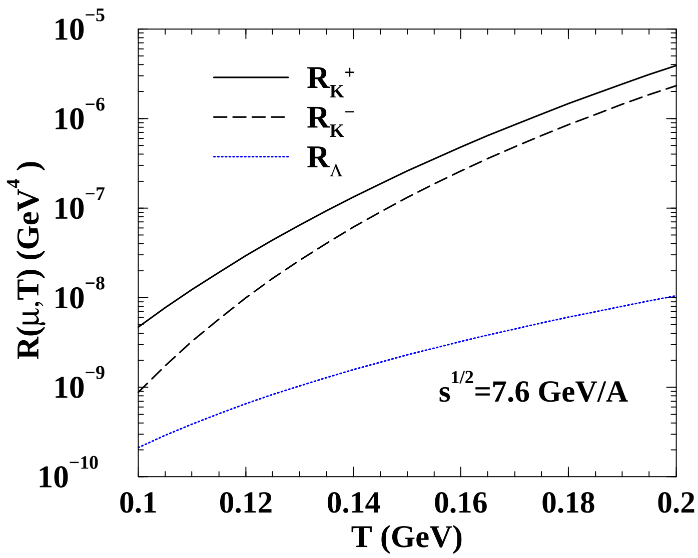

Figure 8.8: Rate of production of K^+, K^- and Λ at $\sqrt{s_{NN}} = 7.6$ GeV.

rapidity (large μ_B) K^- yield is smaller than K^+ due to large K^- nucleon absorption. The rate of productions for Λ is displayed in Fig. 8.8 and Fig. 8.9. The production rate is much less compared to kaons as the phase space and production cross section is less. The rates for $\sqrt{s_{NN}}$=7.6 and 200 GeV are displayed. In Fig. 8.10 the variations of R^+ with $\sqrt{s_{\rm NN}}$ are depicted. The experimental data on R^+ is well reproduced if a partonic initial phase (scenario-II) is assumed beyond $\sqrt{s_{\rm NN}}$=8.7 GeV. A "mindless" extrapolation of hadronic initial state (scenario-I)for all the $\sqrt{s_{\rm NN}}$ up to RHIC energy show an increasing trend in disagreement with the experimental data at higher $\sqrt{s_{\rm NN}}$. In both the scenarios, I and II, the curves at higher $\sqrt{s_{\rm NN}}$ (RHIC energies) becomes flatter. That is because at higher energies the K^+ productions in the hadronic phase are dominated by mesonic interactions and the production rates from mesons are same for all $\sqrt{s_{\rm NN}}$ for a given temperature range. But at lower energies the rates of kaon productions are dominated by the effective interactions among the baryonic degrees of

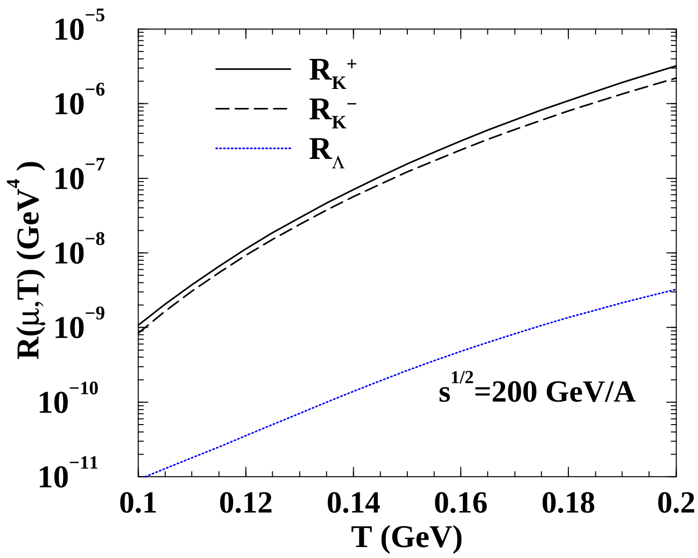

Figure 8.9: Rate of production of K^+, K^- and Λ at center of mass energy=7.6 GeV.

freedom. The composition of matter formed in heavy ion collision changes from baryon to meson dominated region with the increase in colliding energy. The μ_B changes from 86 MeV to 28 MeV as $\sqrt{s_{\rm NN}}$ varies from 62.4 GeV to 200 GeV (Table 8.1). The change in the K^+ production in the hadronic phase due to the change in μ_B mentioned above is marginal - resulting in the flatness in R^+ at higher energies. The decrease of the value of the R^+ beyond $\sqrt{s_{\rm NN}}$=7.6 GeV showing 'horn' like structure is realized when an initial partonic phase is considered. Such a non-monotonic behavior of R^+ can be understood as due to larger entropy productions from the release of large color degrees of freedom (resulting in more pions yield) compared to strangeness beyond energy 7.6 GeV .

In the lower panel of Fig. 8.10, the variations of R^- with $\sqrt{s_{\rm NN}}$ is displayed. R^- has a lower value compared to R^+ at lower energies since K^- get absorbed in the baryonic

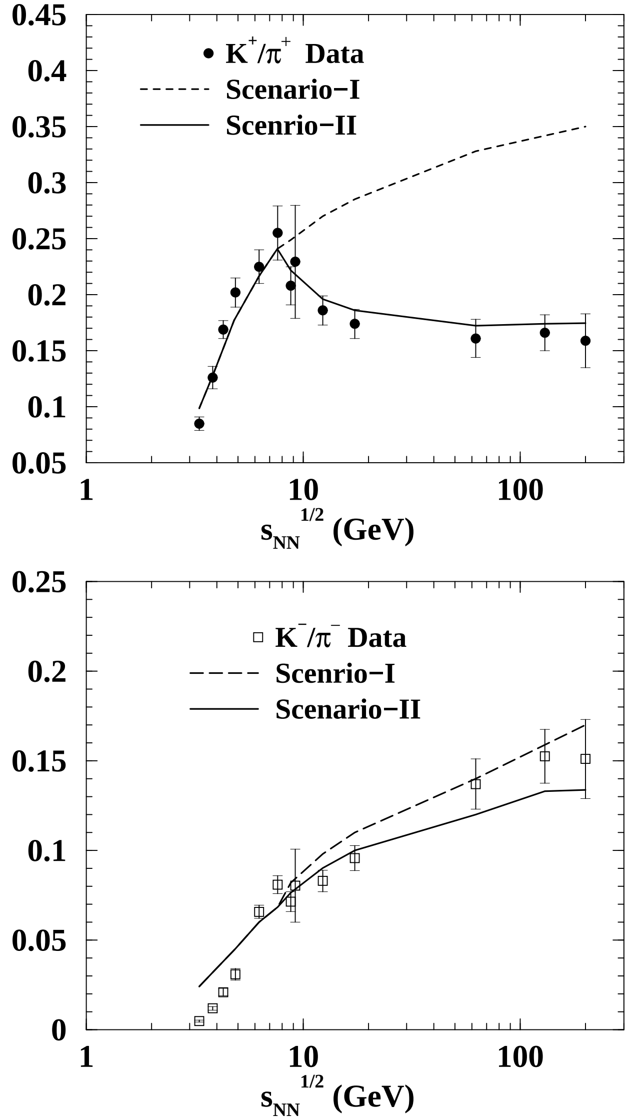

Figure 8.10: **Upper panel**: K^+/π^+ ratio is plotted for different centre of mass energies. Scenario - I represents for pure initial hadronic scenario for all centre of mass energies. Scenario - II represents for the calculation with hadronic initial conditions for low $\sqrt{s_{NN}}$ and partonic initial conditions for higher $\sqrt{s_{NN}}$. **Lower panel**: Same thing for K^-/π^- See text for details.

medium. At higher energies K^- is closer to K^+ because production of K^+ and K^- is similar in baryon free medium, which may be realized at higher collision energies. The variation of R^+ can be understood from the results displayed in Fig. 8.11 where the variation of densities of K^+, K^- and π^+ are depicted with centre of mass energies in the upper panel of the figure. The π^- productions are assumed to be similar as π^+. The dotted and dashed lines are for K^+ and K^- productions respectively and long solid line is for π^+ density. The inset in the upper panel of the Fig.8.11 show K^+ and K^- densities as a function of $\sqrt{s_{NN}}$. The slopes of the number densities of K^+, K^- and $\pi^\pm$ are displayed in the lower panel of the curve. The sharp change in the slope of K^+ compared to K^- at low $\sqrt{s_{NN}}$ (high μ_B) makes difference in the ratios R^+ and R^-. Where as at high $\sqrt{s_{NN}}$ (low μ_B) the slopes are almost same which makes the ratios similar. Also it explains the constancy of ratio at higher centre of mass energies. In the upper panel of Fig. 8.12 the R^+ is depicted as a function of $\sqrt{s_{\rm NN}}$ for other scenarios (III, IV and V). We observe that when the strange quarks and kaons are formed in complete equilibrium but their secondary productions are neglected during the evolution (scenario III) then the data is well reproduced. It is also important to note that in the scenario (IV), when the system is formed in equilibrium (as in III) but the productions of strange quarks and kaons are switched on through secondary processes then the data is slightly overestimated at high $\sqrt{s_{\rm NN}}$. However, we have seen that the data is also reproduced well in the scenario II as discussed above. This indicate that the deficiency of strangeness below its equilibrium value as considered in (II) is compensated by the secondary productions. In scenario V we assume that vanishing initial strangeness and observed that the production of strangeness throughout the evolution is not sufficient to reproduce the data. The productions from secondary processes are small but not

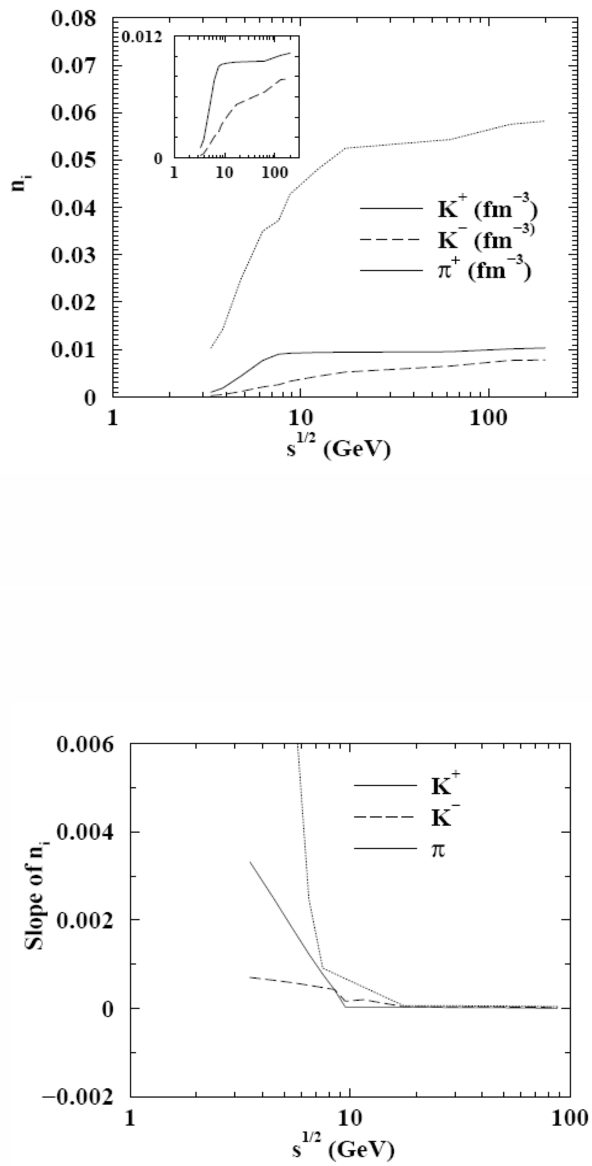

Figure 8.11: **Upper panel:** The variation of density with centre of mass energies. **Lower panel:** The variation of slope of density with centre of mass energies.

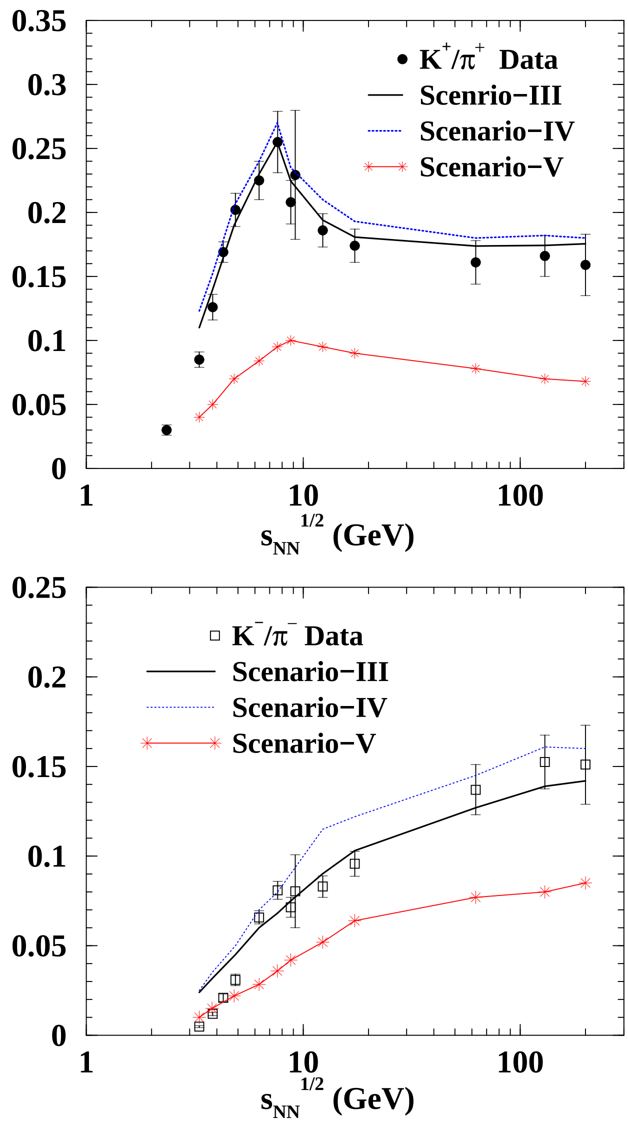

Figure 8.12: **Upper panel:** K^+/π^+ ratio for different centre of mass energies. Scenario-III assumes complete equilibrium of strange quarks and hadrons. The production through secondary processes have been ignored. Scenario IV is same as III with secondary productions processes are on and scenario V represents zero strangeness initially but secondary productions are switched on. **Lower panel:** Same as Fig. 8.12 for K^-/π^-.

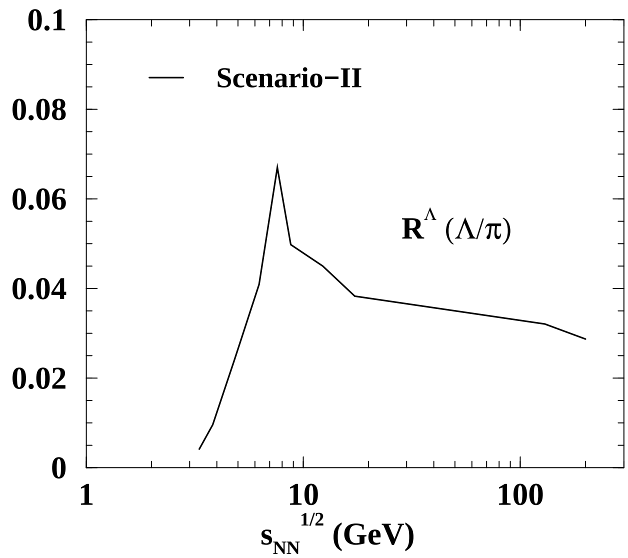

Figure 8.13: The ratio R^{Λ} at various center of mass energies.

entirely negligible (V). In the lower panel of Fig. 8.12 the R^{-} has been displayed as a function of $\sqrt{s_{\mathrm{N}N}}$. A trend similar to the results shown in Fig. 8.12 is observed. The data is overestimated for the intermediate $\sqrt{s_{\mathrm{N}N}}$ in the scenario IV, reproduced well in scenario III and underestimated for the scenario V.

In Fig. 8.13 the R^{Λ} is displayed for the scenario (II). It shows a behavior similar R^{+}.

The inclusion of Σ, Ω do not change the productions of K^{+}, K^{-} drastically. Here we solve the Boltzmann equations including Σ with the K and Λ to show the differences. The equations have been solved for ratio of r_i where (should not be confused with $R_i(= n_i/\pi^i)$ with $r_i = n_i/n_i^{eq}$. The n_i and n_i^{eq} are the non-equilibrium and equilibrium densities of the species i. The strangeness productions for QGP phase ($s, \bar{s}$ quarks), Mixed phase ($s, \bar{s}$ quarks, K, Λ, Σ) and hadronic phase (K, Λ, Σ) have been considered using the following equations in terms of ratio r_i.

In the QGP phase the evolution equation of strangeness is given by:

$$\frac{dr_{\bar{s}}}{d\tau} = \frac{R_{\bar{s}}(T)}{n_{\bar{s}}^{eq}}[1 - r_s r_{\bar{s}}] \tag{8.20}$$

where, $r_i = n_i/n_i^{eq}$, n_i and n_i^{eq} are the non-equilibrium and equilibrium densities of the species i in the QGP phase. R_i is the rate of production of particle i at temperature T.

When the temperature of the QGP phase approaches the transition temperature T_c due to expansion, then the s and $\bar{s}$ quarks hadronize to strange hadrons like K^+, K^-, Λ etc. The evolution of K^+ $(u\bar{s})$ in the mixed phase is governed by the following equation:

$$\begin{aligned}\frac{dr_{K^+}}{d\tau} &= \frac{R_{K^+}(T_c)}{n_{K^+}^{eq}}(1 - r_{K^+}r_{K^-}) + \frac{R_\Lambda(T_c)}{n_{K^+}^{eq}}(1 - r_{K^+}r_\Lambda) \\ &+ \frac{R_\Sigma(T_c)}{n_{K^+}^{eq}}(1 - r_{K^+}r_\Sigma) + \frac{1}{f}\frac{df}{d\tau}\left(\delta\frac{r_{\bar{s}}n_{\bar{s}}^{eq}}{n_{K^+}^{eq}} - r_{K^+}\right),\end{aligned} \tag{8.21}$$

Similar coupled equations can be written for Λ and $\Sigma(uus)$. In the above equation f represents the fraction of hadrons in the mixed phase at time τ. The last term stands for the hadronization of $\bar{s}$ quarks to K^+ [255, 257]. Here δ is a parameter which indicates the fraction of $\bar{s}$ quarks hadronizing to K^+. The value of $\delta = 0.25$ if we consider that $\bar{s}$ hadronizes to K^+ and K^0, Λ and Σ with equal probabilities. The initial values of $\bar{s}$ quarks are taken close to their equilibrium values. However, a small change in the initial value of $r_{\bar{s}}$ does not change the final results significantly. Similar equations are solved for hadronic phase. We solve for scenario (II) for T_c=175 MeV and μ_B=0. Even

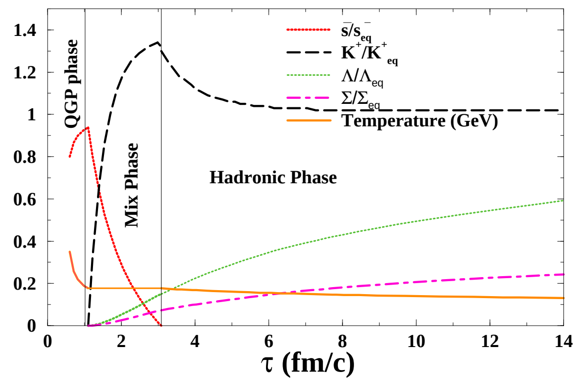

Figure 8.14: The time evolution of the ratio of non-equilibrium to equilibrium density of quarks/various hadrons when initial phase is assumed to be QGP ($T_i > T_c$). Here $\bar{s}$, K^+ etc. stand for their corresponding number densities.

with lower initial values of $r_{\bar{s}}$ the system reaches equilibrium very fast due to their production at the high temperature heat bath. We solve the above-mentioned coupled set of differential equations numerically. In Fig. 8.4 the ratio r_i's are shown with the time τ [57].

8.5 Summary and Conclusions

The evolution of the strangeness in the system formed in nuclear collisions at relativistic energies have been studied within the framework of momentum integrated Boltzmann equation. The Boltzmann equation has been used to study the evolution of s and $\bar{s}$ in the partonic phase and K^- and K^+ in the hadronic phase. The calculation has been done for different centre of mass energies ranging from AGS to RHIC. We get a non-monotonic variation of K^+/π^+ with $\sqrt{s_{NN}}$ when an initial partonic phase is assumed for $\sqrt{s_{NN}} = 8.76$ GeV and beyond. A monotonic rise of K^+/π^+ is observed when a pure hadronic scenario is assumed for all centre of mass energies. The K^-/π^- data is unable to differentiate between the two initial conditions mentioned before.

Some comments on the values of the initial parameter are in order at this point. We have seen that a 10% variation in the initial temperature does not change the results drastically. We have assumed that the initial density of strange quarks or kaons depending on the scenario (I) or (II) is about 20% away from the corresponding equilibrium density. Results from a scenario where strange quarks or kaons are formed in complete equilibrium and the production is ignored during the evolution then the data is well reproduced (scenario III). If the the strangeness is produced in equilibrium and the production is included during the expansion stage then the data is overestimated. However, if the system is formed with zero strangeness then the theoretical results underestimate the data substantially. This indicate that the production of strangeness during the expansion of the system is small but not entirely negligible. The deficiency assumed in scenario (II) is compensated by the production during evolution.

Chapter 9

Summary

With a brief introduction to the basic building blocks of matter and their interactions, we have discussed the properties of QCD in chapter 1. The phenomenology of relativistic heavy ion collisions and the production of QGP under the extreme condition of temperature has been outlined. Different experimental programs aiming to create QGP and several signals to detect it have also been discussed. In the chapter 2, the thermal emission rates for both dilepton and photon productions have been described. The rates from thermal medium like QGP and hadronic matter have been discussed within the framework of thermal field theory. The photon production rate from QGP has been considered from the annihilation ($q\bar{q}\rightarrow g\gamma$) and Compton ($q(\bar{q})g \rightarrow q(\bar{q})\gamma$) processes using hard thermal loop (HTL) approximation. Higher order processes like : $gq\rightarrow gq\gamma$, $qq\rightarrow qq\gamma$, $qq\bar{q}\rightarrow q\gamma$ and $gq\bar{q}\rightarrow g\gamma$ have also been taken into account. For the photon rate from hadronic phase we have considered an exhaustive set of hadronic reactions and the radiative decays of higher resonance states. The relevant reactions are: (i) $\pi\,\pi \rightarrow \rho\,\gamma$,

(ii) $\pi\,\rho \rightarrow \pi\gamma$ (with all possible mesons in the intermediate state) , (iii)$\pi\,\pi \rightarrow \eta\,\gamma$ and (iv) $\pi\,\eta \rightarrow \pi\,\gamma$, $\rho \rightarrow \pi\,\pi\,\gamma$ and $\omega \rightarrow \pi\gamma$. The corresponding vertices are obtained from various phenomenological Lagrangian. The reactions involving strange mesons: $\pi\,K^* \rightarrow K\,\gamma$, $\pi\,K \rightarrow K^*\,\gamma$, $\rho\,K \rightarrow K\,\gamma$ and $K\,K^* \rightarrow \pi\,\gamma$ have also been incorporated in the present work. Contributions from other decays, such as $K^*(892) \rightarrow K\,\gamma$, $\phi \rightarrow \eta\,\gamma$, $b_1(1235) \rightarrow \pi\,\gamma$, $a_2(1320) \rightarrow \pi\,\gamma$ and $K_1(1270) \rightarrow \pi\,\gamma$ have been found to be small for $p_T > 1$ GeV. All the isospin combinations for the above reactions and decays have properly been taken into account. The effects of hadronic form factors have also been incorporated in the present calculation.

For dilepton or lepton pair productions from QGP phase we have considered the annihilation of quarks and anti-quarks ($q\bar{q} \rightarrow l\bar{l}$). The QCD corrections through the processes $q\bar{q} \rightarrow gl^+l^-$ $gq(\bar{q}) \rightarrow q(\bar{q})l^+l^-$ have also been taken into account. The lepton pair productions from hadronic matter have been considered from the decay of vector mesons ρ(I=1, J=1, P=-1), ω(I=0, J=1, P=-1) and ϕ(I=0, J=1, P=-1) to l^+l^- using the vector meson dominance model taken from [93]. We have included the continuum in the vector mesons spectral functions and four pion annihilation process (as some author considers), therefore, have not been considered here to avoid over counting.

Chapter 3 deals with the space time evolution of the matter formed in relativistic heavy ion collision. (2+1) dimensional relativistic ideal hydrodynamics with longitudinal boost invariance and cylindrical symmetry is considered to describe the space time dynamics. The inputs like T_i, τ_i, T_f and EoS to the hydrodynamic calculation have also been discussed. The parameters are constrained from the available experimental data.

In chapter 4 we have studied the photon productions in terms of invariant yield from heavy ion collisions. Using thermal field theory and relativistic hydrodynamics as discussed in chapters 2 and 3 we have estimated the net invariant yield of direct photons from Au+Au collisions at RHIC energy $\sqrt{s_{NN}}$=200 GeV [52] and from Pb+Pb collisions at SPS energy $\sqrt{s_{NN}}$=17.3 GeV [51, 54]. Also we have predicted for thermal photons from Pb+Pb collision at LHC energy (for hadron multiplicity, dN/dy=4000). For RHIC energy (mid rapidity) we have assumed an initial QGP phase with an initial temperature T_i=400 MeV and initial thermalisation time τ_i=0.2 fm. Those are constrained together from the experimentally measured hadron multiplicity. The freeze out temperature T_f has been taken to be 120 MeV which is also constrained from the p_T spectra of hadrons(pions and kaons). With these inputs the photon spectra measured by PHENIX collaboration were explained reasonably well. This value of T_i is much larger than the value of the QGP-hadron transition temperature T_c predicted by the lattice quantum chromodynamics at zero baryonic chemical potential. Hence at RHIC, the possibility of initial hadronic state seems to be ruled out. The data for different centralities have also been explained with the same production and expansion mechanism. The sensitivities of different input parameters like transition temperature T_c, strong coupling constant α_s and equation of states, radial velocity (v_r) to the p_T spectra have been studied. Similarly photon spectra at $\sqrt{s}_{NN}$=17.3 GeV, SPS energy, have been discussed with initial temperature T_i=200 MeV and τ_i=1 fm with lattice EoS and shown in [51]. From the initial temperature T_i inferred for spectra at both energies we say the data along with the theoretical evaluation supports the formation of an initial QGP phase at $\sqrt{s}_{NN}$=17.3 GeV Pb+Pb collision and at $\sqrt{s}_{NN}$=200 GeV Au+Au collision. Finally we have predictions for p_T spectra of photons from Pb+Pb collision at LHC energy.

In chapter 5, the dilepton (dimuon) productions in heavy ion collision have been discussed using formalism discussed in chapters 2 and 3. The productions have been estimated considering two scenarios of the expanding system : (I) with the assumption of an initial QGP state and (II) with the assumption of an initial hadronic state. We have compared the theoretical evaluation of the spectra with the dimuon data taken from In+In collision at $\sqrt{s_{NN}}$=17.3 GeV or E_{lab}=158 A GeV by NA60 collaboration. The invariant mass spectra normalized with the charge hadron multiplicity, $(dN/dMdy)/(dN_{ch}/dy)$ have been evaluated as a function of invariant mass M for different p_T windows for scenario(I). We have also evaluated the transverse mass spectra $(dN/m_T dm_T \equiv dN/p_T dp_T)$ of the pair for various M windows as a function of $m_T - M$ for both scenarios (I) and (II) and finally compared with the data. It has been observed that the scenario(I) with the initial QGP phase explains the data reasonably well, where as, the scenario (II) fails to reproduce. Our study is restricted up to low mass region (LMR: $M < 1.5$ GeV). A non-monotonic behavior of the inverse slope parameter, $T_{\rm eff}$ is observed when extracted from the transverse mass spectra of the thermal lepton pairs as a function of invariant mass. This non-monotonic trend of $T_{\rm eff}$ may possibly indicate the origin of lepton pairs from a partonic phase formed initially in the collisions. The theoretical analysis of both M-spectra and $m_T - M$ spectra supports the formation of QGP in In+In nuclear collision at $\sqrt{s_{NN}}$=17.3 GeV SPS energy.

In chapter 6 we have studied the variation of R_{em}, the ratio of the transverse momentum spectra of photons to dileptons and argued that measurement of this quantity would be very useful to determine the value of the initial temperature of the system formed in heavy ion collisions. We have observed that R_{em} reaches a plateau beyond

$p_T = 1.5$ GeV for all M windows. The value of R_{em} in the plateau region depends on T_i. However, the effects of flow, the dependence on the values of T_c and v_0 get canceled away in the ratio, R_{em}. The effect of EoS on R_{em} is found to be the least in the mass window $1.2 < M(GeV) < 1.3$. For M above and below the ρ peak and $p_T \geq 2$ GeV the contributions from quark matter dominates, therefore these regions ($p_T \geq 2GeV$ and $1.2 < M(GeV) < 1.3$) could be chosen to estimate the initial temperature of the system formed after the collisions.

In chapter 7 we discussed the importance of the evaluation of ratio of the p_T spectra in extracting the thermodynamic (temperature) information of the system. It was argued in the literatures that the non-monotonic behavior of T_{eff} with M as observed from the dimuon data of In+In collisions at SPS energy is because of the presence of two thermal sources- QGP and hadronic matter. To address this issue more closely we have theoretically evaluated the dimuon spectra for SPS, RHIC and LHC energies and the non-monotonic behavior of T_{eff} is observed for SPS and RHIC energies. However a monotonic rise of T_{eff} has been noticed for LHC energy. Hence it is argued in this chapter that the non-monotonicity of $T_{\rm eff}$ may not be a direct answer to prove the presence of two thermal sources as it depends on both average temperature, T_{av} and flow velocity v_r of the system. We then extract radial flow v_r using both photon and dilepton p_T spectra simultaneously. In the present work we focus on the extraction of v_r from the ratio, $R_{\rm em}$ for various M windows. The $v_{\rm r}$ obtained from the analysis of both the spectra vary with M non-monotonically for SPS, RHIC and LHC energies but not the T_{eff}. The non-monotonic behavior of v_r may be interpreted as due to the presence of two different kinds of thermal sources of lepton pairs of the expanding system.

In chapter 8 we have studied the strangeness productions in heavy ion collision at various centre of mass energies starting from AGS to RHIC and explore the possibility of QGP formation. The study of strangeness to entropy ratio is a subject of high interest and the ratio, $R^+ \equiv K^+/\pi^+$ (ratio of the multiplicities) is one such currently debated issue. R^+ is measured experimentally as a function of centre of mass energy ($\sqrt{s_{NN}}$). It is observed that the R^+ increases with $\sqrt{s_{NN}}$ and then decreases beyond a certain value of $\sqrt{s_{NN}}$ giving rise to a horn like structure, whereas the ratio, $R^- \equiv K^-/\pi^-$ increases faster at lower $\sqrt{s_{NN}}$ and tend to saturate at higher $\sqrt{s_{NN}}$. In the present work we have employed a microscopic model for the productions and evolution of strange quarks and/or hadrons. Here we have examined whether the K^+/π^+ experimental data can differentiate between the following two initial conditions or two scenarios : (I) the hadronic phase for all $\sqrt{s_{\rm NN}}$ or (II) the partonic phase beyond a certain threshold in $\sqrt{s_{\rm NN}}$. Other possibilities like formation of strangeness in complete thermal equilibrium and evolution in space time (III) without and (IV) with secondary productions of quarks and hadrons have been considered. (V) Results for an ideal case of zero strangeness in the initial state have also been presented. For the strangeness productions in the partonic phase we consider the processes of gluon fusion and light quarks annihilation. For the production of K^+ and K^- an exhaustive set of reactions involving thermal baryons and mesons have been considered. The time evolution of the densities are governed by the Boltzmann equation. The Boltzmann equation has been used to study the evolution of s and $\bar{s}$ in the partonic phase and K^- and K^+ in the hadronic phase. The calculation has been done for different centre of mass energies ranging from AGS to RHIC. We get a non-monotonic variation of K^+/π^+ with $\sqrt{s_{NN}}$ when an initial partonic phase is assumed for $\sqrt{s_{NN}} = 8.76$ GeV and beyond. A monotonic rise of K^+/π^+ is observed when a pure hadronic scenario is assumed for all centre of mass energies. The K^-/π^- data is unable to differentiate between the two initial conditions mentioned before. We also evaluate the Λ/π productions for the scenario (II) and observe the similar non-monotonic horn when plotted against $\sqrt{s_{NN}}$.

Bibliography

[1] Vaisheshik Darshan (by Kanad), Indian philosophy; Subodh Kapoor, The Indian Encyclopaedia, Vol.1, P.5643, Cosmo Publications, ISBN 8177552570 (2002).

[2] Helmut Satz, University of Bielefeld Zermany, Nucl. Phys. A **862-863**, 4 (2011).

[3] C. N. Yang and R. Mills, Phys. Rev **96**, 191 (1954).

[4] G. Sterman *et. al.*, Rev. Mod. Phys. **67** 157-248 (1995).

[5] T. Muta, *Foundations of Quantum Chromodynamics: An Introduction to Perturbative Methods in Gauge Theorie*, World Scientific, Singapore, 1998.

[6] M. E. Peskin and D. V. Schroeder, *An Introduction to Quantum Field Theory*, Addison-Wesley Pub., 1995.

[7] R. K. Ellis, W. J. Stirling and B. R. Webber, *QCD and Collider Physics*, Cambridge University Press, 1996.

[8] t'Hooft and M. Veltman, Nucl. Phys. B**44**, 189-213 (1972); t' Hooft (1972) Unpublished, Nucl. Phys. B **254**, 11 (1985).

[9] L. D. Faddeev and V. N. Popov, Phys. Lett. B **25**, 29 (1967).

[10] M. Schmelling, arxiv:hep-ex/9701002, (1997).

[11] D. J. Gross and F. Wilczek, Phys. Rev. Lett. **30**, 26 (1973); H. Politzer, Phys. Rev. Lett. **30**, 1346 (1973).

[12] K. Wilson, Phys. Rev. D **10**, 2445 (1974).

[13] J. C. Collins and M. J. Perry, Phys. Rev. Lett. **34**, 1353 (1975);

[14] S. Gupta, X. Luo, B. Mohanty, H. G. Ritter and N. Xu, Science, **332**, 1525 (2011); S. Borsanyi *et al.* , J. Phys. G, **38**, 124101 (2011); A. Bazavov *et al.*, for Hot QCD Collaboration, J. Phys. G, **38**, 124099 (2011).

[15] R. Fitzpatrick, PHY380L, Introduction to Plasma Physics *a graduate level lecture course, (Spring 1998)*, The Institute for Fusion Studies, The University of Texas at Austin.

[16] E. V. Shuryak, Phys. Rept. **61**, 71 (1980); Phys. Rep. **115**,151 (1984).

[17] F. F. Chen, *Introduction to plasma physics and controlled fusion*, vol. 1, Springer Publication, ISBN-10:0306413329, (1984).

[18] J. A. Bittencourt, *Fundamentals of Plasma Physics*, vol. 1, Springer Publication, ISBN-10:0387209751, (2004).

[19] S. A. Chin, Phys. Lett. B, **78**, 552, (1978)

[20] S. Slegt, PhD. Thesis, KVI, University of Groningen, NL-9747 AA Groningen.

[21] J. Alam, S. Chattopadhyay, T. Nayak, B. Sinha and Y. P. Viyogi, J. Phys. G, **35** issue 10 (2008). (Proc. QUARK MATTER 2008).

[22] I. Arsene *et al.* (BRAHMS Collaboration), Nucl. Phys. A **757** (2005) 1; B. B. Back *et al.* (PHOBOS Collaboration), Nucl. Phys. A **757** (2005) 28; J. Adams *et al.* (STAR Collaboration), Nucl. Phys. A **757** (2005) 102; K. Adcox *et al.* (PHENIX Collaboration), Nucl. Phys. A **757** (2005) 184.

[23] STAR Collaboration, Nucl. Phys. A **757**, 102-183 (2005);

[24] J. Kapusta, P. Lichard, and D. Seibert. Phys. Rev. D **44**, 2774 (1991), *Erratum-ibid* **47**, 4171 (1993).

[25] E. L. Feinberg, Nuovo Cimento Sco. Ital. Fis. A **34**, 39 (1976).

[26] J. Rafelski and B. Muller, Phys. Rev. Lett. **48**, 1066 (1982).

[27] J. Rafelski and R. Hagedron, "From Hadron Gas To Quark Matter. 2", in it Statistical Mechanics of Quarks and Hadrons, H. Satz, ed. (North Holland 1980)pp.253-272, also; Preprint CERN-TH-2969, October 1980.

[28] S. V. Afanasiev *et al*, NA49 Collaboration, Phys. Rev. C **66**, 054902 (2002).

[29] I. G. Bearden *et al*, BRAHMS Collaboration, Phys. Rev. Lett. **88**, 202301 (2002).

[30] I. G. Bearden *et al*, BRAHMS Collaboration, Phys. Rev. Lett. **90**, 102301 (2003).

[31] J. Cleymans, A. Muronga, Phys. Lett. B **388**, 5 (1996); J. Cleymans, M. Marais and E. Suhonen, Phys. Rev. C **56**, 2747 (1997)

[32] J. Cleymans *et al.*, Phys. Rev. C **57**, 3319 (1998).

[33] S. Hamieh, K. Redlich, A. Tounsi, Phys. Lett. B **486**, 61 (2000).

[34] B. I. Abelev *et al.*, STAR Collaboration, Phys. Lett. B **673**, 183 (2009).

[35] M. Gazdzicki, Acta Phys. Polon. B **34**, 187 (2004).

[36] M. Gazdzicki *et al.* Acta Phys. Polon. B **42**, 307 (2011).

[37] J. Rafelski, Phys. Rep. **88** (1982) 331; Nucl Phys. A **418** (1984)215c.

[38] Jajati K. Nayak, S. Banik and J. Alam, Phys. Rev. C **82**024914 (2010)

[39] A. Andronic, P. Braun-Munzinger and J. Stachel, Phys. Lett. B **673**, 142 (2009).

[40] S. Chatterjee, R. M. Godbole, and Sourendu Gupta, Phys. Rev. C **81**, 044907 (2010).

[41] Boris Tomasik, Evgeni E Kolomeitsev, Eur. Phys. J. C **49**, 115 (2007).

[42] T. Matsuiand H. Satz, Phys. Lett. B **178**, 416 (1986).

[43] H. Satz, Talk given at Brookhaven National Lab, June 7, 2011.

[44] R. L. Thews, M. Schroeder and J. Rafelski, Phys. Rev. C, **63**, 054905 (2001).

[45] L. Grandchamp and R. Rapp, Phys. Lett. B, **523**, 60 (2001).

[46] P. Broun-Munzinger and J. Stachel, Phys. Lett. B, **490**, 196 (2000).

[47] L. Grandchamp and R. Rapp, Nucl. Phys. A, **709**, 415 (2001).

[48] F. Abe it et al., for CDF Collaborations, Phys. Rev. D **48**, 998 (1993).

[49] M. Gyulassy, P. Levai and I. Vitev, Nucl Phys. B **571**, 197 (2000); *ibid* Phys. Rev. Lett. **85**, 5535 (2000).

[50] H. Zhang, J. F. Owens, E Wang and X. N. Wang, Phys. Rev. Lett. **98**, 212301 (2007).

[51] P. Mohanty, J. K. Nayak, J. Alam and S. Das, Phys. Rev. C **82**, 034901(2010).

[52] J. Alam, J. K. Nayak, P. Roy, A. K. Dutt-Mazumder and B. Sinha, J. Phys. G **34** 871 (2007).

[53] J. K. Nayak, J. Alam, S. Sarkar and B. Sinha, Phys. Rev. C **78**,034903 (2008).

[54] J. K. Nayak, Jan-e Alam, S. Sarkar and B. Sinha, J. Phys. G **35**c 054001(142)(2008).

[55] J. K. Nayak, J. Alam, T. Hirano, S. Sarkar and B. Sinha, Phys. Rev. C **85**,064906 (2012).

[56] J. K. Nayak and J. Alam, Phys. Rev. C **80**,064906 (2009).

[57] J. K. Nayak, J. Alam, P. Roy, A. K. Dutt-Mazumder, B. Mohanty, Acta. Phys. Slova **56**,27 (2006).

[58] T. Abott *et al*, E802 Collaboration, Phys. Rev. C **50**, 1024 (1994).

[59] L. Ahle *et al*, E866 Collaboration, Phys. Rev. C **58**, 3523 (1998).

[60] L. Ahle *et al*, E866 Collaboration, Phys. Lett. B **490**, 53 (2000).

[61] I. Bearden *et al*, NA44 Collaboration, Phys. Rev. C **66**, 044907 (2002).

[62] J. K. Nayak, S. Banik and J. Alam, Nucl. Phys. A **862-863**,286 (2011).

[63] H. A. Weldon, Phys. Rev. D **42**, 2384 (1990).

[64] A. H. Mueller, Phys. Rev. D **4**, 150 (1971); C. E. DeTar, D. Z. Freedman, and G. Veneziano, *ibid* **4**, 906 (1971).

[65] P. V. Ruuskanen, in "Particle Production in Highly Excited matter", (H. H. Gutbrod and J. Rafelski, Eds.) Plenum, New York (1993).

[66] M. Le. Bellac, "Thermal Field Theory", Cambridge University Press, Cambridge, UK, (1995).

[67] L. D. McLerran and T. Toimela, Phys. Rev. D **31**, 545 (1985); H. A. Weldon, Phys. Rev. D **42**, 2384 (1990).

[68] N. P. Landsman and Ch. G. van Weert, Phys. Rep. **45**C, 142 (1987).

[69] H. A. Weldon, Phys. Rev. D **26**, 1394 (1982).

[70] H. A. Weldon, Phys. Rev. D **28**, 2007 (1983); R. L. Kobes and G. W. Semenoff, Nucl. Phys. B **260**, 714 (1985); Nucl. Phys. B **272**, 329 (1986).

[71] J. Alam, S. Sarkar, P. Roy, T. Hatsuda and B. Sinha, Ann. Phys. **286**, 159 (2000).

[72] H. A. Weldon, Ann. Phys. **228**, 43 (1993).

[73] A. Das, *Finite Temperature Field Theory*, World Scientific Singapore, (1997).

[74] R. Kobes and G. Semenoff, Nucl. Phys. B **260**, 714 (1985); **272**,329(1986).

[75] F. Gellis, Nucl. Phys. B **508**, 483 (1997).

[76] R. Baier, H. Nakkagawa, A. Niegawa, and K. Redlich, Z Phys. C **53**, 433 (1992).

[77] R. D. Pisarski, Nucl. Phys. B **309**, 476 (1988); Phys. Rev. Lett. **63**, 1129 (1989); E. Braaten and R. D. Pisarski, Nucl. Phys. B **337**, 569 (1990). ibid **339**, 310 (1990).

[78] P. Aurenche, F. Gelis, H. Zaraket and R. Kobes, Phys. Rev. D **58**, 085003 (1998).

[79] S. Jeon *etal.*, Nucl. Phys. A **715**, 795 (2003).

[80] B. G. Zakharov, JETP Lett. **80**, 1 (2004).

[81] S. Turbide, C. Gale, S. Jeon, and G. D. Moore, Phys. Rev. C **72**, 014906 (2005).

[82] R. Baier, H. Nakkagawa, A. Niegawa and K. Redlich, Z. Phys. C **53**, 433 (1992).

[83] P. Aurenche, F. Gelis and H. Zaraket, Phys. Rev. D **61**, 116001 (2000); P. Aurenche, F. Gelis and H. Zaraket, Phys. Rev. D **62**, 096012 (2000)

[84] P. Arnold P, G. D. Moore and L. G. Yaffe, J. High Energy Phys. **11**, 057 (2001); P. Arnold, G. D. Moore and L. G. Yaffe, J. High Energy Phys. **12** , 009 (2001); P. Arnold, G. D. Moore and L. G. Yaffe, J. High Energy Phys. **06** , 030 (2002)

[85] O. Kaczmarek and F. Zantow, Phys. Rev. D **71**, 114510 (2005).

[86] R. J. Fries, B. Müller, and D. K. Srivastava, Phys. Rev. Lett. **90**, 132301 (2003).

[87] S. Turbide, R. Rapp and C. Gale, Phys. Rev. C **69**, 014903 (2004).

[88] J.J. Sakurai, *Currents and Mesons*, (University of Chicago Press, Chicago, 1969); F. Klingl, N. Kaiser, and W. Weise, Z. Phys. A **356**, 193 (1996); H.B. O'Connell, B.C. Pearce, A.W. Thomas, and A.G. Williams, Prog. Part. Nucl. Phys. **39**, 201 (1997).

[89] H. Gomm, Ö. Kaymakcalan, and J. Schechter, Phys. Rev. **D30**, 2345 (1984).

[90] C. Song, Phys. Rev. **C47**, 2861 (1993).

[91] R. Rapp and C. Gale, Phys. Rev. C **60**, 024903 (1999).

[92] C. Gale and J. Kapusta, Nucl. Phys. B **357**, 65 (1991).

[93] S. Ghosh, S. Mallik and S. Sarkar Eur. Phys. J. C **70**, 251 (2010); S. Ghosh, S. Sarkar and J. Alam arxiv:1009.1260 [nucl-th];

[94] E. V. Shuryak, Rev. Mod. Phys. **65** 1 (1993).

[95] P. Lichard and J. Juran, Phys. Rev. D **76**, 094030 (2007).

[96] V.L. Eletsky, M. Belkacem, P.J. Ellis and J. I. Kapusta, Phys. Rev. C **64**, 035202 (2001).

[97] R. A. Schneider and W. Weise, Phys. Rev. C **64**, 055201 (2001).

[98] J. Cleymans, J. Fingberg and K. Redlich Phys. Rev. D. **35**, 2153 (1987);

[99] T. Altherr and P. V. Ruuskanen, Nucl. Phys. B **380**, 377 (1992).

[100] M. H. Thoma and C. T. Traxler, Phys. ReV. D **56**, 198(1997).

D. H. Rischke and M. Gyulassy, Nucl. Phys. A, **608** , 479 (1996) .

[101] L. D. Landau and E. M. Lifshitz, *Fluid Mechanics* (Pergamon; Addision-Wesley, New York, 1959).

[102] Y. Hama, T. Kodama, and O. Socolowski Jr, Brazil J. Phys. **35**, 24(2005).

[103] P. Huovinen and P. V. Ruuskanen, Ann. Rev. Nucl. Part. Sci. **56**, 163 (2006).

[104] C. Eckart phys. Rev. **58**, 919(1940).

[105] H. Grad, Commun. Pure Appl. Math. **2**,331 (1949).

[106] I. Muller, Z. Phys. **198**,329 (1967).

[107] W. Israel, Ann. Phys. (N.Y.)**100**,310(1976).

[108] J. M. Stewart Proc. R. Soc. London, Ser. A **357**, 59(1977); W. Israel and J. M. Stewart, Ann. Phys. (N.Y.)**118**, 341(1979).

[109] D. H. Rischke, in *Hadrons in Dense Matter and Hadrosynthesis*, edited by J. Cleymans *et al.*, Lecture Notes in Phys. **516** (Springer, Berlin, 1999).

[110] P. Houvinen, Acta. Phys. Pol. B **33**, 1635(2002).

[111] T. Hirano, Y. Nara, Phys. Rev. Lett. **91**,082301(2003); Phys. Rev. C **69**, 034908 (2004).

[112] P. F. Kolb and U. Heinz, nucl-th/0305084 (2003).

[113] D. H. Rischke *et al*, Nucl. Phys. A **595**,383(1995).

[114] R. Bair, P. Romatschke, Eur. Phys. J. C. **51**, 677 (2007); P. Romatschke, Int. J. Mod. Phys. **E19**, 1 (2010).

[115] A. Muronga, Phys. Rev. C. **69**, 034903 (2004).

[116] B. Schenke, S. Jeon and C. Gale Phys. Rev. C. **82**, 014903 (2010).

[117] G. S. Denicol, H. Niemi, E. Molnar and D. H. Rischke, arxiv:1202.4551 (2012).

[118] J. Y. Ollitrault, Eur. J. Phys. **29**, 275 (2008).

[119] H. Song, U. Heinz, Phys. Rev. C. **77**, 064901 (2008).

[120] T. Hirano, Phys. Rev. C **65**,011901(2001).

[121] T. Hirano *et al.*, Lect. Note Phys. **785**, 139 (2010).

[122] Mikolaj Chojnacki, PhD. Thesis at Institute of Nuclear Physics, Krakow, Poland (2009).

[123] S. Weinberg, The Astronomical Journal **168**, 175 (1971).

[124] J. D. Bjorken, Phys. Rev. D **27**, 140 (1983).

[125] Gersdorff H Von, M. Kataja, L. McLerran and P. V. Ruuskanen, Phys. Rev. D **34** 794; Phys. Rev. D **34** (1986).

[126] S. J. Brodsky, J. F. Gunion and J. H. Kuhn, Phys. Rev. Lett. **39** 1120 (1977).

[127] A. Adil and M. Gyulassy, Phys. Rev. C, **72** 034907 (2005).

[128] T. Hirano and Y. Nara, J. Phys. G, **30** S1139 (2004).

[129] R. C. Hwa and K. Kajantie, Phys. Rev. D **32**,1109 (1985).

[130] M. Asakawa and T. Hatsuda, Phys. Rev. D **55**, 4488 (1997).

[131] F. Karsch, E. Laermann and A. Peikert Phys. Lett. B **478**, 447 (2000).

[132] M. Cruetz, Phys. Rev. D **21**, 2308 (1980).

[133] H. Satz, *"The Thermodynamics of Quarks and Gluons"* in the book **The Physics of the Quark Gluon Plasma** Lect. Note. Phys. **785** 1-21, Springer-Verlag, Berlin Heidelberg (2010).

[134] J. Engels *et al.*, Z. Phys. C **42**, 341 (1989).

[135] V. Goloviznin and H. Satz, Z. Phys. C **457**, 671 (1993).

[136] F. Karsch, A. Patkos and P. Petreczky Phys. Lett. B **401**, 69 (1997).

[137] M. M. Aggarwal *et al* WA98 Collaboration, Phys. Rev. Lett. **85**, 3595 (200).

[138] S. Adler, PHENIX Collaboration, Phys. Rev. Lett. **94**, 232301 (2005).

[139] H. Buesching for PHENIX Collaboration Nucl. Phys. A **774**, 103 (2006).

[140] R. K. Ellis, W. J. Stirling and B. R. Webber, *QCD and Collider Physics*, Cambridge University Press, 1996

[141] L. E. Gordon and W. Vogelsang, Phys. Rev. D **50** (1994) , 1901 .

[142] R.D. Field, *Application of Perturbative QCD*, Addison-Wesley Pub. Company, N.Y. 1989.

[143] M. L. Miller *et al.*, Annu. Rev. Nucl. Part. Sci. **57**, 205-43 (2007).

[144] C. Y. Wong, *Introduction of High Energy Heavy Ion Collisions*, World Scientific, Singapore, 1994.

[145] L. E. Gordon and W. Vogelsang Phys. Rev. D **48**, 3136 (1993).

[146] S. S. Adler *et al.* (PHENIX collaboration), Phys. Rev. Lett. **91** (2003) 072301.

[147] P. Roy , J. Alam , S. Sarkar, B. Sinha and S. Raha S, Nucl. Phys. A **624**, 687 (1997).

[148] S. Turbide, C. Gale, S. Jeon and G. D. Moore, Phys. Rev. C **72**, 014906 (2005).

[149] T Renk Phys. Rev. C **67**, 064901 (2003).

[150] S. Sarkar, J. Alam, P. Roy, A. K. Dutt-Mazumder, B. Dutta-Roy and B. Sinha, Nucl. Phys. A **634**, 206 (1998).

[151] P. Roy, S. Sarkar, J. Alam and B. Sinha, Nucl. Phys. A **653**, 277 (1999).

[152] J. Alam , P Roy and S. Sarkar, Phys. Rev. C **71**, 059802 (2005).

[153] J. Alam, P. Roy and S. Sarkar, Phys. Rev. C **68**, 031901 (R) (2003).

[154] K. L. Haglin, J. Phys. G **30**, L27 (2004).

[155] K. Ozawa *et al*, Phys. Rev. Lett. **86**, 5019 (2001).

[156] F. Bonutti *et al.* Nucl. Phys. A **677**, 213 (2000).

[157] M. A. Kagarlis *et al* Phys. Rev. C **60**, 025203 (1999).

[158] M. Naruki *et al*, Phys. Rev. Lett. **96**, 092301 (2006).

[159] I. Flrohlich *et al*, nucl-ex/0610048 (2006).

[160] C. Djalali, Quark Matter 2006, Nov. 14-20, 2006, Shangahi, China.

[161] S. Damjanovic *et al*, J. Phys. G **31**, S903 (2005).

[162] G. Agakichiev *et al* Phys. Lett. B **422**, 405, (1998).

[163] R. Rapp and J. Wambach, Adv. Nucl. Phys. **25**, 1 (2000)

[164] S. Sarkar, J. Alam and T. Hatsuda, J. Phys. G **30**, 607 (2004).

[165] G. Q. Li, C. M. Ko and G. E. Brown, Nucl. Phys. A **606**, 568 (1996).

[166] R. Rapp, G. Chanfray and J. Wambach, Nucl. Phys. A **617**, 472 (1997).

[167] J. Alam, S. Sarkar, T. Hatsuda, T. K. Nayak and B. Sinha, Phys. Rev. C **63**, 021901(R) (2001).

[168] J. Alam, P. Roy, S. Sarkar and B. Sinha, Phys. Rev. C **67**, 054901 (2003).

[169] "First Three Years of Operation of RHIC" Nucl. Phys. A **757**, 1 (2005).

[170] J. Cleymans, H. Oeschler, K. Redlich and S. Wheaton, J. Phys. G **32**, S165 (2006).

[171] G. E. Brown and M. Rho Phys. Rep. **269**, 333 (1996).

[172] S. S. Adler *et al.* PHENIX Collaboration, Phys. Rev. C **69**, 034909 (2004).

[173] G. E. Brown and M. Rho, Phys. Rev. Lett. **66**, 2720 (1991).

[174] G. E. Brown and M. Rho, nucl-th/0509001; nucl-th/0509002 (2005).

[175] B. D. Serot and J. D. Walecka, Advances in Nuclear Physics **16** Plenum, New York (1986).

[176] D. Kharzeev and M. Nardi, Phys. Lett. B **507**, 121 (2001).

[177] B. Mohanty and J. Alam, Phys. Rev. C **68**, 064903 (2003).

[178] F. Karsch, Nucl. Phys. A **698**, 199 (2002).

[179] S. Katz, Nucl. Phys. A **774**, 159 (2006).

[180] M. Cheng *et al.*, Phys. Rev. D **74**, 054507 (2006).

[181] D. Enterria and D Peressounko Eur. Phys. J. C **46**, 451 (2006).

[182] F. D. Steffen and M. H. Thoma, Phys. Lett. B **510**, 98 (2001).

[183] P. Huovinen, P. V. Ruuskanen and S. S. Rasanen, Phys. Lett. B **535** (2002) 109.

[184] K. Gallmeister and B. Kampfer, Phys. Rev. C **62**, 057901 (2000).

[185] D. Peressounko and Yu E. Pokrovsky, hep-ph/0009025 (2000).

[186] D. K. Srivastava and B. Sinha, Phys. Rev. C **64**, (2001) 034902.

[187] E. V. Shuryak, hep-ph/0608177.

[188] P. Kovtun, International Conference on Strong and Electroweak Matter 2006, Brookhaven National Laboratory, May 10-13, 2006.

[189] S. Caron-Huot, P. Kovtun, G. Moore, A. Starinets and L. G. Yaffe, J. High Energy **0612**, 015 (2006).

[190] A. Adare *et al.* (PHENIX collaboration), Phys. Rev. Lett. **104** (2010) 132301

[191] C. Bernard *et al*, Phys. Rev. D **75**, 094505 (2007).

[192] A. Andronic, P. Braun-Munzinger and J. Stachel, Nucl. Phys. **A**, **772**(2006)167; Erratum ibid **678**, 516 (2009).

[193] T. Hirano and K. Tsuda, Phys. Rev. C **66**,054905 (2002).

[194] T. Renk, Phys. Rev. C **71**, 064905 (2005; J. Phys. G **30**, 1495 (2004).

[195] K. Gallmeister, B. Kämpfer and O. P. Pavelenko, Phys. Rev. C **62** (2000) 057901.

[196] R. Chatterjee, D. K. Srivastava and S. Jeon, Phys. Rev. C **79**, 034906 (2009).

[197] A. Arnaldi (for the NA60 collaboration), Phys. Rev. Lett. **100** 022302 (2008).

[198] S. Damjanovic (for the NA60 collaboration), J. Phys. G. **35** 104036 (2008).

[199] R. Arnaldi (for the NA60 collaboration), E. Phys. J. C. **61** 711 (2009).

[200] H. van Hees and R. Rapp, Phys. Rev. Lett. **97** 102301 (2006).

[201] J. Ruppert, C. Gale, T. Renk, P. Lichard and J. I. Kapusta, Phys. Rev. Lett. **100** 162301 (2008).

[202] K. Dusling and I. Zahed, hep-ph0701253.

[203] E. Cooper and G. Frye, Phys. Rev. D **10**, 186 (1974).

[204] Y. Aoki, Z. Fodor, S. D. Katz and K. K. Szab, Phys. Lett. B **643**, 46 (2006).

[205] S. Gupta, X. Luo, B. Mohanty, H. G. Ritter and N. Xu, Science **332**, 1525 (2011).

[206] M. Floris for NA60 Collaboration, J. Phys. G **35**, 104054 (2008).

[207] P. Braun-Munzinger, J. Stachel, J. P. Wessels and N. Xu, Phys. Lett. B **344**, 43 (1995); **365**, 1 (1996); P. Braun-Munzinger, I. Heppe and J. Stachel, *ibid* **465**, 15 (1999); J, Cleymans and K. Redlich, Phys. Rev. Lett. **81**, 5284 (1998); F. Becattini, J. Cleymans, A. Keranen, E. Suhonen and K. Redlich, Phys. Rev. C **64**, 024901 (2001); P. Braun-Munzinger, D. Magestro, K. Redlich and J. Stachel, Phys. Lett. B **518**, 41 (2001); M. Kaneta and N. Xu, J. Phys. G **27**, 589 (2001).

[208] R. Chatterjee, E. S. Frodermann, U. W. Hienz and D. K. Srivastava, Phys. Rev. Lett. **96**, 202302 (2006).

[209] F.-M. Liu, T. Hirano, K. Werner and Y. Zhu, arXiv:0906.3566 [hep-ph]

[210] J. Alam, S. Sarkar, P. Roy, T. Hatsuda and B. Sinha, Ann. Phys. **286**, 159 (2000).

[211] M. Harada and C. Sasaki, Phys. Lett. B **537** 280 (2002).

[212] R. S. Hayano and T. Hatsuda, arXiv:0812.1702 [nucl-ex]

[213] J. Alam, D. K. Srivastava, B. Sinha and D. N. Basu, Phys. Rev. D **48** 1117 (1993).

[214] B. Sinha, Phys. Lett. B **128**, 91 (1983).

[215] S. Raha and B. Sinha, Phys. Rev. Lett. **58** 101 (1987).

[216] N. Armesto, N. Armesto, N. Borghini, S. Jeon, U.A. Wiedemann (ed), J. Phys. G: Nucl. Part. Phys. **35** 2008.

[217] H. Appelshauser *et al* (for NA49 Collaboration), Phys. Rev. Lett. **82** 2471 (1999).

[218] B. K. Patra, J. Alam, P. Roy, S. Sarkar and B. Sinha, Nucl. Phys. A **709** 440 (2002).

[219] S. S. Adler et al (for PHENIX collaboration), Phys. Rev. C **69** 034909 (2004).

[220] H. Buesching (for PHENIX collaboration), Nucl. Phys. A **774** 103 (2006).

[221] E. V. Shuryak, Nucl. Phys. A **661** 119 (1999).

[222] R. Rapp, Nucl. Phys. A **661** 33 (1999).

[223] S. Adler, (for PHENIX collaboration), Phys. Rev. D **71** 071102 (2005).

[224] T. Renk and J. Ruppert, Phys. Rev. C **77** 024907 (2008).

[225] H. van Hees and R. Rapp, Nucl. Phys. A **806** 339 (2008).

[226] S. Leupold, W. Peters and U. Mosel, Nucl. Phys. A **628** 311 (1998).

[227] E. Schnedermann, J. Sollfrank and U. Heinz, Phys. Rev. C **48**,2462 (1993).

[228] C. M. Hung and E. Shuryak, Phys. Rev. C **57**,1891 (1998).

[229] S. Damjanovic (for NA60 Collaboration), J. Phys. G **35**,104036 (2008).

[230] A. Toia (PHENIX collaboration), J. Phys. G **35**, 104307 (2008).

[231] C. Alt *et. al*, for NA49 Collaborations, Phys. Rev. C **77** (2008) 024903.

[232] B. I. Abelev *et. al* for STAR Collaboration, arxiv:0909.4131(2009).

[233] I. G. Bearden *et. al* for BRAHMS Collaboration, Phys. Rev. Lett. **94** (2005)162301.

[234] S. V Afanasiev *et. al* for NA49 Collaboration, Phys. Rev. C **66** (2002)054902.

[235] M. Gazdzicki and M. Gorenstein, Acta Phys. Polon. B **30** (1999) 2705.

[236] B. Tomasik and E. E. Kolomeitsev, Eur. Phys. J. C **49**, 115 (2007); B. Tomasik, nucl-th/0509101.

[237] S. Chatterjee, R. M. Godbole and Sourendu Gupta, Phys. Rev. C **81**, 044907 (2010).

[238] J. Cleymans, H. Oeschler, K. Redlich and S. Wheaton, hep-ph/0510283.

[239] M. Gazdzicki, J. Phys. G **30** (2004) S701.

[240] Jajati K. Nayak, J. Alam, B. Mohanty, P. Roy and A. K. Dutt-Mazumder, Acta Phys. Slov. **56**, 27 (2006).

[241] J. Letessier and J. Rafelski, Eur. Phys. J. A **35**, 221 (2008).

[242] A. Tawfik, Fizika B **18**, 141 (2009).

[243] J. Rafelski and B. Muller, Phys. Rev. Lett **48** (1982) 1066.

[244] P. Koch, B. Muller and J. Rafelski, Phys. Rep. **142**, 167 (1986).

[245] J. Rafelski and J. Letessier, Acta Phys. Polon. B **30**, 3559 (1999).

[246] M. Gazdzicki, Acta Phys. Pol. B **35**, 187 (2004).

[247] M. Gorenstein, J. Phys. G **28**, 1623 (2002).

[248] E. Kolb and M. S. Turner, Early Universe, Westview Press.

[249] G. E. Brown *et. al* Phys. Rev. C **43** (1991) 1881.

[250] C. Amslar *et al.*, Phys. Lett. B **667** (2008) 1.

[251] J. Q. Wu and C. M. Ko, Nucl. Phys. A **499** (1989) 810.

[252] J. Randrup and C. M. Ko, Nucl. Phys. A **343**, 519 (1980); *ibid***411** (1983), 537.

[253] G. Q. Li, C. H. Lee and G. E. Brown, Nucl. Phys. A **625** (1997) 372.

[254] C. M. Ko, Phys. Rev. C **29** (1984) 2169.

[255] J. Kapusta and A. Mekjian, Phys. Rev. D **33** (1986) 1304.

[256] J. Alam, S. Raha and B. Sinha, Phys. Rep. **273**, 243 (1996).

[257] T. Matsui, B. Svetitsky, L. D. McLerran, Phys. Rev. D **34** (1986) 783; Phys. Rev. D **34** (1986) 2047.

[258] J. D. Bjorken, Phys. Rev. D **27**, 140 (1983).

[259] T. S. Biro, E. van Doom, B. Muller, M. H. Thoma and X. N. Wang, Phys. Rev. C **48** 1275 (1993).

[260] J. Alam, P. Roy, S. Sarkar, S. Raha and B. Sinha, Int. J. Mod. Phys. A **12** (1997) 5151.

[261] O. Ristea for BRAHMS collaboration, Romanian Reports in Physics, **56** (2004) 659.

[262] J. Aichelin and C. M. Ko, Phys. Rev. Lett, **55** (1985) 2661.